UPPER ATMOSPHERE CIRCULATION AND WAVE MOTION

A thesis presented for the degree
of Doctor of Philosophy in Physics,
in the University of Canterbury,
Christchurch, New Zealand.

by

M.J. Smith

1981

ABSTRACT

A fully automated partial-reflection, spaced antenna, winds system has been developed at Birdlings Flat (44°S), using real-time data processing on a minicomputer. This enables almost continuous measurement of the winds between 65km and 100km to be made. Optimal data selection criteria for this location, and the value of simplifications in the data analysis and collection, are examined. The seasonal variation of the prevailing wind is studied in detail. The circulation in the mesosphere is characterized by strong westward winds in summer, and more variable eastward winds in winter. The circulation in the lower thermosphere is in the opposite direction. Long-period wind oscillations are observed throughout the year, and an identification of some of these with atmospheric normal modes, is strongly suggested in summer. Baroclinic instability may also occur in the summer mesosphere. Stratospheric disturbances are found to have significant effects in the 65-100 km region. The variation of atmospheric tides with height and season is also examined.

CONTENTS

LIST OF FIGURES

LIST OF TABLES

CHAPTER 1

INTRODUCTION

The main source of wind data in the 65-105 km height region has come from rocket techniques, usually involving the tracking of an experimental package ejected from the rocket. This includes the radar tracking of dropsondes below 60 km, falling inflatable spheres below about 80 km, and the optical tracking of luminous vapour trails above 90 km. The cost of such rockets, especially the larger ones required to probe above 60 or 70 km, has imposed severe limitations on the use of such methods.

The meteor radar technique has been valuable in the study of winds from 80 to 100 km, particularly when the height of the meteors can be determined. The total reflection of LF radio waves at 90-100 km has been utilized by Sprenger and Schminder (1969) to measure night-time winds since 1957. More recently, powerful VHF radars have been used to measure day-time mesospheric winds (Woodman and Guillan, 1974). All of these techniques suffer from poor global coverage, particularly in the southern hemisphere.

Satellite radiance measurements are assuming a rapidly increasing importance in the understanding of atmospheric dynamics but the present resolution, in time and height, is unable to resolve the dominant dynamical components of the lower thermosphere.

This thesis describes the use of MF radio waves, partially reflected from the D-region and totally reflected from the

lower E-region, to determine upper atmospheric winds, with particular emphasis on acquiring data on a continuous basis. This region of the atmosphere encompasses the upper mesosphere and lower thermosphere. The nomenclature describing the different atmospheric regions is summarized in Fig. 1.1. The stratopause is situated near 50 km and the mesopause at 85-90 km.

Figure 1.1: Classification of the neutral and ionized atmosphere (from Hines et al., 1965).

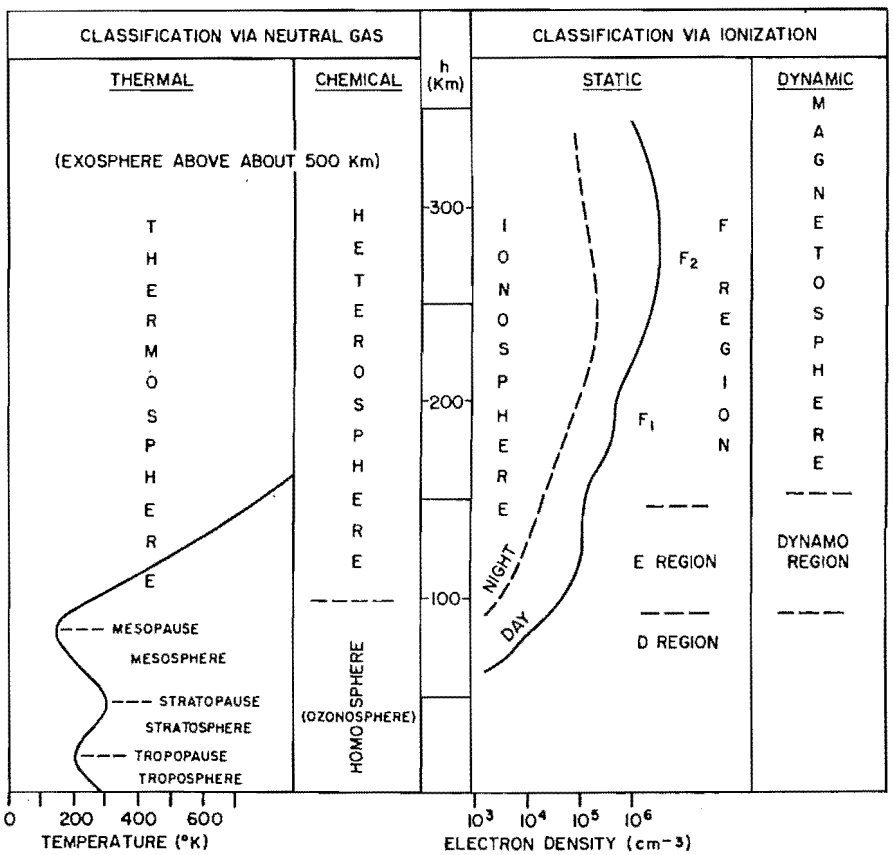

The partial reflection, spaced antenna method was first applied to the D-region by Fraser (1965) at Birdlings Flat (44^{o}S). It has also been used extensively at Saskatoon (52^{o}N) (Manson et al., 1974) and between heights of 80 and

100 km at Adelaide (Stubbs, 1976).

Chapter 2 outlines the partial reflection, spaced antenna method and discusses some of the problems of interpretation of the 'drift' measurements.

The high cost of data processing and the logistics involved in continuous data collection pose a formidable problem. Chapter 3 describes the development of a real-time drifts system, an essential part of this thesis, which enables the measurement of winds on a continuous basis.

Chapter 4 considers in detail the optimization of data yield versus data quality, and the value of simplifications in the data analysis and collection.

The neutral wind can conveniently be subdivided into components of decreasing temporal scale: the prevailing wind, planetary waves, atmospheric tides, internal gravity waves and turbulence. The prevailing wind in the 65-105 km region is dynamically interesting as it lies both in the upper reaches of a wind regime receiving its thermal drive from the upper stratosphere, and at the lower boundary of the quite distinct thermospheric circulation. At these heights, little is known about the behaviour of planetary waves, which are of great importance below. Tidal and gravity waves become dominant features above 80 km, as their amplitudes tend to increase in order to offset the exponential decrease in atmospheric density. In practice there may be significant interactions between the wind components.

In the second part of this thesis, the prevailing wind, planetary waves and atmospheric tides are considered in

Chapters 5,6 and 7 respectively. Each chapter opens with an overview of the theoretical understanding of each topic, upon which later discussion of results is based. Finally, in Chapter 8, the major results of the thesis are summarized and suggestions are given for future work.

CHAPTER 2

THE IONOSPHERIC DRIFTS EXPERIMENT

2.1 THE APPARENT VELOCITY

It was noticed early in the study of ionospheric radio wave propagation that a signal reflected from the ionosphere fluctuates in amplitude. On MF transmissions the radio waves may be totally reflected from the E, E_s or F regions, or partially reflected from the D-region. By using pulsed transmission and suitable aerials, the fading due to interference between the ground and sky waves, multihop echoes or the magnetoionic modes can be eliminated. Pawsey (1935) noted that the fading at two separated points was often similar but with a time delay between amplitude maxima. This suggested that the fading was due in part to the drift of an ionospheric diffracting screen over the receiving stations. The fact that the records at the two stations in the line of drift were not identical indicated that the ionization irregularities composing the diffracting screen were in continuous random motion.

Mitra (1949) made use of the time delays between three spaced antenna to determine the speed and direction of the drift. In this simplest method of analysis, no account is taken of random changes and it is assumed that the contours of constant amplitude in the diffraction pattern have no preferred direction of alignment (that is, the pattern is isotropic). For these reasons the velocity obtained is called the "apparent velocity" and is denoted in magnitude and

direction by V_a and ϕ_a. Fig. 2.1a illustrates contours of constant amplitude in the diffraction pattern drifting over the 3 antennae. A line joining the maxima in the pattern measured at the 3 points, the "line of maxima", moves across the array and for an isotropic pattern will, on average, be perpendicular to the direction of drift.

Rather than considering time delays between individual amplitude features, an average time delay over some recording interval can be conveniently obtained as the time lag to the maximum of the cross-correlation between recordings at pairs of antennae. The correlation function of amplitude, A (measured in space, (x,y), and time, t) for spatial and temporal separations ξ,η,τ is

$$\rho(\xi,\eta,\tau) = \frac{\langle (A(x,y,t) - \langle A \rangle)(A(x+\xi,y+\eta,t+\tau) - \langle A \rangle) \rangle}{\langle (A(x,y,t) - \langle A \rangle)^2 \rangle}$$

A quasi-ergodic assumption is made that the averaging in space and time denoted by $\langle\ \rangle$ will be the same as averaging in time only (Briggs et al., 1950). The temporal autocorrelation between antennae with separations (ξ_o,η_o) is $\rho(\xi_o,\eta_o,\tau)$.

Any two of the three cross-correlations between the amplitude records can be used to determine the apparent velocity. However, consistent with the idea of lines of maxima drifting over the array, the time lags for maximum cross-correlation, $\tau'ij$, (Fig 2.2) are subject to a constraint that when taken in cyclic order their sum should be zero (Barber, 1956). i.e.

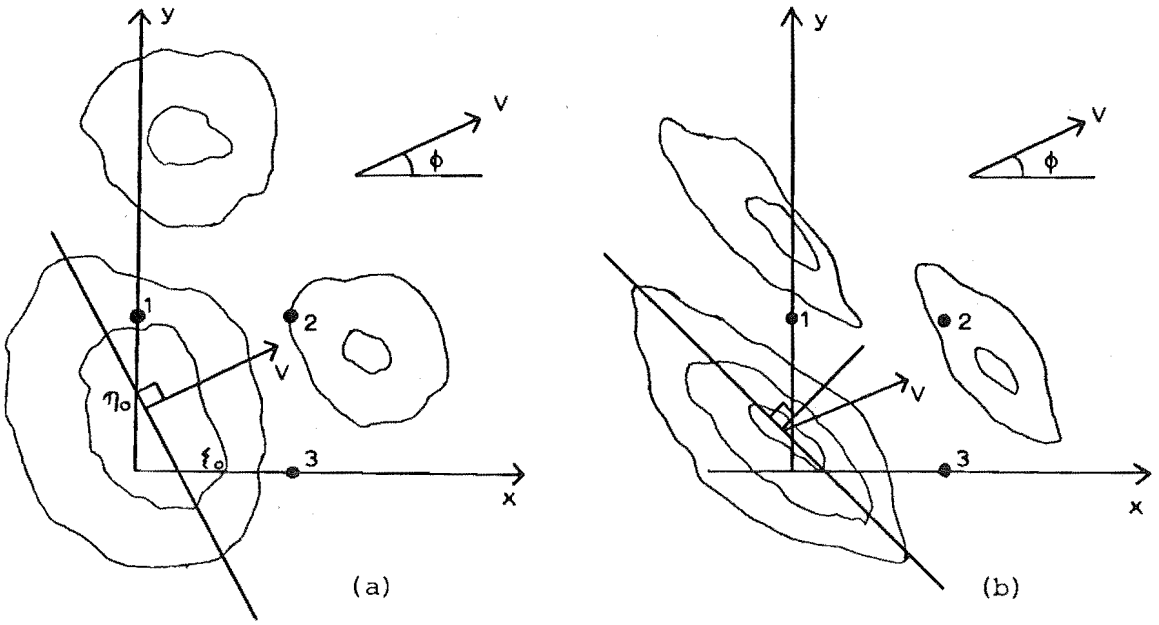

Figure 2.1: Contours of constant radiowave amplitude of (a) isotropic and (b) anisotropic diffraction patterns drifting over 3 antennae: 1,2,3.

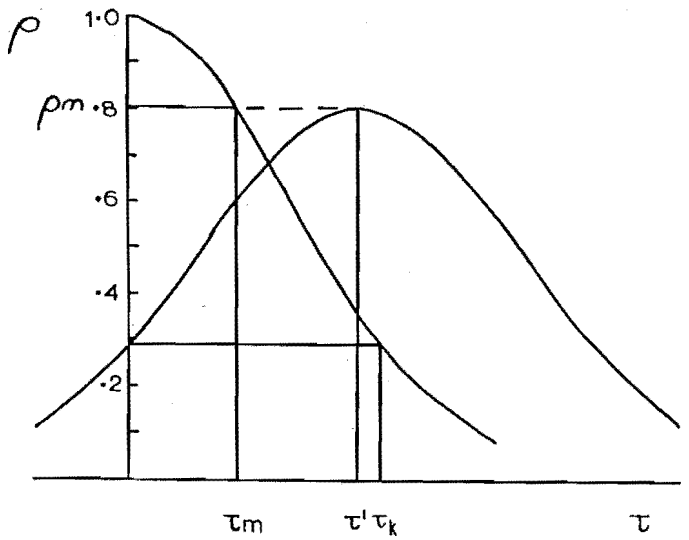

Figure 2.2: Auto- and cross-correlation functions and the parameters obtained from them.

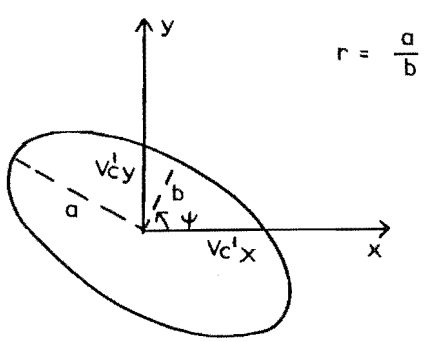

Figure 2.3: The characteristic ellipse.

$$T_e \equiv \tau'_{12} + \tau'_{23} + \tau'_{31} = 0$$

A measure of the deviation from this condition, which gives a good indication of the quality or internal consistency of the data, is the normalised time discrepancy (NTD) defined by

$$NTD \equiv \frac{|\tau'_{12} + \tau'_{23} + \tau'_{31}|}{|\tau'_{12}| + |\tau'_{23}| + |\tau'_{31}|} \qquad (2.1)$$

(Gregory et al., 1979).

The apparent velocity which gives a least squares fit to the three time delays with the geometry of Fig. 2.1 is given by:

$$\frac{1}{V_a^2} = \frac{\tau'^2_x}{\xi_o^2} + \frac{\tau'^2_y}{\eta_o^2} \qquad (2.2)$$

$$\tan \phi_a = \frac{\tau'_y}{\tau'_x}$$

where the least squares fitted time delays are given by

$$\tau'_x = (\tau'_{12} - T_e/3)$$

$$\tau'_y = -(\tau'_{23} - T_e/3)$$

(Fraser, 1970). The derivation is given in Appendix A.

As indicated previously, the apparent velocity will be in error in two circumstances.

(1) If the ground pattern is anisotropic (Fig. 2.1b) the calculated apparent velocity will be too small and in a

direction displaced towards the perpendicular to the direction of elongation (Phillips and Spencer, 1955).

(2) In any real situation changes will occur within the diffraction pattern as it moves. The cross-correlation maximum in the direction of drift will be reduced from a value of 1 by an amount which indicates the importance of the random changes. Also, however, the lag to the correlation peak will be decreased giving an apparent velocity which is too large.

2.2 FULL CORRELATION ANALYSIS

Compensation could easily be made for these two effects if observations were made at a large number of points on the ground, as described by Briggs (1968). However, for most workers, the requirement of a large array of receiving antennae is not practicable. The notable exception is the 89 dipole array at Buckland Park (Briggs et al., 1969). At a station such as Birdlings Flat with only 3 receiving antennae, the spatial correlation is only available at 3 (nonzero) spatial lags. Briggs, Phillips and Shinn (1950) developed a 'full correlation analysis' (FCA) for such a situation which compensates for random changes. The lack of spatial information is overcome by making the assumption that the temporal and spatial correlation functions have the same form. The analysis yields the corrected speed and direction of drift, an indication of the relative importance of random changes, and the spatial scale of the diffraction pattern. The method remains essentially the same today.

Following Briggs (1968), we start by using a coordinate system which moves at the actual drift velocity, $\underline{V}$. The spatial lags in the moving system (ξ_v, η_v) are related to those in a stationary coordinate system (ξ, η) by

$$\xi_v = \xi - V_x\tau; \quad \eta_v = \eta - V_y\tau \tag{2.3}$$

The contours of constant $\rho(\xi_v, \eta_v, \tau)$ are assumed to have the form of concentric ellipsoids centred on the coordinate system origin. It is also assumed that the contours of $\rho(\xi_v, \eta_v, \tau)$ intersect the (ξ_v, η_v) plane in circles, so that the spatial pattern is isotropic. This last restriction is later relaxed to elliptical spatial contours by a simple stretching of the circular contours. The form of the correlation is then

$$\rho(\xi_v, \eta_v, \tau) = F\left(\frac{\xi_v^2}{d^2} + \frac{\eta^2}{d^2} + \frac{\tau^2}{\tau_c^2}\right) \tag{2.4}$$

where d and τ_c are "characteristic" spatial and temporal scales whose ratio is to be determined and F is some unspecified function. Cross terms in $\xi_v\eta_v$ are absent due to the spatial isotropy assumption. The elliptical form can be justified for small lags when only the leading terms of a Taylor expansion are significant. Clearly the spatial correlation

$$\rho(\xi_v, \eta_v, 0) = F\left(\frac{\xi_v^2}{d^2} + \frac{\eta_v^2}{d^2}\right)$$

has the same functional form as the temporal correlation

$$\rho(0,0,\tau) = F\left(\frac{\tau^2}{\tau_c^2}\right)$$

under this assumption, as noted by Briggs (1968).

The correlation in the fixed coordinate system is, from (2.3) and (2.4),

$$\rho(\xi,\eta,\tau) = F\left[\frac{(\xi-V_x\tau)^2}{d^2} + \frac{(\eta - V_y\tau)^2}{d^2} + \frac{\tau^2}{\tau_c^2}\right] \tag{2.5}$$

This function is only known at (ξ,η) values corresponding to our 3 antennae separations: (ξ_o,η_o), $(\xi_o,0)$ and $(0,\eta_o)$, but a range of values of temporal correlation are readily available. Without elaborating further on the form of F, we can use various points on the observed correlations to derive the drift parameters. The value of the spatial correlation between the 2 antennae aligned in the x direction with a separation $(\xi_o,0)$ is

$$\rho(\xi_o,0,0) = F\left[\frac{\xi_o^2}{d^2}\right] \tag{2.6}$$

The temporal correlation falls to this level in a time lag τ_{kx} (Fig. 2.2) given by

$$\rho(0,0,\tau_{kx}) = F\left[\frac{V_x^2\tau_{kx}^2}{d^2} + \frac{V_y^2\tau_{kx}^2}{d^2} + \frac{\tau_{kx}^2}{\tau_c^2}\right] \tag{2.7}$$

From these two equations we have

$$\frac{\xi_o^2}{d^2} = \left(\frac{V_x^2}{d^2} + \frac{V_y^2}{d^2} + \frac{1}{\tau_c^2}\right)\tau_{kx}^2$$

or

$$V_c'^2 \equiv \frac{\xi_o^2}{\tau_{kx}^2} = V_x^2 + V_y^2 + V_c^2 \qquad (2.8)$$
$$= V^2 + V_c^2$$

where the ratio $\frac{d}{\tau_c}$ has been defined as V_c which, having the units of a velocity, is termed the characteristic velocity. Historically, the quantity V_c' has been called the fading velocity; it is the velocity needed to describe the fall-off in the autocorrelation function as being caused solely by the drift of a steady pattern. In the present isotropic case, V_c' is independent of direction.

The components of apparent velocity (V_x', V_y'), can be obtained from the time lag, τ', to the maximum of the cross correlations.

$$\frac{\partial \rho(\xi_o, 0, \tau)}{\partial \tau} = 0 \quad \text{at} \quad \tau_x'$$

giving

$$V_x' \equiv \frac{\xi_o}{\tau_x'} = \frac{1}{V_x}(V_x^2 + V_y^2 + V_c^2)$$
$$= \frac{1}{V_x}(V^2 + V_c^2) \qquad (2.9)$$

Substituting from(2.8) we obtain the x component of the 'true velocity', $\underline{V}$:

$$V_x = \frac{V_c'^2}{V_x'} \qquad (2.10)$$

Similarly for $\rho(0, \eta_o, \tau_y')$ we obtain

$$V_y = \frac{V_c'^2}{V_y'}$$

also, $\tan \phi = \frac{V_y}{V_x}$.

The 'true velocity' can therefore be obtained from V'_c and V' which can be calculated directly from the measured correlations.

The other quantities of interest are the spatial and temporal scales of the changes in the pattern. These can be defined at any level of correlation but it is usual to use the 0.5 level. We have seen the spatial correlation falls to a value $\rho(\xi_o,0,0)$ in a distance ξ_o in the x-direction, and that the autocorrelation takes a time lag τ_{kx} to fall to this level. The lag for the autocorrelation to fall to 0.5 ($\tau_{0.5}$) can be easily found. Since the spatial correlation is assumed to have the same functional form as the temporal correlation, it will fall to 0.5 in a distance:

$$d_{0.5} = \xi_o \frac{\tau_{0.5}}{\tau_{kx}} = V'_c \tau_{0.5} \qquad (2.11)$$

In the more general case of anisotropic irregularities the above spatial scale will depend on direction. $d_{0.5}$ (and V'_c) are then defined in the direction of drift.

The autocorrelation measured by a stationary observer will fall off in a way which depends not only on the random changes taking place within the pattern in time, but also on the steady drift. This can be seen from the form of the autocorrelation at the 0.5 level:

$$\rho(0,0,\tau_{0.5}) = 0.5 = F\left(\left(\frac{V^2}{d^2} + \frac{1}{\tau_c^2}\right)\tau_{0.5}^2\right) \qquad (2.12)$$

The time scale, or "lifetime" of internal changes actually

occuring within the pattern should be measured by an observer moving with the steady drift velocity, $\underline{V}$ (Briggs, 1977). From equation (2.4) the autocorrelation such an observer would measure falls to 0.5 in a time $T_{0.5}$ given by:

$$\rho(0,0,T_{0.5}) = 0.5 = F\left(\frac{T_{0.5}^2}{\tau_c^2}\right) \tag{2.13}$$

The time scales measured by the stationary and moving observers are therefore related by:

$$\frac{T_{0.5}^2}{\tau_c^2} = \left(\frac{V^2}{d^2} + \frac{1}{\tau_c^2}\right)\tau_{0.5}^2$$

i.e.

$$T_{0.5} = \left(1 + \frac{V^2}{V_c^2}\right)^{\frac{1}{2}} \tau_{0.5} \tag{2.14}$$

It is the lifetime $T_{0.5}$ which will be of direct importance to the turbulent lifetimes in the ionospheric diffracting screen. Manson and Meek (1980) have used $T_{0.5}$ to calculate a turbulent velocity parameter and the associated energy dissipation.

2.3 EXTENSIONS OF THE METHOD

Phillips and Spencer (1955) extended the full correlation analysis method to accommodate anisotropic patterns by assuming that the spatial correlation could be described by elliptical contours which are obtained by a uniform stretching

of the isotropic contours. The spatial behaviour can therefore be described in terms of a 'characteristic ellipse', with major and minor axes in the ratio r, and oriented at angle ψ with respect to the x axis (Fig. 2.3). These parameters can be obtained from the measurements of $(V_c')_i$ in the 3 directions of the arrays since, from (2.11), V_c', while having the units of velocity, really describes the spatial behaviour of the ground pattern. The magnitude of V_c' in the direction of drift is denoted by $(V_c')_v$.

The apparent velocity corrected for anisotropy, V', is given by

$$V_a = V' \cos(\phi-\phi_a)$$

where

$$\tan(\phi-\phi_a) = \frac{(r^2-1)\tan(\phi_a-\psi)}{1+r^2\tan^2(\phi_a-\psi)}$$

gives the correction to the apparent velocity direction (Phillips and Spencer, 1955). The true velocity is given by (cf. (2.10))

$$V = \frac{(V_c')_v^2}{V'}$$

with

$$(V_c')_v^2 = \frac{1+(r^2-1)\cos^2\psi}{1+(r^2-1)\cos^2(\phi-\psi)} (V_c')_x^2$$

Fooks (1965) pointed out that when the correlations are low it is preferable to use an alternative form of τ_k which was originally derived by Briggs et al. (1950):

$$\tau_k^2 = \tau'^2 + \tau_m^2 \qquad (2.15)$$

where τ_m is the temporal lag required for the autocorrelation to fall to the same value as the peak of the cross-correlation (Fig. 2.2). The relationship can be shown by equating the autocorrelation at τ_m with the cross-correlation at its maximum value (at $\tau = \tau'$). i.e.

$$\rho(0,0,\tau_{mx}) = \rho(\xi_o,0,\tau'_x)$$

For the isotropic spatial correlation assumed in (2.5) this implies:

$$\frac{V_x^2\tau_{mx}^2}{d^2} + \frac{V_y^2\tau_{my}^2}{d^2} + \frac{\tau_{mx}^2}{\tau_c^2} = \frac{(\xi_o - V_x\tau'_x)^2}{d^2} + \frac{V_y^2\tau'^2_x}{d^2} + \frac{\tau'^2_x}{\tau_c^2}$$

$$(V_x^2+V_y^2+V_c^2)\tau_{mx}^2 = \xi_o^2 - 2\xi_o V_x\tau'_x + (V_x^2+V_y^2+V_c^2)\tau'^2_x$$

After substituting from (2.8) and (2.9) this reduces to

$$\tau_{kx}^2 = \tau'^2_x + \tau_{mx}^2$$

Kelleher (1965) reported that the equation was also valid for anisotropic patterns.

The expression has the advantage that it makes use of the correlations at a higher level where the statistical variations are smaller. This is useful at Birdlings Flat where the antenna spacing is such as to give fairly low cross-correlations for D-region returns and sometimes even

negative values at zero lag. The calculation of τ_k from (2.15) makes use of the width of the autocorrelation in contrast to the original method which depends on the width of the cross-correlation at its intercept with the $\tau = 0$ axis.

In the computer implementation of the equations at Birdlings Flat, the temporal lags $\tau_{0.5}$, τ_m, τ' are found from a least squares fit of a polynomial to a section of the experimental correlations. The use of a third or fourth order polynomial caters for skewed cross-correlations which are sometimes observed (v. Section 2.4.3).

Other approaches to the problem have been described by Briggs and Spencer (1955), Keneshea et al. (1965), Little and Ekers (1971) and others. A significant contribution was that of Fedor (1967) who introduced a statistically rigorous approach by fitting sections of the observed correlations to a Gaussian function on a least squares basis. He also allowed for any number of aerials, and the use of spaced frequencies to determine three-dimensional structure, although the validity of this interpretation has been questioned by Briggs (1972). Although the method is mathematically more correct, the assumption of Gaussian correlations is often violated in practice. The implementation of the drifts analysis on a minicomputer in real-time also places restraints on the degree of sophistication which may be employed. In an application of his method Fedor found that the 'best-fit' method differed from the simpler method by less than 5%; such differences are insignificant

when atmospheric variation is taken into account. Gregory et al. (1979) have employed a simplified full correlation analysis for use on a microprocessor based system, but this method also suffers from the assumption of Gaussian correlations.

2.4 PRACTICAL ASPECTS OF THE ANALYSIS

2.4.1 The Similarity of the Spatial and Temporal Correlation Functions

A major assumption made in the full correlation analysis is that surfaces of constant $\rho(\xi,\eta,\tau)$ are ellipsoids. The mathematical basis for this is valid only for small lags, a condition which is often violated in the experimental situation. It is therefore important to test this assumption or the resulting effect that the temporal and spatial correlations have the same shape. The latter can be tested when a number of receiving antennae are available to calculate the spatial correlation. Kelleher (1966), using F-region reflections, found differences especially when V_c was large. Many of his correlations were periodic suggesting the presence of a fringe-like diffraction pattern which is common in F-region data. The determination of velocity is difficult when there are fringes, as motion in the direction of the fringes cannot be detected, but fortunately for the present work, this type of echo is seldom seen in D-region data where random diffraction patterns predominate (Felgate and Golley, 1971). Studies by Golley and Rossiter (1970) and Brown and Chapman (1972) on E-region reflections found good similarity in the shapes of the correlations.

Recently Briggs and Maude (1978) have shown how the assumption can be avoided by making use of time lags at the intersection points of the correlations. The method, however, is not suited to many of the observed correlations at Birdlings Flat where this intersection is often ill-defined. This may be due to the low correlations obtained from our fairly wide antenna spacing.

2.4.2 The Triangle Size Effect

Kelleher (1966) found that the 'true velocity' depends upon the size of the triangle formed by the receiving antennae - the so-called 'triangle size effect'. Golley and Rossiter (1970) studied this problem using the large Buckland Park array, and found that as the triangle size was increased the 'true velocity' increased to a limit which was in good agreement with the actual velocity obtained from spatial correlation measurements. They proposed that the cause of the triangle size effect was the depression of the cross-correlation values due to instrumental factors such as differences in receivers or digitizing channels or coupling effects (Fedor and Plywaski, 1972). The depression of the cross-correlation would most affect high values of correlation where the slope is smallest (Brown and Chapman, 1972). These high values are obtained from an antenna spacing small compared to the ground diffraction pattern scale, hence the observed discrepancy in velocities at small spacings. Chandra (1978) has supported his conclusion from theoretical studies. Another effect observed when a right-angled triangle is used,

is a tendency for the characteristic ellipse to be aligned with its major axis along the hypoteneuse of the triangle (Beynon and Wright, 1969). This is probably a related phenomenon since the two shorter sides of the triangle would have higher cross-correlation values giving an underestimate of pattern size in these directions and therefore a rotation of the ellipse towards the longest side.

2.4.3 Experimental Correlation Functions

A radio wave returned from the ionosphere contains both amplitude and phase information. Full utilization of this information requires the calculation of complex correlation functions whose magnitudes are then used in the full correlation drifts analysis. However, it is simpler experimentally to use a linear detector in the receivers and measure amplitude only. Alternatively, quadratic detectors measuring signal intensity could be used. In both of these cases the calculated correlations will in general differ from the complex correlations. Bramley (1951) has shown that for a randomly phased received signal (i.e. Rayleigh distributed) the following relationship holds:

$$\rho_A \simeq \rho_I = \rho_C^2 \qquad (2.16)$$

where ρ_A, ρ_I and ρ_C are the correlations of amplitude, intensity and complex amplitude. The relationships are shown diagrammatically in Fig. 2.4. When a specular component is present in the angular spectrum, Bramley obtained:

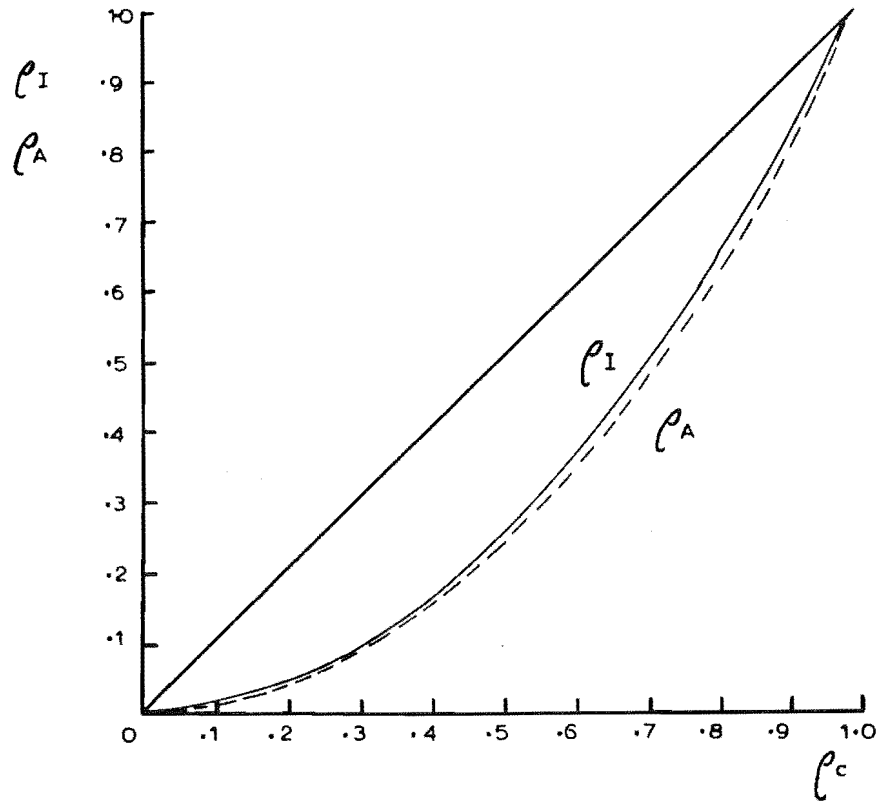

Figure 2.4: Relationships between ρ_C, ρ_I and ρ_I (adapted from Rogers and Walker, 1973).

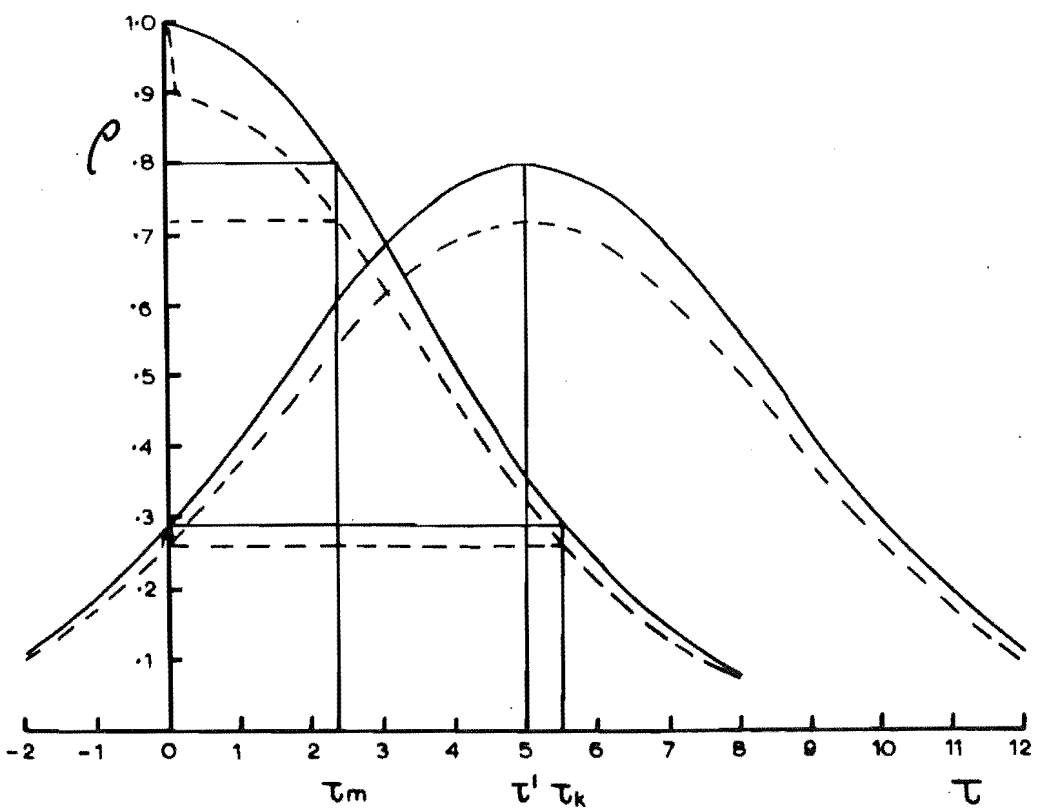

Figure 2.5: Effect of high frequency noise on the correlation functions.

$$\rho_A \simeq \rho_I = \rho_C$$

For the case of a Rayleigh distributed signal the correlation function of amplitude will clearly be narrower than that of complex amplitude. It should be asked whether this change in correlation will affect the 'true velocity' or other parameters obtained in the full correlation analysis.

Firstly, on the basis of (2.16), the position of the maximum of a cross-correlation, τ', and hence V_a are not expected to be altered. The second important parameter obtained from the correlations is τ_m, the temporal lag required for the autocorrelation to fall to the value of the cross-correlation maximum. Earlier this was seen to occur (e.g. in the x direction) when

$$\rho_C(0,0,\tau_m) \equiv F\left(\frac{\tau_m^2}{\tau_c^2}\right) = \rho_C(\xi_o,0,\tau') \equiv F\left(\frac{(\xi_o - V_x\tau')^2}{d^2} + \frac{\tau'^2}{\tau_c^2}\right)$$

The amplitude correlation will in general be a function G of ρ_C, i.e. $\rho_A = G\{\rho_C\}$. For a Rayleigh distribution $G\{\rho_C\}$ is simply ρ_C^2. Therefore the value of τ_m for amplitude correlations must satisfy

$$G\left\{F\left(\frac{\tau_m^2}{\tau_c^2}\right)\right\} = G\left\{F\left(\frac{(\xi_o - V_x\tau')^2}{d^2} + \frac{\tau'^2}{\tau_c^2}\right)\right\}$$

i.e.

$$\rho_A(0,0,\tau_m) = \rho_A(\xi_o,0,\tau')$$

The point that emerges clearly is that the function G will

have an equivalent effect on both the auto- and cross-correlations, resulting in no change in the derived value of τ_m and in turn τ_k (from (2.15)), V_c' and V (the'true velocity'). However, the lag $\tau_{0.5}$, for the autocorrelation of amplitude to fall to 0.5 will be different, since when

$$\rho_A(0,0,\tau_{0.5}) = G\left\{F\left(\frac{\tau_{0.5}^2}{\tau_c^2}\right)\right\} = 0.5$$

the complex correlation, $F\left(\frac{\tau_{0.5}^2}{\tau_c^2}\right)$, has only fallen to $G^{-1}(0.5)$. From (2.11) this will directly affect the spatial scale size derived from the FCA. For data approaching a Rayleigh distribution, the scale size derived from correlations of amplitude will be significantly smaller than those obtained from the complex correlation.

Experimental confirmation of these results has been given by Pfister (1971). He analyzed both the correlations of amplitude and the complex correlations of amplitude and phase and found no systematic difference in calculated speed or direction. But larger structures were obtained from the complex correlations.

The receivers used at Birdlings Flat (Section 3.3) employ an additional logarithmic amplification after the video output of the linear stage. This enables a wider dynamic range of signals to be measured. In order to test the effect of this nonlinear alteration of the signal on the correlations, a computer simulated study was carried out. A series of random amplitude values was generated and smoothed

so as to give a Gaussian correlation. The correlation of amplitude and correlation of the logarithm of the amplitude were then computed and compared. For the same length of data as used at Birdlings Flat the difference at high values of correlation was barely measurable. At the 0.3 correlation level the difference was 0.02; at the 0.1 level it was 0.03. The effect of using a logarithmic receiver output is therefore considered to be negligible.

In the presence of noise of a much faster fading rate than the signal reflected from the ionosphere, a spike may appear at the origin of the autocorrelation functions. Some workers have reduced the effect of this spike by interpolating each autocorrelation to zero lag and renormalizing the autocorrelation by this factor (S_i). The correct application requires the 3 autocorrelations to be treated separately. The correction $(S_i S_j)^{\frac{1}{2}}$ is then applied to the cross-correlation between receivers i and j (Vincent and Rottger, 1980). Meek (1978) has used a correction factor from the mean autocorrelation. If there are significant differences in the high frequency noise between receivers or aerials this will be slightly inaccurate.

In the real-time drifts system described in Chapter 3, the autocorrelations from the 3 receivers are not calculated separately, in the interest of efficiency. So a correction for a noise spike would have to be made on the basis of the mean autocorrelation. Such a correction would however involve an undesirable amount of additional computing time. Fortunately, for the present implementation of FCA, it is

not necessary. This is because the parameters involved in the FCA are obtained from temporal lags which depend on equating certain values of auto- and cross-correlations. High frequency noise will reduce these values by the factor S in both auto- and cross-correlations, leaving the values of τ_m and τ_k unchanged. This is illustrated for Gaussian correlations in Fig. 2.5 where 10% noise has been introduced. The reasoning is identical to that concerning complex correlations discussed above, except that now the function G is replaced by a constant factor S. As before the 'true velocity' is unchanged, but $\tau_{0.5}$ (and hence the scale sizes) will be in error. The correct value of $\tau_{0.5}$ can be simply obtained by finding the lag for the autocorrelation to fall to S x 0.5. In this way considerable effort in rescaling correlations can be avoided.

The shape of the observed cross-correlations often differ markedly from the well behaved, singly-peaked, Gaussian-like forms implicitly assumed by the theory. Oscillatory correlations may be produced by fringelike diffraction patterns such as would be produced by interference between specular reflections from large-scale undulations of a fairly smooth reflecting screen. Magneto-ionic mode interference may also be a cause.

Cross-correlations which are broadened or have multiple peaks could be caused by changes in velocity over the recording interval. The finite height resolution of the experiment also allows the combination of signal from different heights at a nominal sampled height. If the vertical wind

shear is significant, correlations may be broadened when scatter is received over a continuum of heights, or separate peaks may appear if reflections are from discrete layers. Haug and Petersen (1970) have shown how a simple model with a few differently behaved screens can produce irregularly shaped correlations as observed.

A direct consequence of the broadening or skewness of the cross-correlation is that the intersection point with the $\tau = 0$ axis will be altered. If τ_k is calculated directly from this intersection point, V_c' will also be altered, while V' will be unchanged. This may lead to negative values of V_c^2 and a breakdown of the full correlation analysis, since from (2.8) and (2.10)

$$V_c^2 = V_c'^2 - V^2 = V_c'^2 \left(1 - \frac{V_c'^2}{V'^2} \right) \tag{2.17}$$

If instead τ_k is calculated from (2.15), V_c' will not be affected by the width of the cross-correlation since it uses the autocorrelation width. So it is to be expected that use of (2.15) will be less affected by distorted cross-correlations. When several patterns are superimposed the height of each cross-correlation peak will be lower than that which would be obtained with a single pattern (MacDougall, 1966). This will also affect the 'true velocity' and may result in negative V_c^2.

Skew correlations will also occur in the presence of dispersion (McGee, 1966), that is, when the velocity of different Fourier components depends on frequency. Jones

and Maude (1965) attributed dispersion to dispersive surface gravity waves but Hines (1974,p107) has disputed the theoretical basis for their interpretation.

2.4.4 The Ground Diffraction Pattern

Since the Fresnel diffraction pattern is observed on the ground, the scale of the wavefront emerging from the ionospheric screen is a factor of 2 smaller (see Section 2.5.1). Furthermore the relationship with the actual scale of the ionospheric irregularities is generally not simple. Ratcliffe (1956) examined the case where the irregularities impose a random change in the complex phase, of standard deviation ϕ_m, on the emerging wavefront. He showed that only for a shallow screen where ϕ_m is less than 1, and a specular component dominates the angular spectrum, will the size of the irregularities be of the same order as the emerging wavefront. For a deeper screen ($\phi_m >> 1$) interference effects between the components of the angular spectrum result in a diffraction pattern size smaller than that of the irregularities by a factor $1/\phi_m$. Additionally the correlation of amplitude will be approximately equal to the square of the correlation of complex amplitude in this case, introducing a further difference in scale.

Consequently the ground diffraction pattern scale sizes measured by the drifts experiment are only simply related to the ionospheric irregularity scale size in the case of a shallow diffracting screen. If change is observed in the ground pattern sizes it is not possible to determine whether

this is due to a change in the lateral size of the irregularities or the 'depth' of the screen.

2.5 MOTION OF THE NEUTRAL ATMOSPHERE

2.5.1 The Point Source Effect

The velocity of the diffraction pattern at the ground is actually a factor of 2 larger than that of the ionospheric diffracting screen. This is because of the 'point source effect' whereby the scale size of the diffraction pattern (and hence the velocity) obtained from point source illumination is twice that obtained from plane wave illumination of the screen (Ratcliffe, 1956). Doubts were raised by Wright (1968) about the applicability to the ionosphere but subsequently Fedor and Plywaski (1971) found that aerial coupling had been causing the conflict in his results. Experiments confirming the effect have been made by Felgate (1970) and Wright (1972) who observed the displacement of the diffraction pattern when the radio wave source was given an instantaneous displacement. Subsequent comparisons of the winds with other methods confirm the validity of the point source effect.

2.5.2 The Effect of the Geomagnetic Field

The drifts experiment detects motion of ionization irregularities, so the degree to which this reflects the motion of the neutral atmosphere should be examined.

In regions of the atmosphere where the neutral density is sufficiently great, collisions between charged and neutral particles will ensure that ionization irregularities move with the neutral particle velocity. The collision frequency exceeds the gyrofrequency up to a height of 140km for ions but only up to about 70 km for electrons (Kent and Wright, 1968). So the possibility of magnetic field effects on the motion must be considered. The work of Clemmow et al. (1955) indicates that due to the creation of a polarization charge, cylindrical irregularities will move with the neutral wind when the ratio of electron collision frequency to gyrofrequency exceeds 10^{-2}, or below about 80 km. For isotropic irregularities this height should be extended to well above the E region (Tsedelina 1965). Villars and Feshbach (1963) concluded that the magnetic field will not affect turbulence induced irregularities below 100 km and have little effect up to 120 km. It seems likely then that the ionization irregularities detected by the drifts experiment in the D- and E-regions will in fact move with the neutral wind. Stubbs (1977) did however find a tendency for the characteristic ellipse describing the spatial behaviour of the ground diffraction pattern to be aligned towards the direction of the geomagnetic field above 100 km.

2.5.3 The Wave Interpretation of Ionospheric Drifts

Hines (1960, 1972) challenged the interpretation of ionospheric drifts as a measure of the neutral wind. He argued that internal gravity waves may impose undulatory

ionization irregularities upon an undisturbed ionosphere. In this situation the irregularity motion determined at the ground would be that of the horizontal trace velocity of the wave, not of the ambient wind. The argument was primarily intended for regions where there are no preexistent ionization irregularities, that is, above the turbopause in the upper E-region.

In the D-region, scattering irregularities are thought to exist due to turbulence. Conventional scattering theory indicates that the drifts experiment would be most sensitive to irregularities with scale sizes of about half the probing radio wavelength or about 60-70 m. However, Hines (1960, 1975) also suggested that even in the lower D-region these irregularities could be the result of the imposition of phase variations of gravity waves with horizontal wavelengths less than a few hundred metres. To avoid viscous quenching, these gravity waves would have to propagate at an angle from the vertical and the reflected radio waves were need to come from off-vertical angles of $> 5^{o}$ at 60 km and $> 15^{o}$ at 70 km. Fortunately, if this is indeed the case, the measured winds would not be in error since the intrinsic period of these waves would have to exceed 5 minutes resulting in a motion which would only differ by about 1 ms^{-1} from the background wind (Hines, 1975).

It may not be necessary to involve such a mechanism since VHF radar studies, which are most sensitive to irregularities with sizes of the order of metres, have reported horizontally stratified structures in the lower

D-region similar to those found by MF partial reflections (e.g. Cunnold, 1975). These results suggest that irregularities are present on a vast range of scales - certainly smaller than could be imposed directly by gravity waves. In addition, the eddy diffusion coefficients observed in the turbulent layers are likely to quench the small scale waves which Hines' hypothesis requires. Hocking (1979) has studied the angular spectrum of D-region reflections and found that echoes from below 80 km probably come from within $2\text{-}3^{o}$ of the vertical. This contradicts Hines' prediction of off-vertical reflections from small-scale, gravity wave induced irregularities in the lower D-region. It therefore appears more likely that radio wave scattering in the lower D-region is from turbulence induced irregularities blown along in the background wind.

This is not to say that gravity waves are unimportant; they may well be the source of the turbulence. The thermodecline of the mesosphere is especially unstable to wind shears such as produced by short vertical wavelength gravity waves. Also Hodges (1967) has shown that excessive temperature perturbations in the wave can produce instability resulting in thin layers of turbulence which propagate with the wave. However most D-region ionospheric layers remain fairly constant in height. Theoretical studies (Geller et al., 1975) also show that Kelvin-Helmholtz instabilities produced in the vicinity of critical layers may decay into thin turbulent layers. In any event the dissipation of gravity waves by eddy viscosity will provide the energy for the production of

turbulence. As well, of course, when irregularities are already present due perhaps to turbulence, the perturbation velocity of a gravity wave will be superimposed upon the neutral background wind and as such will be measurable by the drifts experiment.

Observations of the D-region often show evidence for stratified layers (Gregory, 1961) and in the upper D-region, ledges of ionization possibly caused by complex D-region chemistry (Mechtly and Smith, 1968). Hines (1975) suggested that gravity waves could impose undulations on these existing ledges of ionization and again result in the drifts experiment measuring the wave horizontal trace velocity. Indeed Fraser and Vincent (1970) have found that reflected signals sometimes have coherent phase variations such as could be produced by a small number of specular reflections from an undulating reflector. The wavelength and periodicity of such a moving screen were found to be 10 km and 10 minutes in keeping with a gravity wave hypothesis. When the deformation of such a screen is increased, further points on the screen are able to provide specular reflections. Slack (1946) has shown that as few as 5 specular points (which are able to overlap within the receiver) can produce a diffraction pattern that is essentially indistinguishable from a random scattering model. The important difference would be that in the former case the derived drift velocity is related to that of the wave phase velocity, rather than the neutral wind.

Alternatively, it can be argued that the coherent phase changes were due to the passage of a single cloud of ionization

(Fraser and Vincent, 1970) carried along by the ambient wind. The presence of a small number of specular points would produce the same coherent phase changes as the wave induced irregularity, but now the drift velocity would be that of the neutral wind. The limited lifetime and lack of periodicity of most of Fraser and Vincent's echoes is not inconsistent with this.

In view of the good agreement which is often found between drift results and independent measurements (Section 2.6), in order to preserve a wave-induced irregularity model Hines (1968) suggested possible mechanisms whereby the irregularities would in fact move with the neutral wind. A gravity wave approaching a critical layer (where the background wind velocity matches the wave phase speed) would produce an enhanced ionization disturbance which would receive observational emphasis in the drifts experiment. The very fact that the wave is approaching a critical layer ensures that it will be moving at the background wind velocity. Another occasion for agreement would be when a broad spectrum of waves with no preferred direction of propagation is present, contributing only to an increase in the random component of the background wind in the long term. However, the middle atmosphere is expected to impose directional filtering on the wave spectrum originating in the troposphere (Hines and Reddy, 1967).

2.6 COMPARISONS WITH OTHER METHODS

Questions concerning the ability of the partial reflection drifts method to measure neutral wind motion can only be put at rest by direct comparison with other techniques. The presence of short temporal and spatial scale variations in the atmosphere requires that the measurements to be compared be carried out closely spaced in time and position.

A comparison of D-region partial reflection drifts measured over 6 hours near noon with meteor winds made by Rossiter (1971) showed significant discrepancies. However, a more detailed study by Stubbs (1973) and Stubbs and Vincent (1973) showed excellent agreement. On occasions though, short-term differences were observed, with the meteor wind values showing the most variability. Considering the fact that successive meteor echoes may have separations of the same order as gravity wave scales, a certain amount of discrepancy is not unexpected. Ionospheric drifts using total reflections from the E-region have also been compared with meteor radar winds by Felgate et al. (1975) and Wright et al. (1976). In both cases good agreement was obtained most of the time. A more direct comparison with the neutral wind was made by Vincent et al. (1977). They compared drift measurements in the 60-90 km region with wind measurements made from observations of falling spheres and dropsondes ejected from rockets. The spatial and temporal overlap of the measurements was better than previous comparisons and again excellent agreement was obtained.

The works above provide rather convincing evidence that the partial reflection drift experiment does in fact

measure the neutral wind. In veiw of the controversy that has surrounded the experiment in the past, however, opportunities to make further comparisons with other methods should be utilized. During the first ten days of October, 1977, a joint experiment was conducted with the meteor radar facility near Christchurch. The meteor radar equipment is described in detail by Baggaley and Poulter (1978). The meteor radar zonal and meridional wind components were determined separately by observing alternatively west and south for one hour intervals. Only the first day of the meteor data has as yet been analyzed and without height information. Since meteor echoes from all heights were combined, the partial reflection data from 80 to 100 km were similarly averaged.

The results from the two methods are compared in Fig. 2.6, with the error bars representing the standard error of the means. The daytime winds compare well. The smaller scatter and smaller error bars on the meteor wind results reflects the large number of individual wind evaluations from this method. The partial reflection data was degraded substantially at night by interference. There may be some difference between the two methods in the mean height of the compared data, with the Gaussian-like meteor distribution peaking near 95 km while drifts values have a more even distribution over the height interval. The observing regions are also separated by approximately 260 km. Both of these factors may introduce some scatter between the results. Nevertheless the limited amount of data available confirms previous findings that wind measurements by the meteor radar and partial reflection methods are in agreement. A more detailed analysis of these data is planned.

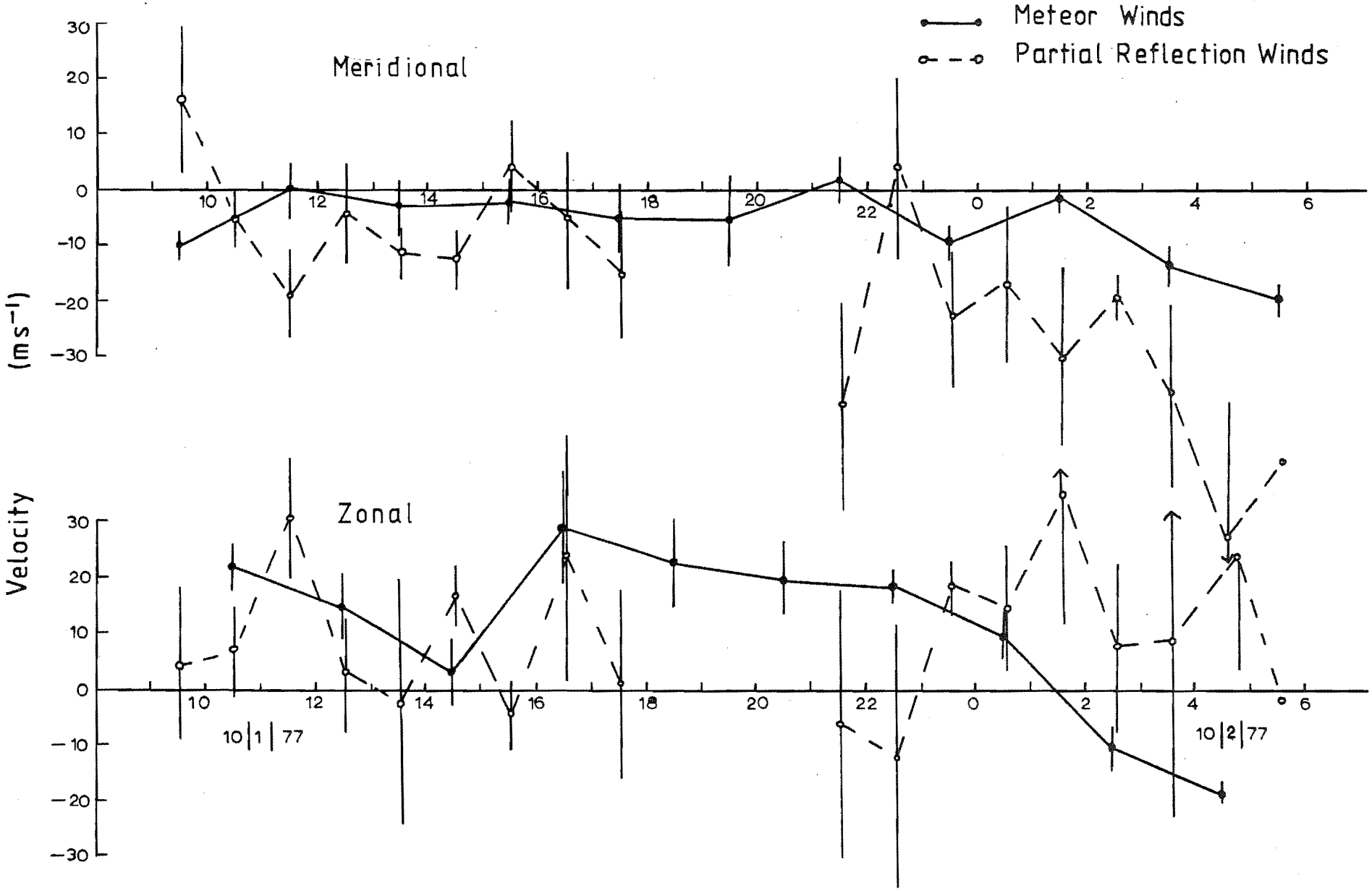

Figure 2.6: Comparison of meteor radar and partial reflection wind measurements.

CHAPTER 3

EXPERIMENTAL DETAILS

3.1 INTRODUCTION

This chapter gives a brief description of the transmitting and receiving equipment, and the development of a real-time partial reflection drifts analysis system.

The data were recorded at the Physics Department field station at Birdlings Flat at latitude $43^{\circ}50'S$, longitude $172^{\circ}40'E$, geomagnetic latitude $47^{\circ}S$, and magnetic shell number 2.6. Measurement of weak D-region partial reflections requires sensitive reception equipment and a low-noise site. Birdlings Flat is some 50 km from Christchurch city and separated from it by hills, and so suffers little interference from this source. However, being situated on the coast, local trawlers are a serious source of interference.

3.2 TRANSMITTING EQUIPMENT

The transmitter operates on a fequency of 2.40 MHz (λ = 125 m) and has a peak power of up to 100 kW. A pulse width of 30 μ sec was used. This, together with the pulse repetition frequency and various switching functions was controlled remotely by the on-line minicomputer.

The transmitting array used is a broadband array (for use with a swept-frequency radar) which consists of four rows of two colinear three-wave dipoles (Fig. 3.1). The

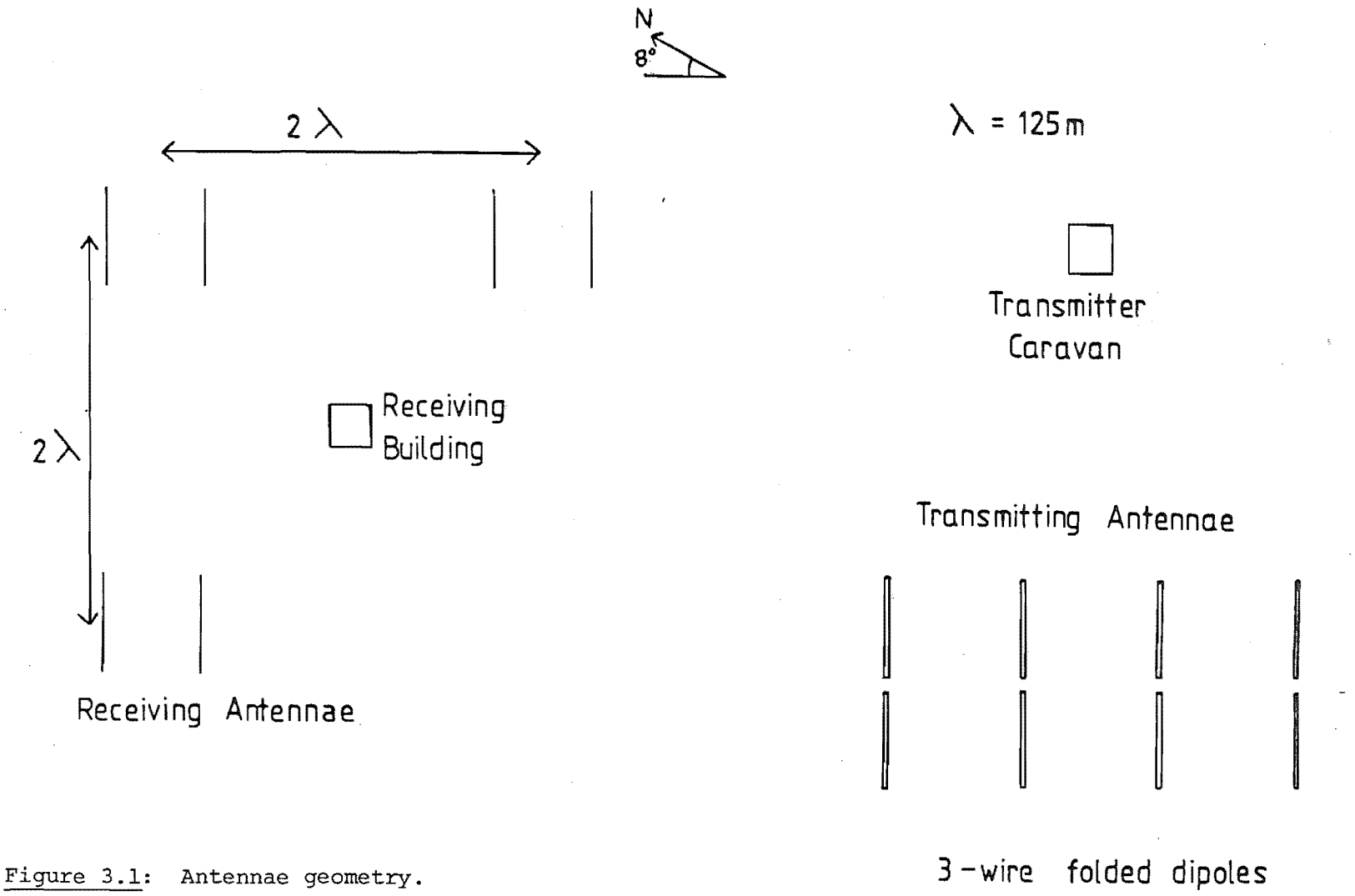

Figure 3.1: Antennae geometry.

calculated main lobe width is 19°, slightly narrower than the narrowband array which it replaced.

The 30 μ sec pulse width corresponds to a range resolution of 4.5 km. A shorter pulse width would give improved height resolution, but this advantage would be offset by the increased noise and interference accepted by the wider receiver bandwidth which would be required. A further contribution to the uncertainty in vertical resolution is the presence of oblique echoes which, although having the same range as a vertical reflection, will originate from a different height. This effect should not be severe below about 80 km, where Vincent and Belrose (1978) and Hocking (1979) have shown that the anisotropic nature of the irregularities limits the reflections to within a few degrees of the vertical. The transmitting antenna beamwidth will also impose attenuation on oblique echoes. The partial reflections were sampled at 2.5 km height intervals by the analogue-to-digital (A/D) converters. The same echo can therefore be measured in two adjacent height samples. When short period and short vertical scale effects are being studied, such as caused by internal gravity waves, care must be taken to ensure that the measured wind changes are not in fact due to changes in the height of echoes (Manson et al., 1973). In the present work, attention is turned to longer period oscillations. If the echoes are uniformly distributed within the sampling regions on average, the long term winds should give accurate height profiles.

All measured heights refer to the virtual height, but Fraser and Kochanski (1970) showed that the pulse retardation was less than 1 km below an altitude of 100 km.

3.3 RECEIVING EQUIPMENT

The receiving arrays each consist of two broadside, parallel in-phase dipoles. (The aerials were built with tuned-traps for use in a dual frequency experiment. These traps were physically shorted out for the winds experiment.) The centre of each array is connected by 600 ohm open-wire transmission line to the receiver building. Three arrays forming a right-angles isoceles triangle with sides of 250 m (2 λ) were used for the drifts measurements (Fig. 3.1).

Golley and Rossiter (1970) showed that when an aerial separation small compared to the diffraction pattern size is used, the 'true velocity' will systematically underestimate the actual velocity. The present aerial spacing of 250 m should give little bias for E-region measurements where Golley and Rossiter recommended a spacing of 300 m. The D-region pattern scales are much smaller and consequently the measured winds should be hardly affected by the 'triangle size effect' on the basis of the results of Golley and Rossiter (1971). For the same reason any bias in D-region results introduced by the use of a right-angled triangle should be small. In fact a smaller antenna spacing than that used here would have the advantage of giving a greater number of records with cross-correlations at a significant level (Golley and Rossiter, 1971). Meek (1978) found a major increase in data yield when a triangle with sides of 1.2 λ was used, compared with 2λ.

Three solid state receivers were used with a bandwidth at the 3dB level of 60 kHz. The minimum detectable signal

was 1μV. The receivers had two outputs: a linear output of 66 dB dynamic range and a logarithmic output of 70 dB dynamic range. The latter was preferred in dealing with the large dynamic range of the D-region partial reflections.

3.4 COMPUTER HARDWARE

In 1973 a DEC PDP-8/E minicomputer with 8 K of core storage was installed at Birdlings Flat. This machine has a 12 bit word size and a memory access cycle time of 1.2 μ sec. Data is input to the computer through track and hold circuits and three 10-bit analogue to digital (A/D) converters which sample at 2.5 km height intervals. The principal data storage medium is a 7-track, buffered magnetic tape unit, with papertape available as a backup medium. Both the A/D converters and the magnetic tape transfer data via the data break system. A software accessible millisecond clock, derived from the 9.6 MHz master oscillator, controls the timing of transmitter pulses. The other important item of hardware is the station control register (SCR) which gives software control of equipment by latching a 6-bit command onto various addressable rack-mounted modules. A block diagram of the complete system is shown in Fig. 3.2.

Initially the minicomputer was used as a flexible data collecting system, controlling the timing and the transfer of the digitized data to magnetic tape for subsequent analysis on the larger computer on campus. Attenuation of input signals was controlled manually.

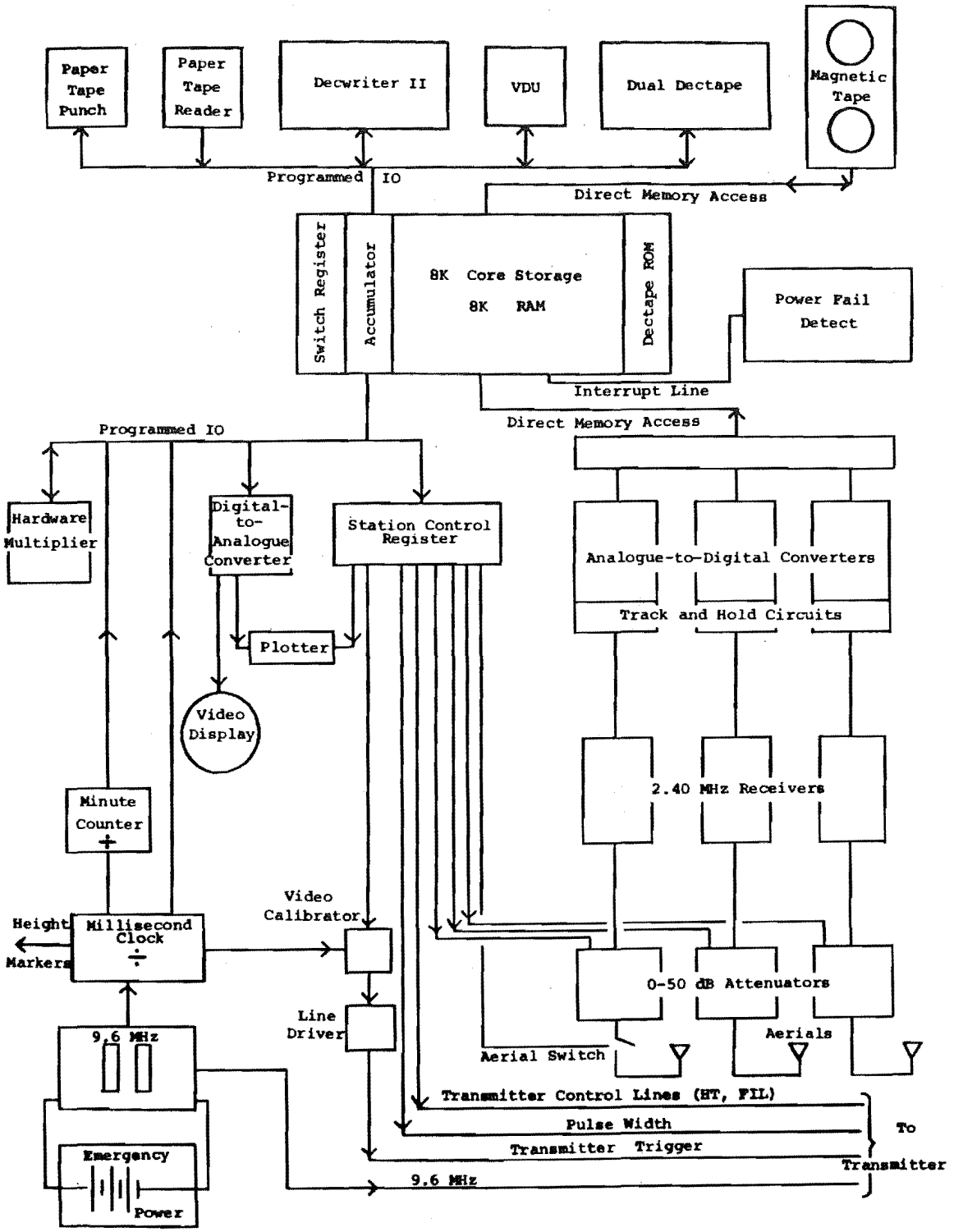

Figure 3.2: Real-time winds system hardware based upon a PDP-8/E minicomputer.

Although this system was adequate for short (< 1 day) data collection runs, it soon became apparent that both the volume of data collected and the cost of analysis would prohibit extended data runs needed to study tides and planetary scale waves. A viable alternative was sought in a real-time processing system.

3.5 REAL-TIME DATA PROCESSING

An on-line drifts system with immediate data processing must satisfy certain requirements.

(1) It must be fast enought to yield a density of data suitable for analysis on the time scales of interest.

(2) It should monitor and optimize the input signal levels.

(3) It must be able to run the experiment without operator intervention. For example, data below 80 km need not be analysed at night because of the absence of partial reflections.

The numerical calculations involved in the 'full correlation analysis' determination of velocities and characteristic ellipse parameters are most easily carried out in a high level language. For this, an Algol-60 system, "Rogalgol", (developed by Dr R.H. Abbott) was found to be both fast and economical in memory usage. This particular dialect of Algol is typically three times as fast as the comparable DEC OS/8 Fortran IV system, although occupying

only about a third of the memory space. In real terms the storage comparison is even more favourable because of the availability of dynamic arrays in Algol. Other attractive features are the flexible input/output routines and the ability to converse easily with machine language.

The largest proportion of processing time in the drifts analysis is involved with calculating the correlation functions. There are several approaches to speeding up this calculation.

The simplest approach is that used by Fraser (1965) who used tetrachoric correlations (the polarity coincidence method) where only the sign of the signal about its mean is used. If the probability distribution of the data is known there is no loss of information in this method, although for a given variance the integration time should be increased by a factor of 2.46. A similar method but with a smaller variance of the correlation, is to clip only one of the components of the product. The correlation calculation reduces to a series of additions and subtractions rather than multiplications, which on the PDP-8 can be done fairly quickly in triple precision arithmetic. The multibit by one-bit correlation between series x and y, r_B, is related to the normalized multibit by multibit correlation, $\rho_{xy}(\tau)$, by

$$r_B(\tau) = \left(\frac{2}{\pi}\right)^{\frac{1}{2}} \frac{\rho_{xy}(\tau)}{\sigma_{xx}}$$

where σ_{xx}^2 is the variance in the series x and τ is the time lag between the series (Hagen and Farley, 1973). Note

that the power in each signal also has to be calculated.

A problem that arises with both of these methods is that to subtract the mean either the whole series needs to have been recorded or assumptions must be made about the stationarity of the mean over very short time intervals.

Memory availability often dictates that the correlations be accumulated as the data is acquired. Otnes and Enochson (1972, p231) show how this can be done using storage of only three times the maximum lag.

An evaluation trial was carried out using only 8K of memory but requiring considerable intermediate storage of data on magnetic tape and the smaller program storage Dectapes. Drift velocities were obtained from eight heights every 20-25 minutes. This prototype system established the practicability of using a small minicomputer for calculating real-time drifts and delineated the major areas requiring improvement. Increased speed and less dependence on intermediate storage were clearly required.

The addition of 8K of semiconductor memory enabled the entire program (including a full correlation analysis) as well as eight heights of data to be held concurrently in memory, as shown in Fig. 3.3. An important contribution to this software from Dr G.J. Fraser is gratefully acknowledged. The limitation to eight heights (20 km) at a time was not found to be serious, since echoes from a greater height range would undoubtedly exceed the dynamic range of the equipment. A structure diagram of the drifts program is found in Fig. 3.4. At the initialization stage

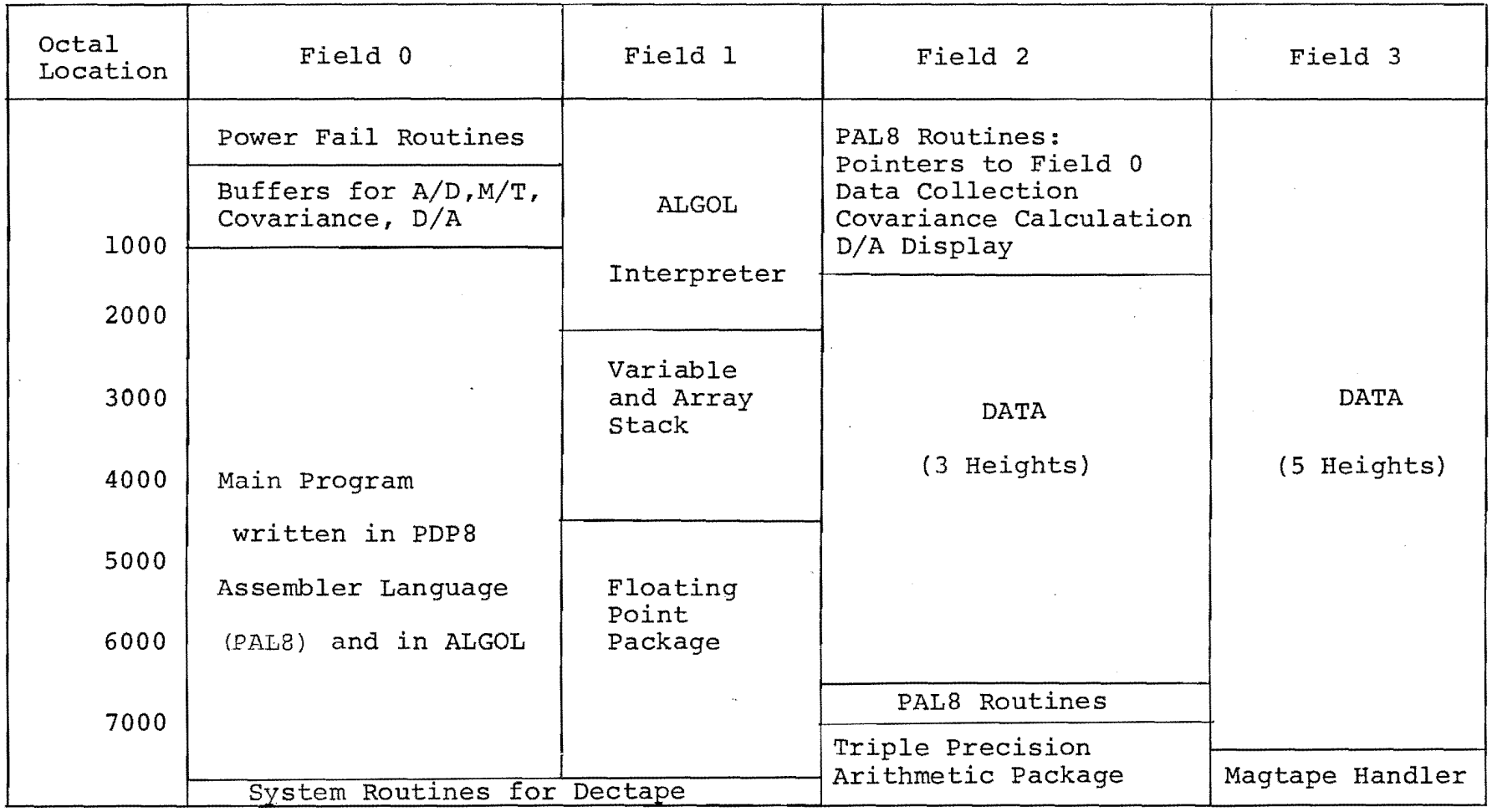

Figure 3.3: Memory Map for PDP8 Drifts Program using 16K Memory.

(A Field is a 4K division of PDP8 memory which can be addressed with a single 12-bit word.)

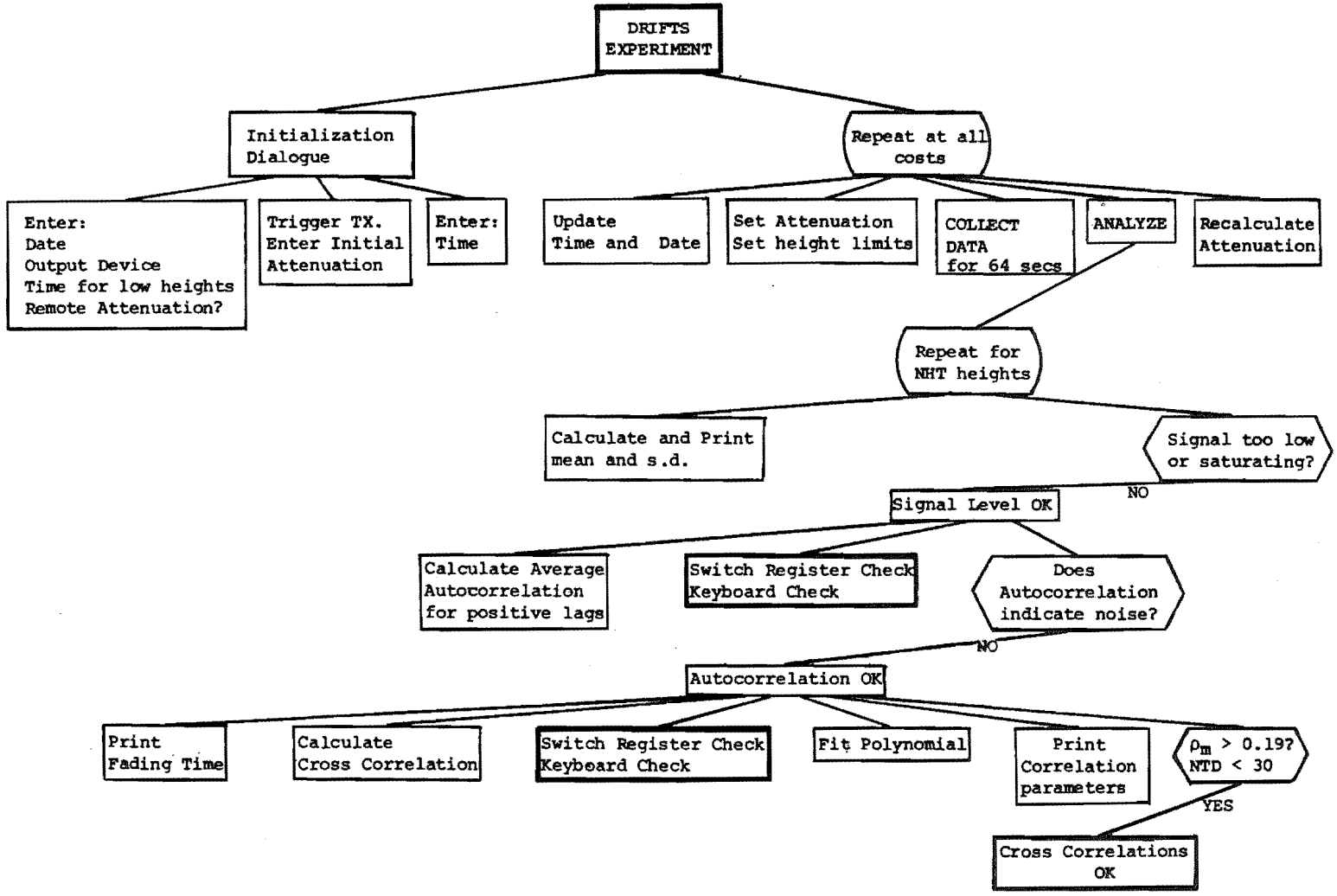

Figure 3.4: (Part 1) Structure diagram of the real-time drifts program.

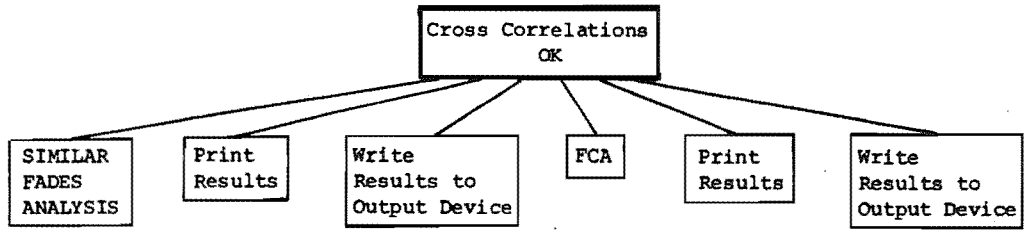

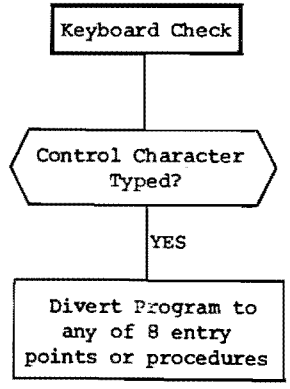

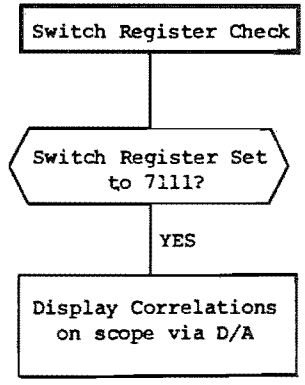

Figure 3.4. (Part 2)

parameters including the date, time and output device (7-track magnetic tape, papertape or Dectape) are entered. Two other parameters entered are the daylight times between which data is to be recorded between 65 and 80 km (in addition to the usual 80 to 102.5 km range). Other operating parameters such as the number of heights, the maximum number of correlation lags, pulse repetition frequency and height ranges could be changed at this point. Data from eight heights are collected for 256 pulses 0.25 seconds apart, that is, for 64 seconds. This comprises one 'scan'.

To cover the dynamic range of the D-region echoes, the height interval 65-102.5 km was usually covered in three scans, each with a different value of attenuation in front of the receivers. The attenuators were designed to be controlled either manually, or programmatically via the Station Control Register, with a range of 0-50 dB in 5 dB steps (Appendix B). The optimum value of attenuation for each scan was determined on the basis of the mean amplitude on the previous scan of these heights.

At different stages during the analysis the data at a certain height was checked to ensure that it satisfied certain criteria, such as minimum signal to noise levels, in order to minimize the time spent processing data which was of no use. These criteria are detailed in Chapter 4.

Since the entire data series are held in memory with the new system, the mean value can easily be evaluated and subtracted, thus avoiding the problems associated with subtracting local means from small blocks of data when

correlations are accumulated. Initially multibit by one-bit correlations were used. However a further development was a hardware multiplier built in the Physics Department Electronics Workshop. It could perform an unsigned multiplication in only a few machine cycles, enabling full multibit by multibit correlations to be calculated at a speed only slightly slower than the multibit by one-bit correlations. Having calculated the average autocorrelation and the cross-correlation functions, a least squares fit was made near the peaks of a fourth order polynomial and τ_m and τ' found. Cross-correlations at zero lag were first interpolated across in case of a noise spike at that position.

The apparent velocity was calculated by the least squares method of Equation 2.2. Then, if the data quality was satisfactory, full correlation analysis as extended by Phillips and Spencer (1955) was used to evaluate the 'true velocity' and the diffraction pattern parameters. These were written to the output device together with the date, time and height. The drifts system, in its final form, calculated the winds from eight heights in three to five minutes, depending on data quality, enabling the full height range of 65 to 102.5 km to be covered in approximately ten to fifteen minutes.

An important aspect of maintaining unbroken, lengthy data collection runs is the need for hardware backup. Spare receivers were always maintained. Also the output from the analysis could be directed to papertape in the event of magnetic tape failure (which occurred for several extended

periods). On the rare occasions that both the magnetic tape unit and the papertape punch were simultaneously out of operation, Dectapes were used as temporary storage until transfer to magnetic tape or papertape could be made. Also, since a Dectape could hold up to 3 days of results, it could be used over the weekend period when magnetic tape was unavailable.

Power failures are a frequent problem at Birdlings Flat (especially in the duck season). Even a short voltage drop results in the loss of the drifts program from semiconductor RAM and the magnetic tape being switched irrevocably off-line. To overcome this problem, use was made of hardware which detected the falling mains voltage and caused a hardware interrupt. A routine then had 1 msec to save necessary information, such as date and time, in non-volatile core memory and set up registers to enable a bootstrap to a recovery program on Dectape when the power came back on. A battery kept a minute counter going during the power failure, so that the time and date could later be updated. The recovery program directed subsequent output of drifts parameters to the paper tape punch (the magnetic tape being off-line) and altered the pulse repetition frequency slightly. The PRF change could be heard in Christchurch, acting as a warning that a failure had occurred and that there was only up to 30 hours of papertape operation left. If for any unforseen reason the magnetic tape ran out, a similar sequence of events to the power failure was set in motion.

Beyond the obvious (and important) aspect of economy, on-line, almost real-time drifts, afforded other advantages.

After each correlation calculation the program could be directed to display the correlations on an oscilloscope by way of a digital-to-analogue converter. The correlations could also be printed if required. Thus correlations could be observed in real-time and directly related to the behaviour of the ionosphere monitored on an adjacent oscilloscope. The effect of interference, unusual events such as meteor echoes, and the lowest usable echo strength could be studied. Any faults in the equipment - aerials, receivers, A/D converters - became immediately obvious from either the shape of the correlations or the drifts printout, greatly improving fault detection.

CHAPTER 4

CONSISTENCY OF WIND DATA

4.1 DATA EDITING

Data editing is necessary at different stages in the data collection and analysis in order to remove poor quality data. The criteria upon which data is rejected must be optimised to produce good quality data which satisfies the assumptions of full correlation analysis (e.g. NTD ~ 0), yet not be so stringent that the data yeild is too low to be of sufficient statistical significance in subsequent analysis.

A coarse selection of data is made during the on-line drifts program before the results are written to magnetic tape. The data must satisfy the following conditions:

(i) The receiver output should not be too low nor saturating too often.

(ii) The autocorrelation should fall to 0.5 and the cross-correlations should reach their maximum values within the maximum lag used (i.e. 8 sec).

(iii) The average autocorrelation should not have fallen below 0.32 by a lag of 0.25 sec. Faster fading than this is assumed to be noise.

(iv) The maximum of each cross-correlation must be greater than 0.19.

(v) The normalised time discrepancy (NTD) must be less than 0.3.

This coarsely selected data is then analysed on the larger computer on campus - a Burroughs B6700 - where more stringent quality control is imposed. Based on studies of velocity-height profile consistency, on the reliability of individual drift records and on studies by other experimentors (Meek et al., 1979; R.A. Vincent, private communication), the data was accepted if it satisfied the following criteria:

(1) The fading time (the time for the autocorrelation to fall to 0.5) must be greater than 0.5 sec. This is to exclude interference, especially at night.

(2) $V_a < 175$ m/s and $V' < 250$ m/s.
Observations made with the real-time drifts system indicated that apparent velocities faster than this in the D-region invariably occurred when interference was present (due to a radioteletype station or lightning). Some of the data was contaminated by regularly timed marine broadcasts. This data was characterized by a large shift of the signal mean level due to the strong carrier, and identical velocities at heights. Where obvious, this data was removed manually. Sometimes E-region records with very slow fading rates and high cross-correlations with small time lags were observed. These records have the characteristics expected of a shallow specularly reflecting screen. On the basis of data rejection for $V_a < 175$ m/s, some of these records may have been rejected, but as discussed in Section 2.5.3, these velocities may well be the horizontal trace velocities of a perturbing gravity wave.

(3) NTD > 0.2.

The NTD gives an indication of the internal consistency of the data.

(4) $V_a/V < 3.0$ and $|\phi_a - \phi| < 90^o$.

In cases of very large time changes or extreme elongation of the diffraction pattern, the correction made by full correlation analysis must be regarded as suspect (e.g. Manson and Meek, 1977).

(5) $V_c^2 < 0$, unless $-|V_c| > -30$ and $\frac{|V_c|^2}{V'^2} < .25$.

This last criterion requires further comment. Strictly speaking when V_c^2 is negative the analysis breaks down and the data should be rejected. However, Fraser and Vincent (1970) have noted that merely statistical fluctuations in V_c' and V may cause negative V_c^2, since

$$V_c^2 = V_c'^2 - V^2 = V_c'^2 \left(1 - \frac{V_c'^2}{V'^2}\right) \qquad (4.1)$$

The situation is most likely to occur when the random changes are small so that V_c' and V' (and hence V) are of similar magnitude. In such cases V' is likely to be a good estimate of the true velocity. Vincent (private communication) has suggested that V' then be used instead of V.

The importance of the correction for random changes in the pattern can be judged from the ratio $\frac{V_c^2}{V^2}$. Rearranging equation (2.9) in the direction of drift,

$$VV' = V_c^2 + V^2$$

$$V' = \frac{V_c}{V} + V$$

$$\frac{V'-V}{V} = \frac{V_c^2}{V^2}$$

Thus $\frac{V_c^2}{V^2}$ is the correction to V' as a fraction of V and so indicates the importance of random changes. Although strictly applicable only to cases with $V_c^2 > 0$, the ratio $\frac{|V_c|^2}{V^2}$ has been used here to distinguish cases with relatively small random changes.

The situation is clearly illustrated in the graphical example of Fig. 4.1. The V_c' ellipse is shown intersected by a solid line AB. The perpendicular from AB to the origin is the apparent velocity V_a and $(V_c')_V$ is given by the line from the origin to the point of contact of the tangent to the ellipse parallel to AB. V', the apparent velocity corrected for anisotropy, is the length of this line to its intersection with AB. Clearly when the line AB intersects the ellipse, V_c' is greater than V' and from (4.1) V_c^2 will be negative. In this example $\frac{|V_c|^2}{V^2} = .09$, indicating that the time changes in the pattern are small. On the basis of other criteria the example illustrated is of good quality (e.g. NTD = .14). Therefore the use of V' instead of V in such cases, as suggested by Vincent, will be a useful and meaningful contribution to the data acquisition rate.

Variations in the rejection criteria have been studied for the effect on the consistency of height-velocity profiles and their standard errors of the mean. The standard error of

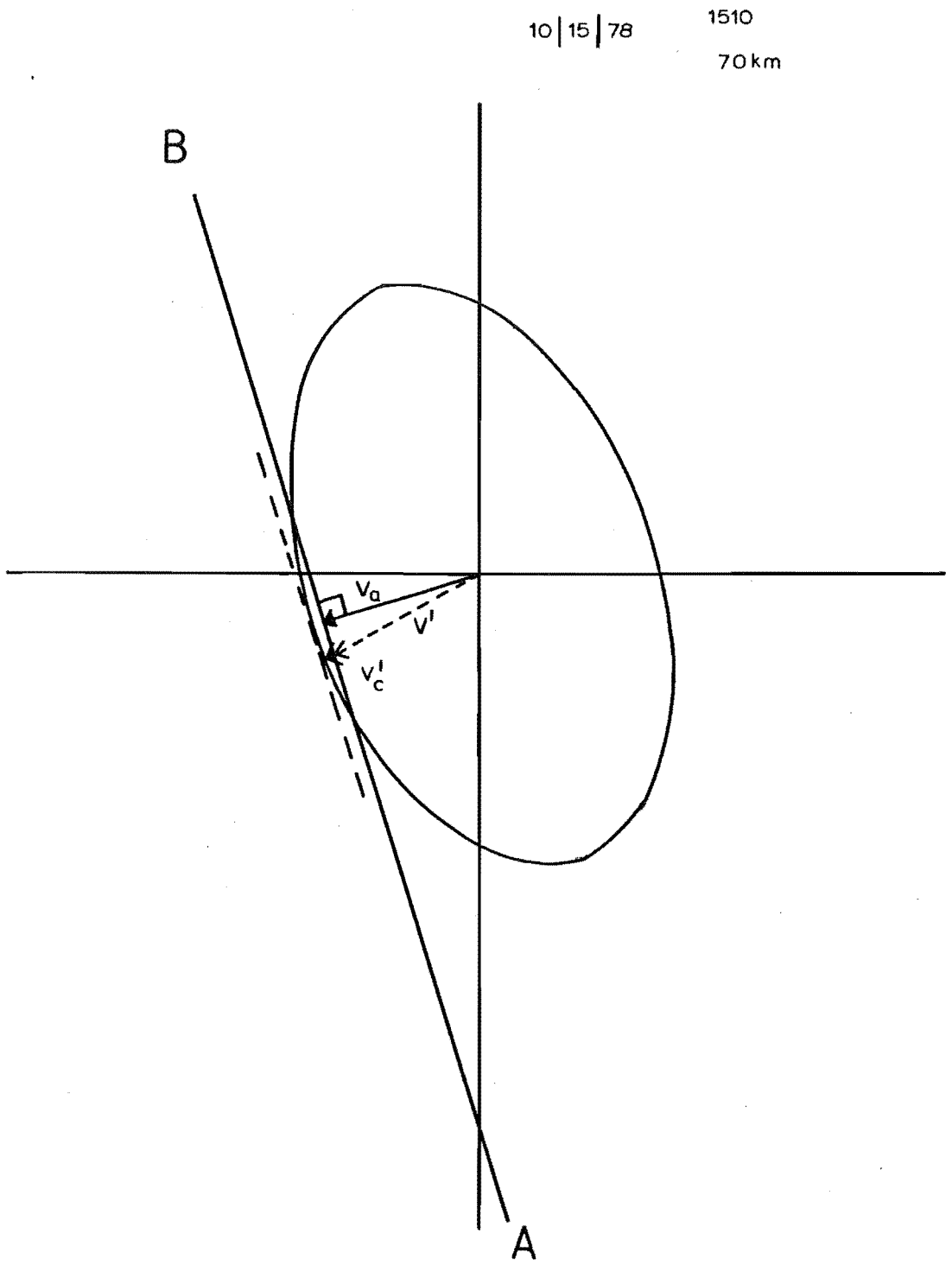

Figure 4.1: The characteristic ellipse with $V_c^2 < 0$.

of the mean (s.e.) is related to the sample standard deviation (s.d.) by s.e. = s.d./$\sqrt{N-1}$ where N is the number of points in the sample. Sample profiles of 3h wind averages were taken from a data set with 6,040 drifts records taken over a period of 9 days. A typical profile is shown in Fig. 4.2. The error bars in the figure are the s.e. and the numbers down the right hand side indicate the number of individual velocities contributing to the average at that height. The s.e. will reflect the effect of gravity wave activity over the sampling interval of 3h as well as the uncertainties in the velocity estimates. The rejection criteria must aim to minimize the latter contribution by rejecting poor quality data.

When data with $V_c^2 < 0$ were completely rejected the profiles were only changed slightly, typically less than 6 ms^{-1}, yet the s.e. were nearly always degraded, reflecting the lower data rate which was reduced by 6%. This result gives support to the use of data with $V_c^2 < 0$ when the random contribution is small. More stringent control over the degree of anisotropy acceptable was exercised by only using data with $|\phi_a - \phi| < 45^o$. This gave a significant (19%) reduction in data yeild. Even for the worst sample studied, with 50% data reduction, no significant change in the velocity profile was made but the s.e. was improved for only 2 of the 10 heights. The use of this criterion clearly rejected a lot of useful and reliable data. Among the other variants tried, was the use of poorer quality data with NTD up to 0.3, but the increased data yield (of 4%)

served to increase the scatter rather than improve the statistics.

It is concluded that the data rejection criteria described previously are the optimum in terms of data quality versus data yeild at this location.

4.2 THE USE OF APPARENT VELOCITIES

There are often practical advantages in using the apparent velocity rather than 'true velocity'. The apparent velocity requires less numerical computation (a factor of significance in real-time drifts) and since the last 2 data acceptance criteria ((4) and (5)) apply only to the calculation of the 'true velocity', the simpler and less stringent conditions give a higher yield of data. The disadvantage is that the velocities may be inaccurate due to diffraction pattern anisotropy and random changes. The apparent velocity has been widely used at Birdlings Flat (Fraser, 1968), and also at Saskatoon, Canada in measurements of noon winds (Manson et al., 1974; Gregory and Manson, 1975a, 1975b; Manson et al., 1978) and for internal gravity wave studies (Manson and Meek, 1976). It is therefore of considerable interest to examine the agreement and statistical range of variations (s.e.) of apparent and 'true' velocities over different time scales.

A study by Meek et al. (1979) indicated that the Saskatoon noon mean profiles of apparent velocity agreed well with those of 'true velocity' below 100 km, but above

this height, the apparent velocity was too large by a factor of about 50%. Their comparison for 3h profiles of Adelaide data showed that the apparent velocity was significantly larger than the 'true velocity' at all heights. They also found that samples of 'true velocity' sampled closely in space and time showed greater consistency than the apparent velocity. Thus the lower yield of the 'true velocity' data is compensated by increased reliability. The greater consistency is expected since the 'true velocity' makes compensation for random changes, and as Manson et al. (1979) note, for this reason the use of the 'true velocity' is especially desirable in gravity wave studies.

Fig. 4.2 shows a 3h mean noon wind profile of the 'true velocity' at Birdlings Flat using the selection criteria of Section 4.1. Also shown are the apparent velocities obtained using the same criteria. For 7 of the 10 heights shown the magnitude of the apparent velocity exceeds that of the 'true velocity', this result being fairly typical. The difference is not as marked as in the Adelaide data, however. Thus the correction made for the overestimation of velocity due to random changes is more important than the correction for the underestimation of velocity magnitude due to anisotropy, particularly for large velocities. For the majority of cases (75%) the s.e. of V_a were larger than those of V. The profiles of apparent velocity produced by using only criteria (1)-(3) above showed close agreement with those using the full criteria. However, despite an improved data yield of 23%, the s.e. were actually increased in the

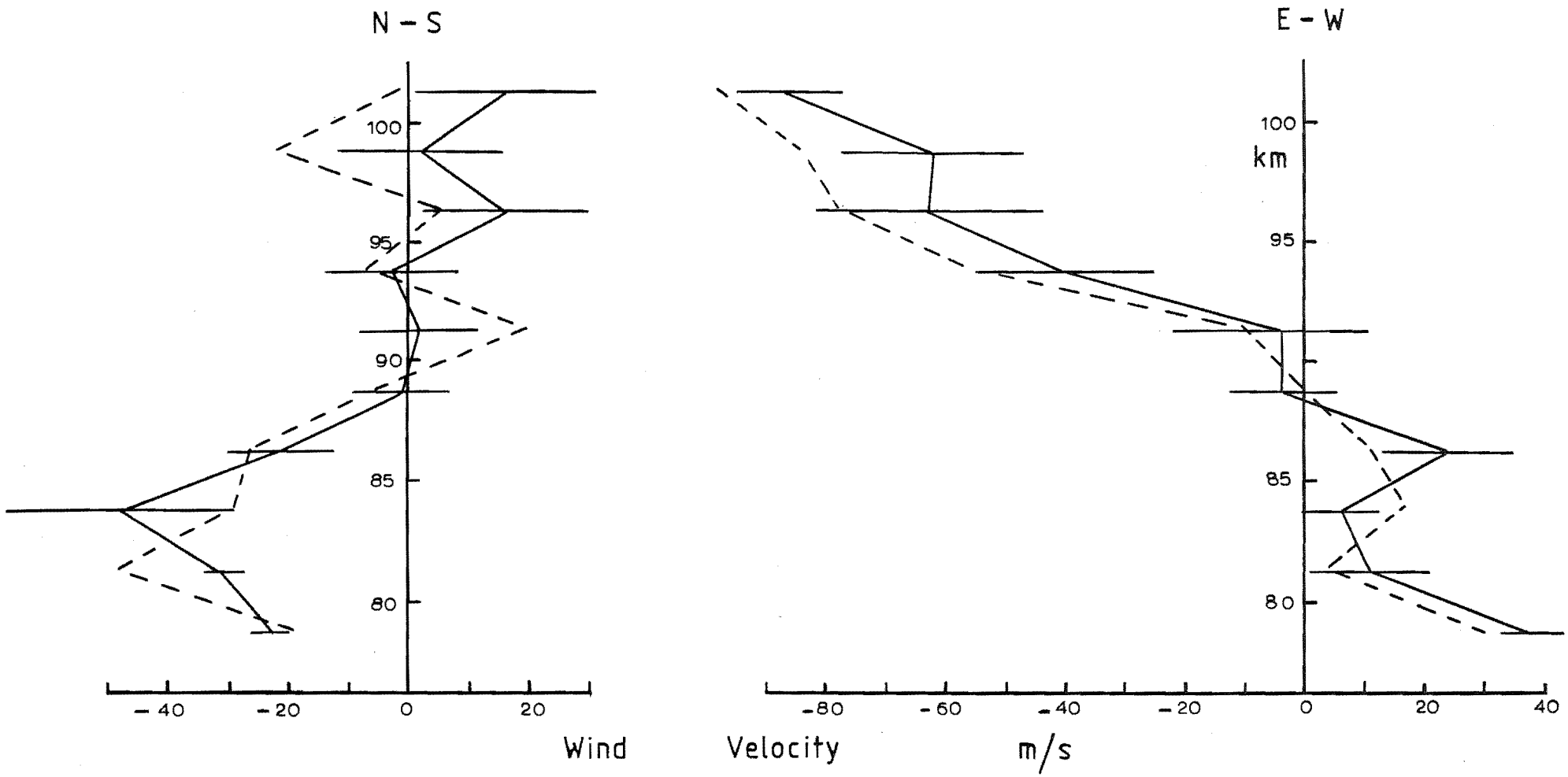

Figure 4.2: Three hour mean wind profiles of V_t (——) and V_a (---).

majority of cases, consistent with the additional data being of poorer quality.

The larger scatter of apparent velocity places limits on the confidence one may have in short term averages. With longer vector averages some of the scatter may be expected to average out. Fig. 4.3 shows the variation of daily averages of apparent and 'true' velocities over a period of 26 days. The agreement between the two estimates is very good. They seldom differ by more than 5 ms^{-1}, with the average of the absolute differences increasing from 2 ms^{-1} at 86 km to about 5 ms^{-1} at 101 km. As expected, the standard deviations of apparent velocities over 24 hours are larger than those of the 'true velocity', but the larger number of contributing velocities results in a slightly smaller s.e. The s.e. of the 'true' velocities increases with height from typical values of 3-5 ms^{-1} at 86 km to 6-8 ms^{-1} at 101 km. This increase is consistent with the presence of gravity wave activity which increases in amplitude with height.

Apparent velocities from Birdlings Flat have been used in tidal analyses (Smith, 1980). A comparison of monthly mean tides using 'true' and apparent velocities is shown in Figs. 4.4a and 4.4b. The agreement of phases is excellent, showing no systematic differences. The only serious disagreement occurred in the centre of the eastward phase of the semi-diurnal tide of Fig. 4.4b, but in this region the phase change with height was rapid and the uncertainties in phase are naturally very high. Accordingly, the s.e. of the phase

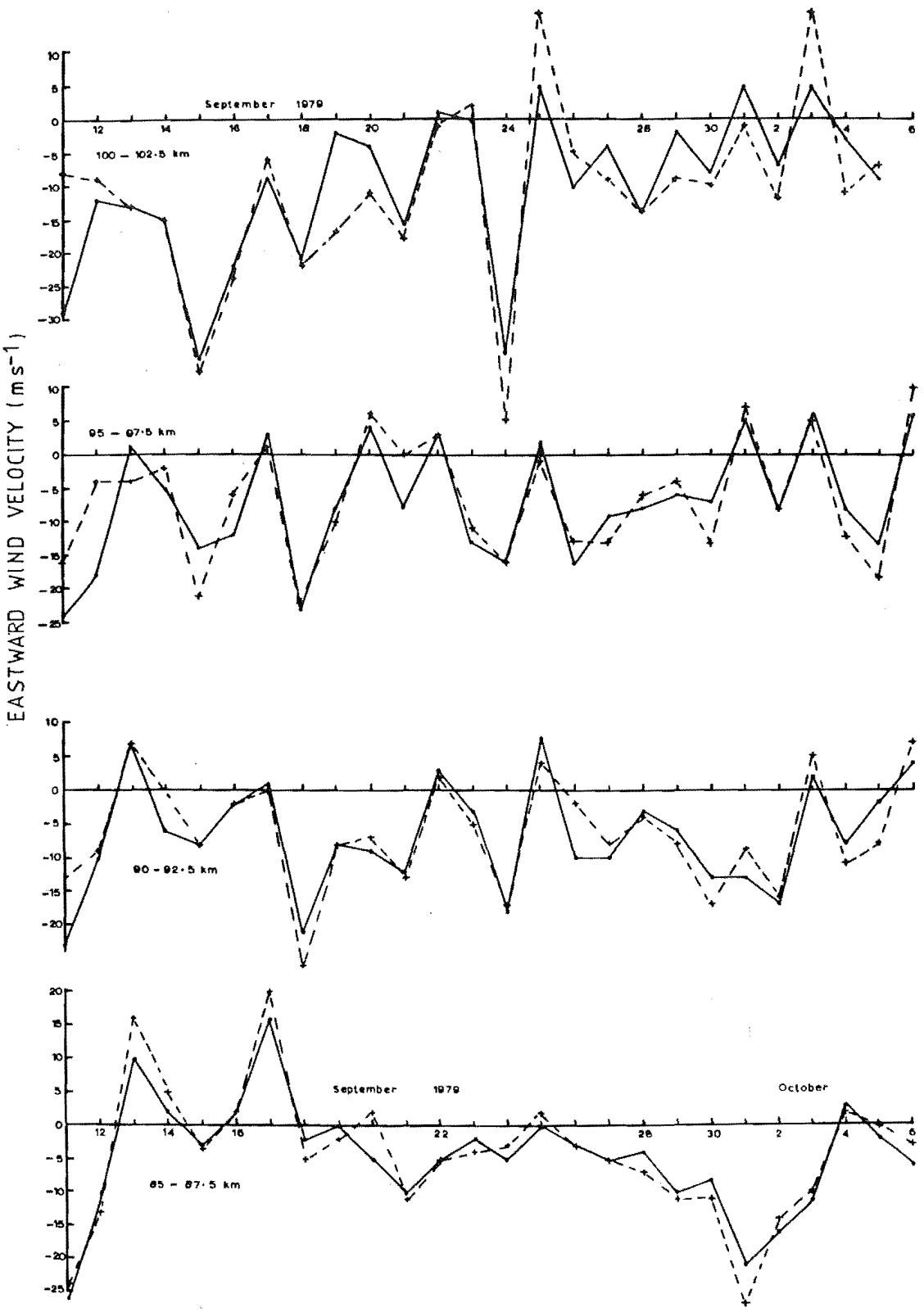

Figure 4.3: Comparison of daily mean apparent and 'true' zonal winds.

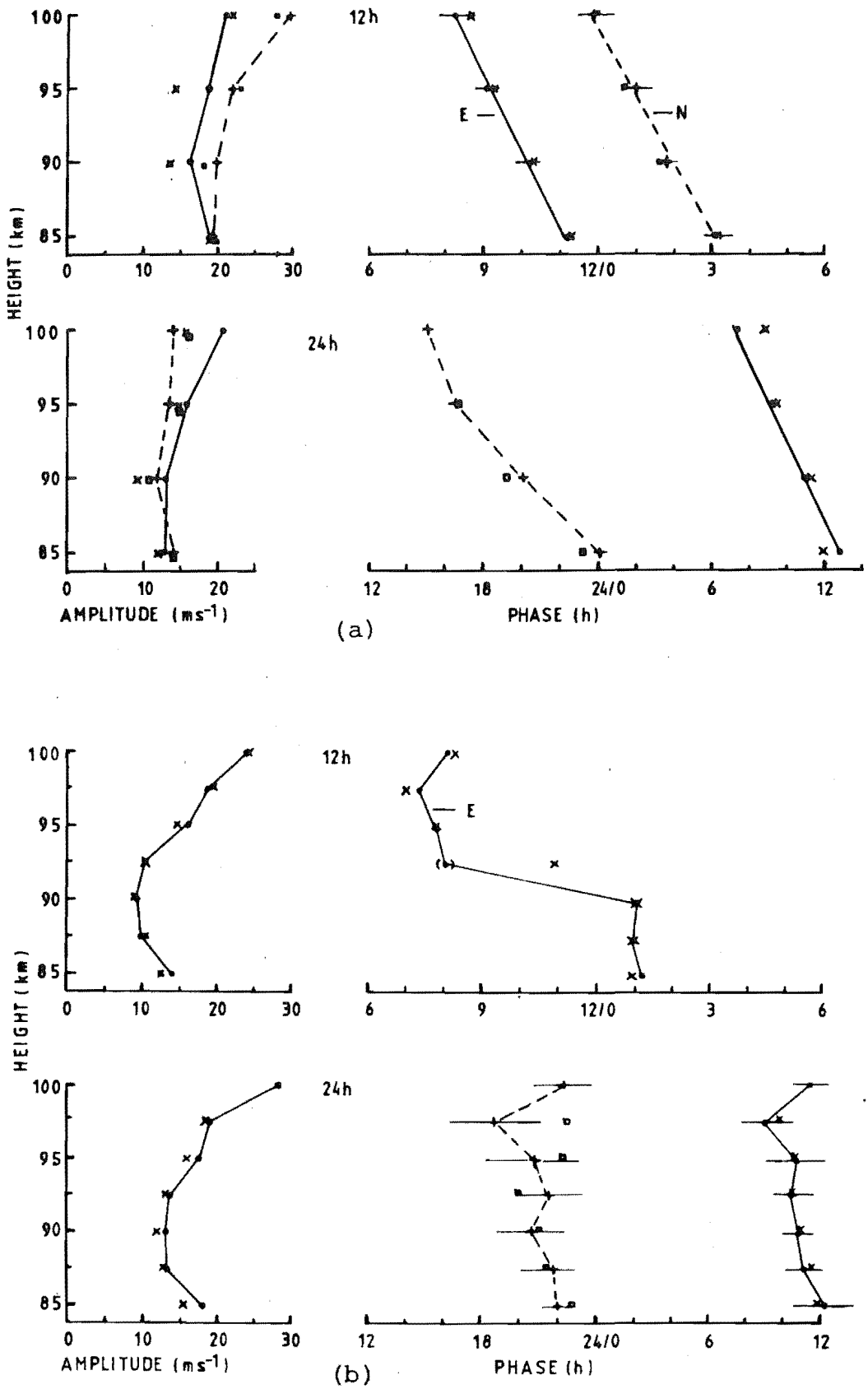

Figure 4.4: Comparison of tides obtained using 'true' (•,+) and apparent (×,□) velocities in (a) April 1979 and (b) September 1979

indicated that these points were unreliable. Differences in amplitude were not severe but the amplitude of the tides obtained using the apparent velocity did tend to be smaller. This may be explained by the greater scatter of the apparent velocities about the tidal periods resulting in smaller amplitudes being fitted to these periods.

In summary, the apparent velocity has greater scatter than the 'true velocity' on short time scales and tends to give larger magnitudes. Long-term averages over 24 hours however, show excellent agreement and previously published Birdlings Flat data should be quite consistent with 'true velocity' estimates.

4.3 DATA LENGTH

The experimental correlations will naturally be subject to sampling errors whenever a finite length of data is used (Awe, 1964 a,b). At the same time the motion of the atmosphere is subject to changes on a vast range of time scales, from days down to less than a minute. There inevitably arises a conflict between taking a data record long enough to ensure statistical reliability yet short enough to be statistically stationary. A commonly used length is 3 minutes. For real-time drifts the additional constraints of storage and data processing time make a shorter data length desirable. In addition, for gravity wave studies shorter data lengths are preferable for the increased temporal resolution (Vincent and Ball, 1977). One-minute data samples

have been used by Vincent et al. (1977) and the velocities were found to agree well with the neutral wind as measured by rocket techniques. Meek et al. (1979) found that the consistency in height and time of 1-minute samples showed only slight degradation over 3-minute samples at Adelaide, although the percentage of acceptable velocities was smaller. However, Saskatoon data showed a significant decrease in consistency.

To investigate the yield and quality of shorter samples at Birdlings Flat, a 3 hour recording of 3-minute samples separated by 7 minutes was studied. Average velocity-height profiles have been formed from data using (a) the first of the 3 minutes, (b) the second minute, (c) the third minute and (d) the entire 3 minutes. Ionospheric changes over 3 minutes are not expected to be large and such changes that may exist on this small time scale (e.g. acoustic waves and turbulence) should average out over 3 hours. Consequently the four profiles shown in Fig. 4.5 are expected to show good agreement. The number of velocities contributing to each point is shown down the right hand side of the diagram. (It should be pointed out that since this data was taken instrumental improvements have resulted in an increased data rate.)

The low zonal wind speeds are typical of the spring period of circulation change from winter westerlies to summer easterlies (see Chapter 5). The high data yield at 66.5 km was associated with a steady, strongly reflecting layer at this height, which was also accompanied by an

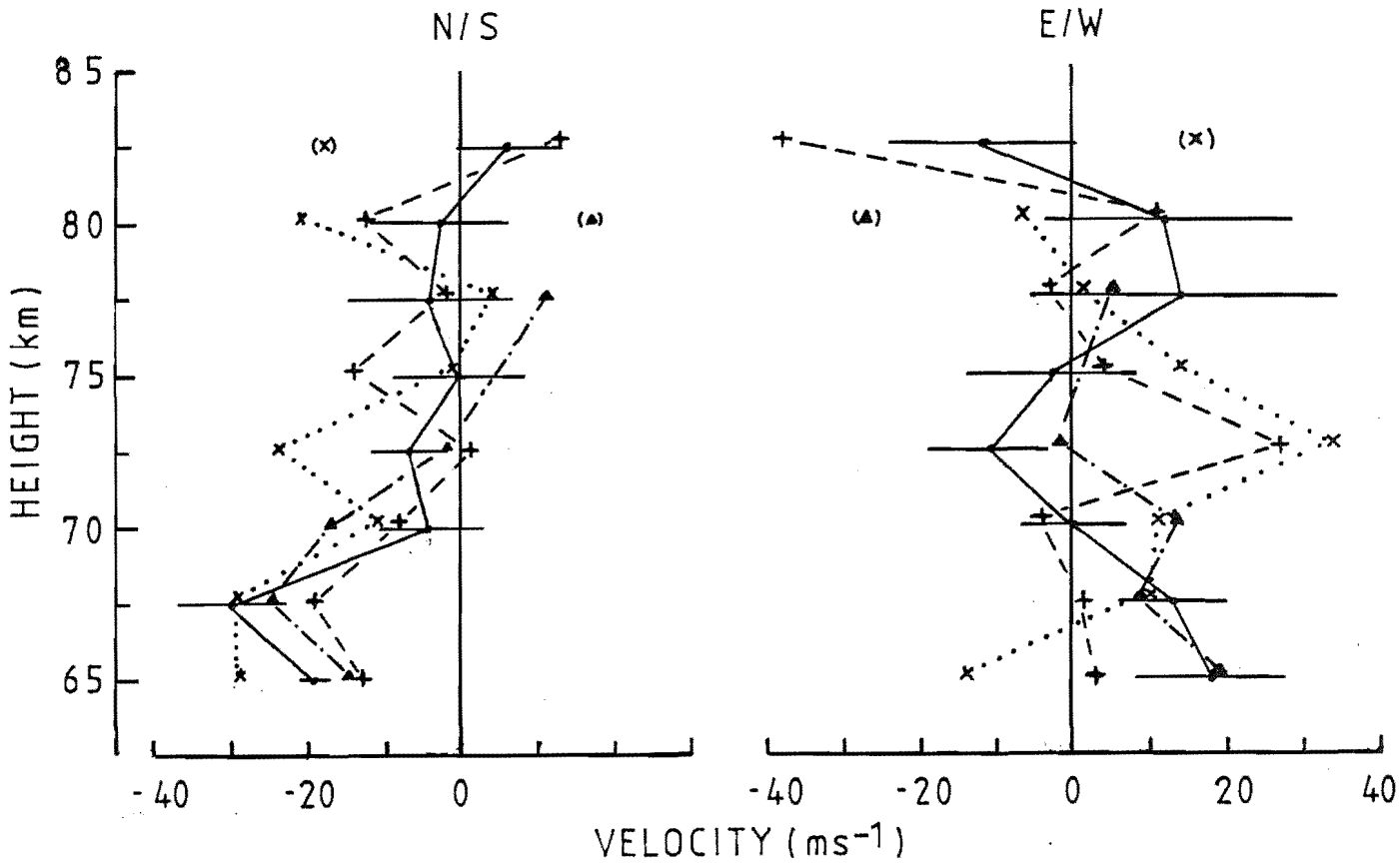

(a)	(b)	(c)	(d)
6	2	1	0
4	2	3	1
3	7	2	3
4	3	3	0
4	2	2	3
6	5	5	5
7	10	11	12
3	4	4	3

Figure 4.5: Average velocity-height profiles for 1 and 3 minute samples. (a) —— (b) --- (c) ... (d) -•-• .

extremum in the southward velocity component. A layer of strong reflection associated with a wind maximum has also been observed by Hocking (1979). Data may be poorly distributed over the 3 hours at heights with a very low number of velocities. In such cases the influence of longer period changes may make them unsuitable for comparison. For example, on closer inspection of individual velocities, the large zonal wind speeds of profiles (b) and (c) at 71.5 km were found to be caused by unusually high velocities which occurred in the last 30 minutes of the 3 hours. At the heights suitable for comparison the profiles agree to within 15 m/s and within their s.e.

Of direct interest is the amount of data obtained from the different samples. The 1-minute samples consistently gave a much larger yield than the 3-minute sample. It is not clear whether this is due to real changes in velocity or pattern orientation over the 3 minutes. If in fact significant changes in velocity do occur over 3 minutes, the shorter samples would be expected to show greater variability, as found by Meek et al. (1979), since the 3-minute drifts would incorporate these variations in V_c to some extent.

It is concluded that 1 minute samples are a satisfactory length and in fact give a higher data yield than the 3-minute samples. For the majority of the data in this thesis samples of 256 points spaced at 0.25 sec, that is 64 seconds long, are used.

4.4 DIURNAL DISTRIBUTION OF DATA

There is a very pronounced variation in the quantity and quality of data collected over a period of 24 hrs. The absence of solar radiation at night results in not only much weaker D-region partial reflections but also a complete absence of detectable echoes below 80 km. The decrease in absorption at night also allows considerable radio interference from long path propagation. This occurs after sunset.

The distribution of usable echoes over 24hrs averaged over a month long September data run is shown in Fig. 4.6. The results for the 79-81 km height range indicate the virtual absence of detectable echoes between 1900 and 600 hrs. At heights of 84 - 86 km the echoes, although still present, are much weaker at night and sometimes badly contaminated by interference from after 2000h till the early morning. Above this, in the upper D-region, echoes are stronger and present throughout the day. But again interference degrades the signal to noise ratio at night.

The poorer night-time data quality has usually required the combination of adjacent heights in order to get sufficiently dense data for tidal analyses, and has also prevented tidal analyses being made below about 82 km.

4.5 NOON WINDS AS A MEASURE OF THE PREVAILING WIND

In later chapters the climatology of the prevailing wind and the long period (> 1 day) planetary scale oscillations which may be superimposed,are discussed. It is often necessary

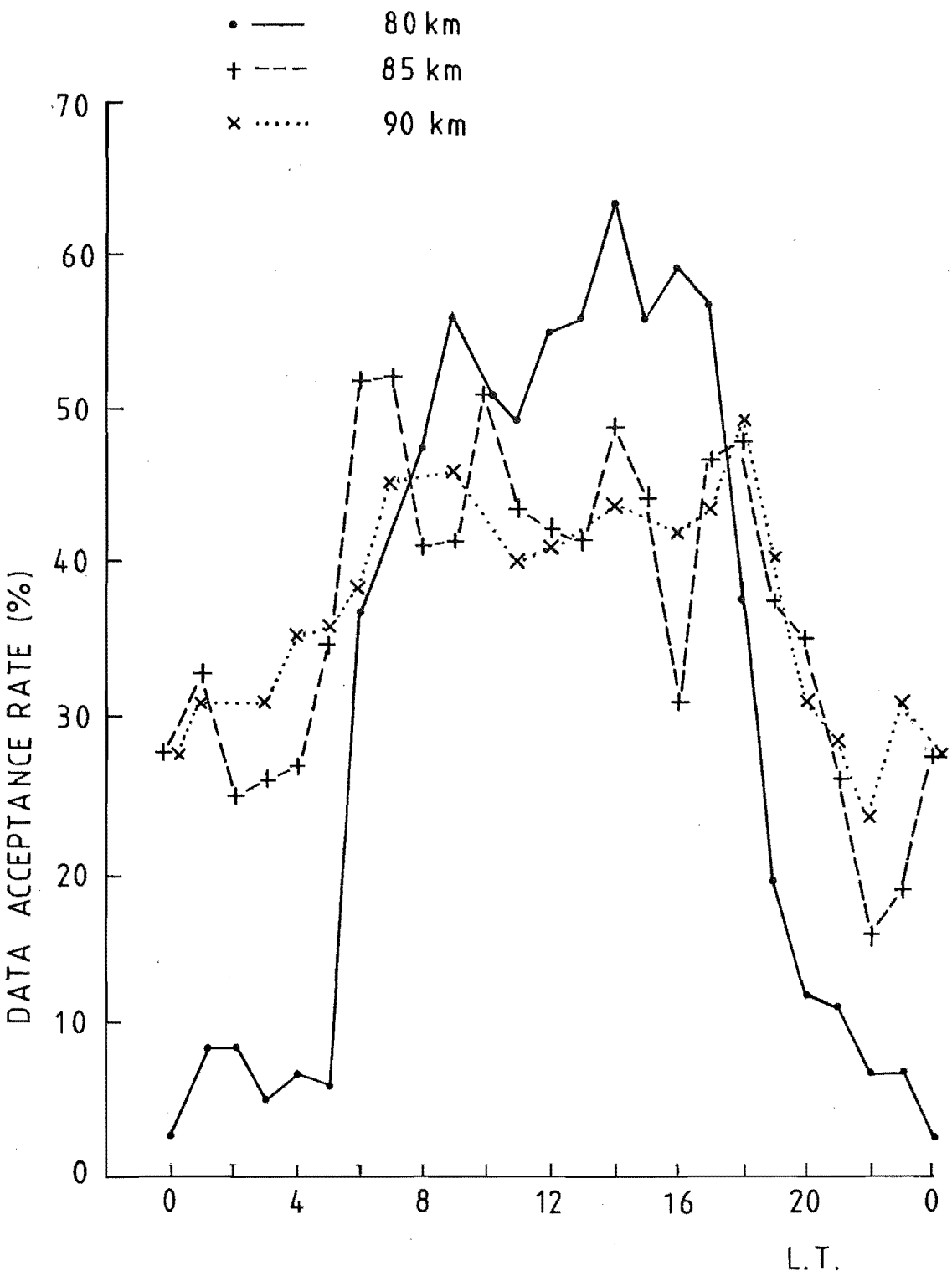

Figure 4.6: Diurnal distribution of data acquisition rate.

or expedient to estimate the prevailing wind from measurements over a limited period centred on noon. However, both tides and internal gravity waves may contribute to the noon averages. The effect of such incomplete sampling of the wind is discussed here.

Below 80 km the sampling is incomplete by necessity - the reduction in solar radiation at night restricts adequate partial reflections to the daytime. Before the introduction of real-time drifts analysis, the logistics of continuous data recording often dictated that prevailing wind estimates at all heights were based on noon values (Fraser, 1968; Manson et al., 1974). Fraser (1968) was interested in seasonal variations in the wind, and from an analysis of Adelaide meteor wind data, concluded that the tidal components were of sufficient irregularity over the course of a month, to make only a small and possibly negligible contribution to monthly averages. Manson et al. (1978) found that on a day to day basis the noon winds reproduced the daily means well below 100 km, typically within 5-10 ms^{-1}, but with occasional differences exceeding 20 ms^{-1}. Above 100 km only the trend in the winds agreed.

Fig. 4.7 shows a comparison of 24h, 6h (1000 - 1600) and 2h (1200-1400) averages of daily winds over a 26 day period. The mean component of a harmonic analysis of daily winds in terms of mean, diurnal and semidiurnal components was generally within a few ms^{-1} of the 24h average, with the largest difference being 7 ms^{-1}. Data from 2 heights have been combined for display on the graphs. It is

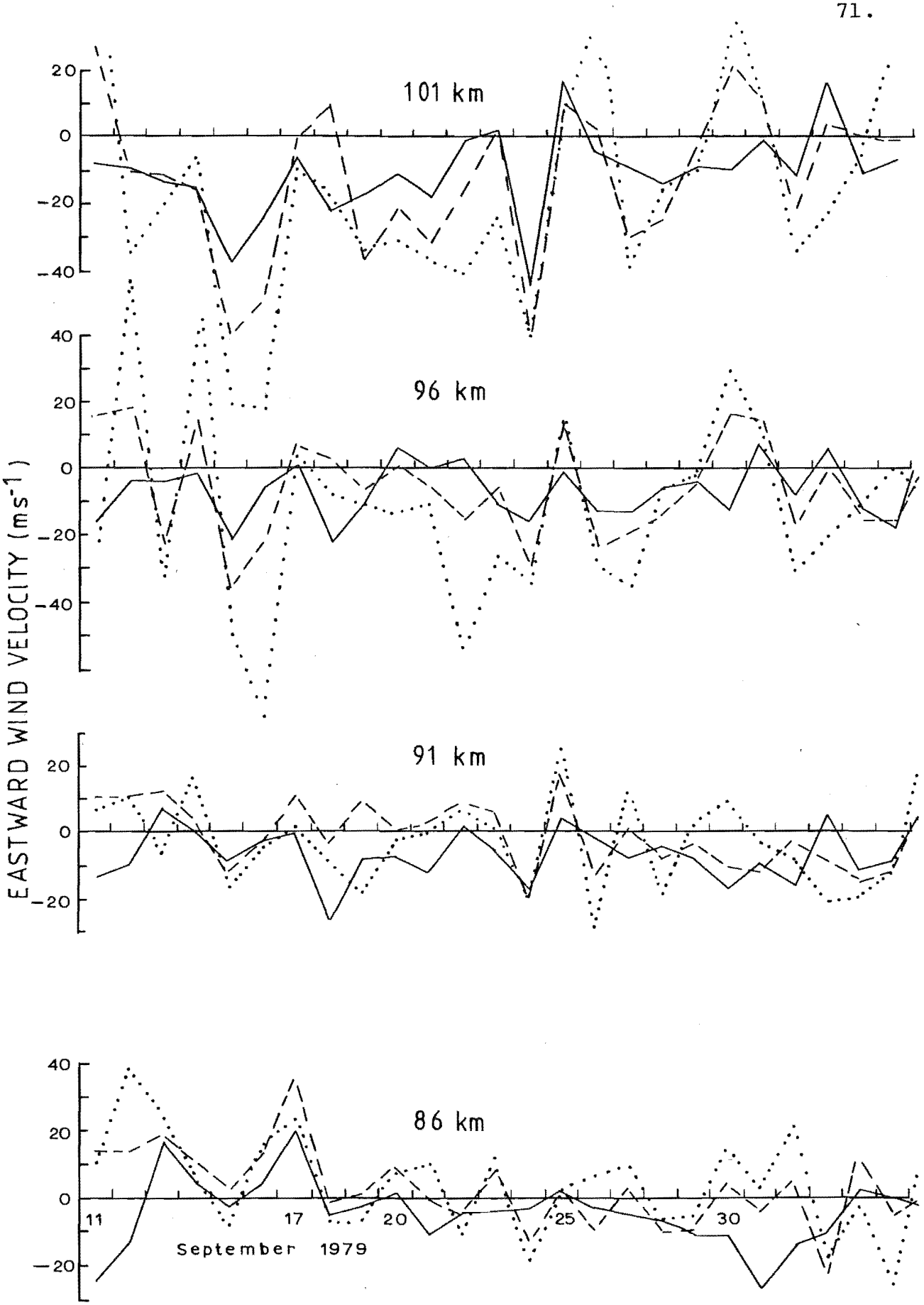

Figure 4.7: Comparison of 24h (——), 6h (---) and 2h (•••) zonal wind averages.

immediately apparent that the 6h and 2h averages show much greater day to day variations than the daily mean values. Looking at the 86 km data, it can be seen that at times (e.g. 13-20 September) both 6h and 2h averages do exhibit very good agreement with the 24h average, (within about 5-10 ms^{-1}), but at other times (30 September - 2 October) the differences can be large. Differences become more pronounced at higher heights with discrepancies of 25-30 ms^{-1} not uncommon. At 100 km, the 2h averages occasionally show extreme differences. The agreement of the 6h averages is generally better than the 2h averages, as may be expected from the more complete coverage of full cycles of gravity waves and the semidiurnal tide.

A comparison of the general trend of the wind with the more rapid fluctuations smoothed out by 3 passes of a Hanning filter, is shown in Fig. 4.8. Again it is apparent that although the 24h mean is followed at times (especially at 101km) there are occasions for significant discrepancies both in magnitude and general trend. One aspect that now emerges clearly, is that for the 86 and 91 km heights the short term averages give an eastward velocity significantly more positive than the daily averages. However at the higher heights the 6h means, on average, are not noticably biased while the 2h mean even shows a bias towards westward velocities.

Consideration of the tides explains a large amount of these differences. It will be shown in Chapter 7 that the tides vary both in phase and amplitude from day to day.

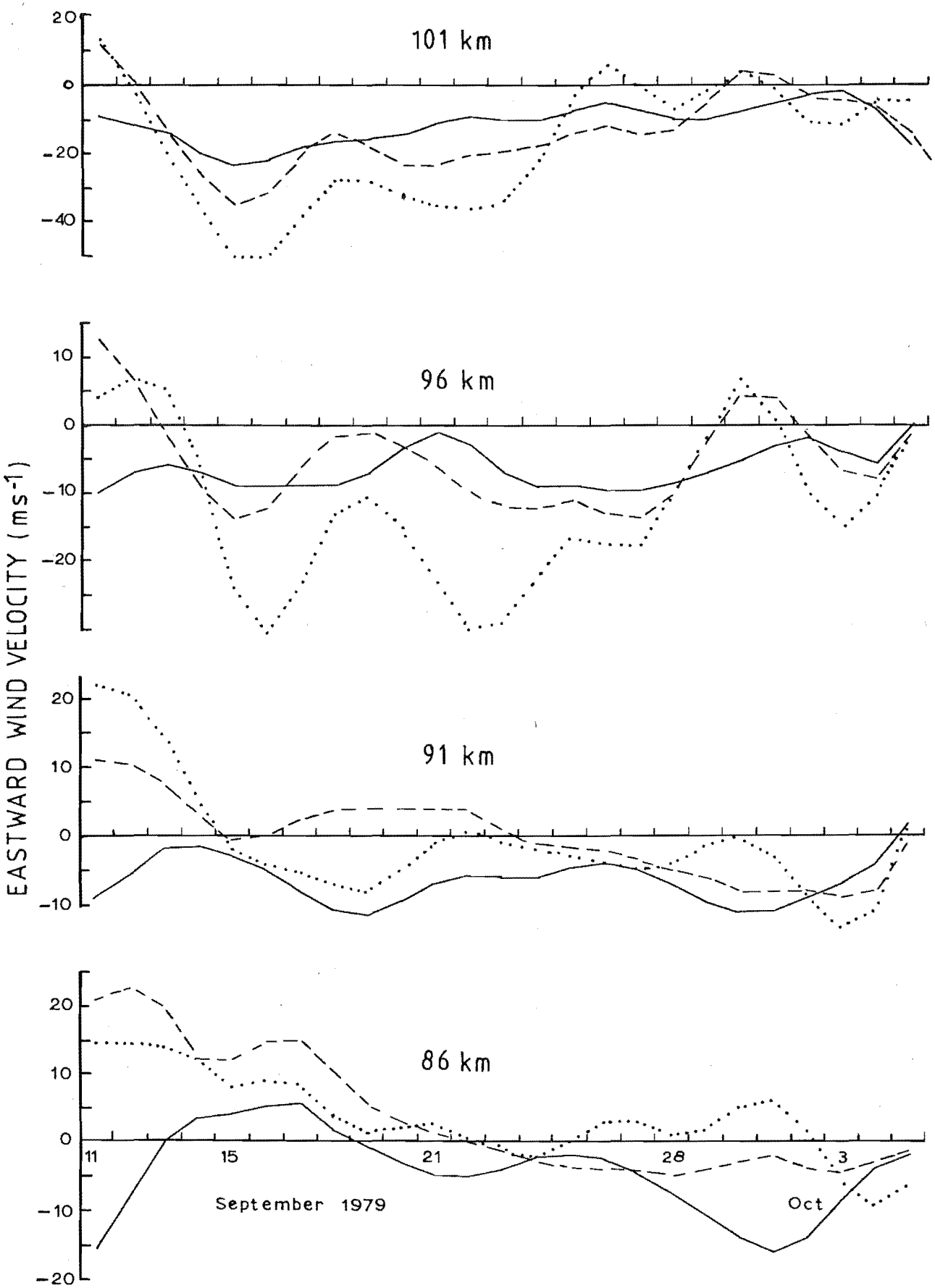

Figure 4.8: Comparison of 24h (——), 6h (---) and 2h (•••) zonal wind averages after smoothing with one pass of a Hanning filter.

A phase shift of 3 hours in the semidiurnal tide will significantly affect the 2h averages; such changes are common. The average tide for this particular month was shown previously in Fig. 4.4b and is also shown in Table 4.1. The diurnal tide shows a maximum at noon, while the semidiurnal tide has a maximum on average at about 1300h below 93 km but closer to 730 and 1930 above this. So below 93 km both tidal components will reinforce near noon to give increased eastward winds in accord with Fig. 4.8. Above 93 km, the semidiurnal tide reverses phase to have a maximum westward velocity at about 1330, while the diurnal tide now maximizes a little earlier at 900-1030. This again is in qualitative agreement with Fig. 4.8. Closer analysis at times of specific discrepancies such as at 86 km on 11-12 September and 30 September - 2 October, showed that on these occasions the amplitude of the diurnal and semi-diurnal tides was strong but also the times of maxima were closely timed near midday.

How well then, can monthly averages of noon winds be expected to reveal the prevailing wind? As Fraser (1968) noted, changes in the phase of the tides will significantly reduce the tidal influence. Table 4.1 shows the amplitude (A) and phase (ϕ) of the vector means of the daily diurnal and semidiurnal tidal components for September, 1979. The monthly algebraic averages of the daily tidal amplitudes are shown in brackets; they are typically three times larger than the amplitude of the vector means indicating that significant phase variations have occurred. The vector

Table 4.1: Monthly averages of tides and wind averages for September, 1979.

Ht.	Dirn.	24h Tide A (ms^{-1})		24h Tide ϕ(h)	12h Tide A(ms^{-1})		12h Tide ϕ(h)	Wind Averages (ms^{-1}) Mean	24h	6h	2h
86 km	E	6	(18)	12.2	4	(14)	1.2	-5	-4	1	3
	N	8	(14)	22.1	3	(13)	10.1	1	0	-2	2
91 km	E	8	(13)	10.8	1	(9)	1.0	-6	-6	-2	-4
	N	4	(9)	20.7	2	(10)	10.7	1	1	1	2
96 km	E	6	(18)	10.5	6	(16)	7.8	-5	-5	-3	-13
	N	4	(16)	20.8	8	(16)	1.2	3	4	6	16

averages of the semidiurnal tide at 91 km are especially low due to the rapid phase change in this region noted previously. The contribution of the tides to noon winds over the month can be found by combining the diurnal and semidiurnal oscillations with the appropriate phases. So for 86 km in the eastward direction, the tides may be expected to contribute a positive offset of nearly 10 ms^{-1}. The monthly average of 2h noon winds as well as 6h and 24h averages, and the mean component from the harmonic analysis, are also shown in Table 4.1. The 2h noon wind at 86 km is 8 ms^{-1} more eastward than the average mean value; this can be accounted for by the tides. The eastward tidal contribution at 91 km is less than 8 ms^{-1} and at 96 km less than 2 ms^{-1}. At the latter height, this is insufficient to explain the discrepancy between the 2h averages and the prevailing wind. Long period gravity waves with preferred directions of propagation may be influencing these short term averages.

Table 4.1 shows clearly the decreasing reliability of shorter term averages as estimators of the monthly mean prevailing wind. Even so, the maximum error of 2h noon averages was only 13 ms^{-1}. In the absence of fuller diurnal coverage, noon winds are still valuable for synoptic studies. As an indicator of day to day prevailing wind changes or planetary wave activity, however, short period averages have been shown to be quite misleading on occasions, particularly in the upper height regions.

CHAPTER 5

THE PREVAILING WIND

5.1 CURRENT STATUS OF CIRCULATION MODELS

The general circulation arises in response to the uneven distribution of thermal heating of the atmosphere. Models of upper atmospheric circulation fall into two areas: those which are concerned with the stratosphere and mesosphere where solar absorption by ozone dominates the heat budget, and those which consider the thermosphere where oxygen is the dominant species in the heat budget.

5.1.1 Stratospheric and Mesospheric Circulation

In the middle atmosphere, there is strong heating in the 35 - 75 km region with the solar absorption by the 2000 - 3000 Å wavelength range of ozone (Murgatroyd, 1971). Against this heating must be balanced radiative cooling by the infra-red emission of carbon dioxide (15μ band) and a lesser contribution from ozone. This cooling is a maximum in the high temperature regions and so tends to restore a thermal balance. The net radiative effect has been calculated by Murgatroyd and Goody (1958), and Leovy (1964). They found a strong seasonal dependence, with heating in the summer hemisphere peaking around 50-60 km, and cooling in the winter hemisphere. At the equinoxes net heating occurs in equatorial regions. This diabatic differential heating provides the principal drive for the circulation in the

upper stratosphere, but at other heights further energy sources (and sinks) become important; in the lower stratosphere strong eddy penetration from the large energy reservoir in the troposphere is important (Newell, 1966), while in the upper mesosphere, tidal and internal gravity waves propagating from below become important dynamical factors. The different regions of the atmosphere cannot be treated in isolation.

Murgatroyd and Singleton (1961) calculated the circulation in the meridional plane which would be required to balance the differential heating in the stratosphere. Ascending air in the summer hemisphere was required to produce adiabatic cooling to balance the net radiative heating there, and subsiding air in the winter hemisphere was needed to produce adiabatic heating. A summer to winter flow of 4-5 ms^{-1} was needed to complete this single cell model. However, no account was taken of momentum balance, and the Coriolis torque on this pole-to-pole flow would produce strong eastward accelerations in winter and westward accelerations in summer which must be offset. It was realized that the momentum flux accompanying eddies (or planetary waves) in the stratosphere would be important in momentum considerations, just as it was well known that tropospheric eddies were important in transferring angular momentum to mid-latitudes to maintain the circulation there against surface friction. Accompanying the eddy momentum transfer would also be eddy heat transport which in turn would affect the thermodynamics.

The basic linear equations governing the large scale motions in the atmosphere taking the eddy fluxes into account

are derived in Holton (1975). The dependent field variables are conveniently considered as the sum of a zonal mean (i.e. averaged around a latitude circle), denoted by overbars, plus a residual representing the effects of eddy or wave motion, denoted by primed quantities. Holton has used scaling arguments to simplify the equations governing the seasonal circulation in terms of a Rossby number (U/2L) expansion. To lowest order, the zonal and meridional equations of motion, the thermodynamic equation,and the continuity equation reduce to the following:

$$2\Omega \sin\theta\, \bar{v} = \frac{1}{\cos^2\theta}\frac{\partial}{\partial y}\left(\overline{u'v'}\cos^2\theta\right) + \frac{1}{\rho_o}\frac{\partial}{\partial z}\left(\rho_o\, \overline{u'w'}\right) \tag{5.1}$$

$$2\Omega \sin\theta\, \bar{u} = -\frac{\partial \bar{\Phi}}{\partial y} \tag{5.2}$$

$$N^2\bar{w} = \frac{\kappa \bar{J}}{H} - \frac{1}{\cos\theta}\frac{\partial}{\partial y}\left(\overline{v'\Phi'_z}\cos\theta\right) + \frac{1}{\rho_o}\frac{\partial}{\partial z}\left(\rho_o\, \overline{w'\Phi'_z}\right) \tag{5.3}$$

$$\frac{1}{\cos\theta}\frac{\partial}{\partial y}\left(\bar{v}\cos\theta\right) + \frac{1}{\rho_o}\frac{\partial}{\partial z}\left(\rho_o\, \bar{w}\right) = 0 \tag{5.4}$$

where u,v,w are the zonal, meridional and vertical velocities, Ω and θ are the earth's angular velocity and latitude, $y = a\theta$, and Φ, N^2, H and $\bar{J}$ are the geopotential, Brunt frequency, scale height and zonal mean diabatic heating. Also, $\Phi'_z = \frac{RT'}{H}$, where R is the gas constant. The two right-hand terms of (5.1) and (5.3) are the divergences of eddy momentum and eddy heat fluxes.

The circulation which evolves can be described in the following way. The diabatic heating (cooling) $\bar{J}$ in (5.3),

damped by the divergence of eddy heat flux, must be balanced by the adiabatic cooling (heating) of rising (subsiding) air given by $N^2\bar{w}$. The continuity equation in turn requires a mean meridional flow ($\bar{v}$). The Coriolis torque acting on $\bar{v}$ (equation (5.1)) would give rise to strong zonal accelerations unless balanced by the eddy momentum flux divergences. In the presence of a summer to winter meridional flow, the sense of such an acceleration is to produce westward winds in summer and eastward winds in winter, as is observed in the stratosphere and mesosphere. On shorter time scales, such as during stratospheric warmings, enhanced eddy fluxes can also upset the balance implied in (5.1) and result in zonal wind accelerations (and temperature changes). Equation (5.2) is a statement of the geostrophic approximation: the Coriolis force on the zonal wind is balanced by the meridional pressure gradients.

The main problem in numerically modelling this equation system is the lack of information about the eddy fluxes, which include the effects of all scales of waves, from planetary scale down to small-scale gravity waves. For this reason Leovy (1964) parameterized the eddy flux divergences and was able to qualitatively represent the observed solstice circulation.

More detailed three-dimensional models by Cunnold et al. (1975) and Manabe and Mahlman (1976) have revealed an additional stratospheric high latitude cell in the northern hemisphere winter opposing the dominant summer to winter hemispheric flow. Such a cell has received observational

confirmation by Vincent (1968). This cell is believed to be due to planetary waves which give rise to poleward eddy fluxes. The "non-interaction theorem" (Charney and Drazin 1961; Eliassen and Palm, 1960) states that cancellation between the wave induced meridional cell and the eddy fluxes occurs in the absence of wave transience, damping or critical levels (where the wave phase velocity equals the background wind velocity). The mass circulation in this situation is the same as in the solely thermally driven circulation, and in recent work has been associated with a Lagrangian mean circulation (Dunkerton, 1978). If this indirect high latitude cell extends into the mesosphere, although not affecting the mass transport of conservative traces, it could have important consequences if it affected the subsidence of nonconservative tracers such as NO, which is important in the production of the winter anomaly. Dissipation may be significant at these heights also. Manabe and Mahlman (1976) further deduced a weaker third meridional cell at high latitudes in the southern hemisphere stratosphere in winter. The existence of this cell has been given observational support by Hartmann (1976).

Crane et al. (1980) have modelled the circulation of the stratosphere and mesosphere using planetary wave heat and momentum fluxes deduced from Nimbus 6 pressure modulated radiometer (PMR) data. They used Planck equivalent temperatures and deduced zonal mean and eddy velocities using the geostrophic approximation. The meridional velocities calculated were 3-4 ms^{-1} at 70 km

directed from the summer to winter pole. A much weaker return flow was evident at lower heights. The thermally indirect winter cell was observed up to a height of at least 55 km. Crane et al. also incorporated the observed planetary wave momentum transports into a model to deduce the zonal circulation. They found that the planetary wave momentum flux divergences were incapable of balancing the zonal momentum budget in the mesosphere. A further source of strong damping was required to reproduce the observed zonal winds. Such a requirement has also been found in the models of Manabe and Mahlman (1976) and Holton and Wehrbein (1980). Houghton (1978) has suggested that the divergence of eddy fluxes due to tidal and shorter period internal gravity waves may provide the necessary damping. In the upper mesosphere these waves achieve large amplitudes but through dissipation suffer a divergence of momentum flux. Since satellite measurements do not have the temporal or height resolution needed to measure these waves, ground based observations such as at Birdlings Flat have a valuable contribution to make in elucidating this problem.

If an upward flux of internal gravity waves is responsible for the damping of the Coriolis torque, it should exhibit a seasonal variation. Such a variation may be provided by the filtering of the gravity wave spectrum by background zonal winds as described by Hines and Reddy (1967). A gravity wave which approaches a critical level will suffer absorption. If an intially isotropic spectrum of waves is assumed to originate at tropospheric levels,

then in winter, in the presence of an eastward jet, a large part of this spectrum will be removed, namely waves with phase velocities of 0-60 ms^{-1}. Waves travelling in the opposite direction experience a lesser filtering effect by reflection as they are Doppler shifted closer to the limiting Brunt frequency. Therefore at mesospheric heights where the damping of waves by eddy viscosity will result in momentum deposition, the wave spectrum is expected on theoretical grounds to be biased towards the westward direction - precisely the sense needed to damp the eastward Coriolis acceleration. In summer due to the reversal of the mean winds, the wave spectrum will also be biased in the required sense. Confirmation of such a directional filtering must however, await improved experimental observations.

An important consequence of the circulation in the meridional plane is that the adiabatic cooling associated with ascending air in the summer mesosphere and the adiabatic warming associated with subsidence in the winter hemisphere is sufficient to result in higher mesopause temperatures in winter than in summer. This imbalance may be assisted by chemical heating associated with recombination of subsiding oxygen atoms in the winter hemisphere (Kellogg, 1961). The situation where radiative heating is acting in a region where the temperature is being maintained at a low value is the action of a refrigerator. Thus we have a stratospheric heat engine driving the upper mesospheric refrigerator (Newell, 1966).

5.1.2 Thermospheric Circulation

The principal source of lower thermospheric heating is from absorption of solar EUV and UV radiation. Above 300 km the neutral heating depends upon heat conducted down from the magnetosphere where it is generated by complex magnetospheric - ionospheric interaction processes (Dickinson et al., 1975). In model simulations of thermospheric circulation, Dickinson et al. (1975,1977) found that an additional high latitude heating source was required to explain the observed temperature structure and meridional winds. They suggest that this is due to auroral processes involving Joule heating by ionospheric current systems, and to particle precipitation. This source, which is required to be larger in summer than winter, must increase by a larger factor than solar EUV and UV heating does, from sunspot maximum to sunspot minimum.

An important factor in thermospheric dynamics is ion drag - resulting from the collision of neutral particles with ions, which above 140 km are constrained to move along the earth's magnetic field lines. The correlation between ion drag and the diurnal variation of the wind also results in an effective mean momentum source (Dickinson et al., 1975). These factors were included in the model of Dickinson et al. The resulting meridional circulation was a simple Hadley cell with motion from the summer to winter pole, but modification by the high latitude heat source reinforced the summer flow, and at solar cycle maximum actually generated a reverse cell at high latitudes in winter. This reverse

cell was only found above 150 km, but during geomagnetic storms could be expected to move to lower heights and lower latitudes (op cit). Below about 150 km, the momentum source due to ion drag is fairly weak, and the zonal winds are determined largely by the Coriolis force on the strong meridional flow damped by ion drag. However above this, the balance between the strong ion drag and the zonal momentum source largely determines the zonal wind. The modelled zonal circulation then consisted of mean eastward winds in winter and westward winds in summer. Incoherent scatter radar measurements at heights near 300 km are consistent with this model (Emery, 1978; Babcock and Evans, 1979).

Unfortunately the results below 120 km, the region of direct interest here, are uncertain due to the artificial boundary specifications of eddy processes (Dickinson, 1975). However, somewhere near this height, there must exist a return flow for the predominent thermospheric meridional motion of ascent in the summer hemisphere, drift from summer to winter pole and subsidence in the winter hemisphere. The Coriolis torque on this return winter to summer meridional flow may be expected to generate eastward winds in summer and westward winds in winter.

Modelling of the circulation in the stratosphere/mesosphere and thermosphere has largely treated the two regions independently. However there must exist a region from 90-120 km where the two circulation patterns meet. In this region there will be a transition from the summer to winter flow of the

upper mesosphere and the winter to summer return flow of the lower thermosphere.

5.2 THE OBSERVED CIRCULATION BETWEEN 65 AND 100 km

Wind measurements using the on-line processing system described in Chapter 3 began in June 1978. The aim of continuous data collection was largely achieved except for a three week period in July 1978, and during periods of hardware failure: from December 1978 till February 1979, one week in March 1979, and several weeks in June 1979.

For the purpose of studying the prevailing winds, the zonal and meridional components of the 'true' velocity have been averaged in 7 day sections at 2.5 km height intervals from 64 to 101 km. Such a temporal sampling interval is fine enough to preserve adequate detail of the seasonal changeover periods, yet includes a statistically significant number of data points. As discussed in Section 4.4, data below 80 km is only obtained during daylight hours. The 6h wind averages at these heights should be reasonable estimates of the prevailing wind, particularly since the tidal amplitudes decrease with height. Results for the winter to spring period of 1978, and the complete year from February 1979 are presented separately.

5.1.2 1978

Fig. 5.1 shows the 1978 data in the form of contour maps. Operational considerations - demands of other experiments or the loss of a section of memory - determined that winds

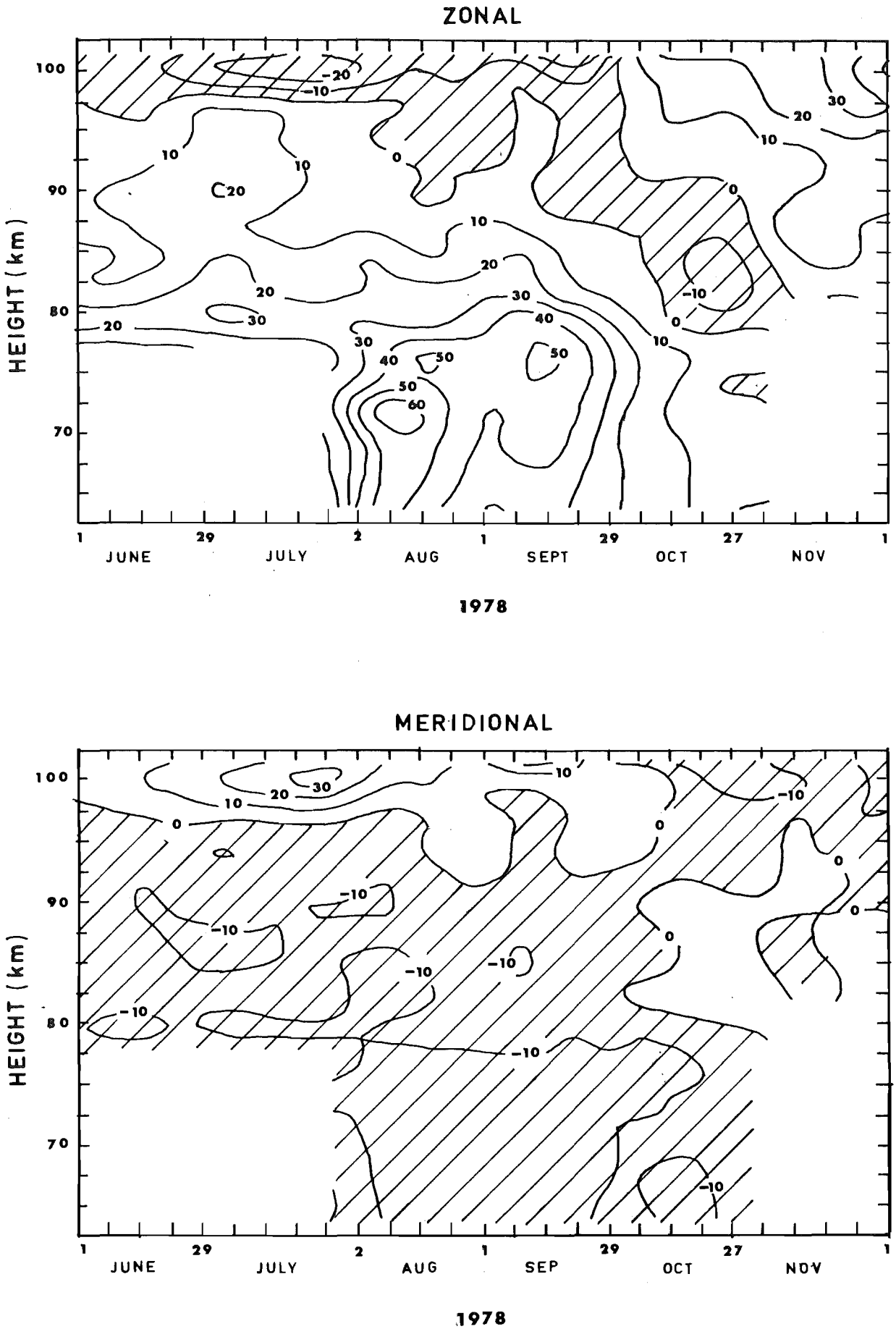

Figure 5.1: Contours of weekly mean winds for 1978.

below 80 km were only obtained during August, September and October. The July gap in the data has been filled by linear interpolation. A simple smoothing in time with weights of 1/4, 1/2, 1/4 has also been applied.

The zonal circulation shows the expected eastward winds in the winter mesosphere, with an indication of a change to westward winds in summer. Maximum eastward velocities in excess of 60 ms^{-1} are reached at 71 km in August. Above 97 km, at the highest levels of measurement, there is evidence for a different wind regime, with westward winds in winter. In the intermediate region, near the mesopause, maximum eastward winds are reached in early July.

In August the upper westward wind regime temporarily descends downward; the meridional wind component is also affected. At the end of August the eastward winds of the mesosphere are also weakened. A major dynamical disturbance thus affected a large region of the atmosphere, from the mesosphere up to the lower thermosphere. This will be discussed further in Section 6.7 in relation to stratospheric temperature measurements.

The change from the winter circulation pattern appears to begin in mid-September as the boundary between the lower level eastward winds and the upper level westward winds begins to descend, reaching 80 km by mid-October. At the end of September a transition to eastward winds occurs in the lower thermosphere. These winds develop to strengths exceeding 30 ms^{-1} in early summer.

The meridional wind component has a significantly smaller amplitude than the zonal. In winter it is directed

poleward below a height of about 97 km, and above this equatorward flow exists. As with the zonal component, the upper region winds change direction in spring, although 1-2 weeks later.

5.2.2 1979

Fig. 5.2 shows smoothed contours for 56 weeks beginning on February 10, 1979. Data below 80 km was not obtained during March 1979 due to memory failure, nor from September 13 to October 12 when efforts were concentrated on the measurement of atmospheric tides from 80 to 100 km. As before, missing data has been filled by linear interpolation.

A monsoonal-type (i.e. seasonally reversing) circulation clearly emerges in the mesosphere. In summer a westward jet develops with maximum speeds of 75 ms^{-1} in early January at 72 km. These strong winds weaken fairly rapidly through February until a complete reversal occurs in late February or early March. This autumn changeover was very similar in both 1979 and 1980.

The autumn and winter eastward winds below the mesopause show considerable variability, with maximum speeds of 75 ms^{-1} occurring in early winter. In August, fluctuations are extreme with several reversals of the dominant flow. Indeed, westward winds can be followed within a few days by eastward winds with speeds up to 60 ms^{-1}. The possible effects of both tidal and internal gravity waves should be averaged out over the 7 day data interval. More likely causes are long period planetary waves or dynamical effects induced by winter warmings

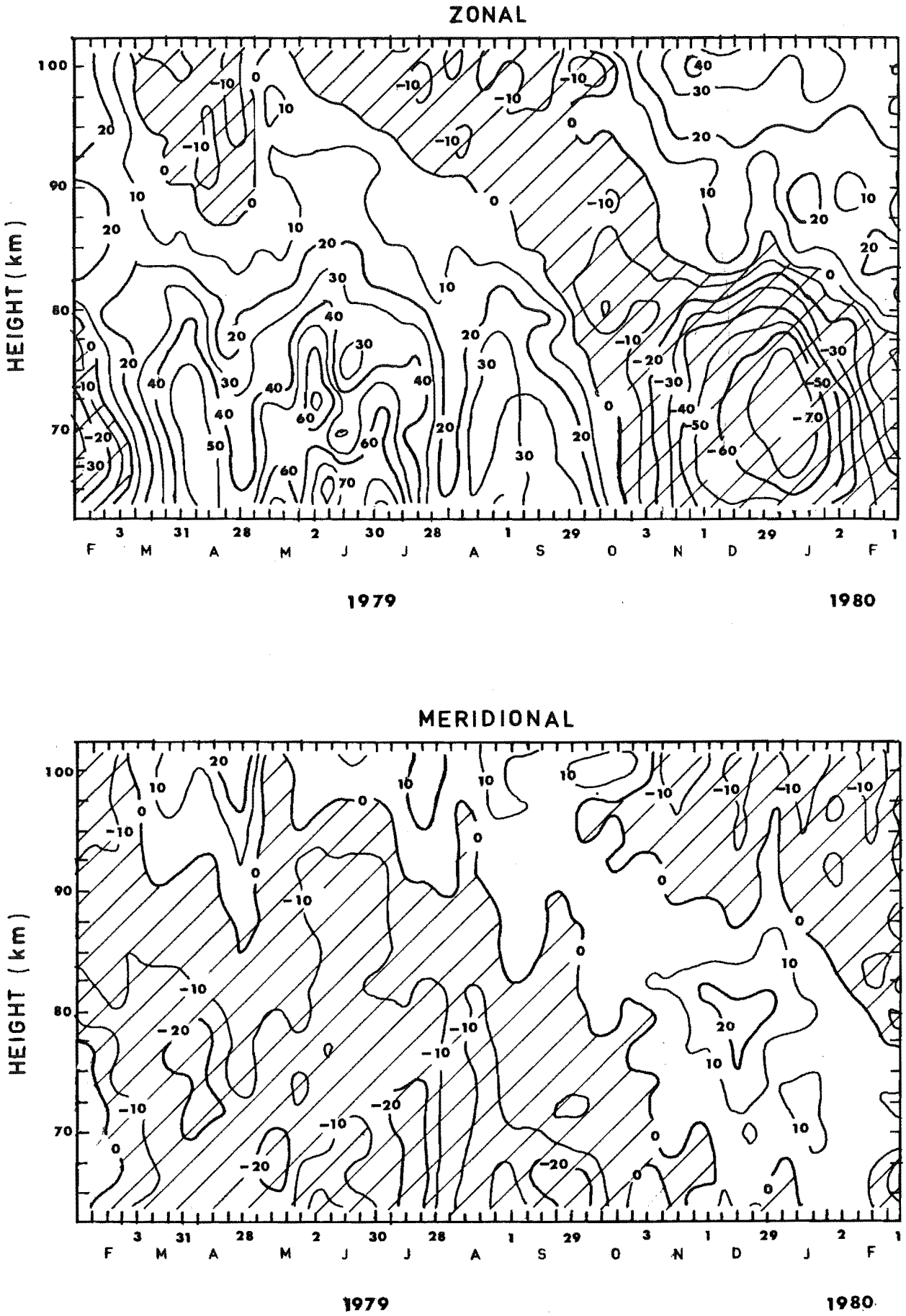

Figure 5.2: Contours of weekly mean winds for 1979/1980.

in the stratosphere. As a result of these fluctuations no well defined jet develops as in summer, and average wind values are substantially reduced from peak values.

In the upper region above 85 km in summer, eastward winds of similar magnitudes ($\sim$ 30 ms^{-1}) to those observed in 1978 develop. These occur from early November through to March when a transition to westward winds occurs slightly after the autumn transition below. These upper level autumn westward winds extend down to 90 km at a time when winds below 85 km weaken, but in May eastward winds abruptly intrude from below causing the elevation of this boundary to above 102 km. The transition height between eastward and westward winds does not remain static after this but steadily decends throughout winter, eventually leading to the establishment of westward winds in the mesosphere in October.

Above a height of 102 km then, eastward winds prevail in summer and westward winds in winter, while the winds below the mesopause are in antiphase. However, in the intermediate region at about 95 km, four transitions of wind direction occur, with eastward winds in mid-winter as well as in summer.

The meridional wind component shows a broadly similar seasonal variation to the zonal component. In summer the flow is towards the equator below 90 km and reaches fairly strong values ($>$ 20 ms^{-1}) in early December around 80 km. It is interesting to note that this maximum does not coincide with the zonal westward jet maximum. The meridional flow

below 80 km reverses to a poleward direction in March. This flow persists until late spring/early summer. The spring meridional changeover lags the zonal change by a week or two.

The flow in the upper wind regime is broadly in the opposite sense to that below.

In many respects the behaviour of the zonal and meridional components is closely related, as might be expected. The upward intrusion of the lower region winds in early May occurs simultaneously in both components and the bridge between the upper winter levels of westward and northward winds to the summer region below is quite similar.

5.2.3 Discussion

A comparison between the 1978 and 1979 June to December winds shows general agreement in trends but certain differences in detail. Both years showed variability in the winter eastward winds but 1979 showed more frequent and stronger reversals during July and August in contrast to the single dominant disturbance in August in 1978. This resulted in generally lower magnitude winter mesospheric winds in 1979. In both years in the 85-90 km region maximum eastward winds occurred near the winter solstice, in mid-June. The band of westward winds which descended at the time of the spring circulation changeover was common to both years but occurred some 2 weeks earlier in 1979, possibly reflecting the weaker eastward circulation in

this year. The 1979 meridional component was generally stronger.

The seasonal changes of the winds can be viewed perhaps more easily from the perspective of plots at a single height. Fig. 5.3 shows smoothed weekly winds in 1979 at four heights.

At 66 km the dominance of an annual component of circulation is clear, although the duration of the westward winds (19 weeks) is significantly shorter than that of the eastward winds (33 weeks). The contrast between the variability in winter and the fairly steady changes in summer is quite marked. Although the meridional component is smaller and consequently more difficult to determine reliably, the present data set also allows meridional seasonal variations to emerge with some degree of significance; a fact reflected in the similarity in changes at nearby heights. At 66 km the wind is directed poleward for the major portion of the year (33 weeks) with a period of very low speeds in spring lasting about 6 weeks, while in summer a weak equatorward wind lasts for about 13 weeks.

Although the observed circulation pattern may be partly influenced by stationary planetary wave activity, it seems likely in view of both its overall consistency and in light of more widely distributed northern hemisphere observations, that it is indicative of the trend of the zonal mean circulation. The summer to winter meridional flow in the mesosphere is consistent with the thermally driven circulation discussed in Section 5.1. The extended period of poleward flow is also to be expected on the basis of the

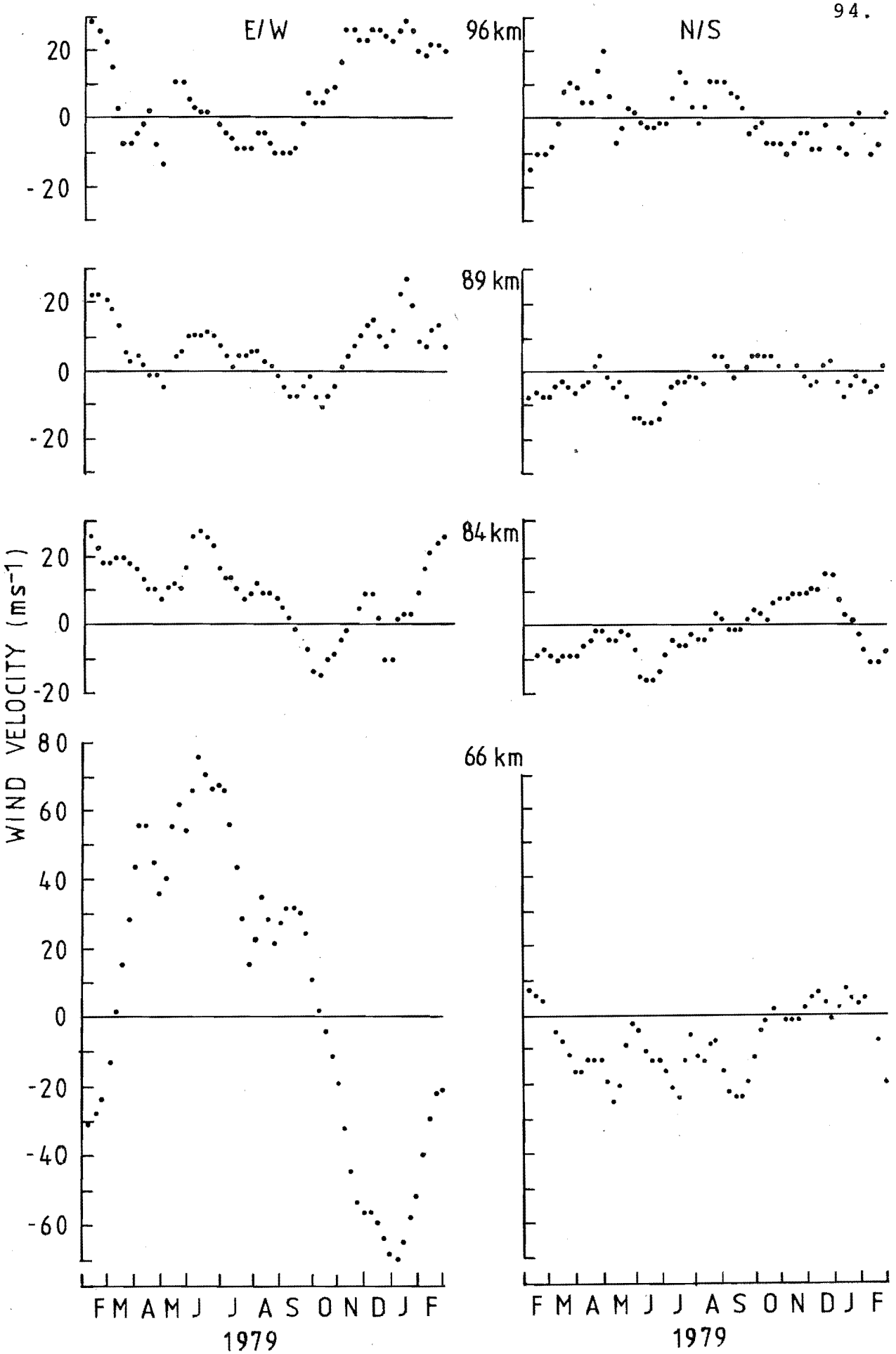

Figure 5.3: Smoothed weekly winds during 1979.

seasonal variation of a simple thermally driven circulation since at the equinoxes net heating at the equator and cooling at high latitude regions would induce a poleward flow in both hemispheres. This in turn may be expected to generate a longer period of eastward winds than westward winds (Holton and Wehrbein, 1980).

The zonal winds weaken with height and by 84 km (Fig. 5.3) the spring/summer winds are partly in the lower westward mesospheric region and partly in the upper eastward region. By 89 km the early winter winds are also characteristic of the upper region and the wind variation consequently appears to be predominantly semi-annual with two periods of westward and eastward winds. Meanwhile the meridional component only reaches significant amplitudes in mid-June, at the winter solstice, when it is directed poleward.

At 96 km (Fig. 5.3) an annual variation, out of phase with the lower region is again apparent. The meridional wind component has also reversed at this height. This upper region is consistent with the circulation pattern of return flow proposed in Section 5.1 to complete the meridional thermally direct cell in the thermosphere.

These results also support the contention of Gregory and Manson (1975) that the semi-annual oscillation in the 80-100 km region is due to the overlap of the two regions of out-of-phase annual variation. This obviates the need for a physical semi-annual generation mechanism such as proposed by Kochanski (1972).

5.3 COMPARISON WITH PREVIOUS MEASUREMENTS AT CHRISTCHURCH

Previous wind measurements were made at Birdlings Flat in 1964 by Fraser (1968). Although based on a much smaller data sample using noon 'apparent' velocities, the seasonal trend of the zonal wind was similar to the present results. The major difference was the much earlier establishment of strong summer mesospheric westward winds which penetrated from below rather than gradually descending from the upper region. They also reached much higher heights - ~ 95 km compared to ~ 85 km. The meridional component was mainly poleward except for a reversal in the summer months in agreement with the 1978/79 results. However the magnitude of Fraser's meridional component often exceeded 60 ms^{-1}. Such unusually large speeds are not reproduced here. Wilkinson and Baggaley (1975) used the meteor radar method to measure winds at a mean height of approximately 95 km in 1971. Both components were small but equatorward winds were indicated in summer and poleward winds in winter, consistent with the flow in the mesospheric regime observed in the present results. The zonal component did not differ significantly from zero except in summer when a westward wind was observed. In contrast significant eastward winds were recorded in 1978 and 1979 near this height. The spread in height of the meteor echoes over the two out-of-phase upper and lower regions may account for some of this discrepancy.

5.4 COMPARISON WITH EMPIRICAL MODELS

5.4.1 Description of the Models

Observations of mesospheric and thermospheric winds have suffered from poor geographic and height distribution making the formulation of empirical wind models difficult. Zonal mean winds were included in the COSPAR International Reference Atmosphere (CIRA) 1965 model for heights between 30 and 80 km based largely upon meteorological rockets up to 60 km and with some data above this available from grenade techniques. However, the Meteorological Rocket Network (MRN) is concentrated in North America, introducing a longitudinal bias. Kantor and Cole (1964) were able to extend the height coverage upwards with the use of data from the radio meteor method at Adelaide (35°S) and Jodrell Bank (53°N), and from chemical releases at Wallops Island (38°N) and Woomera (31°S). The low latitude region of the model above 85 km was improved by Murphy (1969) with the use of 6 nights of luminous trail data recorded at Barbados (13°N). Murgatroyd (1965) made use of E-layer drifts, meteor radar and rocket based techniques to develop latitudinal cross-sections of zonal winds for both solstice and equinox periods.

The common and dominant feature of these models is the monsoonal-type circulation in the stratosphere and mesosphere, with eastward winds in winter and westward winds in summer. Differences between the models of Kantor and Cole, and Murgatroyd, exist in winter above 95-100 km where the former model indicates a return to eastward winds above the small

region of intervening westward winds.

The mean meridional wind speed below 70 km is about an order of magnitude smaller than the zonal speeds, while above this tidal amplitudes reach very large values. These factors have hampered the measurement of the meridional component. However, Groves (1969) produced a model of both zonal and meridional monthly mean winds between 65 and 130 km at intervals of 10° in latitude and 5 km in height. In the region of 85 km there is evidence for a meridional summer to winter flow, but in general the flow is more complicated with unexpected large values occurring at times. The paucity of data in the southern hemisphere has necessitated the combination of data from both hemispheres, ignoring the differences which satellite radiance measurements have revealed. Clearly the acquisition from as wide a range of stations as possible is required.

The zonal winds of Groves (1969) have been included in a slightly changed form in the CIRA 72 model which gives winds from 85 to 130 km. This model has attempted to account for some of the hemispheric and longitudinal asymmetries below 60 km by giving separate hemispheric values in this region and also by modelling North American and European/West Asian data separately. However Groves notes that "above 105 km wind data are almost completely lacking polewards of mid-latitudes", and no attempt is made to give winds above 100 km at 50° or above 85 km at 60 and 70° latitude. The CIRA 72 and Groves (1969) models differ in the strengths of the summer and winter jets and in the upper level summer winds.

5.4.2 Observed and modelled height profiles

For the purposes of comparing model wind values and observations made at Birdlings Flat, mean monthly height-velocity profiles have been formed. The model zonal winds are taken from CIRA 72 and the meridional winds are from Groves (1969). The values have been linearly interpolated to find the values at 45° latitude and for the middle of each month (Fig. 5.4). The sign of the meridional winds has been altered for the southern hemisphere.

The partial reflection data are given at 2.5 km height intervals and have not been smoothed (apart from the inherent effect of finite pulsewidth) in order to indicate the consistency (or otherwise) of the height profiles. Discontinuities in the profiles are possible if reflecting layers exist at strongly preferred heights over extended lengths of time. It should be born in mind that data below 80 - 82 km is only obtained during the day. The number of drift values contributing to each height, ranges from 150 to 550 below 80 km, and from 550 to 1350 above 80 km. Representative error bars (standard errors of the mean) are shown on a few profiles to indicate the magnitude of day-to-day fluctuations over the month and experimental uncertainties. The zonal values are largest at the lower heights, especially in summer when the partial reflections are weak, being typically 10-15 ms^{-1}. The meridional values are significantly smaller, typically 5-10 ms^{-1}.

Figure 5.4a: Monthly mean velocity-height profiles (—— 1979, ••• 1980, --- CIRA 72 and Groves (1969)).

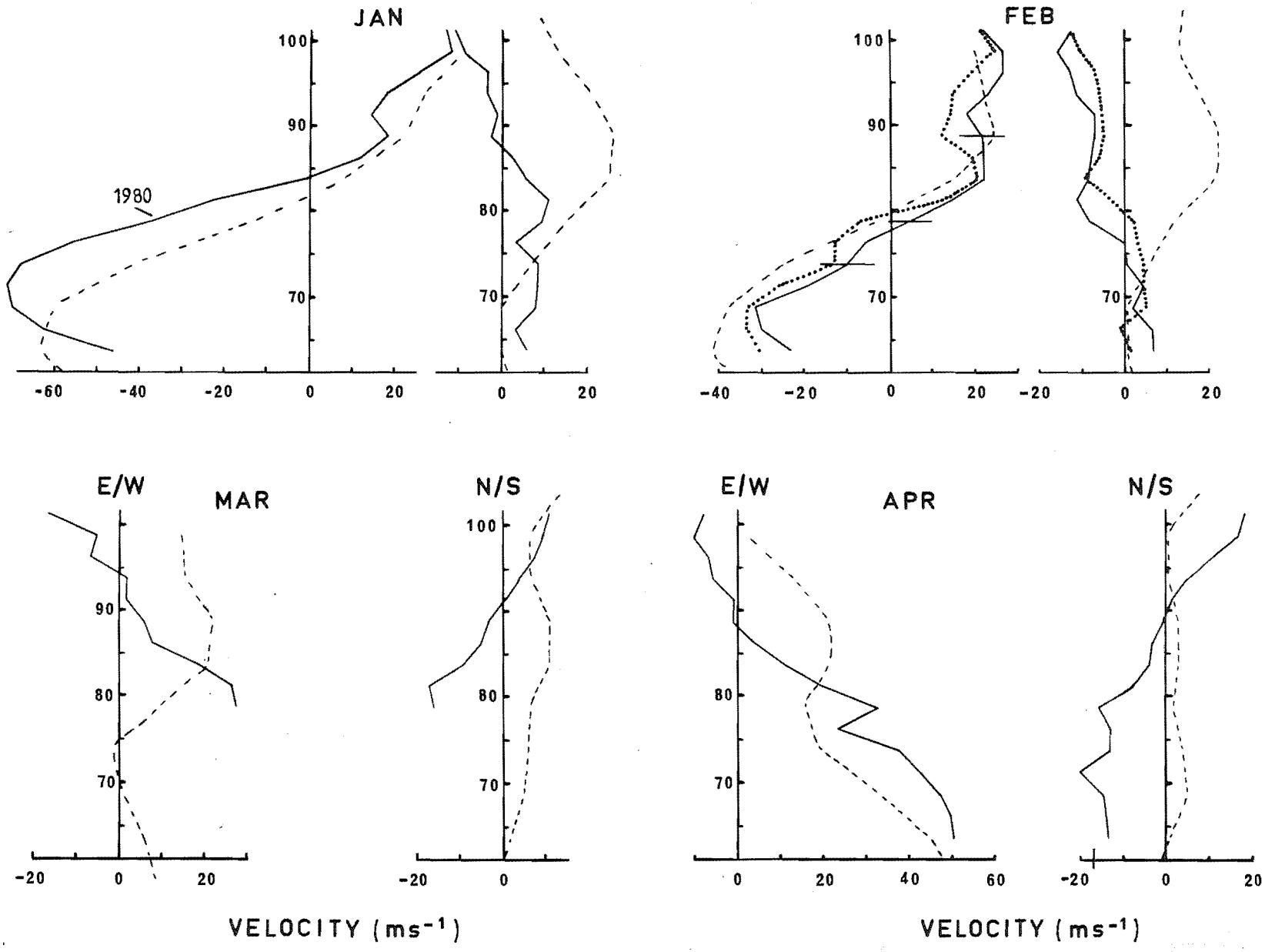

Figure 5.4b: Monthly mean velocity-height profiles. (—— 1979, ••• 1978, --- CIRA 72 and Groves (1969)).

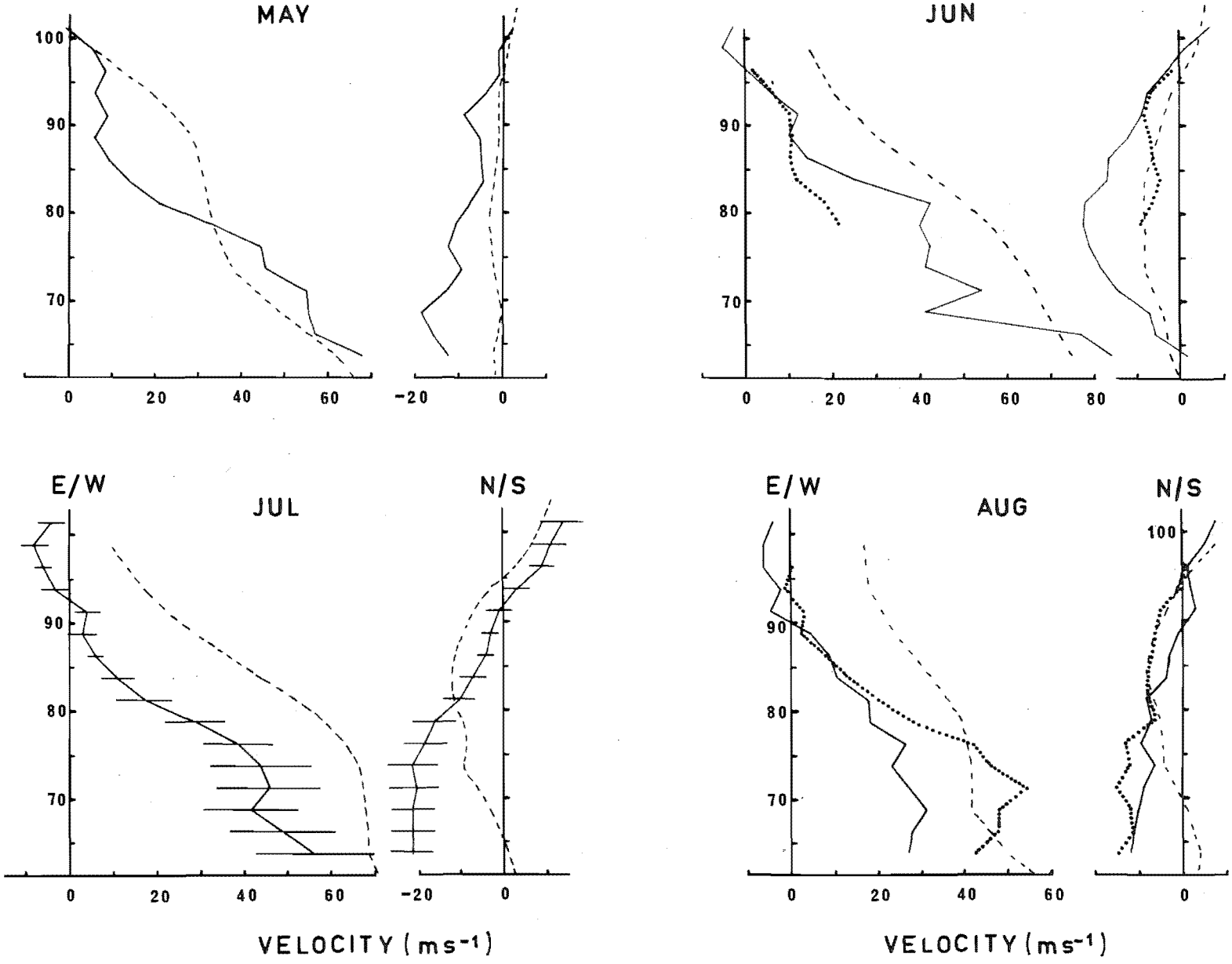

Figure 5.4c: Monthly mean velocity-height profiles. (—— 1979, ••• 1978, --- CIRA 72 and Groves (1969)).

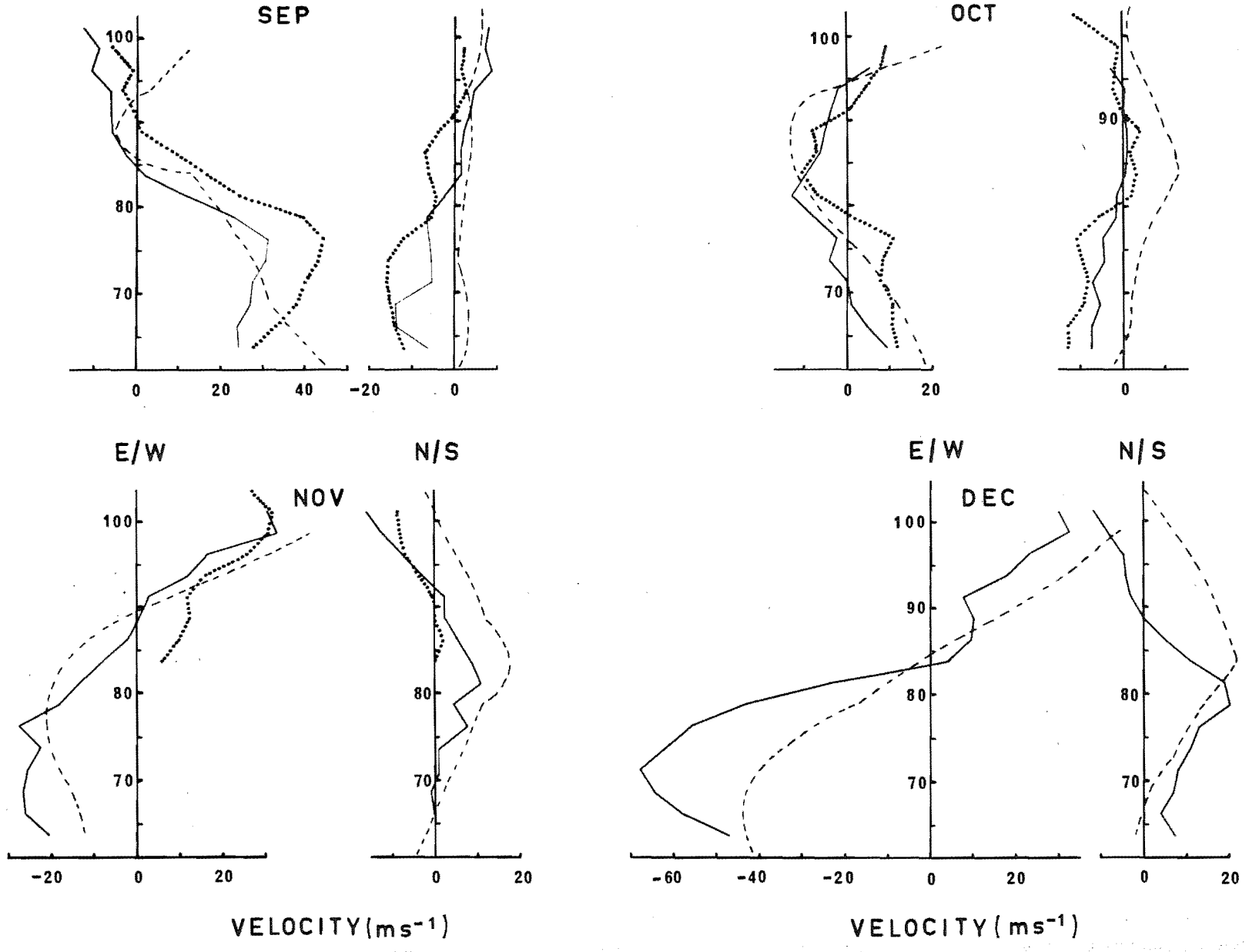

Zonal Winds

The measured summer zonal winds (December-February) show good agreement with the model above ~ 85 km and at all heights in February. The difference at the lower heights arises from the formation of the westward jet earlier in the season and at a higher altitude than the model. It is noted that Groves (1969) does give stronger values at these heights in December than CIRA 72. The consistency of the 1978 and 1979 February profiles is indicative of the relatively undisturbed conditions at this time.

The autumn months of March and April show a strong decrease in the zonal wind above 85 km at Birdlings Flat, actually becoming westward above 90 km. This feature, which was seen as a temporarily descending band of westward winds in Fig. 5.2, is not represented in the CIRA 72 results where a reversal does not occur until ~ 105 km. A similar temporary transition to westward winds has been observed in LF drift measurements at 90-100 km, 51°N, by Sprenger and Schminder (1967) and Schminder and Kürschner (1979). They have termed it the 'autumnal anomaly' and also found an accompanying change in the phase of the semidiurnal tide. No such tidal phase change was seen at Birdlings Flat however (Fig. 7.5). The contour diagram of Fig. 7.2 indicates that winds become more westward at the end of April throughout the mesosphere as well.

In general, the measured winter winds (June - August) are more westward than those of the model, particularly above

80 km. The August results indicate the considerable variability that can occur from year to year. The variations in the mean flow which resulted in the lower monthly mean wind in 1979 can be seen to have had most effect below about 77 km; above this the winds for both years agree well.

During September the winds appear to weaken at the lowest heights, leaving a maximum in the wind profiles for both 1978 and 1979 near 75-80 km. This behaviour is more in accord with the 1969 model than CIRA 72. Apart from this and the later development of the eastward winds observed above 95 km, the spring period is in excellent agreement with the model.

Meridional Winds

The observed meridional wind in summer is directed equatorward up to a height of 80 - 90 km, where a circulation of opposite sense is encountered. The two years of February data are quite consistent in this respect. This behaviour is quite different to that of the model of Groves (1969) in which equatorward winds reach peak values near the mesopause at 85 - 90 km and poleward winds are not evident till much higher heights.

The winter results are in much better agreement. However, the poleward flow below 90-100 km at this time appears to extend to lower heights than the model and is more consistent with simpler opposing cellular flow above and below 90-100 km.

As discussed in Section 5.2, the mesospheric poleward flow persists well into the equinoxes. This is in contrast to the model meridional wind which is much more symmetrical with respect to season. Differences with the model at the equinoxes above 90 km are relatively small.

5.4.3 Discussion

The extent to which differences between the present observations and the model values is due to the influence of hemispheric and longitudinal differences is unknown. However, it is worthy of note that above 85 km in summer, when large differences in meridional winds are found, stationary waves receive their maximum attenuation (Section 6.2). In addition, in winter and at the equinoxes above 90 km, when the agreement is quite good, stationary waves are able to penetrate the stratospheric wind barrier with relative ease.

Elford (1976) also found considerable variability from year to year. A solar cycle modulation of the winds around 95 km was established by Sprenger and Schminder (1969) and recently also found at lower levels in the mesosphere at Saskatoon (Gregory, 1979; 1980, private communication). Such a dependence has not been included in the wind models. A high latitude auroral source of heating which is strongly dependent on solar cycle has been postulated by Dickinson et al. (1975) in the thermosphere. This may possibly influence the lower thermospheric circulation, but a solar cycle dependence of mesospheric winds is more difficult to explain. The recent finding of an apparent solar cycle

modulation of the amplitude of the semi-annual oscillation in the stratosphere by Nastrom and Belmont (1980) poses a similar problem. Those authors suggest that it results from ozone changes associated with magnetic storms.

5.5 SEASONAL WIND COMPONENTS

Seasonal variations in the zonal wind have been frequently decomposed in terms of harmonics of a fundamental period of one year, particularly in the stratosphere where rawinsonde and rocket data are available (Angell and Korshover, 1970; Belmont et al., 1974). A similar analysis of the present data is a useful means of comparing the winds at Birdlings Flat with lower atmosphere data and enables the accurate determination of the timing of the seasonal wind changes.

5.5.1 MEM Spectra

The irregularity of the zonal wind in winter and the shortness of the mesospheric summer wind regime relative to that of winter (Fig. 5.3) indicate a substantial contribution from frequencies higher than 1 yr^{-1}. The length of the 1979 weekly data series (56 points) is not sufficient to give useful frequency resolution of such contributions from a classical spectral analysis. However, the Maximum Entropy Method (MEM) is more suited to time series which are short in comparision to the predominent periods present (Ulrych and Bishop, 1975). In order to resolve two frequencies,

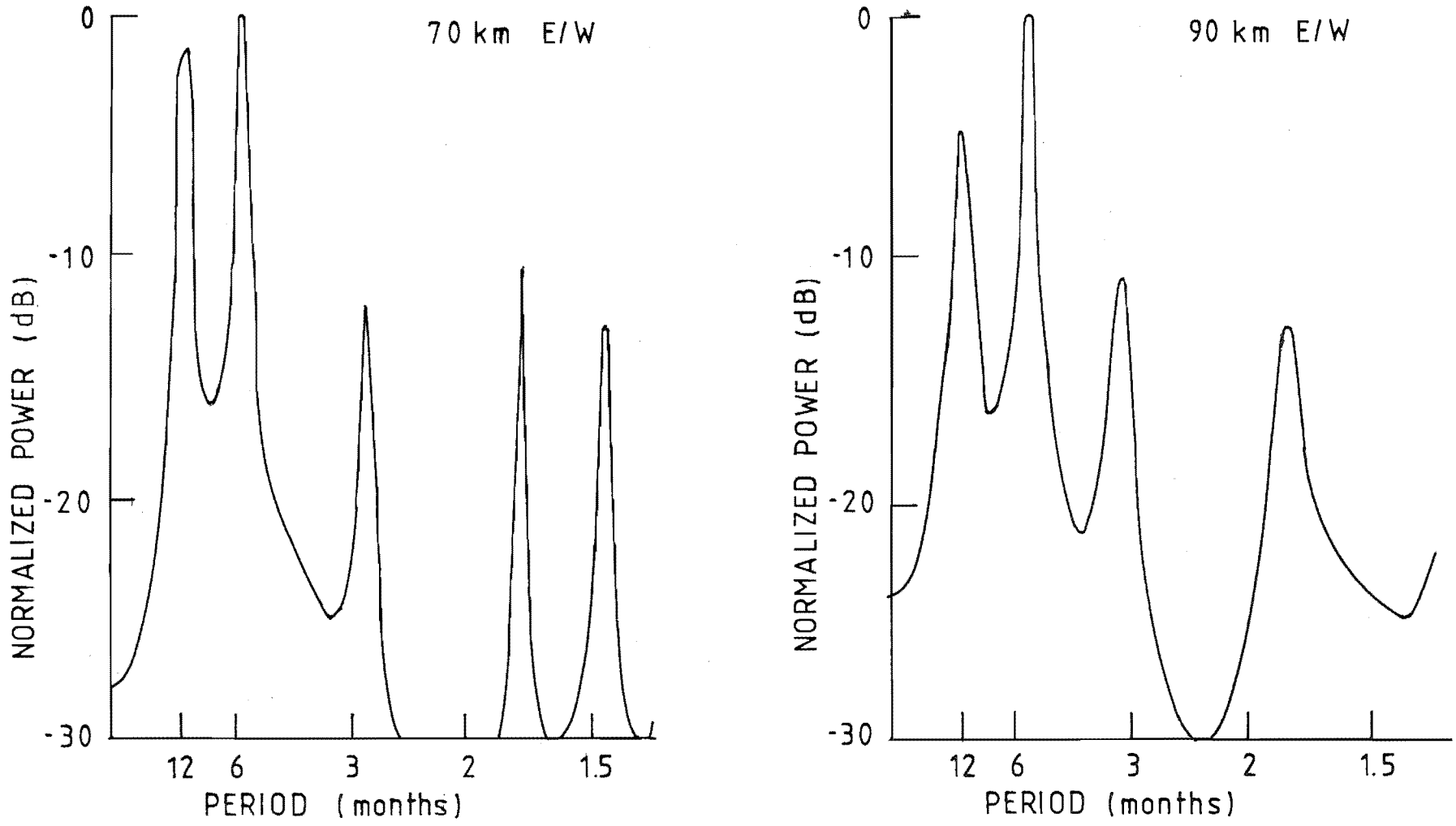

Figure 5.5: MEM spectra of 1979 weekly average zonal winds.

f_1 and f_2, the data length should be greater than $\frac{1}{f_1} - \frac{1}{f_2}$ (op. cit.). Thus in order to resolve the annual and semi-annual components, the 1979 data length is close to the resolution limit of MEM. The method is sensitive to the length of the prediction error filter, M. Although frequency resolution is improved as M is increased towards the number of data points, spurious spectral peaks can arise if M is too large (Chen and Stegen, 1974). Kane (1979) demonstrated that the lower the frequency, the larger the length of prediction error filter required, and filter lengths approaching 90% of the data length gave satisfactory results at low frequencies. A certain amount of experimentation is required to determine the optimum filter length.

The time series for 1979 shown in Fig. 5.3 were analysed with increasing filter lengths. At all heights a strong spectral peak occurred near a period of one year. However, this will be accentuated by the fact that MEM tends to show a spectral peak at the period of the data length, which in this case is close to one year. No semi-annual component could be resolved with filter lengths shorter than 50% of the data length but with greater filter lengths, periods between 23 and 28 weeks emerged strongly at all heights, with the most common period being 26 weeks. At 90 km the semi-annual peak dominated the spectrum (Fig. 5.5).

The most significant other feature which occurred at all heights was a peak near 12 weeks, suggesting that a 3 month oscillation is of importance. At 95 - 100 km this period was shifted closer to 14 weeks.

The above features were quite consistent with further increases in filter length, which only served to narrow the width of spectral peaks and give minor shifts in frequency in the low frequency portion of the spectra under consideration. These features are therefore unlikely to be spurious peaks induced by the analysis method. The 'final prediction error' given by the analysis (Ulrych and Bishop, 1975), was not found to be a satisfactory indicator of optimum filter length. A weaker peak at 16 weeks appeared below 90 km with filter lengths greater than 70% of the data length. This may be indicative of a 4 month oscillation as noted by Belmont et al 1974, but the evidence for it is more tenuous than the periods mentioned above. The spectra also showed peaks at periods shorter than 3 months, but these will not be considered here.

5.5.2 Harmonic Analysis

The MEM results indicate that the dominant seasonal spectral components are harmonics of an annual oscillation. The weekly data have therefore been subject to a weighted harmonic analysis in terms of a mean term and periods of 12, 6,4 and 3 months. The weights applied were the number of wind measurements contributing to each weekly value (Appendix C). The results are shown in Figs. 5.6 and 5.7, where the phase is the time of maximum eastward or northward velocity.

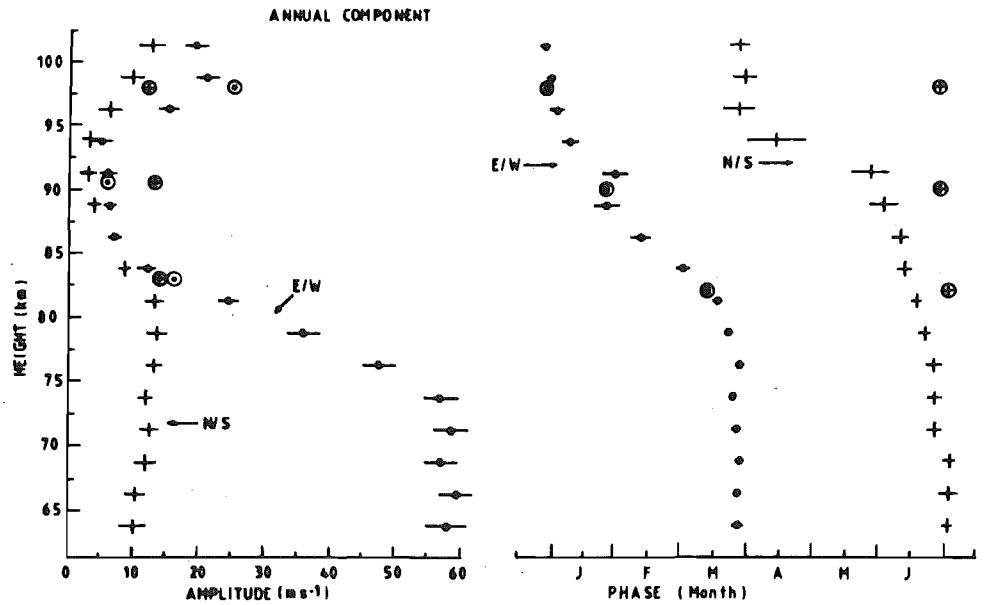

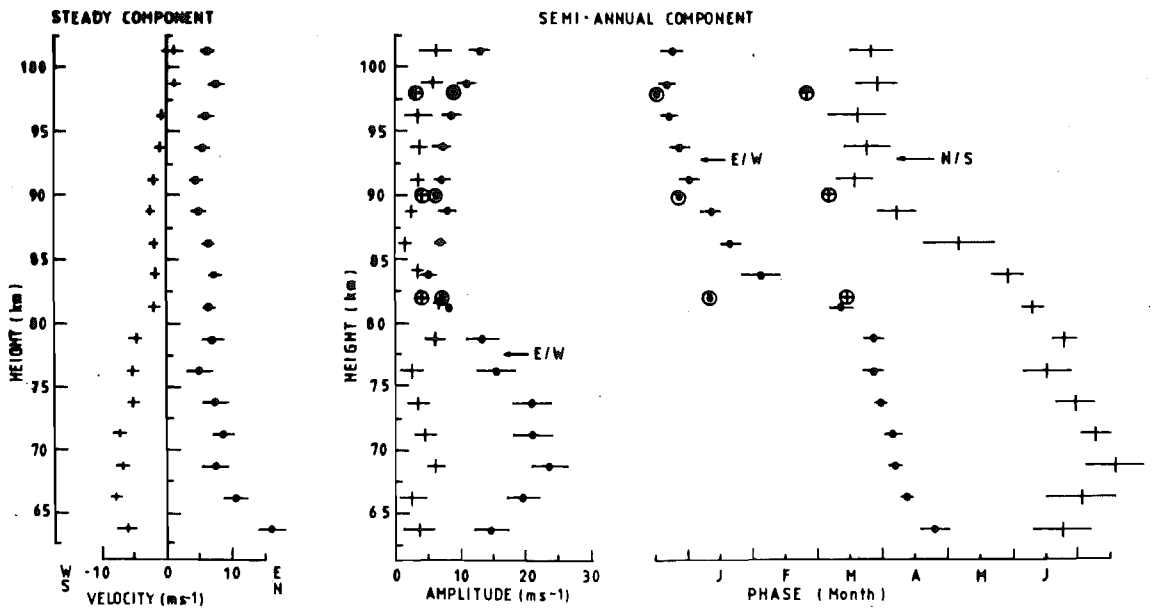

Figure 5.6: Mean, annual and semi-annual wind components.

Steady Component

The zonal constant term lies between 5-8 ms^{-1} at all heights except for evidence of an increase below 67 km. The values are similar to those found by Massebeuf et al. (1979) at 47°N but are less than one half of those found by Belmont et al. (1974) at 65 km between 1960 and 1971. The meridional component shows a slow change from southward values of -6 - -7 ms^{-1} at the lowest heights, to weakly northward values near 100 km.

Annual Component

The annual oscillation shows large amplitudes (~ 60 ms^{-1}) at heights of 65 - 75 km reflecting the strength of the mesospheric monsoonal-type circulation. This value agrees extremely well with the data compiled by Belmont et al. (1974) in contrast to a similar analysis of Saskatoon winds at 52°N (Belmont and Nastrom, 1979). The constant phase below 80 km indicates that maximum winds are reached very close to the solstices, with the zonal and meridional components 180° out of phase. This timing is also in good agreement with Belmont et al. (1974). The strength of the annual variation decreases with height, with minimum values in the 88-94 km region, while the phase undergoes a 180° phase shift by 95 km in the lower thermosphere. The annual variation of the zonal wind at Adelaide, also shown in Fig. 5.6, is very similar, but the meridional component there does not show such a large phase variation. The zonal results are in good agreement with the analysis by Groves (1972) of the model

winds although the amplitude minimum near 90 km appears lower here.

Semi-annual Component

The zonal semi-annual oscillation (Fig. 5.6) has maximum values near 70 km in early April (and October). It is likely that this is due to the strong winds which build up in early April before collapsing during the 'autumnal anomaly'. After a minimum at 86 km there is a small increase in the 86-95 km region where the oscillation is actually larger than the annual oscillation. This is in the region where westward winds are observed in two periods in the year (Section 5.2.3). The phase here is approximately 3 months (180°) in advance of the mesospheric region. These values are in general agreement with Groves (1972) below 95 km. The Adelaide results agree at 90 km and above; the difference in phase below this height is in accord with the latitudinal variation described by Groves.

Three- and Four-Monthly Oscillations

The 3- and 4-monthly oscillations (Fig. 5.7) are both small in amplitude. The 3-month oscillation shows a steady advance of phase with height in the zonal component, while the much smaller meridional component is more erratic. The eastward component of the 4-monthly (terannual) oscillation only reaches appreciable amplitudes in the 70-77 km region. The phase is fairly constant throughout but differs significantly from the values in Belmont et al. (1974) at

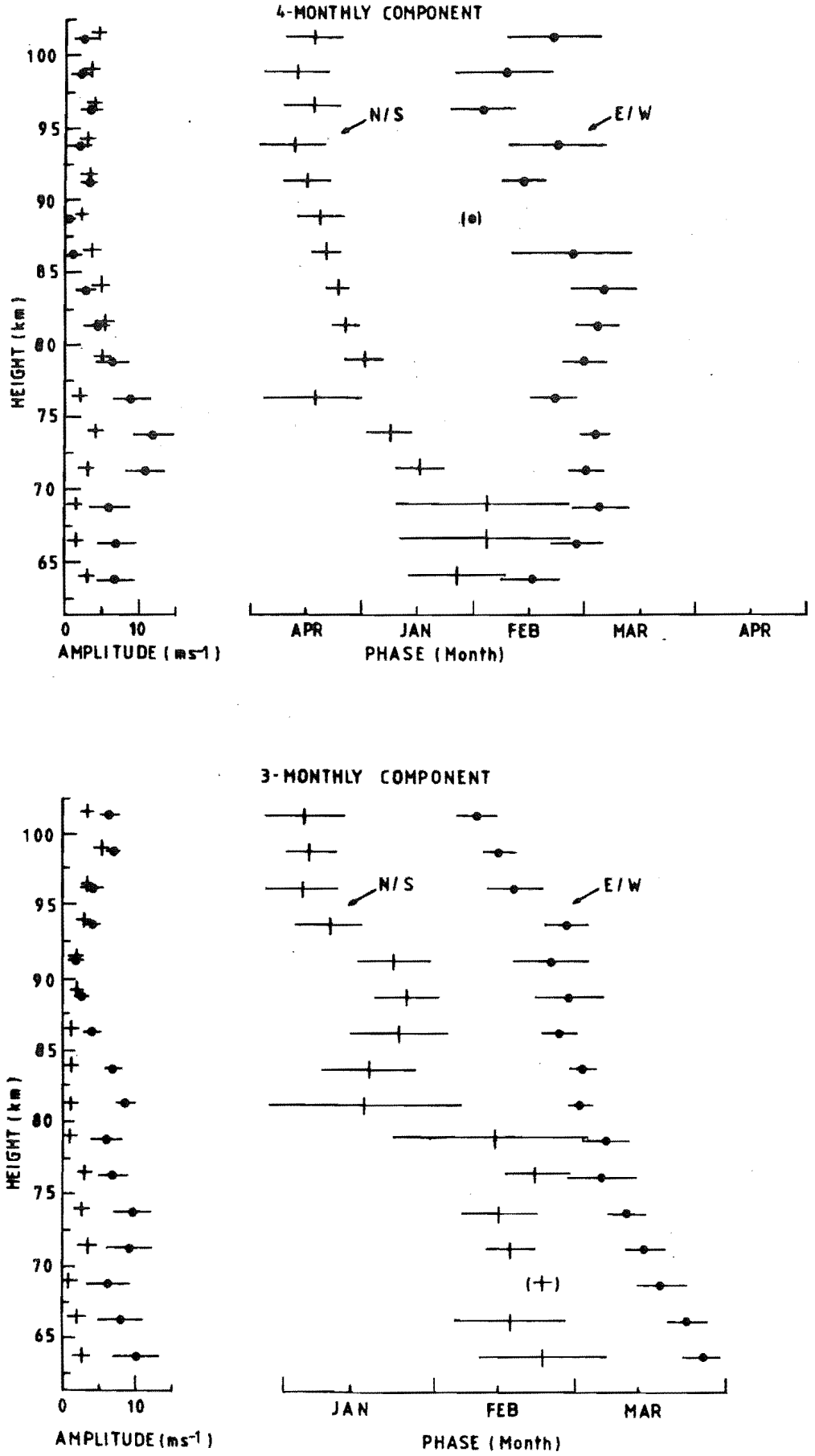

Figure 5.7: 3-monthly and 4-monthly wind components.

65 km. Those authors suggested that at high latitudes it represents the third harmonic of the annual wave due to the square wave form of the high latitude solar input function, in which case it would lag the fundamental annual wave by 2 months. Massebeuf et al. (1979) found such a relationship at Garchy (47°N) but the timing of the first maximum of the eastward wind near the beginning of March at most heights at Birdlings Flat is difficult to reconcile with this theory.

5.6 THE THERMAL WIND

The zonal wind profiles can be used to obtain information about the meridional temperature gradient. The geostrophic wind equation, the equation of state and the hydrostatic equation can be combined to give the thermal wind equation in altitude coordinates:

$$\frac{\partial u}{\partial z} = - \left(\frac{g}{fT}\right)\frac{\partial T}{\partial y} + \frac{u}{T}\frac{\partial T}{\partial z} \qquad (5.5)$$

where u is the zonal wind velocity, y and z are meridional and vertical coordinates, and T,g and f are temperature, acceleration due to gravity and the Coriolis parameter ($2\Omega \sin\theta$).

When the gradient of temperature is taken along a constant pressure surface, the second term on the right-hand side disappears. In practice it is small anyway, since $|\frac{g}{f}| \sim 10^5$ while $u\frac{\partial T}{\partial z}$ is 2 to 3 orders of magnitude

smaller. The zonal wind shear, 'the thermal wind', is therefore proportional to the meridional temperature gradient, with a positive thermal wind indicating warmer temperatures towards the equator than towards the pole.

Figure 5.8: Meridional Temperature Gradients. Hatched areas denote a cool poleward region.

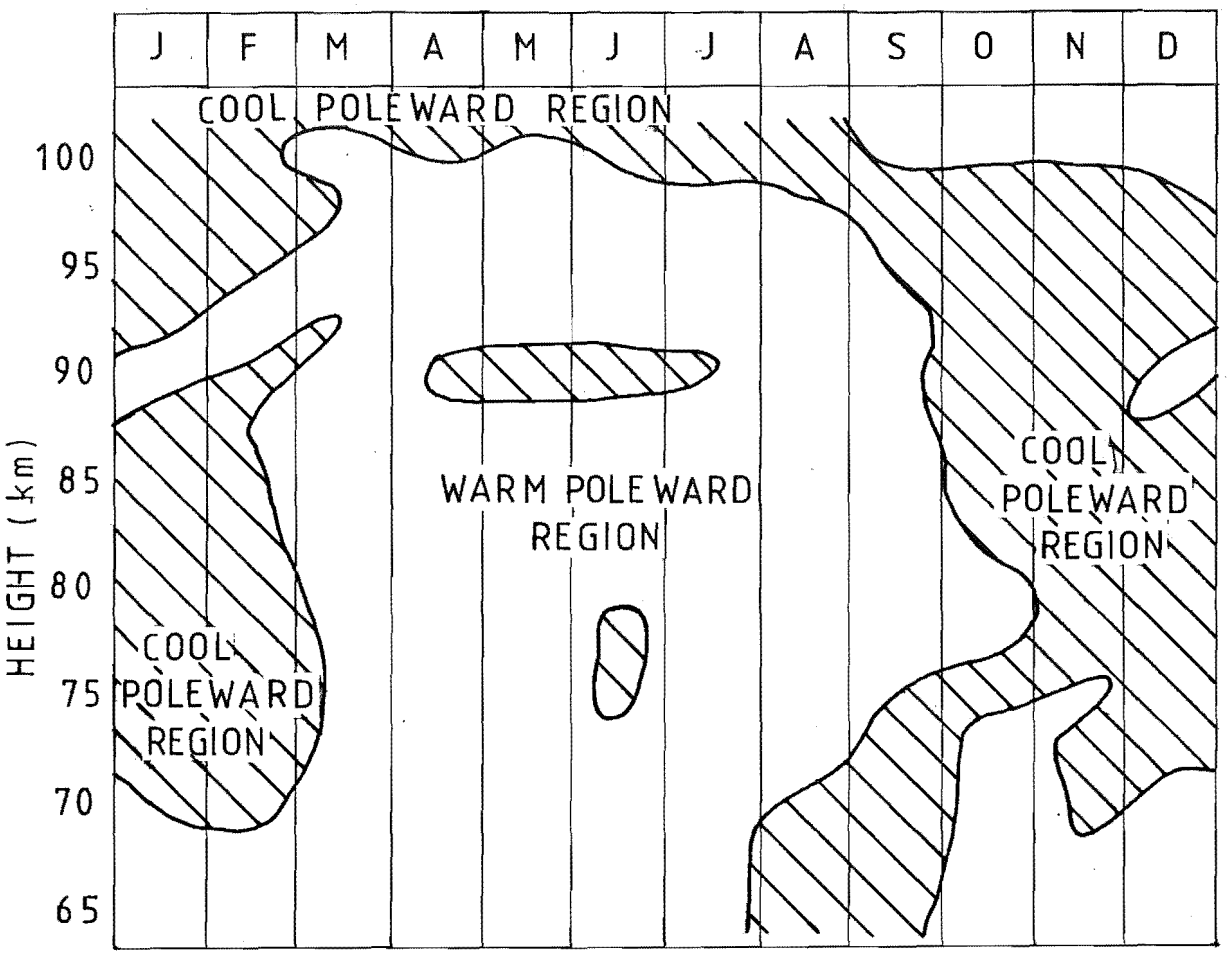

The sense of the poleward temperature gradient has been determined for each month from the profiles of Fig. 5.4, and is shown in Fig. 5.8. In winter a poleward temperature gradient is indicated at all heights up to nearly 100 km.

These conditions also encompass most of the autumn period. In summer, the gradient is reversed above ~ 70 km with cooler temperatures towards the pole. This summer state can be seen to commence in late winter at the lowest heights and penetrate slowly upwards during spring. Below 70 km and above 100 km in summer, the temperature gradient is again poleward.

These conditions are consistent with an upper mesosphere which is warmer in winter than in summer as has been observed by direct rocket sounding measurements (CIRA 72). The agreement with the CIRA 72 temperature model extends to the existence of a warm poleward region in summer below 70 km, but unlike the present results, the model does not depict the short-lived gradient reversal in August-September at these heights.

CHAPTER 6

LONG PERIOD WIND OSCILLATIONS

6.1 INTRODUCTION

Planetary waves are a major factor in the dynamics of the lower atmosphere. Rocket soundings and recent satellite measurements indicate that these waves may extend into the mesosphere. Ionospheric measurements have also shown the presence of long period oscillations. The present chapter studies long period oscillations in the winds of the upper mesosphere and lower thermosphere. Section 6.2 firstly provides a theoretical background upon which later discussion of results will be based. The importance of the measured long period wind oscillations, as determined by their energy densities, is examined in Section 6.4 in terms of seasonal and height variations. In Section 6.5 spectral analysis techniques are used to delineate the periods of importance in the 65-100 km region and their possible association with free modes of oscillation of the atmosphere. One such mode, the 2-day wave, appears as a major feature in summer; it is discussed in Section 6.6. Finally, an association between waves and circulation changes in the stratosphere and in the D-region is shown, with a magnetic storm appearing as an apparent cofactor on one occasion.

6.2 REVIEW OF PLANETARY WAVE THEORY

Long period, planetary scale atmospheric waves which depend on the earth's rotation for their existence, are commonly called Rossby waves. They take their name from Rossby (1939) who considered the waves caused by a disturbance from geostrophic equilibrium on a simple two dimensional, non-divergent beta-plane. The use of a beta-plane approximation is a simplification which ignores the complicated geometrical effect of the earth's curvature while retaining its dynamical importance. The Coriolis parameter $f(\equiv 2\ \Omega \sin \theta)$ is then assumed to vary linearly in the northward y direction such that $\beta \equiv \frac{\partial f}{\partial y}$ is a constant. Here Ω and θ are the earth's rotation rate and latitude. The conservation of absolute vorticity gives rise to wave motion with the following dispersion relation:

$$c = \bar{u} - \frac{\beta}{k^2} \qquad (6.1)$$

where c is the speed of the wave in the zonal (x) direction, $\bar{u}$ is the background zonal wind speed and k is the horizontal wavenumber. The largest scale waves will have the greatest speeds and will always move westward with respect to the background wind. Haurwitz (1940 a,b) extended the work by confining the wave within lateral boundaries and later by considering the nondivergent vorticity equation on a sphere. The imposition of boundaries in both cases limits the phase velocity (and period) to discrete values. A comparison with

observed tropospheric travelling wave motions by Eliasen and Machenhauer (1965) showed similar but somewhat smaller velocities to those predicted. The discrepancy was shown by Diky and Golitsyn (1968) to be due to the assumption of atmospheric nondivergence (i.e. incompressibility). Rossby waves stationary with respect to the earth's surface ($c = 0$) are also important because of their strong forcing by topography and land-ocean termal contrast.

The theoretical understanding of planetary scale waves was considerably advanced by the work of Charney and Drazin (1961). Under an approximation of quasi-geostrophic balance they derived a vertical wave equation of the form:

$$\frac{d^2G}{dz^2} + n^2G = 0$$

where G is related to the wave field variables. The effective 'refractive index' for vertical wave propagation, n, determines whether vertical propagation of wave energy is permitted. The simplest case they consider is for waves on a beta-plane in an isothermal atmosphere with constant background wind speed in the vertical. Then the vertical wave equation gives

$$n^2 = -\frac{N^2}{f^2}\left\{(k^2 + \ell^2) - \frac{\beta}{\bar{u}-c}\right\} - \frac{1}{4H^2} \qquad (6.2)$$

where N is the Brunt-Vaisälä frequency of the undisturbed atmosphere, k and ℓ are the zonal and meridional wavenumbers, and H is the atmospheric scale height. In regions of positive

n^2, there will be vertical propagation with a vertical wave number equal to n, while when n^2 becomes negative wave energy will be reflected. The conditions for vertical planetary wave propagation are then:

$$0 < \bar{u} - c < u_c \tag{6.3}$$

where

$$u_c \equiv \beta/\{(k^2 + \ell^2) + f^2/4H^2N^2\} \tag{6.4}$$

The condition that the waves travel westward with respect to the zonal wind ($0 < \bar{u} - c$) will restrict the penetration of stationary or eastward waves in the summer westward winds, but allow a wide range of westward, stationary and eastward waves in the winter eastward winds. These waves in winter are restricted however, by the condition that $\bar{u} - c < u_c$, which, with typical values of u_c of 40 m/s will clearly inhibit fast travelling westward waves. The value of u_c increases with increasing horizontal scale of the waves, so that in winter small scale waves are excluded the most strongly. In fact Charney and Drazin showed that the strong winter eastward winds in the stratosphere and lower mesosphere will exceed the value of u_c resulting in the trapping of even the large scale stationary waves. This led them to conclude that stationary waves, of large scale, will propagate upwards from the troposphere only at the equinoxes when the eastward winds are moderate.

Observations of stationary planetary waves support this theory in summer, but in winter wave activity is observed to

be stronger than during the equinox periods (McNulty, 1976). Possible reasons for this were investigated by Dickinson (1968a, 1968b). He found that a spherical geometry, rather than a mid-latitude beta-plane, allowed further propagation of large scale waves in winter and also that the variation of zonal winds with latitude guided the stationary waves into wave ducts of weak eastward winds. One of these was between the pole and the strong stratospheric jet. The other, equatorward of the jet, was bounded by a singular zero wind line near the equator where absorption of wave energy was expected to occur. Simmons (1974a) considered more realistic wind profiles and found that the curvature of the wind profile near the jet resulted in a more positive refractive index in this region, and hence permitted propagation in the strong winter eastward winds.

The studies mentioned above have been concerned mainly with stationary waves because of their obvious source of thermal and tropospheric forcing. Observations have confirmed their importance in the stratosphere. However, when only observations at a single location are available, the stationary waves will contribute to the measured local background conditions and only travelling waves will be directly observable. A mechanism for forcing the travelling waves is not so obvious as for stationary waves, although Hirota (1971) has suggested the dynamical interaction of the tropospheric zonal flow with baroclinically unstable waves. In the absence of any well known source of forcing, attention is turned to atmospheric free modes of oscillation which receive

their excitation from the atmospheric "noise" (Geisler and Dickinson, 1976).

Although many of the dynamical properties of these waves can be obtained from a limited beta-plane model, their global extent means that they are more naturally formulated in full spherical geometry. The mathematical formalism for free modes dates back to Laplace (1799) who investigated oceanic tidal oscillations. The linearized primitive equations as applied to atmospheric tidal oscillations are given in Appendix D. For free oscillations the same equations apply except that the thermal forcing (J) is set to zero. In the absence of background winds and viscosity, and assuming periodic motion zonally and with time, the equations are separable into a vertical structure equation involving only the vertical coordinate, and into a horizontal equation - Laplace's Tidal Equation - involving the horizontal co-ordinates (e.g. Siebert, 1961). For free oscillations the appropriate boundary conditions for the vertical structure equation are:

(1) Zero vertical velocity at ground level.

(2) For evanescent solutions, the amplitude should decay rather than grow with height. For propagating solutions, energy should be propagated upwards only (the "radiation condition").

The vertical wave equation has an effective refractive index, Q, given by:

$$Q^2 = \frac{1}{Hh_n}\left(\kappa + \frac{dH}{dz}\right) - \frac{1}{4H^2} \qquad (6.5)$$

where, in tidal terminology, h_n is called the 'equivalent depth' (of a thin ocean on a sphere) and is related to the separation constant.

$\kappa = (\gamma-1)/\gamma$, where γ is the ratio of specific heats

The vertical structure equation, together with the boundary conditions can be solved to find h_n. For an isothermal atmosphere it is found that the only value of h_n that exists is $h = \gamma H$. For an isothermal atmosphere with a temperature of 244 K, h = 10 km. The exact value of h will depend on the model temperature, and the use of realistic temperature profiles may yield additional values. However, a variety of models indicate that the atmosphere has a single dominant equivalent depth and its value is very close to h = 10 km (e.g. Kasahara, 1976; Lindzen and Blake, 1972). Substitution of h = 10 km into (6.5) shows that Q^2 is less than zero. Thus the free oscillations of an isothermal atmosphere are evanescent in the vertical, that is, only external modes exist. However, despite this energy decay with height, the exponential decrease of atmospheric mean density results in an increase of wave amplitude which proceeds as $\exp(\kappa z)$ in the vertical z direction. Such vertical behaviour is characteristic of the Lamb mode, familiar at acoustic frequencies, which has zero vertical velocity at all heights. This mode is of special interest since in an isothermal atmosphere it automatically satisfies the boundary conditions listed earlier.

Having obtained the value of the separation constant, Laplace's Tidal Equation can now be solved as an eigenvalue problem for the frequencies of the atmospheric free modes. The eigenfunctions were found by Hough (1898) in the form of a series of associated Legendre polynomials (the Hough functions). They have more recently been evaluated and tabulated over a range of equivalent depths by Longuet-Higgins (1968). The solutions fall into two classes. Those of the first class are eastward and westward propagating gravity waves, while those of the second class are the westward propagating rotational waves which can be identified with the Rossby waves discussed earlier. The gravity wave solutions did not appear in beta-plane models due to their exclusion by the use of the quasi-geostrophic approximation. Eigenfrequencies for wavenumber 1 westward propagating free modes of oscillation are shown in Fig. 6.1. The frequencies of the free modes in an atmosphere with a 10 km equivalent depth can be read directly from the diagram. The periods of the principal modes are given in Table 6.1 where the indices m and n refer to the zonal and meridional wavenumbers respectively. These periods correspond to the Rossby periods in a horizontally divergent atmosphere on a sphere with no zonal flow.

The zonal and meridional components of the wave perturbation velocity are related to the latitudinal derivatives of the Hough functions and Salby (1979) showed that they are in phase quadrature. Examples of the latitudinal structure of two of the important rotational modes are shown in Fig. 6.2

Table 6.1: Periods in days of atmospheric free modes (i) in an atmosphere with h = 10 km (ii) in realistic solstice and (iii) equinox conditions as determined by Salby (1980c).

m \ n-m	0			1			2			3		
	(i)	(ii)	(iii)	(i)	(ii)	(iii)	(i)	(ii)	(iii)	(i)	(ii)	(iii)
1	1.2	1.19,1.22	1.21	5.0	5.2	5.3	8.3	8.5	9.4	12.5	15.2	16.4
2	1.6	1.64,1.6	1.76	3.8	4.2	4.2	6.0			8.8		
3	2.1	2.18	2.15	3.7			5.6			7.7		

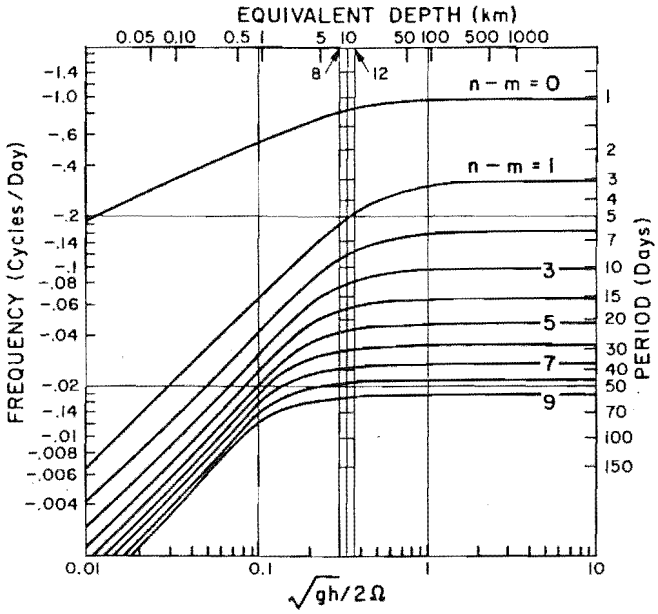

Figure 6.1: Eigenfrequencies of wavenumber 1 rotational free modes as a function of h and latitudinal scale (from Madden, 1979).

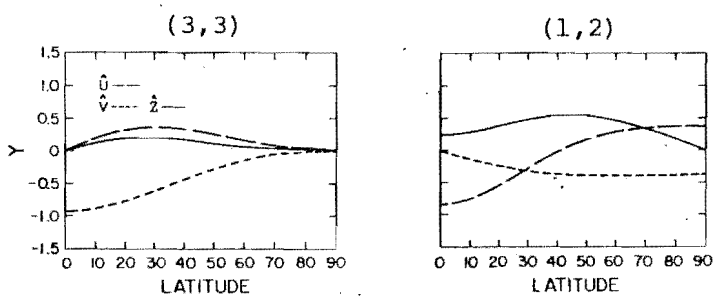

Figure 6.2: Latitudinal structures of rotational waves (from Kasahara, 1976).

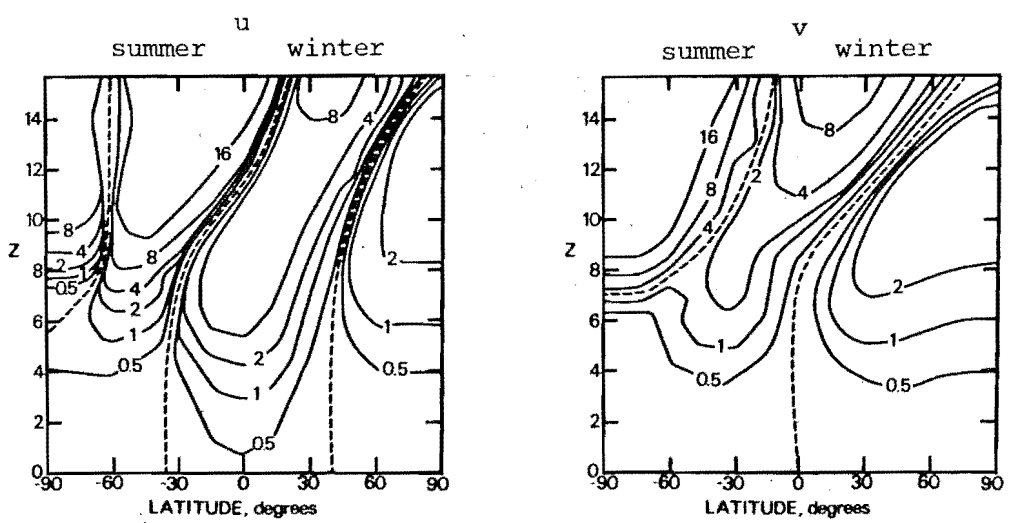

Figure 6.3: Amplitude (ms^{-1}) of zonal and meridional velocity components of the 5-day wave (from Geisler and Dickinson, (1976). Altitude in scale heights (~ 7 km).

from Kasahara (1976). In a baratropic model this structure is invariant with height. The modes with n-m=0 are often referred to as mixed Rossby-gravity modes and are characterized by a large meridional and zero zonal perturbation velocity at the equator (Matsuno, 1966). The n = 3, m = 3 mode (henceforth denoted as the (3,3) mode) with a period of 2 days is one such mode. It can be seen in Fig. 6.2a that at certain latitudes one velocity component may pass through an amplitude mode with an accompanying 180° phase change. Observation of whether u leads or lags v at a particular latitude may prove to be a useful means of distinguishing modes with similar eigenfrequencies.

Salby (1979) extended this work with the inclusion of a realistic vertical temperature profile. By relaxing the condition that the vertical velocity must exactly vanish at the earth's surface, he found a strong atmospheric response at an equivalent depth of 9.6 km and also a weaker response at h = 5.8 km. The first solution was associated with the Lamb structure modified by the variation in temperature; it showed an exponential decay of energy away from the earth's surface. However, unlike the isothermal case, phase propagation was found above 95 km indicating an upwards leakage of energy. Salby interpreted the h = 5.8 km solution as a mode ducted near the stratopause by the temperature structure. The effect of realistic dissipation on the free modes was investigated by Salby (1980a). Dissipation introduced a slow phase propagation with height to the Lamb solution, with an accompanying enhanced vertical leakage of

energy. If a wave is excited by an impulse of energy, then dissipation will not only locally damp the energy but also increase the rate at which energy flows out of that level, giving a lower residence time at any particular height. Because of this factor, Salby considered that the modes with smallest m and n-m, should achieve the greatest amplitude at upper levels despite having shorter damping times. The thermally ducted solution was found to be insignificant if its energy source was at ground level since the energy reaching stratopause heights in the presence of damping was negligible. However, if forcing was applied at 50 km, a ducted solution with h = 6.4 km was able to largely contain the disturbance energy. Salby also found an additional response to forcing near 90 km which he attributed to trapping by the temperature structure below and by viscosity above. Both of these ducted solutions were much weaker than the Lamb structure solution.

It is clear from the simple beta-plane model of the Rossby wave (6.1) that zonal winds may have an important effect on the period of the free modes. The fastest travelling modes, those with the largest spatial scale, are expected to be the least affected. Dickinson and Williamson (1972) and Kasahara (1980) investigated the effect of latitudinally varying winds at tropospheric levels. Kasahara found the expected increase in period for all modes except for a slight decrease for the (1,2) mode, from 5 days to 4.86 days. Changes also occur in the latitudinal structure of the higher index modes. Geisler and Dickinson (1976) made a detailed numerical study of the (1,2) mode, the '5 day wave', in the presence of

Newtonian cooling and zonal winds with vertical shear. They found that the winds had little effect on the period due to a compensation by the temperature gradient at the lower boundary, but the horizontal structure was drastically changed in the upper stratosphere and mesosphere where amplification occurred in a wave cavity formed in the summer hemisphere. Their computed profiles for the zonal and meridional wave velocities are shown in Fig. 6.3. Since the 5 day wave is one of the faster travelling modes, other modes may also be expected to be severely affected by realistic atmospheric conditions, and the well defined latitudinal Hough function behaviour may be restricted to the lowest heights. The requirement for modelling each mode individually has recently been met by Salby (1980c) who examined the response of the lowest order modes at equinox and solstice conditions. He found that spatially varying mean winds resulted in the response of the modes being diffused over a broader band of frequencies, leading to a decrease in the overall atmospheric response. This effect was found to increase with the wavenumber and with latitudinal structure. He considered that the only modes that could be resolved on the basis of frequency were the first three wavenumber 1 modes, the first two wavenumber 2 modes and only the gravest wavenumber 3 mode. The periods of the free modes at solstice and equinox conditions as computed by Salby are shown in Table 6.1. As with the results of Geisler and Dickinson, significant changes in the wave structure were found in the upper atmosphere. Earlier in this section it was discussed how the concept of an

effective refractive index dependent on zonal wind can give a qualitative guide to expected wave penetration. The same principal can be applied to the free modes, which, although fundamentally evanescent in an isothermal atmosphere, can have energy propagation in a realistic atmosphere. Certain wind configurations may enhance wave propagation, while others may exclude it, in which case the rate of energy decay is determined by the 'refractive index'. In accord with the earlier discussion, Salby (1980c) found that the wave energy of a low order mode, having a large westward velocity, tended to be excluded from strong eastward winds and enhanced in westward winds.

The free normal modes discussed above do not transport energy or momentum fluxes vertically or meridionally in an idealistic isothermal atmosphere. For this reason they were thought to be relatively unimportant to stratospheric dynamics compared to forced, stationary waves (Holton, 1975). However, they may have a significant contribution to make, especially at mesospheric heights, for several reasons. Firstly, their increase in amplitude with height, despite an energy decay, may result in large amplitudes in the upper atmosphere (just as the rotational diurnal tide can be of importance). Also, the summer zonal wind profile favours the penetration of westward travelling waves while strongly attenuating stationary and eastward waves even though the stationary waves receive steady forcing in the troposphere. In the extreme, realistic conditions may even form a resonant cavity in the summer mesosphere (Geisler and Dickinson, 1976).

The interaction of the travelling waves with forced stationary waves has been proposed by Madden (1975) to contribute significantly to time variations in the horizontal and vertical heat transport in the stratosphere, while Tung and Lindzen (1979) have suggested that the resonant amplification of free modes may play a crucial role in the initiation of major stratospheric warmings.

External free modes are intrinsic to a barotropic atmosphere. In a realistic baroclinic atmosphere the reflection of a vertically propagating planetary wave by the strong eastward winds in the upper stratosphere (as implied by Charney and Drazin (1961)) gives rise to the possibility of a form of free mode which is intrinsically internal. If the height of the reflection level is a multiple of a half wavelength, a standing wave can form between the ground and the reflection level; with the node at the ground satisfying the lower boundary condition for a free mode. Such internal free modes were found by Geisler and Dickinson (1975) in a beta-plane model. Schoeberl and Clark (1980) used a global spherical model at solstice conditions and found a number of resonant responses due to the strong winds. These occurred for wavenumber 1 at 15 days, for wavenumber 2 at 11 and 22 days and for wavenumber 3 at 12 days. It may be possible that such ducted free modes can leak through the wind barrier and be observed in the mesosphere.

Green (1972) suggested that unstable, short period waves may be generated locally near the winter stratopause through the mechanism of baroclinic instability. The possibility was

examined in greater detail by Simmons (1974b). He found that with a suitable eastward wind shear, instability of local significance could indeed occur in the vicinity of the stratopause. At the winter mesopause in the region of westward shear, no instability was found when even modest Newtonian cooling was included. On the other hand, Simmons (1977) found that baroclinically unstable waves with periods close to one day could develop in regions of large wind shear in the summer mesosphere.

6.3 SUMMARY OF UPPER ATMOSPHERIC PLANETARY WAVE OBSERVATION

Observations of large-scale travelling Rossby waves in the lower atmosphere have recently been reviewed by Madden (1979). The wave most readily identified as a free oscillation is the westward travelling 5-day wave. Madden and Julian (1972, 1973) and Burpee (1976) have shown that the horizontal structure of the wave is as expected for the (1,2) free mode. The amplitude growth of the 5-day wave in the lower atmosphere found by Madden (1978) is not inconsistent with the theoretical value. Rodgers (1976) tentatively identified the 5-day wave in Nimbus 5 SCR measurements at a height near 45 km. The period ranged between 4.5 and 6.2 days. Wave motions analysed by Eliasen and Machenhauer (1969) exhibited the phase speeds expected of Rossby waves and showed little phase change with height. Madden (1978) presented evidence linking a 16-day wave to the (1,4) free mode.

Satellite measurements are assuming increasing importance for observations of both travelling and stationary waves in the stratosphere. Such measurements have shown that quasi-stationary wave activity is weaker in the southern hemisphere than in the northern hemisphere (e.g. Labitzke, 1980), with a consequent increase in the relative importance of travelling waves in the southern hemisphere. This is particularly marked for wavenumber 2 which Deland (1973) found to propagate eastward in the southern hemisphere winter in contrast to the stationarity observed in the northern hemisphere. Hirota (1976) found that the penetration of travelling waves near 45 km was in broad agreement with the Charney and Drazin conditions (equation 6.3). Satellite measurements of stationary waves have been extended to 85 km with the development of the Pressure Modulated Radiometer (PMR) on Nimbus 6 (Hirota and Barnett, 1977).

Observations of planetary waves in the lower thermosphere from ground based techniques have been hampered by the difficulties involved with maintaining continuous data collection. Results from several 10-20 day meteor radar runs were presented by Clark (1975). Roper (1978) also used the meteor radar technique to obtain winds in the 80 - 100 km region on a systematic basis. Salby and Roper (1980) found regularly occurring frequencies in the power spectra of this data. They associated these oscillations with atmospheric free modes on the basis of the observed periods.

Data runs of several days to a week are more numerous and have revealed the repeated occurrence of a 2 day

oscillation in late summer (e.g. Muller and Nelson, 1978). This oscillation will be discussed in detail later.

Long period oscillations have also appeared in ionospheric measurements of absorption (Deland and Friedman (1972); Fraser and Thorpe (1976)). Oscillations in E-region virtual height have been associated with stratospheric temperature measurements by Cavalieri (1976) and Brown and John (1979).

6.4 PLANETARY WAVE ENERGY DENSITIES

6.4.1 Seasonal Variation

The day to day fluctuations of the daily mean winds in the upper mesosphere and lower thermosphere measured at Birdlings Flat (e.g. Fig. 4.3) often show variations which appear periodic, at least for limited time intervals, suggesting an identification with planetary scale waves. An assessment of the dynamical importance of these oscillations has been made from the r.m.s. deviations of daily winds from the mean for each month. In Section 5.2 seasonal trends were shown to be significant. In order to reduce the contribution from this source, a linear trend has been subtracted from each month prior to the calculation of the r.m.s. values. In making comparisons between different months it is also important that the lengths of the time series are approximately equal so that deviations for the same range of periods are compared. In the data to be discussed, 30 $\pm$ 5 days were used unless otherwise specified. Comparison of values from above

and below about 80 km may be biassed by the restriction in sampling of the latter data to day-light hours with a possible additional variation due to day to day tidal changes.

The r.m.s. amplitudes of the zonal and meridional wind components have been combined to estimate an overall $\overline{v^2}$ for the long period oscillations. The energy densities, $\rho_o \overline{v^2}$, for each month are shown in Fig. 6.4. The values of atmospheric density, ρ_o, were obtained by interpolating the CIRA 72 values to a latitude of 45^o and to the middle of each month.

The main features of the energy densities are the high values in summer and, except for August 1979, low values towards late winter. A minimum in March at the autumnal equinox also seems to occur. In general, zonal amplitudes were clearly larger than those of the meridional component. An exception to this occurred in summer above 80 km when the meridional component dominated. Figures 1-4 of Manson et al. (1979) also show largest values of long period oscillations, for 10 day samples at 90 km, occurring in summer at Saskatoon. Elford (1976) found that the summer variability in the meridional wind component was two to three times larger in summer than in winter for the years 1966-1969 at Adelaide, although there was little seasonal variability from 1969-1972.

At first sight the strong planetary wave activity in summer is somewhat surprising since satellite measurements of stratospheric radiance variations show a very pronounced minimum in summer and a maximum in winter (e.g. McNulty, 1976). However, the major contribution to such measurements is from stationary waves, which only contribute to the monthly mean wind at a

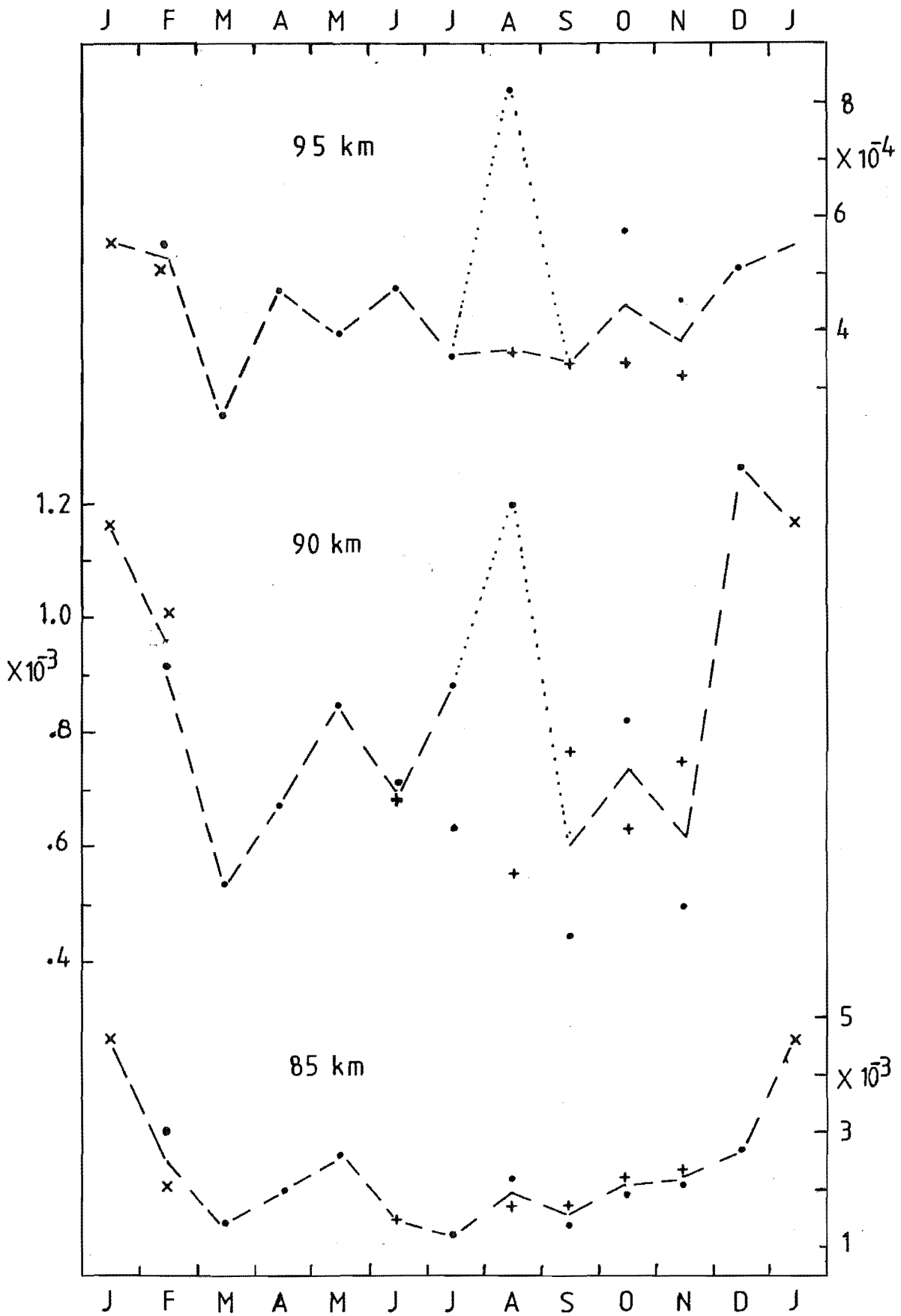

Figure 6.4: Annual variation of the energy densities. + - 1978; • - 1979; × 1980.

single station. The stratospheric variations are in qualitative accord with the restrictions on wave penetration imposed by the background winds as discussed in Section 6.2, with the exclusion of stationary waves in the summer westward winds. The present observations, however, are confined solely to travelling waves and the Charney and Drazin condition $\bar{u} - c > 0$ will allow the penetration of fast, westward travelling waves in summer. Indeed, Hirota (1976) found almost solely westward travelling waves at 45 km in summer. Above this height the summer westward winds continue to increase up to 65-70 km. This should confine the spectrum of waves increasingly to faster westward waves. This, coupled with the fact that only the lowest wavenumber waves are significant at these heights, suggests that only short period westward travelling waves will reach the upper mesosphere in summer. In contrast, in winter a wider range of periods is expected since eastward, stationary and westward waves are all able to penetrate through the stratosphere, although the condition $\bar{u}-c < u_c$ will restrict the very fast moving westward waves. The stationary waves are not directly observable here, but their centres of activity are sometimes observed to wander. Such quasi-stationary waves may show up as long time scale changes in the wind and contribute to the long period spectral variance. Fig. 5.2 illustrates the strong variations which occur in winter on time scales greater than a week. In addition to wind variations due to wave perturbation velocities, large non-periodic changes are possible through wave-mean flow

interactions. Such effects are associated with stratospheric warmings and will be considered in Section 6.7.

In order to test the likelihood that the summer energy densities are due primarily to short period waves, the time series were subject to a low pass filter and the energy densities recalculated. A simple Hanning filter was used whose amplitude response falls to a half at a period of 4 days, and to a quarter at 3 days (Appendix E). This filter is preferable to an equally weighted moving average since such a filter introduces high frequency ripples to the filtered output (Fig. E.1) The annual variation of the energy densities with short periods attenuated is shown in Fig. 6.5. Comparison with Fig. 6.4 shows that the summer values have indeed been reduced considerably more than the winter values, confirming the importance of short period waves in summer.

The atmospheric response to the short period travelling waves in summer is strong, not only in these results but also at Saskatoon and Adelaide. In seeking an explanation for these observations it is significant that the numerical models of Geisler and Dickinson (1976) and Salby (1980b) indicated that the zonal wind and meridional temperature gradient may lead to enhanced amplitudes of planetary free modes in the summer mesosphere. A further possible reason for the large summer energy densities is the presence of baroclinically unstable waves. It is shown in the next section that such waves are likely to be generated in summer near the height of reversal of the zonal wind gradient, around 70 km. Furthermore they will theoretically have short periods at this height.

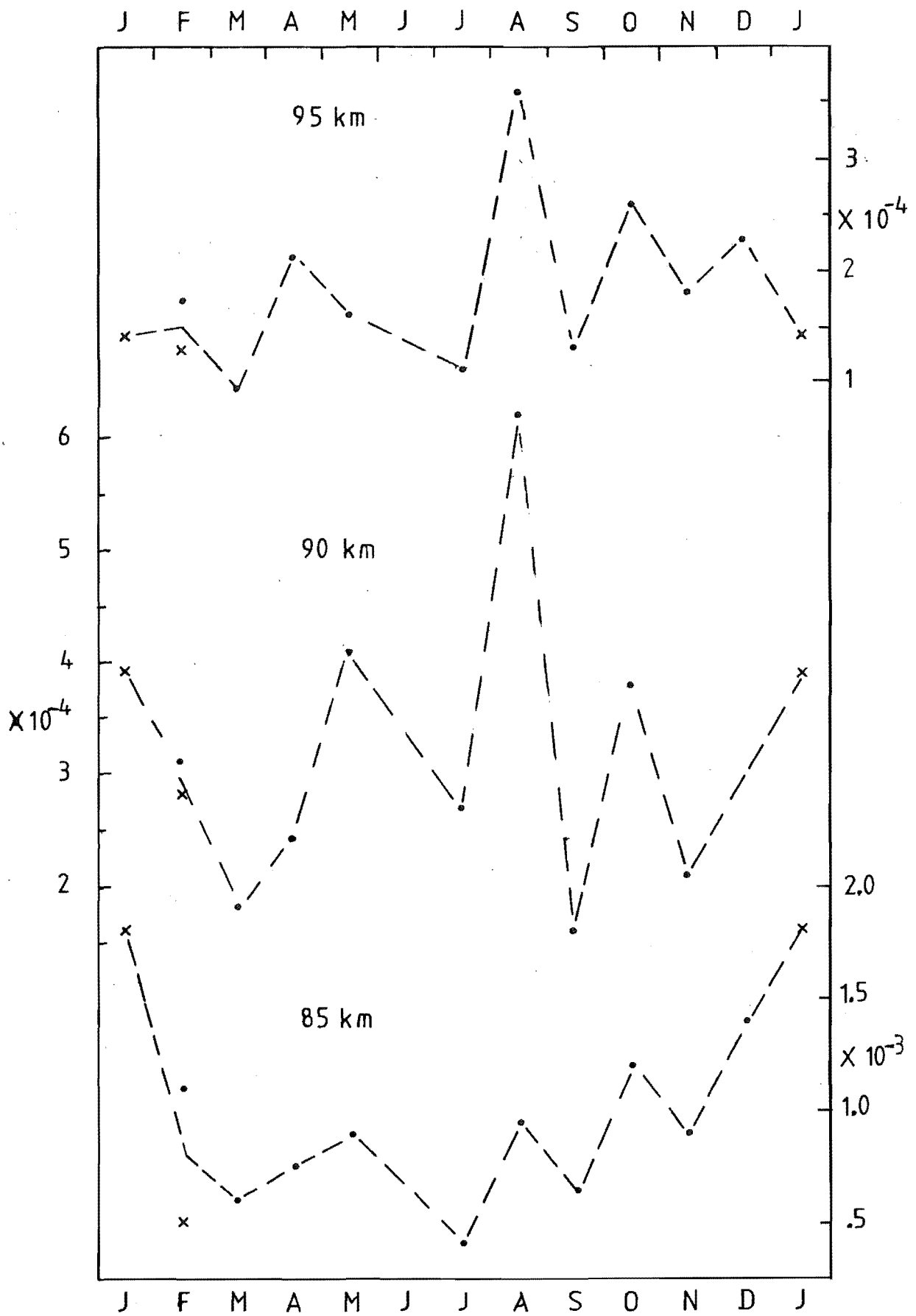

Figure 6.5: Annual variation of the smoothed energy densities.

6.4.2 Vertical Variation

The vertical structure of the long period energy densities is shown in Fig. 6.6. The energy densities decay with height above 70 km at all times. Over certain height intervals the energy densities often fall off at a constant exponential rate (e.g. autumn, Fig. 6.6). On such occasions it is convenient to parameterize the energy decay by assuming a fall off according to e^{-z/h_o} (Vincent and Stubbs (1976); Manson et al.(1979)). Such an energy density decay is predicted for rotational free modes in an inviscid isothermal atmosphere. It is also expected to occur for internal gravity waves of sufficient amplitude to have become superadiabatic. Hodges (1969) showed that the generation of turbulence by such a wave would lead to self-attenuation such as to maintain constant wave amplitude with height, and hence energy density decay with $h_o = H$.

A variety of factors will influence the rate of planetary wave energy density decay in a more realistic atmosphere. In a barotropic atmosphere, normal modes of oscillation will have an energy decay which is dependent on temperature (Salby, 1979). The atmospheric mean temperature is fairly constant with height near the mesopause but increases rapidly in the thermosphere. This increase will reduce the rate of energy decay.

Dissipation by eddy and thermal damping is important in any realistic model at these heights; both of these factors are height dependent. Since thermal relaxation times in the mesosphere become comparable to planetary wave

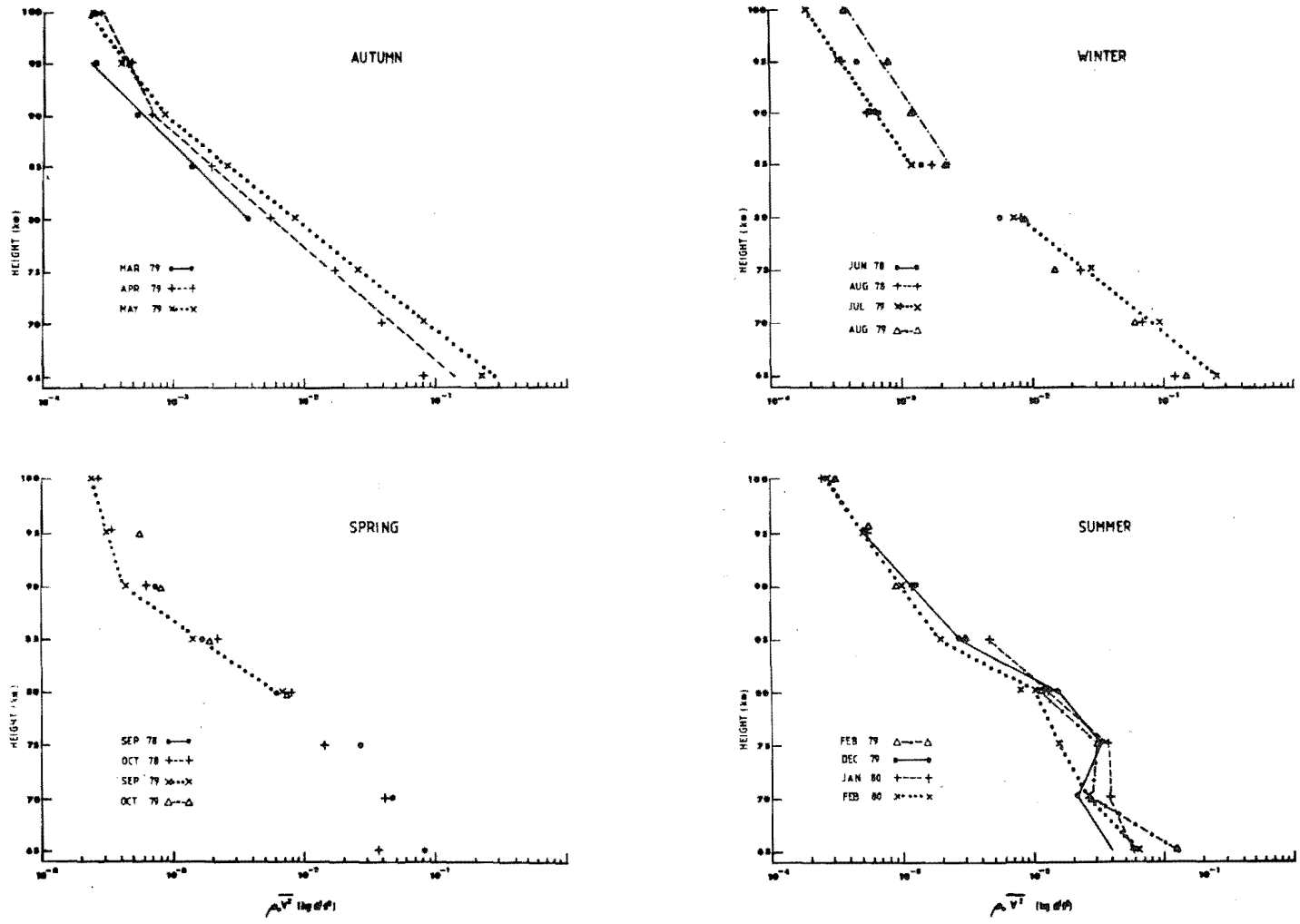

Figure 6.6: Vertical structure of energy densities.

periods, damping is likely to figure prominently in energy density decay rates. The importance of realistic wind profiles (and latitudinal temperature gradients) on amplitude growth has already been noted. Wind shear will also remove the degeneracy in vertical structure of the barotropic normal modes (the separation constant becomes frequency dependent). The composite profiles shown here will include contributions from a number of modes, each probably having a different decay rate. In the strong summer westward winds, two interesting effects may occur. Firstly, waves may be generated locally through baroclinic instability near regions of large wind shear and secondly, the westward jet may provide a critical level for fast moving westward waves. Linear models predict a trapping of wave energy just below the critical level and absorption of energy by the mean flow (Dickinson, 1970).

In view of the variety of factors involved there is ample reason to expect a departure from a simple constant exponential decay of energy density with height. However, the autumn profiles (March - May, 1979) in Fig. 6.6 exhibit a remarkably constant decay up to 90-95 km. The decay constants, h_o, for the months involved are very similar, decreasing from 5.5 km in March to 4.5 km in May, as shown in Table 6.2. At higher heights the energy fall off lessens. It is noted that the difference in the spread of data over the day above and below about 80 km does not appear to have altered the evaluation of the variances of the autumn long period oscillations. The summer values for which shorter

Table 6.2: Values of h_o (km) during 1979/1980

Ht	Mar	Apr	May	Jul	Aug
> 90 km		11.7	~ 7.5	8.2	8.5
80-90 km	5.5	4.8	4.5		

Ht	Sep	Nov	Dec	Jan	Feb
> 90 km	17		~ 6	6.6	7.4
80-90 km	3.6	3.7		4.2	

periods are more important, may be more seriously affected.

The winter months (July,August 1979) also show a change to a slower energy decay rate at the upper levels but the height at which this change occurs is 5-10 km lower than in autumn. The monthly mean wind profiles for the autumn and winter months are not significantly different (Fig. 5.4), suggesting that the influence of wind shear on the propagation conditions was not the major factor involved. Dissipation rates of turbulent energy have however been shown to have a strong seasonal variation in this height region. Roper and Elford (1963) and Roper (1966) observed large values in early autumn and late winter/early spring near 90 km. This variation of eddy damping is in the correct sense to account for the low planetary wave energy densities observed in March and late winter. Although the decay rates in July and August

are the same, the energy densities in the upper region in August 1979 are significantly larger than in July, or in August 1978. The fact that such a difference is not evident at the lower heights indicates that an explanation of increased forcing from below in August is not tenable. The mean zonal winter jet values (Fig 5.4) are significantly lower in August, 1979 than in both July 1979 and August of the previous year. Such a weakened eastward jet would theoretically allow enhanced penetration of planetary waves. The weakening of the flow may in turn be associated with a deceleration of the zonal wind characteristic of stratospheric warmings. The evidence for such an explanation is discussed in Section 6.7.

The spring profiles indicate a strong fall in energy density in the 80-90 km region, with weaker decay above. Data below 80 km for September and October 1979 were only obtained for part of the month and consequently their calculated energy densities may not merge smoothly into the upper region.

A common feature of the profiles is the slower energy density decay above a height of 85 - 90 km. This is the approximate height of the mesopause, above which the positive thermospheric temperature gradient gives rise to an increasing 'refractive index'. This may account for part of the change. The square of the refractive index for an atmosphere with an equivalent depth of 10 km has been calculated as a function of height in Table 6.3 to illustrate this point. Values of atmospheric scale height from the CIRA 72 mean reference

Table 6.3: Refractive index squared of the CIRA 72 Mean Reference Atmosphere with h = 10 km.

Height (km)	H (km)	$\frac{dH}{dz}$	n^2
75	6.15	-.06	-2.9×10^{-3}
80	5.86	-.06	-3.4×10^{-3}
85	5.57	-.01	-3.1×10^{-3}
90	5.54	-.02	-2.6×10^{-3}
95	5.75	.06	-1.5×10^{-3}
100	6.16	.1	-3.2×10^{-4}
105	6.91	.2	1.8×10^{-3}

atmosphere were used.

Zonal mean winds will also be of importance in determining the rate of energy density decay. Below a height of about 90 km, the prevailing wind from autumn through till late spring consists of strong eastward winds with a westward shear. Salby (1980b) found that such conditions tended to reduce the vertical growth of the amplitude and phase gradient of free modes in his numerical model. Above 90 km the observed winds have a very weak shear and are often westward, favouring amplitude growth. In summer, Salby's model indicates that wave amplitudes would be enhanced in the westward wind conditions below $\sim$ 85 km. The strong eastward winds which develop above this height are not so favourable. Both the background

wind and temperature structure appear likely to be important in determining the variation of wave amplitude with height.

6.4.3 Baroclinic Instability in the Summer Mesosphere

A feature of the summer profiles which does not appear at any other time of year, is the very weak decay or in fact growth of wave energy density which occurs near 70-75 km. This is in the region of the strongest westward winds where baroclinic instability would be most likely. Trapping below a critical layer is not likely to be responsible, since any associated buildup in wave energy should occur beneath the layer which, at this latitude, will be beneath this wind maximum.

Simmons (1977) found that for baroclinic instability to occur in the summer mesosphere an eastward shear in the zonal wind greater than 2 ms^{-1} km^{-1} was necessary above the westward jet and that the change in shear should occur over a small height range, typically ~ 5 km. Those figures were for a Newtonian cooling rate of 5 days. For a faster cooling rate of 1.5 d, a shear of 4 ms^{-1} km^{-1} would be required. The summer mean wind profiles (Fig. 5.4) show that the reversal in shear does occur within such a short height range. In January the eastward shear just above the reversal at 74 km is 6 ms^{-1} km^{-1}. The values in December and February are smaller - 3.6 ms^{-1} km^{-1} and ~4 ms^{-1} km^{-1} respectively. Such conditions should support growing baroclinically unstable waves, especially in January. These values

represent monthly means, so it is quite likely that on individual days conditions which are strongly baroclinically unstable may occur.

Simmons estimates that the waves will decay to half amplitude within about 15 km above the westward wind maximum, and have no phase change with height except very close to the wind maximum. The waves are therefore most likely to be observed between 70 and 90 km. The summer energy density profiles lend support to the possibility that baroclinic instability does in fact occur, since in the 70 - 75 km region constant or increasing energy densities are observed, except for February 1980.

Further expected properties of such waves are given by Simmons. The most unstable disturbance should have a zonal wavelength near 5,000 km and a phase speed close to the speed of the zonal wind. At mid latitudes with a jet maximum of 70 ms^{-1}, this implies a period close to 1 day, making the resolution of baroclinically unstable waves from the diurnal tide difficult. Even if a larger wavelength is assumed, the phase velocity will be faster in the westward direction. For example, using Simmons' largest unstable wavelength of 9000 km and the corresponding phase velocity of 2 ms^{-1} eastward with respect to the background wind, the period is found to be 1.5d. The amplitude of the waves however, will ensure their observability in the present analysis.

6.5 SPECTRAL ANALYSIS OF WIND DATA

6.5.1 Analysis Methods

A graph of hourly winds shows variations on a wide range of time scales. Generally the 12h and 24h tides dominate. In order to see the long period variations more clearly it is convenient to view the data after application of a numerical filter. The simplest form is a low-pass filter to remove the tidal frequencies. Such filtering could be achieved with repeated passes of a 3-point Hanning filter or with a moving average of suitable length. An ideal filter amplitude response will have a sharp fall off at the required cut-off frequency and negligible sidelobes beyond this point. The filter should also not alter the phase. Numerical filters which approximate this ideal through the application of a least squares technique have been developed by Behannon and Ness (1966) and are used here (Appendix E). The filters can be tailored as low-pass, band-pass or high-pass. The amplitude response of these filters can be made to roll off more sharply than the Hanning or moving average filters, and have much smaller sidelobes than the latter. The subtraction of an equally weighted moving average from the original data has been used by various workers to achieve a high-pass filter. However, this should be avoided as it has been shown (Webster and Lyon, 1975; Owens, 1978; Kennedy, 1980) that the sidelobes can produce large spurious oscillations in the filtered output.

Fig. 6.7 shows winds for March-April 1979 after application of a low-pass filter with a half-amplitude cutoff at

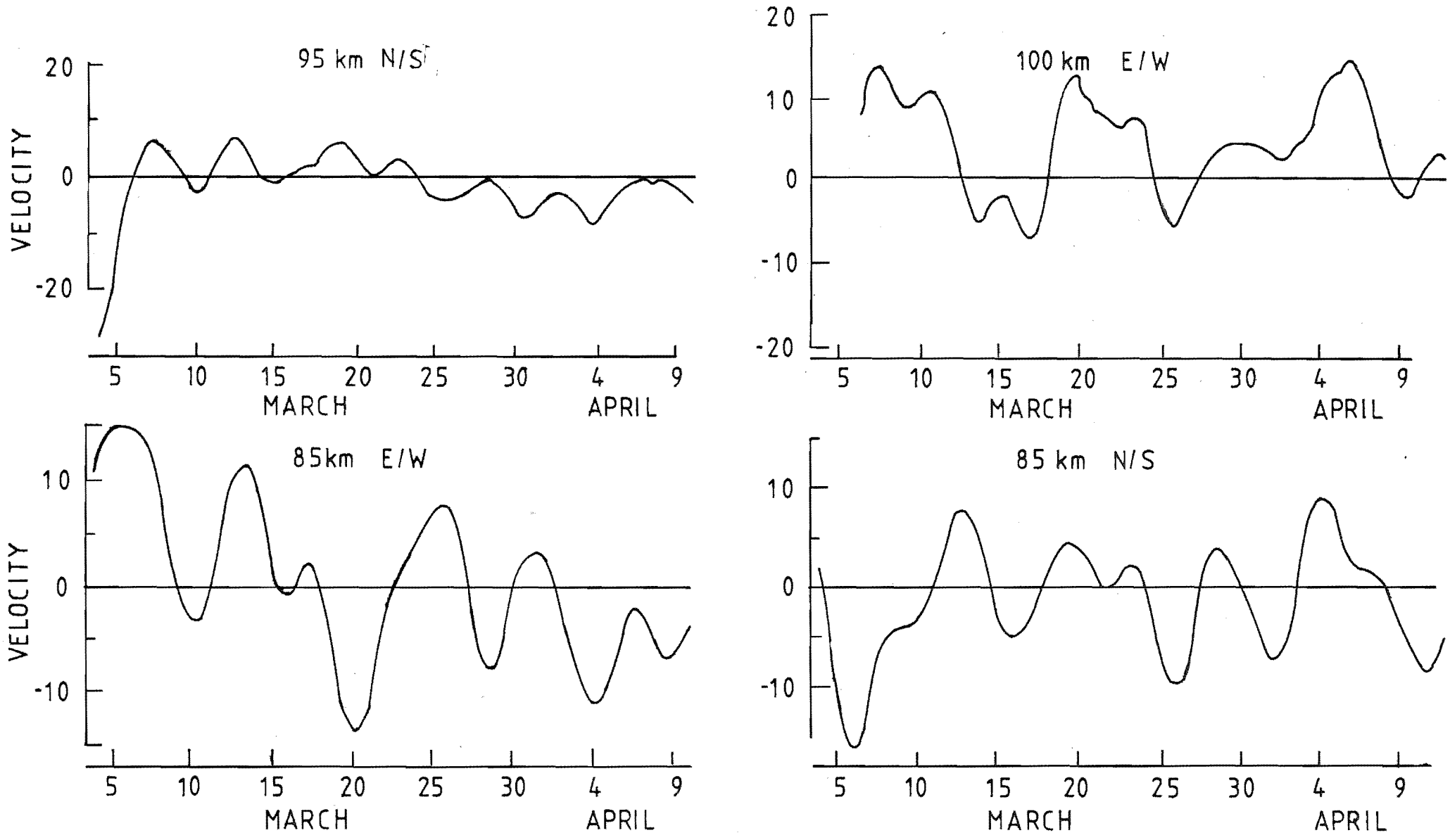

Figure 6.7: Autumn winds in 1979 after low-pass filtering.

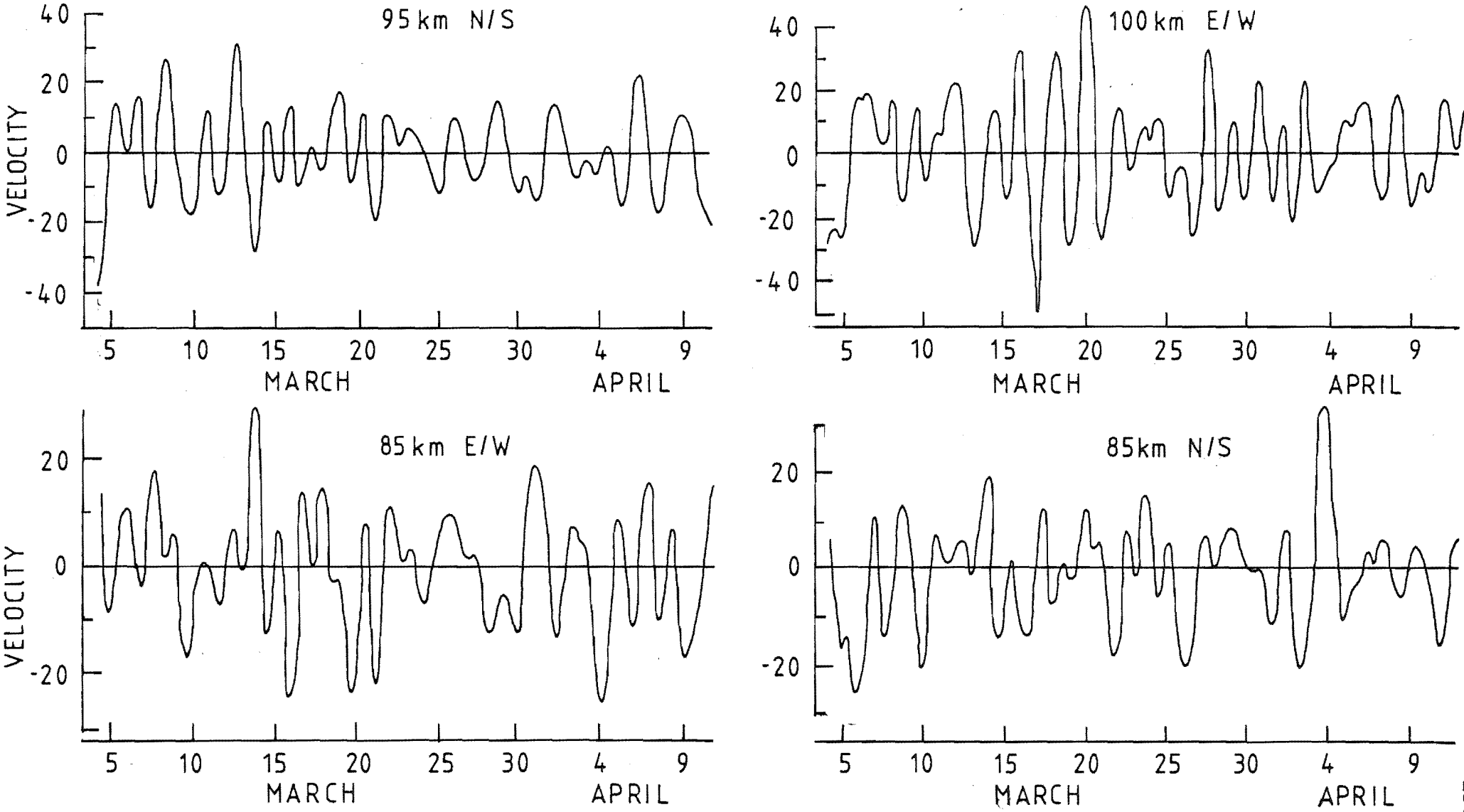

Figure 6.8: Autumn winds in 1979 after band-pass filtering.

5 days. It can be seen that the oscillations are often transient (hence the term 'transient waves' often used in stratospheric studies), with variations in both amplitude and frequency. Long lived oscillations can be seen, however; for example there is a persistent 5-6 day periodicity in the northward wind component at 95 km. At 100 km the eastward component shows a long period oscillation of 11 - 12 days period with other periods superimposed. Not only are there changes in behaviour in time, but also with height, and between the eastward and northward components. The same data is shown in Fig. 6.8 after application of a band-pass filter with half-amplitude points at 11.1 and 1.3 days. Again a range of periodicities are present, from less than 2 days to 6-7 days. The oscillations in this bandwidth are considerably stronger than in the lower frequency band.

The long, continuous data collection runs have enabled power spectral analysis to be performed with good frequency resolution, since the resolution is proportional to the data length; the spectrum frequency spacing, Δf, equals $1/N\Delta t$, where N is the number of data points spaced by a time interval Δt. Month-long data series unbroken by significant gaps were obtained regularly; the longest unbroken run was 3 months long. Periodograms were calculated using a fast Fourier transform (FFT) routine (e.g. Bloomfield, 1976). The ends of the data were first tapered by a cosine bell in order to reduce spectral leakage due to the finite data length (Bingham et al., 1967). A brief description of the method is given in Appendix G. The cross-periodogram

between the eastward and northward time series was also used to identify common periodicities and their phase difference.

Although the length of the time series enables good spectral resolution, it is clear that the data is in general non-stationary in character resulting in periodograms with low stability. Not all peaks in the periodograms will indicate distinct atmospheric waves. Planetary waves not only have a limited residence time at a particular height but they may be amplitude modulated as the transmission characteristics of the atmosphere change. A wave of frequency f modulated at δf will give rise to adjacent sidebands in the spectrum at $f \pm \delta f$. A more complicated situation occurs if the phase of the oscillation also varies in time, that is, the modulating function is complex valued. Such a change may be caused by varying background winds at lower heights. In general, energy will be spread into adjacent frequencies. For these reasons it is desirable to smooth the raw periodogram to obtain a higher number of degrees of freedom and spectral estimates with lower variances, albeit at the expense of spectral resolution. This also enables the coherence (the correlation between time series within the spectral bandwidth) for the cross-power spectrum to be calculated.

The other approach which may be taken is to obtain the auto- (cross-) power spectra from the Fourier transform of the auto-(cross-) correlations of the data. The frequency resolution is then dependent on the number of lags used in

the calculation of the correlations. Since the length of the correlation function is typically a fifth of the data length, the spectral resolution from this method is considerably lower than in the periodogram. Also the choice of suitable window on the correlation to reduce sidelobe leakage assumes greater importance than the window on the original data. The spectra from the two methods have been compared and found to be very similar when sufficient smoothing is applied to the periodogram, as expected. However, the advantage in using the periodogram method lies in being able to start with very good resolution and then increase the spectral smoothing to reduce the variance in the spectral estimates at the cost of resolution.

6.5.2 The Observed Spectra

Fig. 6.9 shows the power spectra, cross-spectrum and phase for hourly data in June 1978. The first two weeks of this month covers the time of a Coordinated Tidal Observation Program (CTOP) run. The eastward and northward components have largest values of power at 24 and 12 hours respectively. The tides are the principal components of the spectra most of the year. An exception to this occurs during January when a 2-day wave is exceptionally strong. The 12h component is generally the stronger of the tidal components. It also has the more stable phase, a fact which emerges from the spread in power about the frequency in question and from the coherence of the cross power. The dominance of the 12h tide can be seen clearly in the

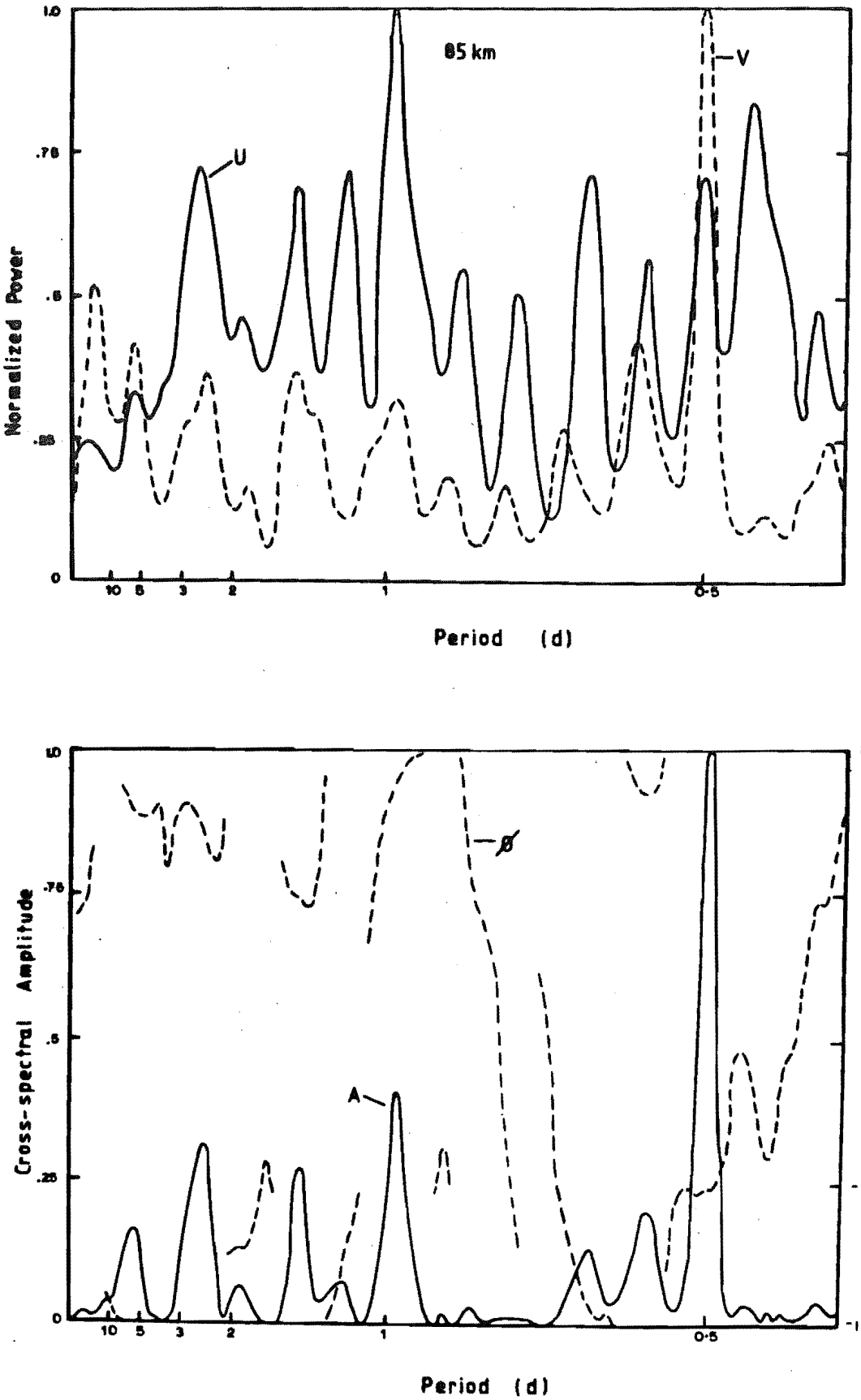

Figure 6.9: Power spectra and cross-spectral amplitude and phase of June 1978 winds.

cross-spectrum in Fig. 6.9. The phase at 12h, -94^{o}, is consistent with the theoretical expectation that, for a single tidal mode, the eastward component leads the northward by 90^{o}. In contrast, the phase difference between the eastward and northward components of the more variable diurnal tide is 160^{o}. The spectral peak sometimes shows a small shift from 24h, in this case to 23.5h.

The power spectra show high frequency peaks other than those of the tides. Internal gravity waves are known to be important at these heights (e.g. Vincent and Stubbs, 1977). The power spectra here also suggest that they have strong amplitudes. The dispersion relation for gravity waves of frequency ω on a rotating plane is

$$n^2 = \frac{(\omega_b{}^2 - \omega^2)k^2}{\omega^2 - f^2} - \frac{1}{4H^2}$$

(Lindzen, 1971), where n, k, ω_b, H, f are respectively the vertical and horizontal wavenumbers, the Brunt frequency, atmospheric scale height and the vertical component of the rotation rate. For vertical propagation of a gravity wave ($n^2 > 0$) the frequency must not only be less than the Brunt frequency, but also greater than f. On a sphere, this lower limiting frequency, the inertial frequency, will vary with latitude and at 44^{o}S is: $2\pi/2\Omega \sin\theta$ = 17.3h = 0.72d (where θ is the latitude and Ω the earth's rotational frequency). Oscillations are observed with periods greater than this, not only in Fig. 6.9 but also at other times and heights.

The extrapolation of the results for a rotating plane suggests that if the oscillations are due to gravity waves, then they are external and locally generated. Spizzichino (1969) has considered nonlinear interactions between gravity waves and tides as a possible generation mechanism. However, W.L. Jones (private communication) has pointed out that this extrapolation is invalid. In a full rotating, spherical model the solutions need not be evanescent in the vertical but rather, are latitudinally confined towards the equator in a manner described by the Hough functions.

Attention is turned now to oscillations with periods greater than a day. Spectral peaks in Fig. 6.9 occur simultaneously in the eastward and northward directions at periods of 5.3, 2.5, 1.9 and 1.4 days. The cross-spectrum reflects this similarity with its principal peaks at these periods also. The precise location of some of these peaks does in fact show differences between the components, but since they only differ by one frequency division, this is not considered to be significant. In addition to the occurrence of simultaneous peaks in both components, a significant spectral peak occurs at 1.15 days in the zonal wind only. This is not inconsistent with the behaviour of long period planetary waves since the latitudinal structure of the normal modes is generally different for the zonal and meridional components (Fig. 6.2). The barotropic 5-day wave for example, has a node in the meridional component at 40^{o} latitude while the zonal component approaches its maximum value there. The observed spectra can assume quite

different appearances at different heights with the attenuation of certain periods into the noise level and the growth of others. The oscillation near 1.9d in the June 1978 spectra provides a good example of such a variation, with an increase in amplitude of the meridional component with height and a decrease in the zonal. Although the northward spectral peak near 2 days is fairly modest at 85 km, it dominates the low frequency portion of the spectra by 90 km. In contrast, the spectral power at 1.75 days is important only in the eastward component. With poorer spectral resolution this latter period would probably have been associated with the 2-day oscillation, but from the present spectra would appear to exist in its own right. Periods at 2.1 and 1.76d do in fact correspond to the (3,3) and (2,2) free modes.

6.5.3 Planetary Wave Results

It is not practicable to present the spectra for each month and height. Some further examples are shown however in Fig. 6.10. Instead, the dominant features of the spectra, taking into account the persistence in height and in both wind components, will be discussed. A summary of the results can be found in Table 6.4 at the end of this section. Where unbroken time series exist, several months have been combined to give seasonal spectra. In addition to the hourly data above 80 km which were suitable for cross-spectral analysis, daily wind averages were obtained between 65 and 80 km. This data was analysed using the Maximum Entropy Method (MEM) which is specially suited to short time series.

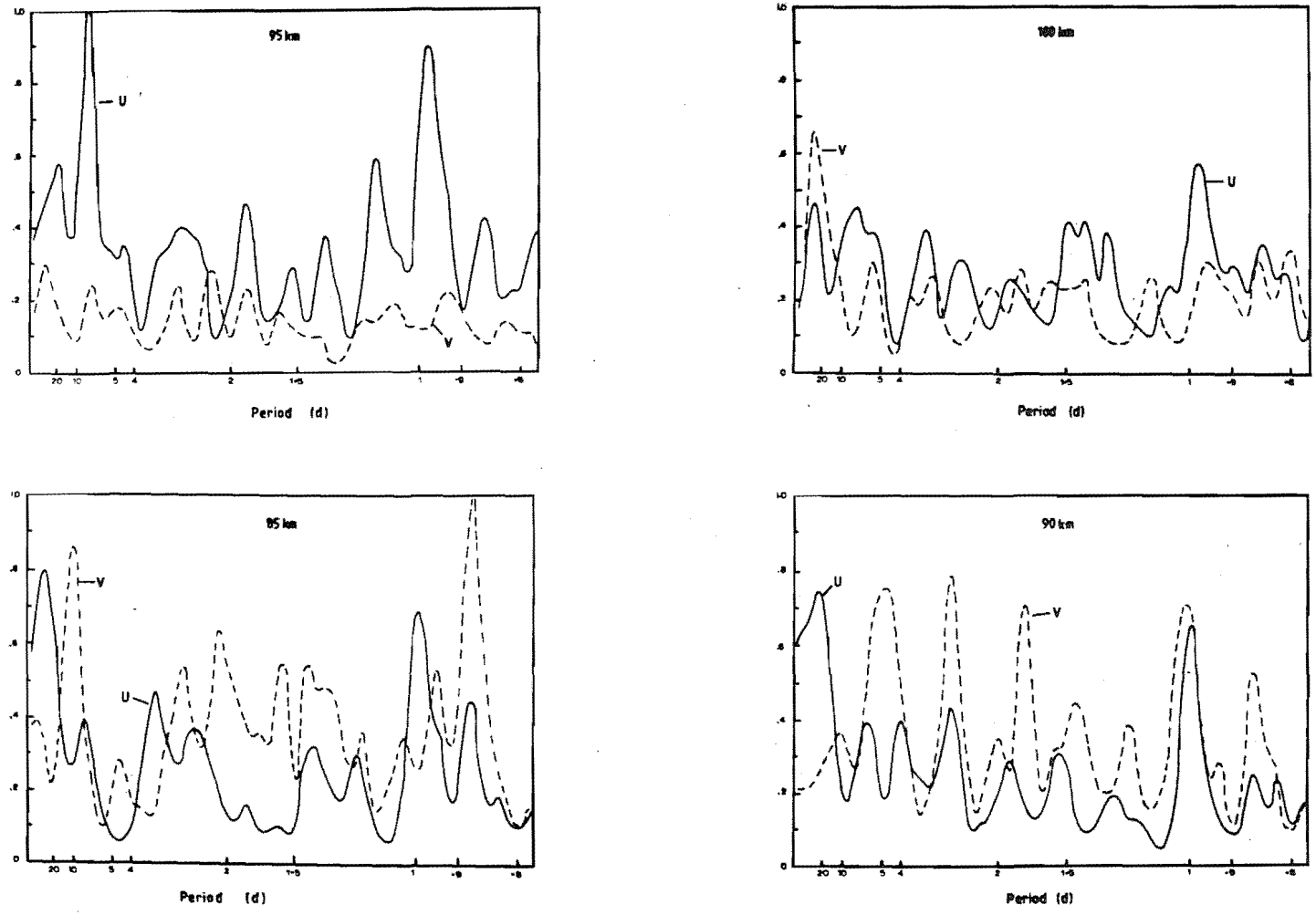

Figure 6.10a: Power spectra of winds from 10 July to 30 September 1979.

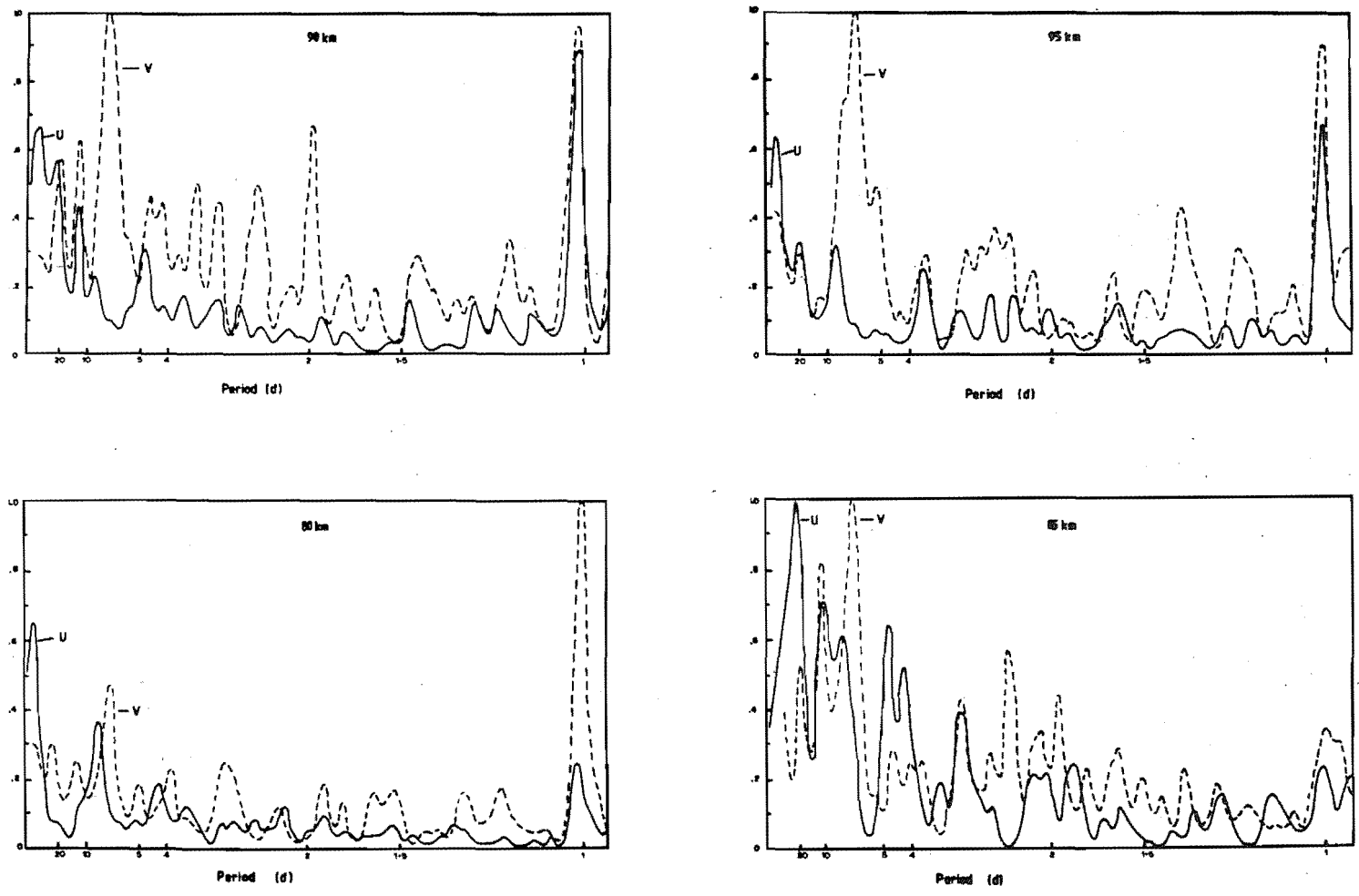

Figure 6.10b: Power spectra of winds from 1 September to 30 November 1979.

Only periods greater than 2.5d can be regarded as significant for this data.

Winter

For the winter month of June 1978 the dominant oscillations which are persistent with height above 80 km appear at periods of 15 ± 5, 5.3, 2, 1.45 days. During the next available winter month, August 1978, the oscillation near 5d was still present. MEM spectra of data below 80 km showed that it extended down to at least 65 km. Analysis of separate sections of August indicated that in the latter part of the month, the period of importance near 5 days was closer to 4.5d with a strong attentuation of the meridional component with height. In addition there were indications of an oscillation with a period close to 7 days over the entire height range. The oscillation near 1.45d was also present in August, particularly in the zonal component. The power near 2 days showed considerable variability of frequency and amplitude with height.

The data for the winter of 1979 provided a further independent sample in which to seek preferred frequencies of oscillation of the winter atmosphere. For this year the occurrence of a steady, discrete spectral peak close to 5 days was not evident. Certainly spectral power was present, but it was diffused between 4.5 - 5.7 d. However the data did show regular behaviour at 7.3 ± .2d over the complete height range of 65 to 100 km with the meridional component attaining the largest amplitudes. The other main contributions

to the data below 80 km were at 11.5, 4.8 and 3.8d. The latter period extended to the upper heights during August. A strong oscillation at 2.5d was present in the upper region in this month; it also occurred weakly at the lower heights.

In the absence of information on the spatial structure of the observed waves it is not possible to make an identification with the free modes whose expected periods were given in Table 6.1. However, on the basis of period, a 5-day wind oscillation with a maximum amplitude in winter, was associated with the (1,2) mode by Salby and Roper (1980). Fraser (1977) associated the 6.5d coherence peak between 30 mb temperature and f_{min} observed by Fraser and Thorpe (1976) with the westward propagating 5-day wave observed in the stratosphere and troposphere. A 5-day oscillation was also persistent in the winds of the present results in the winter of 1978. A property of a free mode in an inviscid, barotropic atmosphere is the phase quadrature between the wind components (Salby, 1979). Although this was not evident here, it does not automatically preclude the observed oscillation from being a free mode since the numerical model of Geisler and Dickinson (1976) indicates that in this height region the meridional wind will pass through a node with an accompanying 180^{o} phase shift (Fig. 6.3). The phase difference between the wind components will therefore be very uncertain. The situation in winter is complicated by the presence of eastward as well as westward waves, as discussed in Sections 6.2 and 6.3. Stratospheric observations by Leovy and Webster (1976) and Hirota (1976)

have found stronger eastward waves than westward. Further to the work of Fraser and Thorpe, Burns (1980), using satellite radiance measurements, found that in winter f_{min} was significantly coupled to a stratospheric wave with a period between 5 and 6 days, but which was of wavenumber 2 and travelled eastward. This finding invalidates Fraser's (1977) identification of the winter oscillation with the 5-day, (1,2) mode which should be wavenumber 1 and travel westward. It therefore appears that identification of upper atmospheric wind oscillations with westward propagating free modes on the basis of frequency alone must remain very tenuous in winter.

With this proviso in mind it is nevertheless noted that the 7.3 $\pm$ .2d period observed in winter coincides with the value of the (2,4) mode which Salby (1980c) found to have a well-defined response in both solstice and equinox conditions. It is also noted that southern hemisphere conditions give a stronger wavenumber 2 excitation than the northern hemisphere (Leovy and Webster, 1976), although these waves are mainly eastward propagating.

Autumn

The spectra during the autumnal equinox were characterized by strong tidal amplitudes. The dominant planetary scale periods were at 8-9, 2.9, 1.58 and 1.2 days. Salby and Roper (1980) also found a frequent occurrence of 1.2d oscillation during autumn and summer, and a 1.6d oscillation in winter. The (1,1) and (2,2) free modes, the gravest wavenumber 1 and 2 modes, have periods of 1.2d and close to 1.6d respectively in a barotropic model.

Spring

The spring months of September, October and November in 1979 were combined with a three hour data averaging interval. The change from the prevailing winter eastward winds to summer westward values showed up as a long term trend in the spectra. The dominant oscillations were at: 11 $\pm$ 5, 6.7 $\pm$ .4, 4.6 $\pm$ 1, 2.9 $\pm$ .1 and 1.9 $\pm$ .1 days. The 6.7d oscillation had largest amplitudes in the meridional component just as the 7d oscillation in winter. This period also appeared in the 1978 September spectra. A further breakdown of the data month by month showed that certain features were not persistent throughout the spring interval. In September 1979 the presence of a strong 11d spectral peak did not enable the 7d period to be resolved, although a 5d oscillation was present. The 1.9-2.0d periodicity was present throughout the equinox period, but was stronger in 1979 than in 1978. Later, in summer, very large amplitudes were reached at this period enabling a more detailed analysis to be made.

The zonal winds during November are generally westward in the mesosphere and more characteristic of summer conditions. It is expected then, that eastward and stationary waves will be more strongly attenuated making an association of observed oscillations with free modes more likely than in winter. A strong feature of November in both 1978 and 1979 was an oscillation near 8.5 days. The asymmetric (1,3) mode has a period of 8.3d in a barotropic atmosphere; Salby (1980c) estimates a period of 8.5d in solstice conditions and a

somewhat longer period of 9.4d at the equinoxes. November 1979 lent a strong contribution to the 4.7d oscillation of the spring spectra. A 1.7d period recurs in November 1978. It is noted that this is within the expected period range found by Salby for the (2,2) mode.

Summer

The summer months provided the most spectacular example of planetary wave activity at ionospheric heights. During January 1980 a 2-day oscillation dominated the spectra reaching amplitudes exceeding even those of the tides. A feature of the wave was the decay in amplitude of the zonal component with height but the growth to large amplitudes of the meridional. The wave will be considered in detail in the next section. During February the meridional activity at 2.0d died down, and the zonal component indicated an increase with height. However the power spectra for the meridional component showed strong activity at 2.6 $\pm$ .1d. This shift in frequency is well within the resolution of the spectral analysis and it was a feature in both 1979 and 1980. It is not clear whether this represents a different mode of oscillation or a shift in frequency of the 2-day wave caused by different background atmospheric conditions. The background wind conditions do undergo a change from January to February with the weakening of the strong summer westward winds. Zonal winds similar to those in February are also found in November up to 85 km, but as noted earlier the preferred frequency of oscillation was at 2.0d.

Unfortunately the data for December 1979 was somewhat intermittent and it was not possible to perform a power spectral analysis.

Oscillations at 1.6 and 1.3d were also frequently observed.

During summer a long period oscillation at 10 $\pm$ 2d was evident. It was also present in the data below 80 km. Harmonic analysis of the February 1980 data revealed an interesting phase structure for this wave (Fig. 6.11). The northward component showed no phase progression with height until a 180^{o} phase change occurred near 95 km. At the same height, the amplitude went through a minimum, suggesting the presence of a standing wave structure. The eastward component was fairly constant in amplitude with a very slow downward phase progression consistent with a vertical wavelength greater than 100 km. A cross-spectral analysis of f_{min} and stratospheric temperatures by Burns (1980) revealed a westward propagating wavenumber 1, ten day wave. This period is somewhat less than the 16-day period which Madden (1978) has tentatively associated with the (1,4) free mode in the troposphere, but it lies within the range expected for the (1,3) mode (Salby, 1980c).

The numerical study by Geisler and Dickinson (1976) predicted large amplitudes for the '5-day' wave in the summer mesosphere because of the formation of a wave cavity. In early summer (November) an oscillation at 4.7d was strong but in January there was no clear tendency for a concentration of power near this frequency. During February

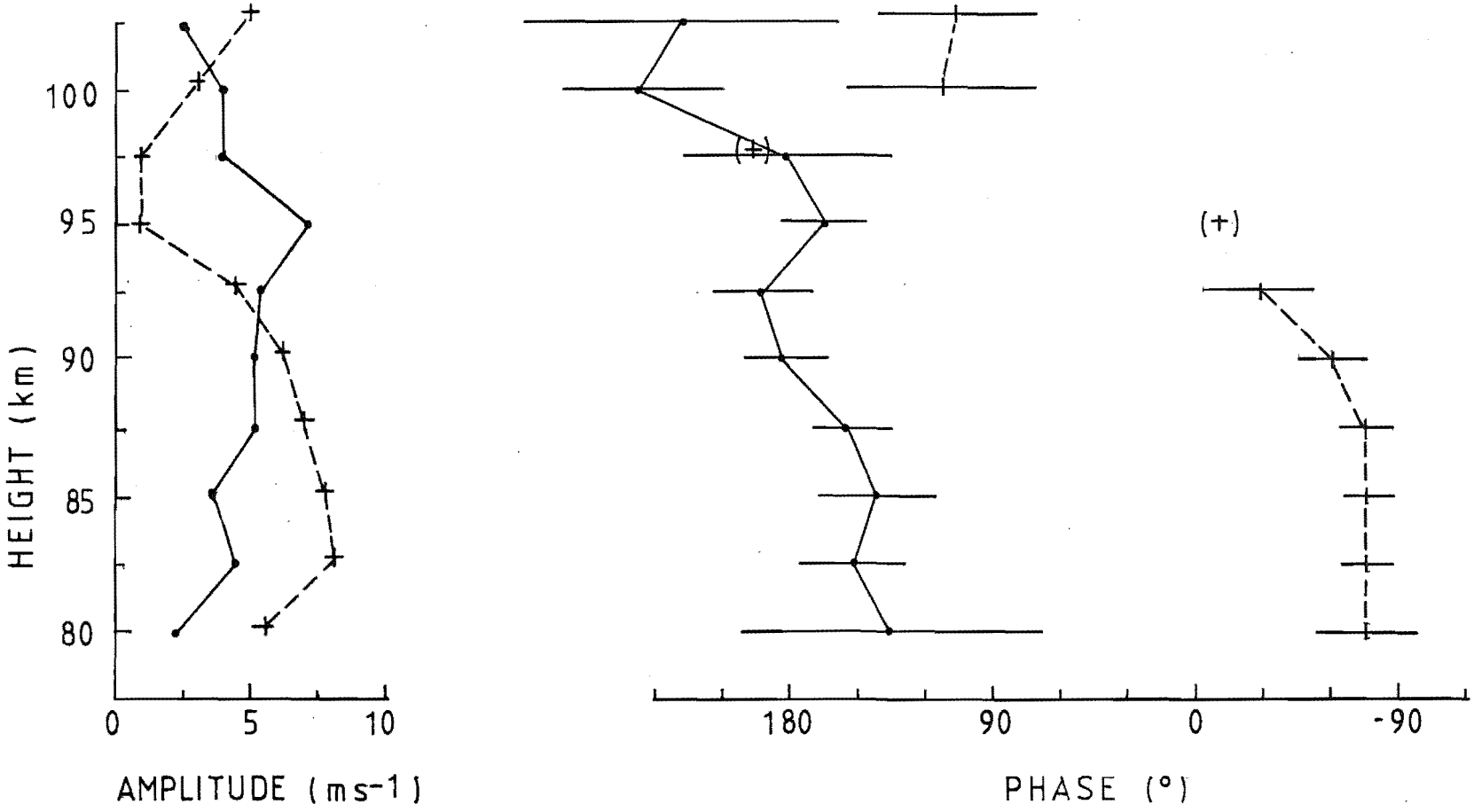

Figure 6.11: Amplitude and phase of a 10d oscillation observed during summer.

1980, a 6-day oscillation was observed and reached amplitudes comparable to the 2-day wave above 88 km. It was also seen in the data below 80 km. These results indicate that a strong atmospheric response near 5 days occurs in early or late summer rather than in mid-summer. The background zonal wind model used by Geisler and Dickinson had strongest summer wind values of -40 m/s at 50 km, 30^{o} latitude. However, the observed summer winds, discussed in Chapter 5, greatly exceed this value in mid-summer. Geisler and Dickinson did try stronger winds (-56 m/s) and found that the summer mesospheric cavity was detuned, and summer amplitudes for the 5-day wave were only twice those of winter as compared to the original order of magnitude difference. They also found that a Newtonian cooling rate of 10 d^{-1} reduced the summer hemisphere amplitudes by a factor of two. Thus the presence of strong (-70 m/s) summer winds and realistic dissipation will qualitatively account for the absence of a strong 5-day wave in January which may have been expected on the basis of Geisler and Dickinson's results. The more moderate winds in November and February are more suited to the formation of a mesospheric wave cavity. Salby and Roper (1980) found minimum amplitudes for a 5 day oscillation in summer; they attributed this to the increased atmospheric unsteadiness at other times of the year which would be required to excite the mode.

Table 6.4: Summary of the periods (d) of dominant long period wind oscillations

Autumn	Winter	Spring	Summer
	15 ± 5 d	11 d	10 ± 2 d
8-9		8.5	
	7.3 ± .2	6.7 ± .4	6.0
	5.0 ± .3	4.6	4.7
	3.8		
2.9	2.5	2.9	2.6 ± .1
	2.0	1.9 ± .1	2.0
1.58		1.7	1.6
	1.45		
1.2			1.3

6.6 THE TWO-DAY WAVE

6.6.1 Previous Observations

The most outstanding observation of a long period wind oscillation was that of the 2-day wave during January and February, 1980. Such an oscillation was originally reported by Muller (1972) who found a 51h periodicity in July and August in the northern hemisphere during 3 to 5 day long meteor radar wind observations. He associated it with an oscillation of a similar period in ground level pressure measurements. Various explanations were put forward to explain the

observations. Muller (1972) proposed that the passage of internal gravity waves from the troposphere to meteor region heights was modulated by tropospheric weather patterns, and that the subsequent energy of dissipation of these waves in the upper atmosphere would similarly be modulated. He argued that the resulting local thermal gradients would in turn set up wind systems. The modulation of the momentum deposition of such gravity waves would have a more direct effect upon the upper level wind systems. Vincent and Stubbs (1977) found small mean flow changes in the upper D-region which they could associate with gravity wave momentum deposition. Muller and Kingsley (1974) cite a mechanism proposed by C.O. Hines involving the diurnal tide. Hines proposed that the dissipation of the tide when reaching meteor heights would create turbulence which would damp the next cycle of the diurnal tide, giving the appearance of a 2-day oscillation. However, at mid to high latitudes the diurnal tide is rather weak and irregular, and this behaviour would be unlikely to account for either the longevity of the oscillations or the spatial structure which subsequent work has revealed. Non linear sub-harmonic generation by the tides was also suggested by Poulter (1978).

Glass et al. (1975) used simultaneous measurements at Garchy and Obninsk to ascertain that the 2-day oscillation was most likely a wavenumber 3, westward propagating planetary wave. Muller and Nelson (1978) confirmed this and from a summary of a variety of meteor radar results, showed that the 2-day wave reached large amplitudes at the end of July

in the northern hemisphere. Craig (1979), using nine years of meteor winds, found that largest values also occurred in summer in the southern hemisphere. The only disagreement with this finding is in the results of Roper (1975) and Salby and Roper (1980) who found largest values in mid-winter; Muller and Nelson (1978) only reported a weak increase in winter. Equatorial stations have reported a large 2-day oscillation in the meridional wind component at solstice, both at stratopause heights (Coy, 1974) and at meteor heights (Kal'chanko and Bulgakov, 1973).

6.6.2 Results

Observations made at Birdlings Flat in the summer of 1980 revealed a strong 2-day oscillation from January 12 till mid February. Smoothed wind values are shown in Fig. 6.12. The oscillation showed a marked phase stability during its lifetime. The power spectra over the most active period show that the period is very close to 48.0h. The amplitude of the meridional component exceeds that of the tides at all heights; the zonal component exceeds that of the tides up to 91 km. A weighted least squares fit of a constant term and periods of 48, 24, 16, 12 and 9.6 hours was made to the two wind components of the hourly data above 80 km. Daytime data distributed between 1000 and 1600 hours (L.T.) was also recorded from 65 to 80 km. A weighted least squares fit of the constant term and a 48 hour period was made to this hourly data. The weights used in both cases were the number of wind measurments within each hour; the

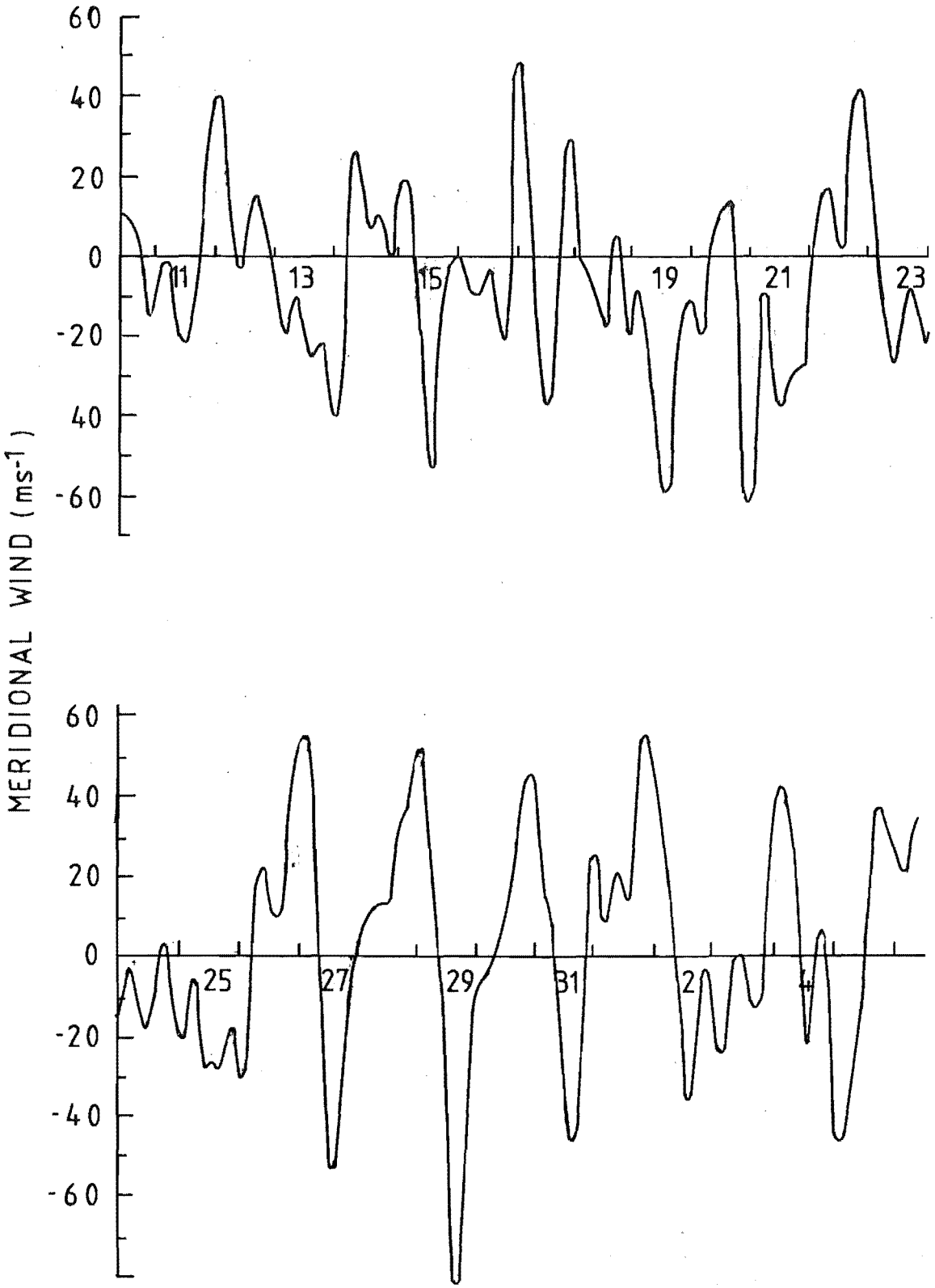

Figure 6.12: Smoothed 3-hourly meridional wind component at 95 km during January/February 1980.

weighting was obviously of particular importance in the analysis of data in the lower height range. Data from adjacent height intervals have been averaged to give added weight to the analysis and this introduces some smoothing with height.

The vertical profile of the amplitude and phase of the 48h oscillation is shown in Fig. 6.13. The phase refers to the hour of maximum eastward or northward velocity. Despite the poor diurnal coverage at the lower heights, the profiles above and below 82 km connect well, suggesting that the lower data can be regarded with some degree of confidence. It is to be noted that the error bars are significantly larger at the lower heights reflecting the lower reliability of this data.

The eastward amplitude shows a slow decay with height from a maximum around 73 km, while the northward amplitude increases with height reaching very large values at 97 km. This growth is probably limited at 97 km. The phase behaviour in the region of full diurnal data coverage is quite linear with height, implying vertical wavelengths in the northward and eastward components of 90 $\pm$ 10 and 60 km respectively. The downward phase progression is consistent with the upward propagation of energy of a westward travelling planetary wave. The northward phase maintains this steady progression down to 70 km where a rapid change is noted. In the 80-85 km region the eastward wind leads the northward by 90° with approximate circular, counter-clockwise rotation of the velocity vector. This relationship is steadily

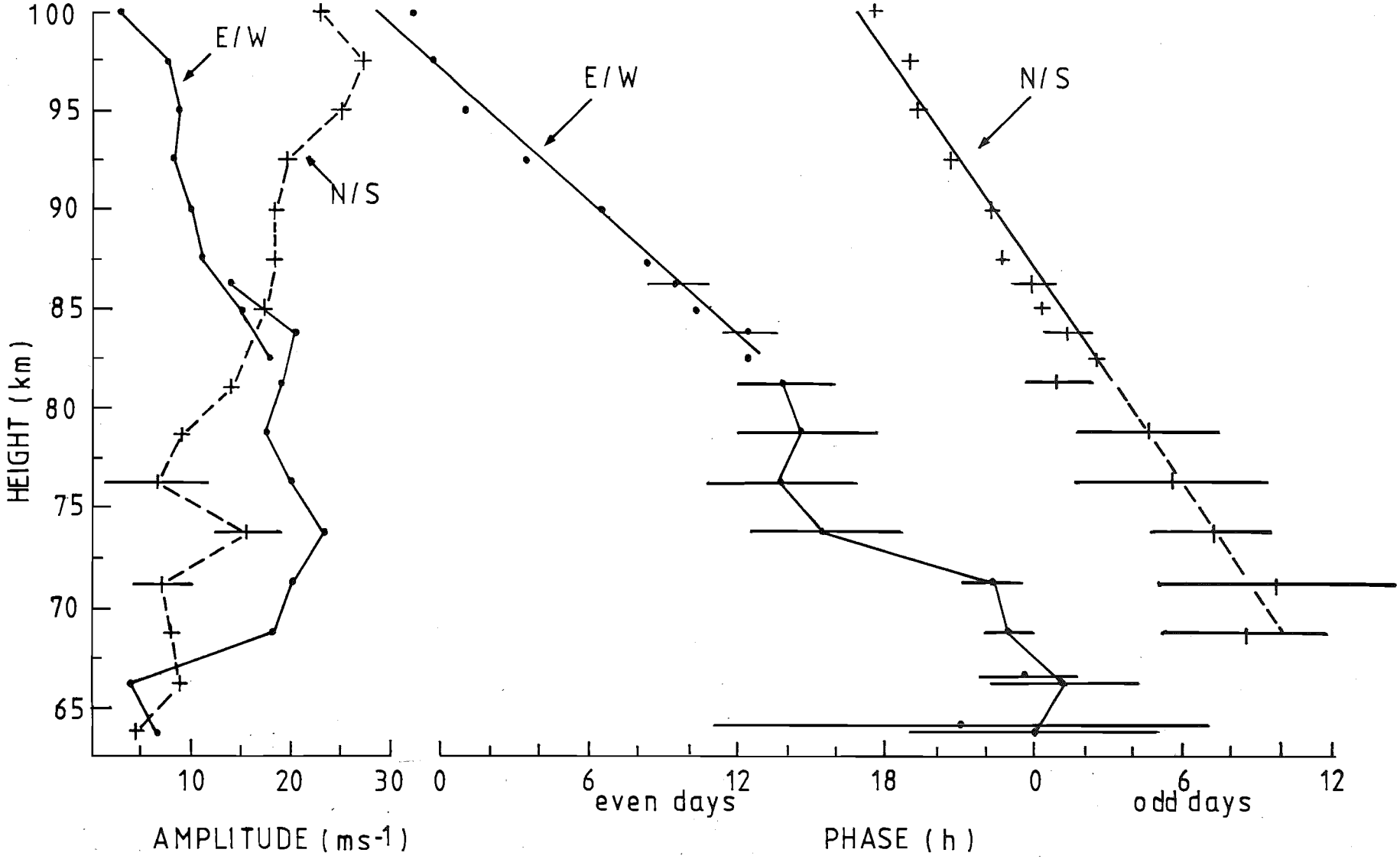

Figure 6.13: Amplitude and phase of the two-day wave from 10 January to 5 February, 1980.

changed above, due to the difference in phase slopes, implying a southward transport of eastward momentum flux by the wave.

Similar partial reflection measurements were also taken over the 80 to 100 km region at Adelaide and Townsville during January and early February. Results of these coordinated measurements have been reported by Craig et al. (1980). The Australian stations also found a dominant meridional component, with larger values than at Birdlings Flat, and a zonal component which decayed with height. Unlike the Birdlings Flat data, the meridional component also showed a slow decay with height. Between 82 and 92 km the three stations showed similar vertical wavelengths in the northward component of about 100 km. The phase differences between Adelaide and Birdlings Flat (and Townsville at 84 and 88 km) were consistent with a wavenumber 3, westward propagating wave if no phase change of the wave in the meridional direction is assumed. This is in agreement with the northern hemisphere observations of the 2-day wave.

6.6.3 Discussion

Salby and Roper (1980) first associated the 2-day wave with (3,3) atmospheric free mode on the basis of its period, which in a barotropic atmosphere whould be 50.4h. This is very close to the commonly reported period of 51h in the northern hemisphere and not significantly different from the present value of 48h. The observed wavenumber gives

additional strong support to this identification. (Muller and Nelson (1978) had earlier made the observation that 6d (the approximate period of the wavenumber 1 (1,2) normal mode) divided by 3 (the wavenumber of the 2-day wave) gave 2d, thus implying a harmonic relationship. This fact however, is coincidental). The barotropic structure of this mode, Fig. 6.2a, shows that the meridional component reaches large values near the equator and falls off with increasing latitude. The zonal component is smaller, with a node at the equator and largest values near 30^{o} latitude. This is in qualitative agreement with the results of Craig et al. (1980) and Kal'chanko and Bulgakov (1973). At mid to high latitudes the zonal and meridional amplitudes are similar. This mode, being the fundamental wavenumber 3 mode, has the fastest westward phase speed of this wavenumber, and will therefore be least affected by background zonal winds in a more realistic model. However, as Geisler and Dickinson demonstrated for the 5-day wave, wind effects can be expected to be significant in the mesosphere.

Of particular interest in this regard is the fact that the (3,3) mode should have a westward horizontal phase velocity of 56 m/s at a latitude of 44^{o}. It can be seen from the zonal wind profile for January in Fig. 5.4 that such a wave would encounter a critical level (CL) (where its frequency relative to the background wind is Doppler shifted to zero) at a height near 66 km. Such a critical level corresponds to a singularity in the wave equations in a linear inviscid model. Theoretical studies have been mainly

concerned with the behaviour of planetary waves near a vertically aligned critical line (which stationary planetary waves encounter near the equator), rather than the present situation of a horizontally aligned critical level. There is therefore some doubt as to the applicability of these results. In a linear model with dissipation, Dickinson (1970) found that absorption of the incident wave took place, but a large amplitude buildup before the CL was considered unlikely because of the long time scales of growth involved (in contrast to an internal gravity wave CL). Nonlinear models (Beland, 1978; Tung, 1979) have stressed the importance of wave reflection. Salby (1980b) used a linear model but with realistic background conditions and found that the wave phase is such as to 'steer' the wave into the CL from low latitudes as well as from below. An increase in phase gradient beneath the layer is expected. This model also indicated large amplitudes of the zonal component in summer in a small region near 70 km, centred at a latitude of 35 - 40^{o}. The meridional component increased with height in a region stretching from high summer latitudes into the winter hemisphere. Salby attributed this latter growth to the weak westward winds and equatorward temperature gradient in his model background conditions. (His model did not include the eastward winds which are observed above 90 km in summer mid to high latitudes.)

The observations of the 2-day wave in Fig. 6.13 show no untoward behaviour of amplitude near the height where the critical level is expected. The northward component of phase

does however undergo a rapid change. The presence of a CL is also expected to introduce latitudinal phase variations below about 80 km, which may affect the calculation of wavenumber from phase differences between stations at different latitudes. The observed behaviour shows remarkable similarities to that of Salby's model, with the zonal wind component reaching a maximum near 75 km, and the meridional component increasing with height. The observations of a larger meridional component at lower latitudes (Craig et al., 1980) is also in accord with the modelled behaviour of the (3,3) free mode.

6.7 COUPLING WITH THE STRATOSPHERE

Since the bulk of the atmosphere's kinetic energy resides in the troposphere, it is likely that the planetary waves observed in the mesosphere and lower thermosphere have their source in this lower region, in the absence of any well-known planetary scale forcing in the upper atmosphere. However, baroclinic instability is an important source of smaller scale planetary waves in the troposphere, but these unstable waves do not penetrate significantly into the stratosphere (Charney and Drazin, 1961). Therefore the large-scale waves which do penetrate to mesospheric heights will be more easily observed in the stratosphere.

6.7.1 Spectral Analysis of Stratospheric Winter Data

The N.Z. Meteorological Service records radiosonde temperatures, heights of pressure levels and winds up to a

height of 25 km above Christchurch. At the time of writing, this data was available up till the end of 1978. The wind data over the winter period at 20 and 25 km is shown in Fig. 6.14. Variations on a long time-scale are important. Frequent gaps in the data at the highest levels made spectral analysis difficult, but the daily winds at 20 km were adequate for analysis after linear interpolation across gaps.

The power spectra of the 20 km winds from June 1 to the end of August are shown in Fig. 6.15. The major difference with the D-region data is the predominance of power in the long period region in the stratospheric spectra. It should be noted that a log scale has been used in Fig. 6.15, whereas the mesospheric spectra were displayed on a linear scale. The interpolation across gaps may have contributed somewhat to this low frequency bias. The dominant periods relevant to the partial reflection observations are at 14 and 10 days. At the upper levels the spectral resolution at the long periods is poor - there is only one frequency interval between 14 and 10.7d. However, long period spectral power does recur near 14d. The stratospheric data also show spectral power at 5.8 and 4.3 days but at these lower periods the lack of stationarity in the data makes frequency identification uncertain. MEM spectra for individual months indicated the importance of power at 4.7d during June and at 5.1d in the zonal component in August. In the partial reflection data a 4.7d oscillation was strong at 80-82.5 km during June (above this a slightly longer period dominated), while in August a 5d oscillation was present from 65 km upwards.

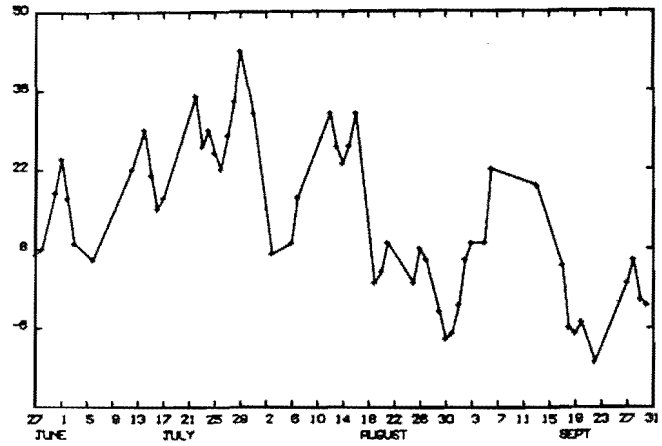

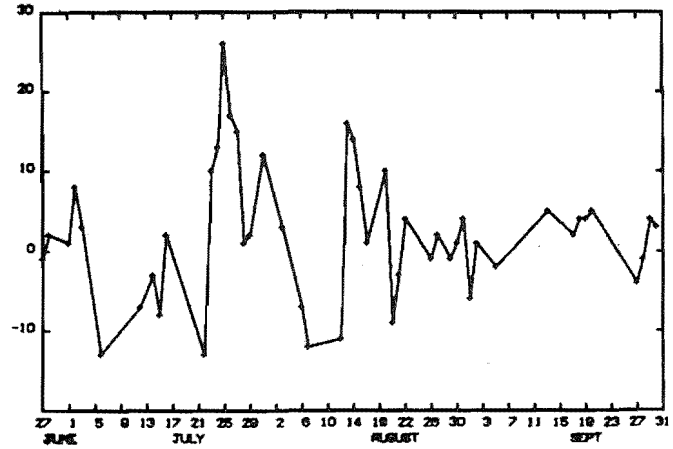

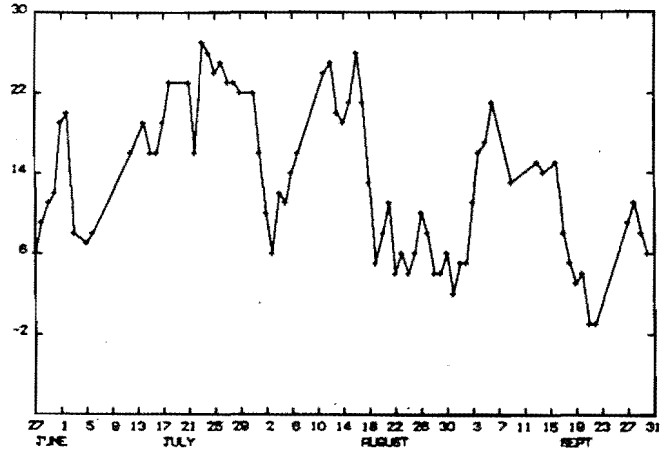

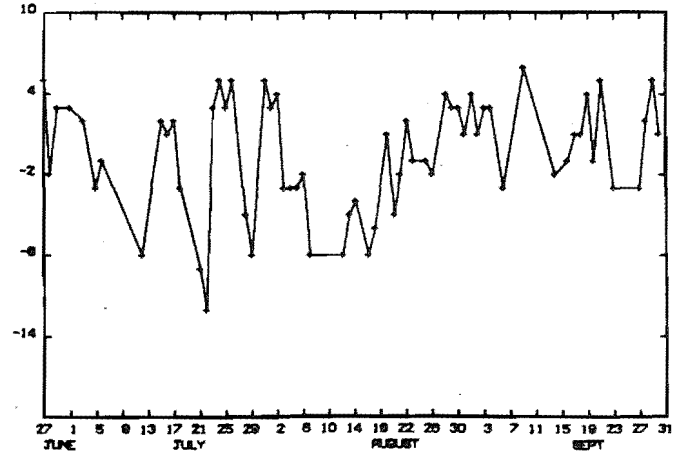

Figure 6.14: Zonal and meridional wind components at 20 and 25 km during winter, 1978.

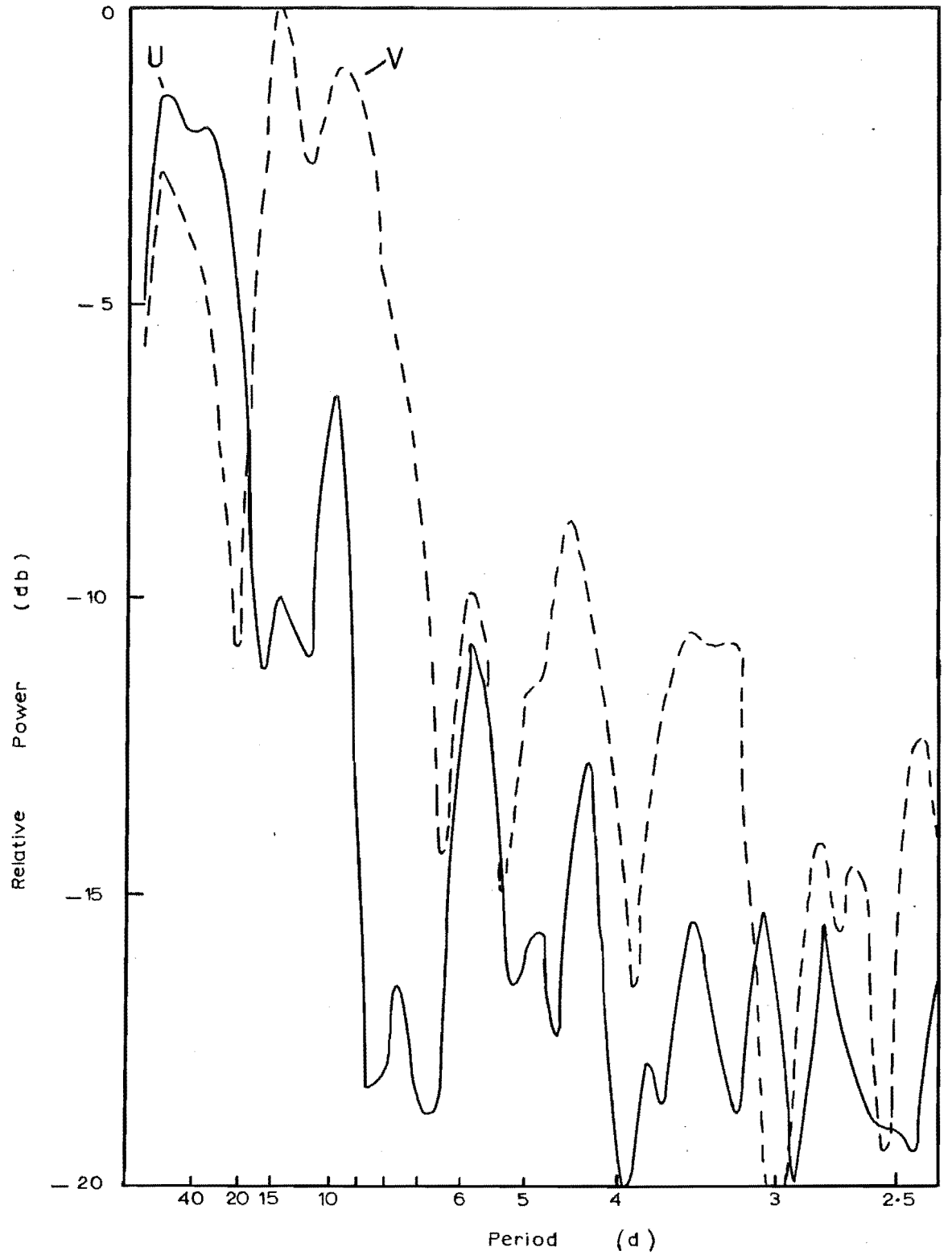

Figure 6.15: Power spectra of winter winds at 20 km.

This comparison is consistent with the upward penetration of travelling planetary waves in winter and the greater penetration of the shorter period waves.

6.7.2 The Response of Mesospheric and Lower Thermospheric Winds to Stratospheric Warmings

Planetary waves provide one form of coupling between the stratosphere and lower thermosphere. Also, large-scale disturbances of the atmospheric flow up to ionospheric heights can occur in association with stratospheric warmings. Sudden stratospheric warmings are observed to follow amplitude increases of planetary waves in the stratosphere which are usually associated with tropospheric blocking (Schoeberl, 1978). Tung and Lindzen (1979) have proposed that this increase occurs when large-scale planetary waves in the troposphere are rendered stationary and resonant by suitable changes in the stratospheric winds. The amplifying planetary wave is usually accompanied by the poleward movement of the wave's thermal centre and also by poleward heat fluxes which can result in drastic increases in high latitude temperatures in the upper stratosphere. On occasions the temperature rise may be sufficient to reverse the usual winter equatorward temperature gradient and result in a breakdown of the polar vortex with a reversal of the winter eastward winds. When such a reversal occurs poleward of 60° latitude at the 10mb level or below, the warming is termed a 'major warming'. Although temperature increases occur in the southern hemisphere which are as large as those in the northern hemisphere, the

colder southern stratosphere with stronger zonal winds is believed to prevent the occurrence of a major warming in the southern hemisphere. The hemispheric difference in temperature is thought to be due to the effect of the varying sun-earth distance on ozone heating (Barnett, 1974). Observations and dynamics of stratospheric warmings have recently been reviewed by Schoeberl (1978) and Holton (1980).

In association with the polar warming, cooling occurs in a region from winter low latitudes across the equator into the summer hemisphere. Temperature changes of the opposite sign occur in the mesosphere (Labitzke, 1972; Houghton, 1978). In the northern hemisphere, reversals in the mesospheric and lower thermospheric winds have been observed during major stratospheric warmings by Hook (1972), Lysenko et al. (1975) and Gregory and Manson (1975b). The behaviour of the upper level winds in the southern hemisphere during disturbed winter stratospheric conditions is examined here.

A contour map of the winds between 65 and 100 km at Birdlings Flat during the late winter of 1978 is shown in Fig. 6.16. The daily data have been smoothed with one pass of a Hanning filter. The usual winter regime of strong eastward winds is seen below 85 km, with a weakening in October at the start of the changeover to the summer circulation. However, two periods of very weak eastward winds occur; one at the end of July and the other, briefly at the end of August. Contours with zonal speeds less than 20 ms^{-1} have been hatched to emphasize this. In the late August period, westward winds descended downwards after August 26

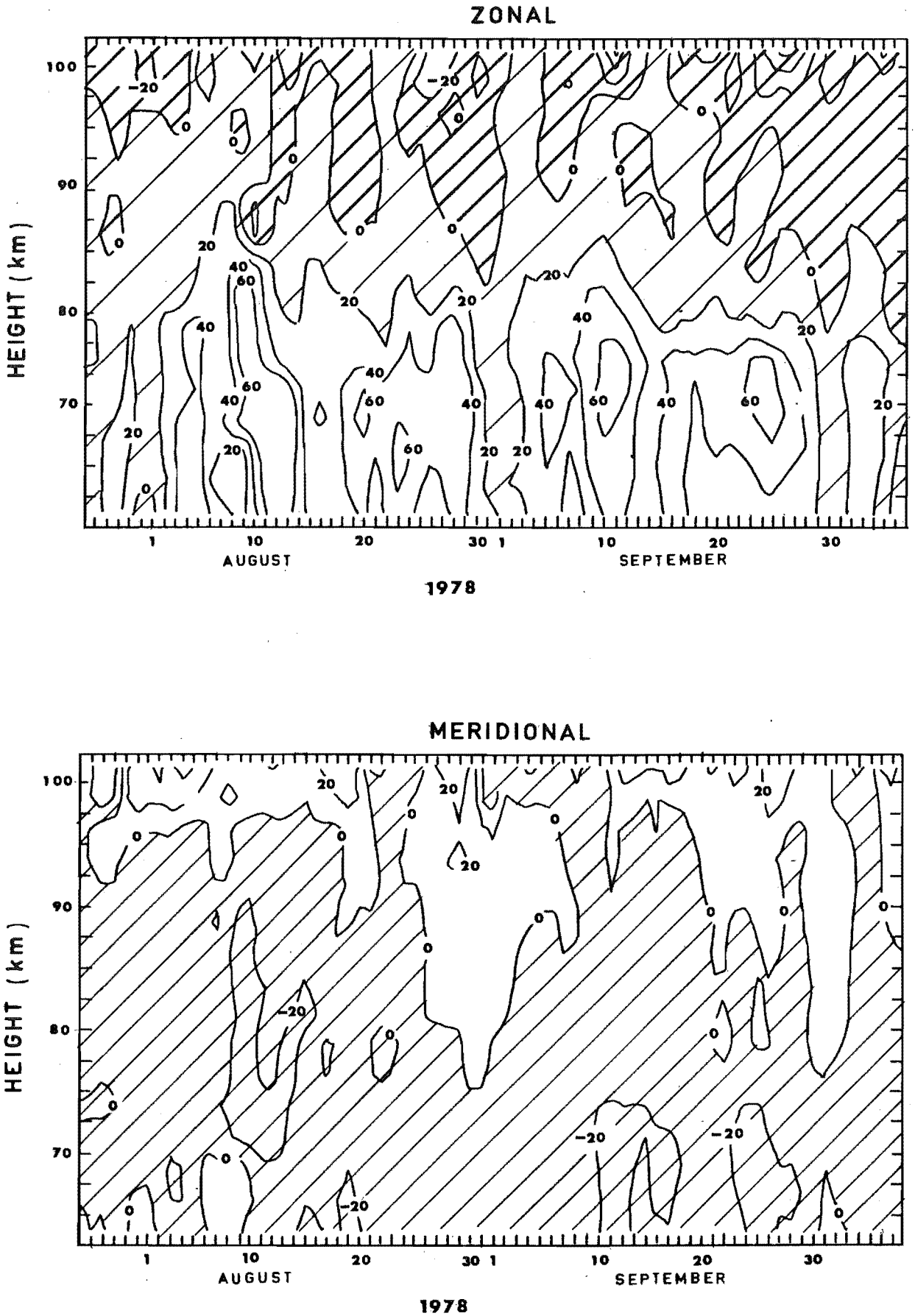

Figure 6.16: Contours of daily winds in winter, 1978.

reaching 80 km by the 31st. (This height and the dates are taken from the unsmoothed data.) The flow below about 85 km showed no similar trend until the abrupt change on August 30-31 when winds less than 20 ms^{-1} extended over the entire height range until September 3. During the same period, the meridional wind component changed to the northward direction down to 76 km.

The change in the thermal wind during the August 30 to September 3 period implied a decreased meridional temperature gradient suggesting that there had been either high-latitude cooling or mid-latitude warming in the mesosphere. It is to be noted that the thermal wind equation assumes that the Coriolis force and the pressure are in geostrophic balance, but when accelerations are taking place this will not apply.

The Meteorological Service zonal winds during the same winter period (Fig. 6.14) were also eastward and increased in strength with height. During the July to September period these winds weakened significantly on two occasions; the first was for a period of a week at the end of July, and the second was for a more extended period, from mid-August to early September. The change was strong enough to result in westward winds at 25 km from August 29 till September 1. The timing of these events strongly suggests an association with the upper mesospheric winds. During this latter period the meridional component was also small in amplitude.

Throughout the period of weak zonal winds in August, the temperature at the 20 mb (~ 27 km) level was building up to sustained high values (Fig. 6.17). The peak value occurred

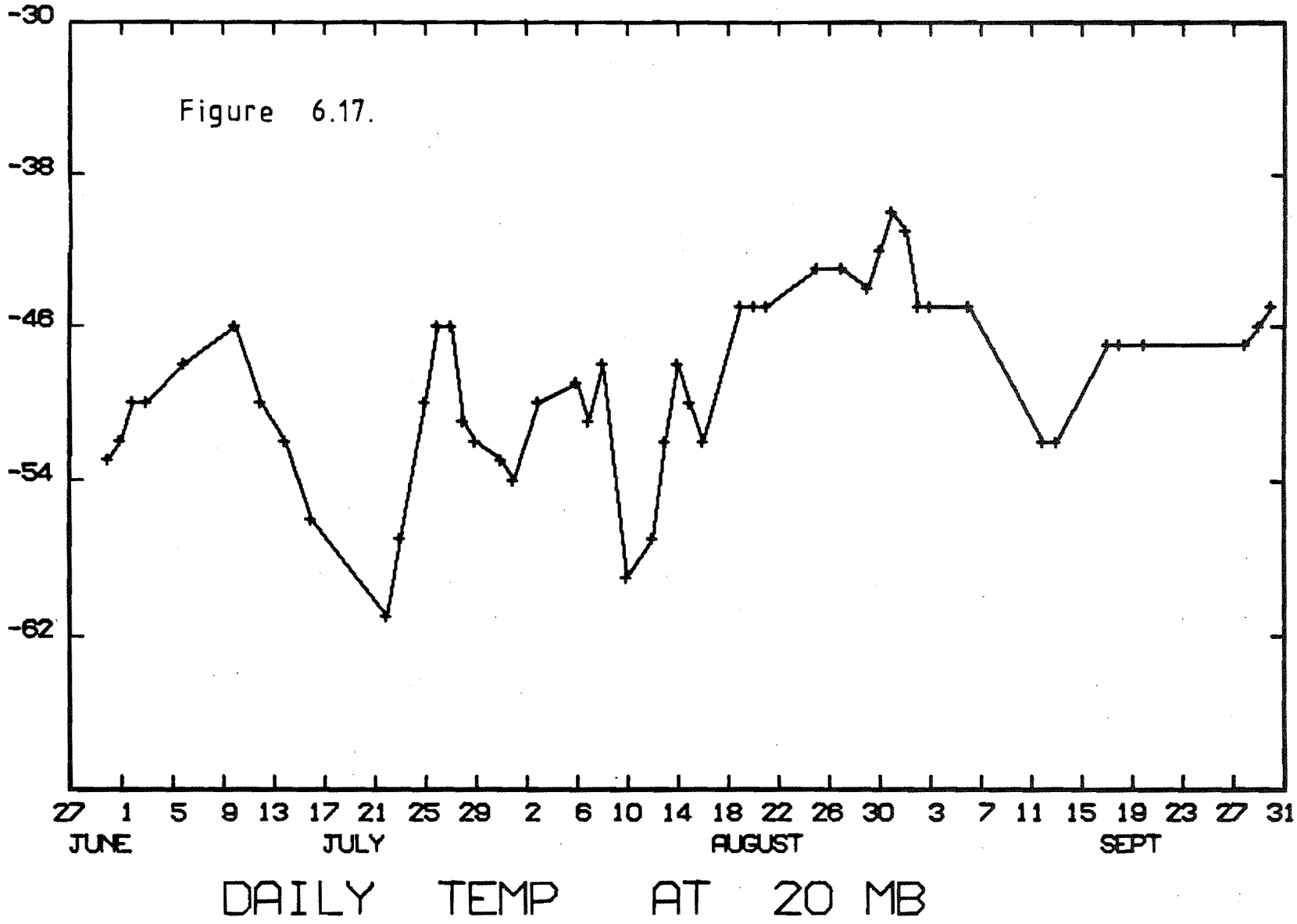
-30
-38
-46
-54
-62
27 1 5 9 13 17 21 25 29 2 6 10 14 18 22 26 30 3 7 11 15 19 23 27 31
JUNE
JULY
AUGUST
SEPT
DAILY TEMP AT 20 MB

Figure 6.17.

on August 31. Although global data, including zonal temperature averages, such as from satellite radiance measurements are required for confirmation, it appears likely that the August wind reversals, both in the stratosphere and in the D-region, were associated with a stratospheric warming. The temperature excursion at 20 mb was not large, but the temperature increases at higher latitudes and in the upper stratosphere will be significantly larger judging by observations of previous warmings (e.g. Quiroz (1978), Figures 8 and 11). The upper level thermal wind, which suggests a cooling of the mesosphere at high latitudes, is also typical of a warming event. The zonal wind change in the upper region commenced not more than a day after the reversal of the stratospheric winds.

Although radiosonde data was not available for 1979, southern hemisphere charts of radiances derived from the Stratospheric Sounding Unit (SSU) on TIROS-N were acquired from the British Meteorological Service. The two main channels have weighting functions which peak near 15 mb (~ 30 km) and 5 mb (~ 38 km).

The major changes in the 1979 winter D-region winds occurred between the 5th and 10th of August (Fig. 6.18), when westward winds were present over most of the 65-100 km height range. This particular month has previously been noted for the unusually strong long-period wind variations in the 80-100 km region (Section 6.4.1), and for the weakness of the monthly-mean eastward jet in the lower mesosphere (Section 5.2). Clearly the westward winds have contributed

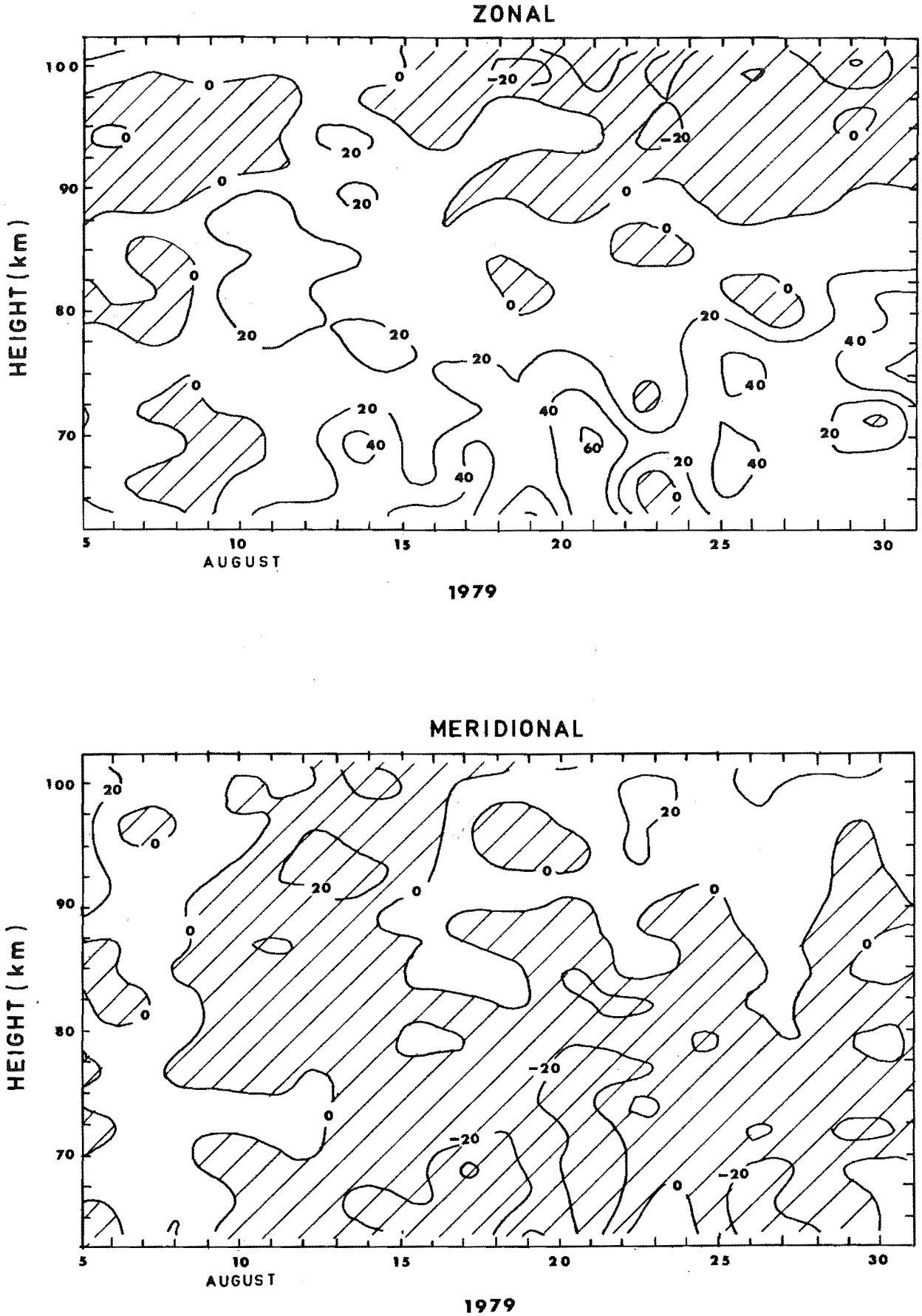

Figure 6.18: Contours of daily winds of August, 1979.

to the latter effect. The thermal wind in the mesosphere was weakly westward (i.e. negative shear with height) from the 7th to 9th of August, increased to eastward values till the 13th, and then reverted to more normal winter westward values above 70 km. This behaviour is consistent with a sequence of mesospheric cooling at high latitudes during the time of westward winds, a stronger cooling of the lower mesosphere from the 10th to the 15th, followed by a recovery to a more usual warm winter mesosphere. During the interval of westward winds, the meridional wind component also showed a change to equatorward winds.

The stratospheric radiance charts at this time show a largely wavenumber 2 temperature disturbance drifting across New Zealand. Temperatures over Christchurch at 15mb reached a peak of -43C on August 7, and had fallen back to -52C by August 16. There was a slight westward tilt of the wave with height. Again there is clearly a coupling between the dynamics of the stratosphere and the upper atmosphere, with little or no time lag.

In late August, a warm centre of a wavenumber 1 disturbance again moved over New Zealand from south of Australia, and led to substantial warming of high latitudes at 15mb. In contrast to the events in early August, no major change in the mesospheric circulation occurred at the same time, indicating that stratospheric changes do not necessarily disturb the upper mesosphere.

6.7.3 Magnetic Storm Effects

Stratospheric warmings have also been associated with changes of a different kind in the mesopause region, with the discovery by Bossolosco and Elena (1963) of a correlation between increases in temperatures at the 10 mb level and the absorption of radio waves in the D-region. Supporting evidence has been given by Shapley and Beynon (1965), Gregory (1965), Manson (1968) and Hargreaves (1973). The relationship between ionospheric absorption and temperature is not simple. Absorption is related to the electron density and the collision frequency in the 80-90 km region, and the electron density is dependent upon neutral and ion chemistry which may be affected both by temperature variations, and by horizontal and vertical transport of minor atmospheric constituents. The winter anomaly in absorption has recently been extensively reviewed by Offerman (1979). The situation is further complicated by the association of electron density (and absorption) with geomagnetic effects.

The 1978 winter geomagnetic and absorption data were examined for any changes associated with the wind and temperature changes discussed in the previous section. The geomagnetic ΣK index at Eyrewell, near Christchurch, is shown in Fig. 6.19a. A major magnetic storm is seen to commence on August 28, with the recovery phase lasting until about October 4. The NOAA Solar-Geophysical Data prompt reports indicated that this was in fact the largest storm of the year with an A_p index of 128 on August 28. (A solar flare also occurred near 500h (L.T.) on August 31 but no

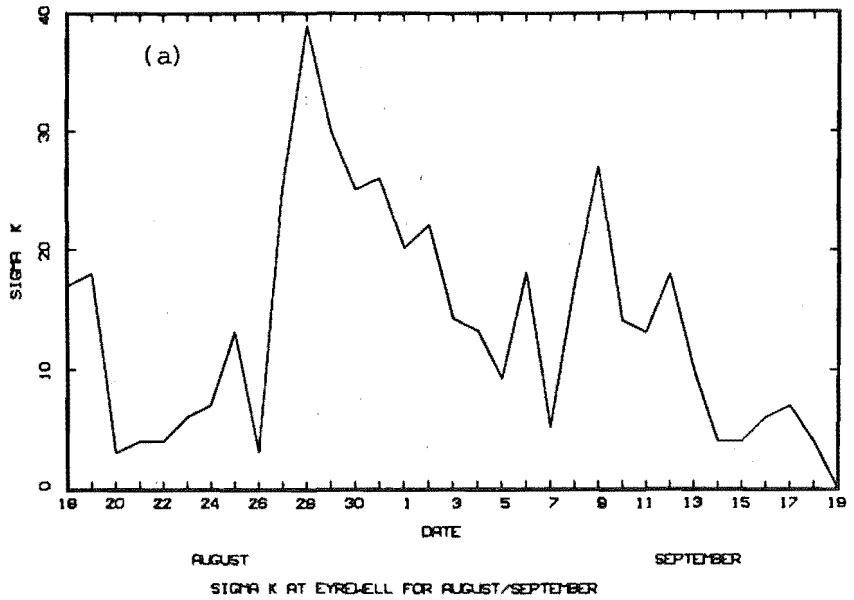
(a)
SIGMA K
0
10
20
30
40
18 20 22 24 26 28 30 1 3 5 7 9 11 13 15 17 19
DATE
AUGUST
SEPTEMBER
SIGMA K AT EYREWELL FOR AUGUST/SEPTEMBER

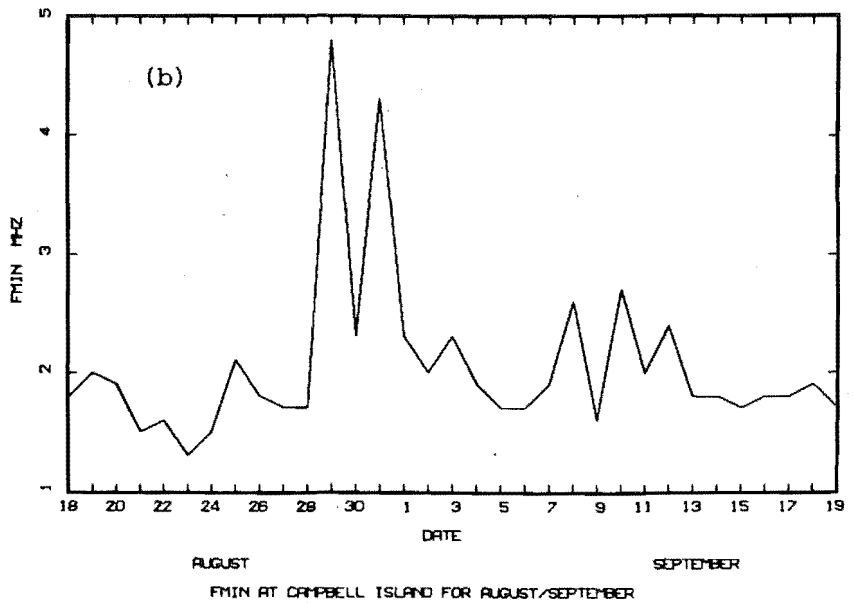
(b)
FMIN MHZ
1
2
3
4
5
18 20 22 24 26 28 30 1 3 5 7 9 11 13 15 17 19
DATE
AUGUST
SEPTEMBER
FMIN AT CAMPBELL ISLAND FOR AUGUST/SEPTEMBER

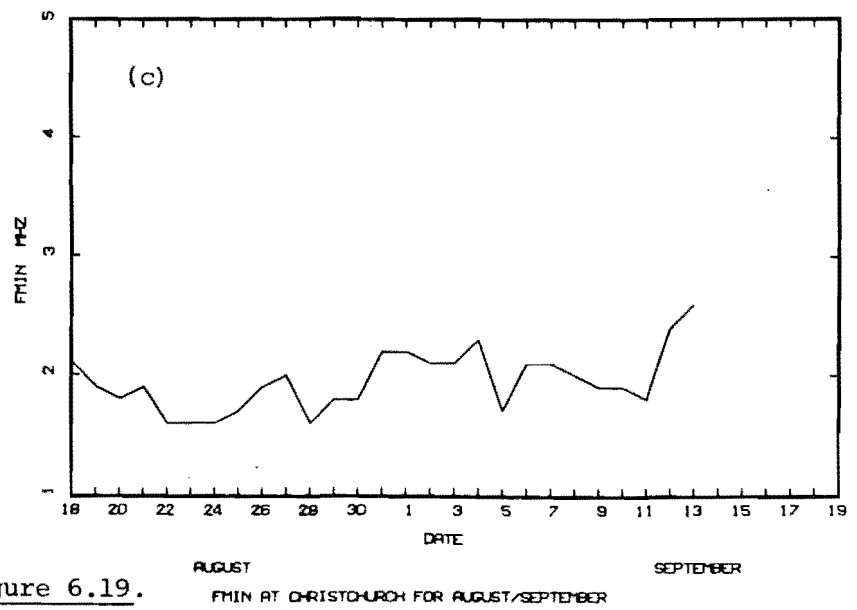
(c)
FMIN MHZ
1
2
3
4
5
18 20 22 24 26 28 30 1 3 5 7 9 11 13 15 17 19
DATE
AUGUST
SEPTEMBER
FMIN AT CHRISTCHURCH FOR AUGUST/SEPTEMBER

Figure 6.19.

effects were seen in the optical or X-ray regions of the spectrum.) Values of f_{min}, a commonly used measure of absorption, at Christchurch and Campbell Island were also available from the DSIR (Fig. 6.19b,c). Campbell Island is located close to the auroral zone (L = 4.0) and therefore absorption effects from particle precipitation would be expected. Hargreaves (1973) has noted that such effects occur typically one day after the ΣK_p peak at high magnetic latitude stations. In accordance with this, a dramatic increase in f_{min} of 3MHz occurs at Camphell Island on August 29 (Fig. 6.19b). The absorption parameter partially recovers on the following day but on the 31st, it again shows a large increase. The solar flare on the 31st occurred too early in the morning to contribute to this second increase in the noon value of f_{min}. Christchurch is at a lower geomagnetic latitude (L = 2.6) where absorption effects associated with geomagnetic phenomena are not so clearly delineated. The f_{min} values show no significant increases on the 29th or 30th of August but increased values are maintained from August 31 until September 4 (Fig. 6.19c).

Two mechanisms can be invoked to explain the increased mid-latitude absorption delayed by 3 days after the onset of the magnetic storm. The first involves the precipitation of energetic electrons initially trapped in the outer radiation belts during the main phase of the storm. Absorption effects produced by the precipitating electrons will be delayed by several days after the onset of the storm as the electrons diffuse to lower L-values, and should persist for almost a

week (Spjeldvik and Thorne, 1975). The increase in absorption at Christchurch is consistent with this. Spjeldvik and Thorne also found from their modelling that the precipitation is strongly latitude dependent, being negligible below invariant latitude $\Lambda = 45^{o}$. This is in agreement with the observations of Lauter and Knuth (1967) who found that precipitation effects disappeared below $\Lambda = 50^{o}$. Christchurch lies close to this limit, $\Lambda = 52^{o}$, but the intensity of the August 1978 storm may have been sufficient to result in the population of relatively low L-values.

An alternative mechanism for the increased mid-latitude absorption is by the modification of the D-region chemistry through transport processes. Enhanced concentrations of nitric oxide (a major source of D-region ionization) have been observed in regions of auroral activity above 90 km by Zipf et al. (1970). Manson (1971) has further suggested that high concentrations will be related to magnetic activity and the associated particle precipitation. Equatorward and downward mixing of this nitric oxide has been proposed to account for the enhanced absorption at mid-latitudes (Geisler and Dickinson, 1968; Strobel et al., 1970). The meridional winds observed at Birdlings Flat are in the correct sense to effect such a transport for a period of about a week after August 26 (Fig. 6.16). A more detailed correlation between the winds and electron densities for this winter is given in Fraser et al. (1981). For a mean northward wind velocity of 5 ms^{-1}, a time delay of several days would be expected between absorption effects at Campbell Island

and Christchurch. This time delay is comparable with the observed delay. Downward transport, such as might be associated with a polar circulation cell, or downward diffusion would also probably be required to introduce the nitric oxide into the 80-95 km region of importance for absorption.

The northward winds below 95 km are not typical of the winter period (Fig. 6.16), and were associated earlier with the warming in the stratosphere. This lends support to the suggestion of Manson (1971) that the anomalous flow patterns which occur during warmings, provide a key link between auroral events and mid-latitude absorption. Further to this however, the schematic summary of the timing of the magnetic, ionospheric and meteorological parameter changes in Fig. 6.20, suggests that the stratospheric temperature

Figure 6.20: Schematic illustration of the timing of related magnetic, ionospheric and meteorological parameters, where u,v and T and zonal and meridional winds and termperature.

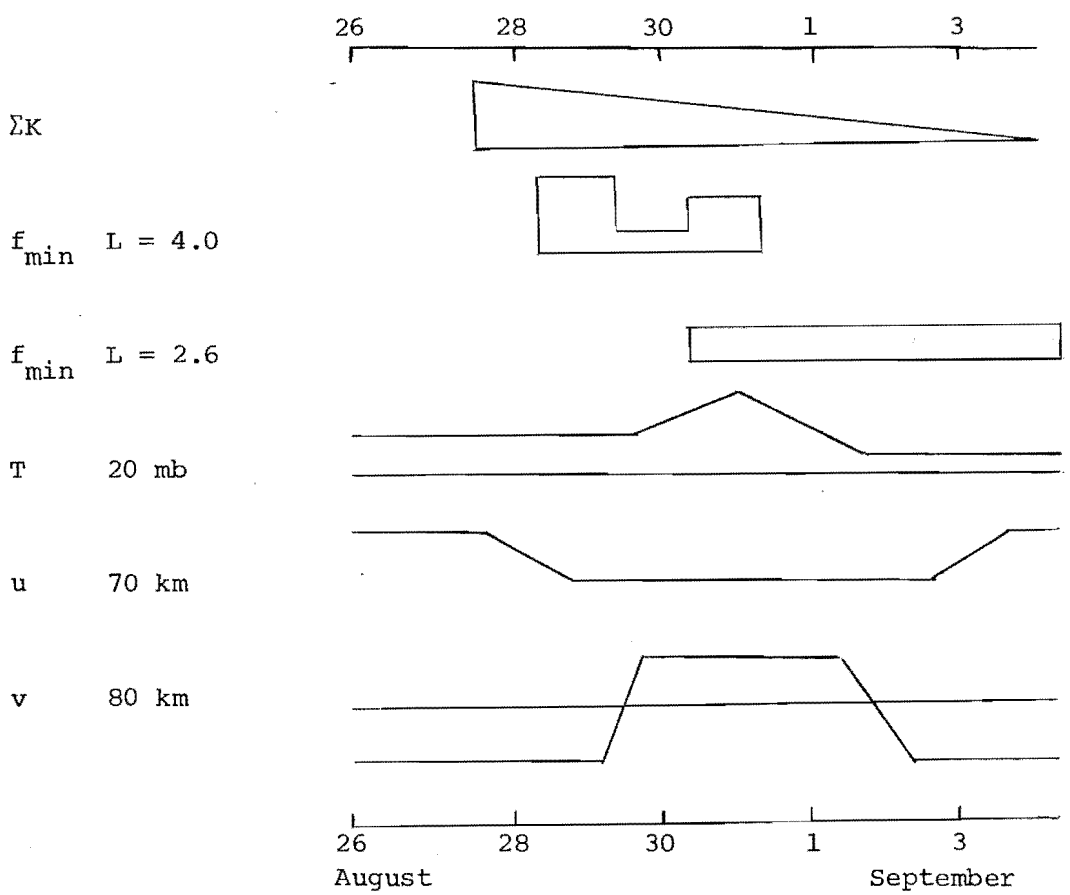

increase at 20 mb on the 31st was itself associated with the magnetic storm. The stratospheric temperature had been building up to sustained high values for several weeks prior to this, and the magnetic storm gives the appearance of being a trigger for an additional sudden increase. This in turn may be associated with the second increase in f_{min} observed at Campbell Island, and the rapid decrease in strength of the mesospheric zonal winds. In the absence of a fuller global coverage of all the parameters involved, such proposals as to cause and effect must remain speculative. The occurrence of stratospheric warmings following several days after enhanced geomagnetic activity has also been noted by Manson (1968), Sinno and Higashimura (1969), Hargreaves (1973) and Essex and Morton (1974).

Manson (1969) determined that energy deposition by precipitating electrons would cause significant heating at high latitudes above 85 km, and he examined the possibility that modifications to the lower thermospheric temperature structure could alter the propagation conditions for the planetary waves which are related to stratospheric warmings. In the present data no magnetic storm related increase in the thermal wind could be discerned.

In summary then, there appears to be an intricate interplay between magnetic storms, ionospheric winds and absorption, and stratospheric temperatures. On the occasion discussed here, the development of a stratospheric warming appears to have been enhanced by the occurrence of a major magnetic storm, with associated increases of auroral and mid-latitude ionospheric absorption.

CHAPTER 7

ATMOSPHERIC TIDES

7.1 THEORY OF ATMOSPHERIC TIDES

Atmospheric tides are those oscillations of the atmosphere whose periods are integral fractions of a solar or lunar day. It is found that the thermally forced solar tide is stronger than the gravitationally excited lunar tide. Since the daily variation of insolation does not follow a simple sinusoidal variation, the higher harmonic content of the forcing can give rise to an important tidal contribution from a semidiurnal (12h) tide as well as the diurnal (24h) tide.

Siebert (1961) and Butler and Small (1963) recognized the importance of insolation by ozone and water vapour in the excitation of atmospheric tides and were able to successfully account for the strength of the semidiurnal component. Observations and theory have been extensively reviewed by Chapman and Lindzen (1970). Although the 'classical tidal theory' described in these works does not consider viscosity or background winds, it was successful in providing at least a qualitative explanation of many aspects of tidal observations. In the classical theory, the tides are described by the linearized primitive equations on a rotating spherical earth. The equations can be consolidated into a single equation involving altitude, z, and latitude, θ, when the tidal solutions are assumed to be periodic in time and longitude, i.e. of the form $\exp i(\sigma t + s\lambda)$, where σ,s and λ are the wave

frequency and zonal wavenumber and longitude respectively (Appendix D). Observations at single stations are concerned with migrating tides which follow the sun, and for $\sigma=1$ these waves have $s = 1$, and for $\sigma = 2$, $s = 2$. Ground level pressure measurements do, however, show a contribution from a non-migrating diurnal tide (Wallace and Tadd, 1974), but Lindzen (1979) considered that it would not be significant at mesospheric heights. A non-migrating tide at meteor heights was suggested by observations of Glass et al. (1975) however. Since measurements are only available at a single latitude in the present work, attention will subsequently be confined to the purely migrating tide.

For a given tide, with fixed σ and s, the equations are separable into vertical and latitudinal dependence. The horizontal structure equation, Laplace's tidal equation, has no contribution from the thermal forcing and is solved in terms of the Hough functions which were used to describe the free normal mode solutions (Section 6.2). In contrast to the free modes whose frequencies were obtained as eigenvalues of the equation, the frequencies of the tides are predetermined by the known forcing. Laplace's tidal equation is then solved to obtain a set of equivalent depths (h_n^{σ}) as eigenvalues corresponding to the eigenfunctions (the Hough functions). Usually only a small number of modes are required for an adequate solution. Each mode is conveniently labelled by an index, n, which increases with the latitudinal structure of the Hough functions, and a tidal mode is then identified by (s,n). The assumption of completeness of the set of Hough

functions provides the justification in expanding the thermal forcing in terms of these functions and so providing the separability of the equations. The solution for the semi-diurnal tide consists only of westward propagating gravity waves i.e. solutions of Laplace's tidal equation of the first class. However, Lindzen (1966) and Kato (1966) recognized that solutions of the second class (related to the Rossby modes) with negative equivalent depths were required to fully describe the diurnal tide.

Once the equivalent depth, which appears in the separation constant, is obtained, the vertical structure equation can be solved for each mode. Consideration of the homogeneous part of this equation yields an effective vertical wavenumber, Q, given by

$$Q^2 = \frac{1}{Hh_n^{\sigma}} (\kappa + \frac{dH}{dz}) - \frac{1}{4H^2} \qquad (7.1)$$

The vertical structure of a mode is therefore determined by the value of its equivalent depth and the background temperature structure (through H). In general a number of modes will interfere to give a complicated vertical structure in amplitude and phase and modal identification on the basis of the observed vertical wavelength ($2\pi/Q$) will not be possible unless one particular mode is strongly dominant. In the mesosphere where $\frac{dH}{dz} < 0$, modes with large positive h_n (the (2,2) and (2,3) modes) may have $Q^2 < 0$ becoming evanescent in this region and being largely trapped below. Some upward leakage of energy will occur however, and the

mode may then resume propagation in the thermosphere. The equivalent depths and vertical wavelengths of the most important modes at 90 and 100 km, as computed from the mean

Table 7.1: Equivalent depths (Chapman and Lindzen, 1970) and vertical wavelengths of the principal propagating tidal components in the CIRA 72 mean reference atmosphere.

Mode	h (km)	90 km λ_z (km)	100 km λ_z (km)
2,2	7.85	evan	170
2,3	3.67	82	61
2,4	2.11	49	41
2,5	1.37	37	32
2,6	.96	29	26
1,1	.69	24	22
1,3	.12	10	9

CIRA 72 standard atmosphere and neglecting viscous effects, are shown in Table 7.1. It can be seen that higher order modes (with larger n) have smaller equivalent depths and will be able to propagate through the mesosphere. These modes also have shorter vertical wavelengths. The diurnal modes with negative equivalent depths will, from (7.1), be vertically evanescent throughout the atmosphere. Despite this they can assume importance at mid- to high- latitudes as discussed below.

The relative excitation of a tidal mode depends upon the matching of the thermal forcing onto the latitudinal and vertical structure of the mode. The forcing due to ozone and water vapour covers a very broad latitude range. The semidiurnal component of this forcing, expanded in terms of Hough functions, matches the (2,2) mode best. The vertical distribution of ozone heating used by Chapman and Lindzen (1970) has a broad vertical extent (with a half width of 40 km) centred near 50 km, while the water vapour heating is strongest near the ground and decreases with height. The broad ozone forcing will be inefficient in exciting short wavelength modes since excitation at one height will suffer cancellation from excitation at a higher height. The (2,2) mode has a very long vertical wavelength and will consequently be excited efficiently, both in the vertical and latitudinal directions. The higher order modes have smaller structure both vertically and latitudinally and will therefore not be excited so efficiently. However they do not suffer from trapping by the mesosphere, as the (2,2) mode does, and may assume importance in the lower thermosphere.

The Hough functions of the propagating diurnal tide are confined near the equator and as such do not match the tidal forcing well despite its fundamentally diurnal nature. Additionally the short vertical wavelengths of these modes (Table 7.1) lead to inefficient forcing by ozone. Of the propagating modes, the (1,1) mode receives the greatest excitation, from heating by tropospheric water vapour. In contrast, the evanescent (1,-2) mode has a broad latitudinal

extent and receives the bulk of the diurnal forcing, especially by ozone heating in the stratosphere. Despite its decay of energy flux with height, it does provide a high latitude complement to the equatorially confined diurnal propagating modes.

The classical theory for the semidiurnal tide was extended by Lindzen and Hong (1974) with the inclusion of vertically varying background winds. They found that higher order modes were generated through coupling with the background wind and other modes. For example, the amplitude of the (2,4) mode in the lower thermosphere due to mode coupling to the (2,2) and (2,3) modes was found to be twice that due to direct thermal forcing. Shorter wavelength modes were therefore expected to be found in the upper atmosphere, particularly at solstices. Hong and Lindzen (1976) also noted that only modest changes in the zonal winds below 100 km were needed to cause large changes in the amplitude and phase of the wind induced modes. Walterscheid and Venkateswaran (1979a,b) developed a spectral form of the tidal equations in the presence of background winds and confirmed the general conclusions of Lindzen and Hong.

Deficiencies in the thermal excitation used in the above models were noted by Forbes and Garrett (1978b). They determined that thermal excitation of higher order semidiurnal modes should be stronger, and that antisymmetric components of heating should be used. Walterscheid et al. (1980) used improved heating rates and found that this factor was actually more important than background winds in enhancing the amplitudes

of the higher order modes. Short wavelength modes were predicted to be most important in winter. The seasonal variation of heating rates contributed to a seasonal variation of tidal amplitudes with larger values in winter than in summer.

Forbes and Garrett (1978b) found that the diurnal heating rates showed little seasonal variation. The water vapour heating for the propagating modes was not altered significantly from earlier models but the ozone heating rate for the (1,-2) mode was found to be a factor of 2 larger. The possibility of an additional heat source in latent heat release in clouds is not thought to be of significance to tides in the upper atmosphere (Lindzen, 1978).

The effect of winds on the diurnal tide has received little theoretical attention, apart from an estimation of the effect on the (1,1) mode at tropical latitudes by Lindzen (1972). In particular, the effect on the strongly forced (1,-2) mode in the mesosphere has not been studied.

The attenuating effects of molecular viscosity, thermal conductivity and ion drag become important above 100 km in the thermosphere. These factors have been studied by Hong and Lindzen (1976), Forbes and Garrett (1976, 1978a) and have been reviewed by Forbes and Garrett (1980). The (1,1) mode which becomes statically unstable at 85 km near the equator is stabilized and damped by molecular viscosity above 108 km (Lindzen and Blake, 1971).

7.2 DAILY TIDES

The importance of diurnal and semidiurnal oscillations of the wind at heights of 80 to 100 km can be seen in the contour plots of wind data in Fig. 7.1. In this example, strong eastward winds occur a few hours before noon each day, and strong northward winds follow several hours after noon. A semidiurnal influence is also evident in the northward winds and in the upper region of the eastward winds. Power spectra of month long data series indicate the dominance of tidal wind oscillations with periods of 24 and 12h (e.g. Fig. 6.9). In Section 6.5.2 it was noted that the diurnal tide is usually more irregular than the semidiurnal tide, showing lower spectral power and greater spread in frequency. This is also apparent from a day by day analysis of the wind.

The daily zonal and meridional components of the tide are obtained by subjecting each 24h segment of data to a weighted least squares fit of a prevailing, 24h and 12h components. The linear regression method used is detailed in Appendix C. The weights used are the number of wind velocities contributing to each hourly mean. Other weighting schemes were tried including weighting by the inverse of the variance and the inverse of the standard errors of the mean of the hourly wind values. No significant differences between the results from these variants was found. The low data rate at night has necessitated the averaging of data from two adjacent height ranges. Errors in the daily tidal components are deduced from the r.m.s. deviation of the

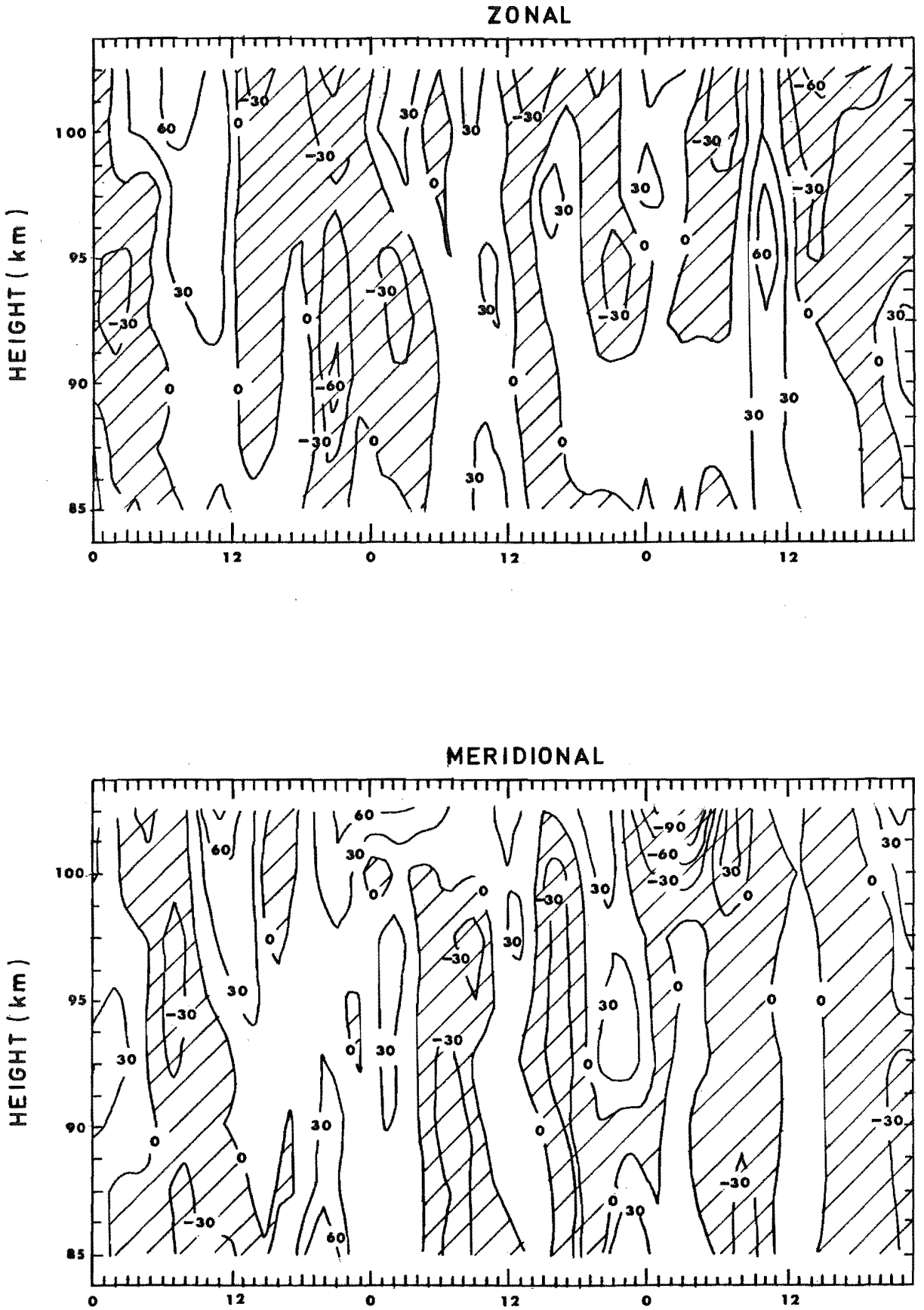

Figure 7.1: Contour plot of hourly wind values of July 1-3, 1979.

measurements from the least squares fitted data. Typical values are 5-10 ms^{-1} in amplitude and 15-45^{o} in phase, indicating significant spread about the fitted data. Gravity waves are likely to contribute to this variance.

Figure 7.2: Phase variation of the semidiurnal tide at 90 km for 8 days in July 1979.

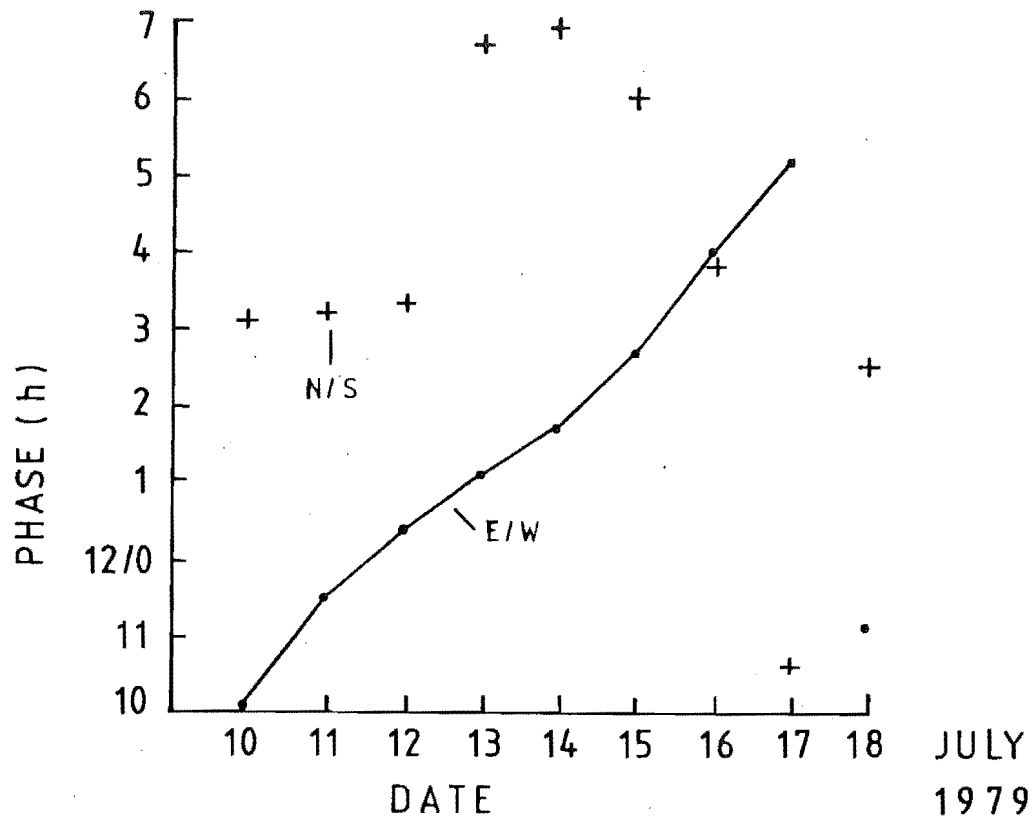

The daily tides obtained from the harmonic analysis generally show considerable variation from day to day. On rare occasions this variation can be very regular. An example of this is shown in Fig. 7.2 where the eastward phase of the semidiurnal tide undergoes a steady phase retardation of 7h over the course of 8 days. The northward phase did not show a similar variation.

The day to day changes in the tide can also be seen by passing the raw wind data through a numerical band-pass filter centred on the chosen tidal frequency (e.g. Glass et al., 1978). The upper diagram of Fig. 7.3 shows a ten day section of data after filtering about a period of 12h with a filter which extends over 48 hours and has half-amplitude points at 16 and 9.7h and negligible side lobes (Appendix E). The amplitude and phase vary considerably, although this is not to be regarded as typical; at other times variations of the semidiurnal tide can be smaller.

A very useful way of presenting the same information is by means of complex demodulation (Bingham et al., 1967). The frequency of interest is first shifted down to zero frequency and a low-pass filter then applied to the resultant time series. This gives directly the time-local amplitude and phase of the required frequency band. Details are given in Appendix F. The method could be used as a substitute for harmonic analysis, although it does not allow for weighting the data points which is necessary when data is sparse or absent. The lower diagram of Fig. 7.3 shows the complex demodulate for the semidiurnal tide using a low-pass filter with the same cut-off characteristics as that used in the upper diagram. The amplitude and phase variations appear more clearly than for the basic broad-band filtering.

An interesting feature of Fig. 7.3 is the amplitude zero accompanied by a 180^{o} phase jump. This is suggestive of the interference between two roughly equal amplitude, out of phase, vectors. One possible explanation is that an

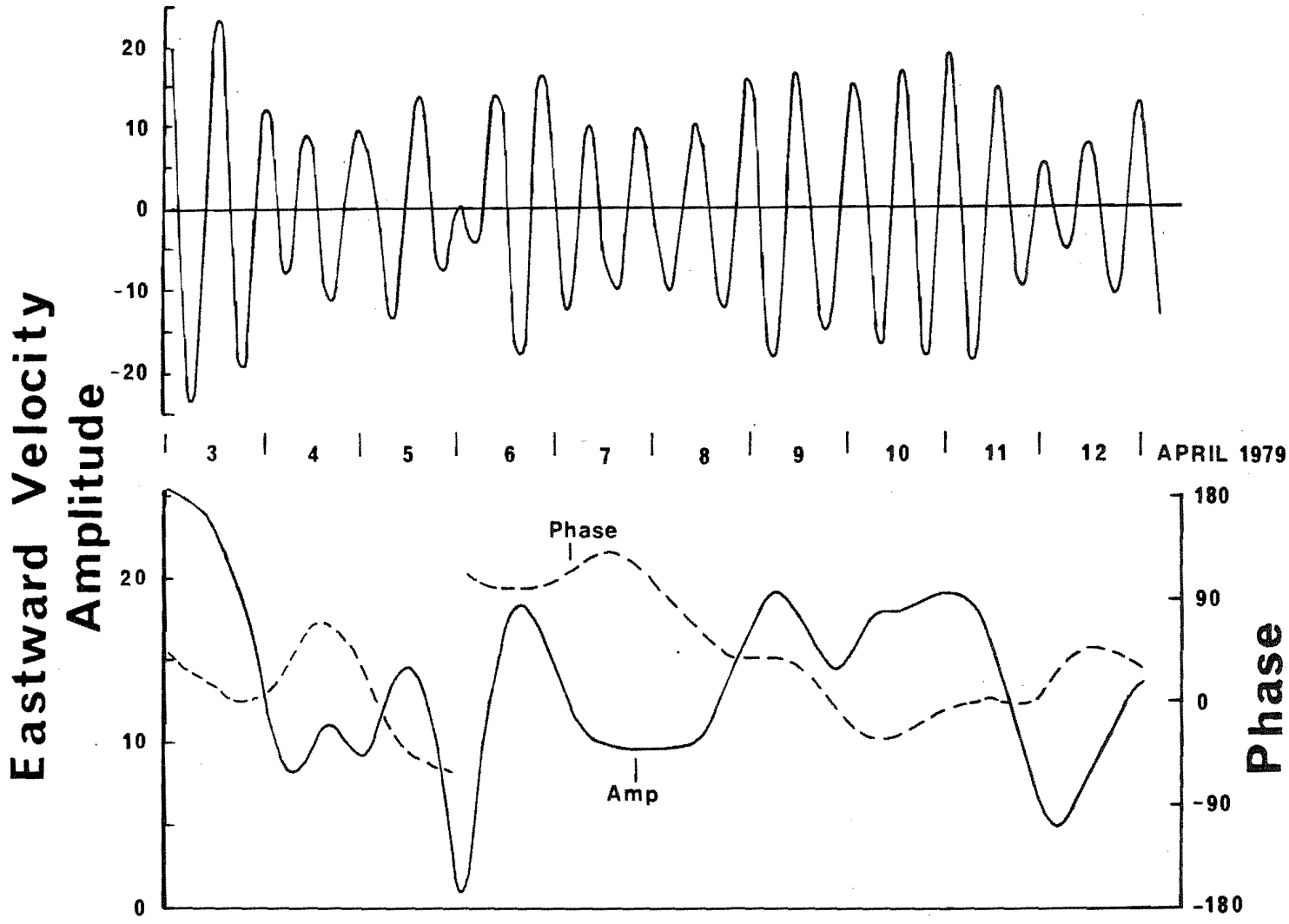

Figure 7.3: The semidiurnal tide as shown by band-pass filtering of data (upper) and by complex demodulation (lower). Filter characteristics are shown in Fig. E.4.

internal gravity wave within the filter pass-band is interfering with the steady tide; the gravity wave will have a vector which rotates in phase with respect to the 12h tide after demodulation. Further weight to this is given by the appearance of a 10.4 h peak in the power spectrum for this month. It should be noted that the least squares method of conventional tidal analysis will also be subject to contamination from oscillations of non-tidal frequencies. The narrow, 24-point data window which is usually used will have a wide frequency response. Consequently fluctuations in the tidal parameters may on occasion be caused by the presence of gravity waves, or in the case of the diurnal tide, planetary waves, at nearby frequencies. In using complex demodulation, direct control over the bandwidth is exercised, enabling possible contamination to be reduced, although care has to be taken that real changes in the tides are not obscured.

Tidal variations may have a number of causes. Lindzen and Hong (1974) found that modest changes in the background temperature structure could result in changes of the order of 30% in the magnitude of the semidiurnal tide in the lower thermosphere. Teitelbaum and Cot (1979) also noted the sensitivity of the modelled tidal response to local temperature fluctuations. Tides excited through mode coupling were found to be very sensitive to zonal wind changes by Hong and Lindzen (1976). Complicated changes in the tide resulting from the superposition of a number of modes may occur when even uniform changes of the thermal excitation occur, since the shorter wavelength modes will be particularly

susceptible to changes of height or width of the excitation region. Fellous et al. (1975) have shown that downward propagating, reflected waves can be important, so changes in the reflection characteristics at higher heights may also be involved.

7.3 THE SEMIDIURNAL TIDE

Since the tides exhibit significant variations from day to day, it is necessary to have a large data sample to gain a representative picture of a tide at a particular time of year. The present data has unprecedented coverage and has enabled tidal averages to be formed for each month. This should indicate any seasonal changes, and also the variation of a tide within a season. Since the data spans 18 months, an indication of year to year variability can also be obtained.

Monthly average phase values have been obtained by vectorially averaging the daily tides. Days where more than 6 hours of data was missing were not used. When phase variations in the tide are large, the amplitudes of the vector averages are small, so a more representative value of daily tidal amplitudes is the arithmetic mean of the daily amplitudes. The mean height profiles for the semi-diurnal tide from June 1978 through to February 1980 for each available month are displayed in Fig. 7.4. The error bars are the standard errors of the mean for the month and the numbers down the right-hand side of each diagram indicate

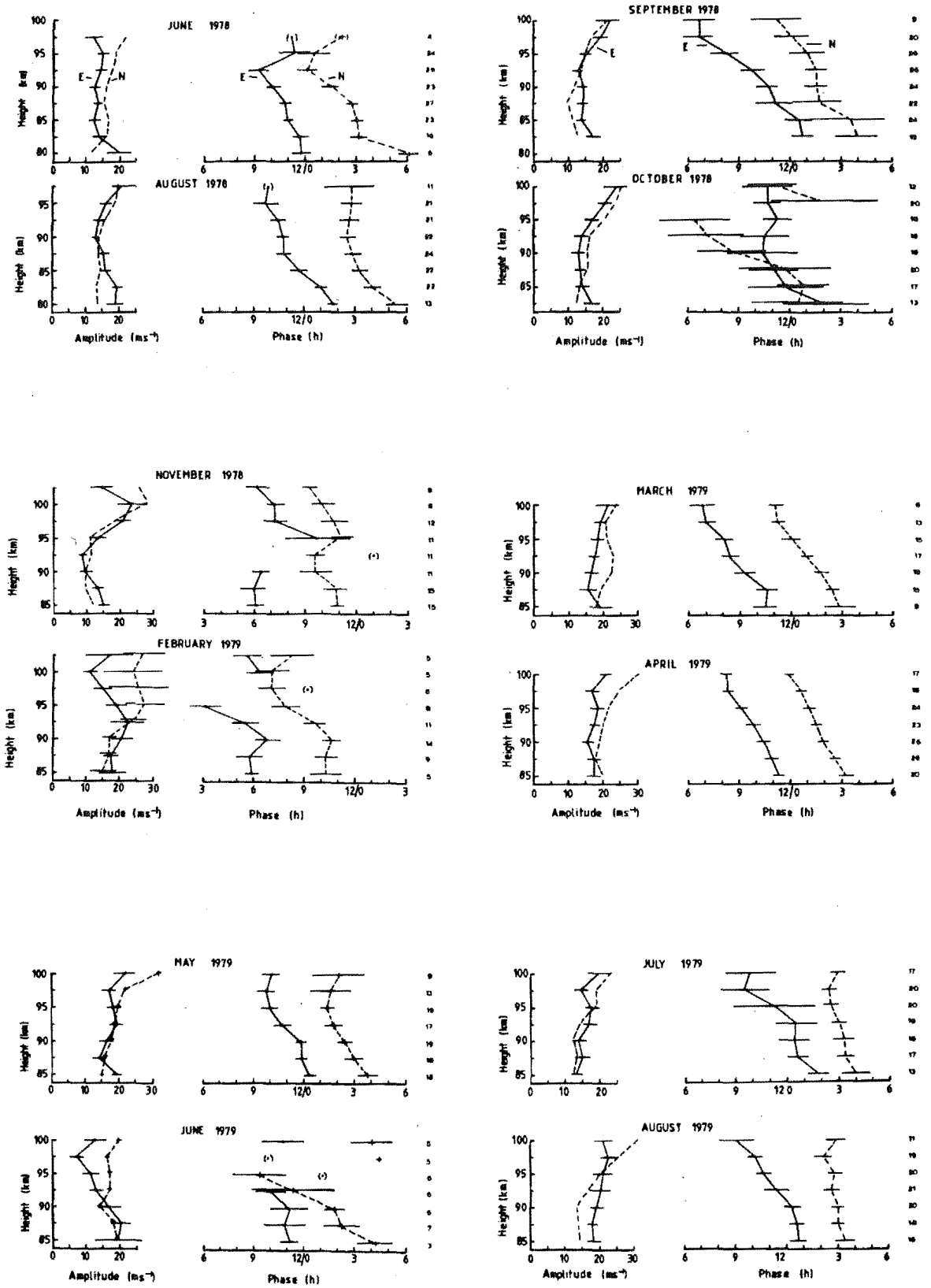

Figure 7.4: Height variation of the semidiurnal tide, June 1978 to February 1980.

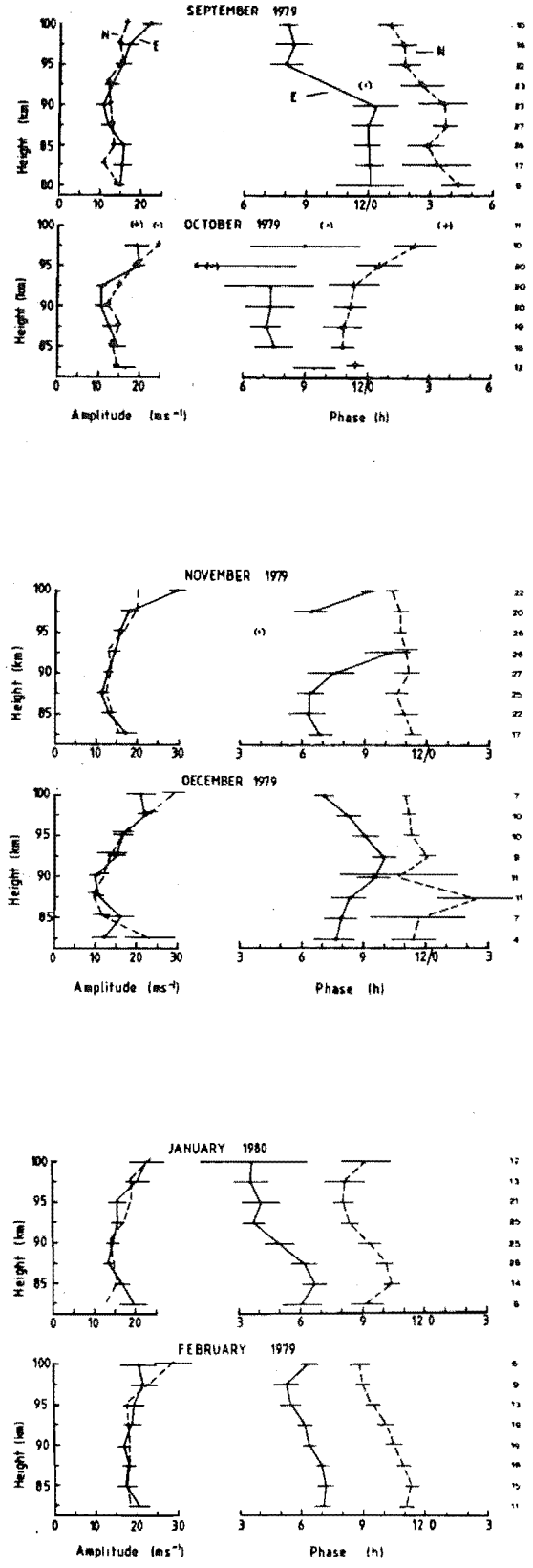

Figure 7.4: Continued.

the number of individual days which contributed to the average. The lowest and highest heights have the sparsest data and should therefore be regarded with caution. The phase is expressed as the local time to maximum eastward (or northward) velocity. This avoids possible ambiguity which can arise when phase is referred to in degrees; such a phase is dependent upon the particular definition used, whether $A \cos(\omega t \pm \phi)$ or $A \sin(\omega t \pm \phi)$.

When a single (unreflected) tidal mode is present the phase profiles are expected to show a constant slope with height (except possibly for very short vertical wavelengths modes when viscosity may lengthen the wavelengths in the upper regions (Hines (1974), p.643)). Upward propagating tidal waves have downward phase progression resulting in the time of maxima decreasing with increasing height. In the southern hemisphere the phase of the eastward tidal component should in general lead the northward component by 90°, consistent with a counter-clockwise rotation of the velocity vector when viewed from above. This is true for the (2,2) mode at all latitudes but the latitudinal structure of the higher order semidiurnal modes involves 180° phase changes at certain latitudes. Blamont and Teitelbaum (1968) showed that as a consequence the sense of tidal rotation would reverse within particular latitude bands. At 44°S the counter-clockwise sense of rotation is in fact preserved for all the semidiurnal modes of importance; the nearest latitude band of reversal is between 39° and 42° for the (2,6) mode. The main diurnal modes also have counter-clockwise rotation at 44°S.

In general a number of modes, each with a different vertical wavelength, will be present. Interference between these modes can result in complicated vertical behaviour in both phase and amplitude, examples of which have been shown by Stening et al., 1978. This may also result in the sense of rotation reversing with height at a fixed latitude.

7.3.1 Results

The observed semidiurnal tide (Fig. 7.4) exhibits a counter-clockwise rotation of the velocity vector on most occasions with the eastward phase leading the northward by close to 3h. The sense of phase propagation is also predominantly downward.

The winter behaviour of the semidiurnal tide can be seen from the profiles for June and August, 1978, and for July and August, 1979. In June, 1978 the eastward component has a fairly steady phase progression between 82 and 92 km, with a slope corresponding to a vertical wavelength close to 45 km. If a single mode was known to be dominant, this would correspond well to the vertical wavelength of the (2,4) mode. Alternatively, it may reflect the behaviour of the superposition of longer and shorter wavelength modes. The abrupt change in phase above 95 km may then be the result of the interference between such modes. The lack of amplitude growth with height, as expected for a single dominant mode, may also be due to modal interference, or it may be indicative of loss processes or wave reflection. The

resolution of such possibilities is not possible with the present data.

The profile for August, 1978 shows a strong phase gradient below 87 km ($\lambda_z \sim$ 30 km) which becomes much weaker above. The two winter months in 1979 also show evidence for short wavelength modes in the eastward components; the inferred wavelength in August 1979 is 45 km. The northward semidiurnal components differ from 1978 by showing more strongly the presence of a long wavelength mode. The vertical wavelengths inferred from the northward phases are close to 100 km. The standard deviation of the phase is also small as would be expected in a simple case of a dominating long wavelength component. A more pronounced amplitude growth is also observed. The data for June 1979 represents a much smaller data sample than other months and is poorly behaved. The northward phase slope ($\lambda_z \sim$ 15 km) is probably too steep to correspond to a tidal mode which could escape significant dissipation.

The significant feature of the summer profiles is their pronounced shift in phase to maximize at earlier times. The northward profiles in November and December in 1978 and 1979 suggest the importance of a long vertical wavelength mode. The eastward component has a more complicated structure with a significant phase discontinuity near 95 km in early summer (November, 1978 and 1979) and also in the late summer of February, 1979. The more regular behaviour in February 1980 is characterized by vertical wavelengths of 78 and 63 km in the eastward and northward components respectively.

The most well defined downward phase progression was observed in autumn (March, April, May 1979). The standard deviations of phase were also small at this time. The vertical wavelengths ranged from 35 km in March, to

Table 7.2: Estimated Vertical Wavelengths (km) of the zonal (E) and meridional (N) components of the semidiurnal tide

1978

	J	J	A	S	O	N	D
E	51		(30)	30	~ev	-	
N	45			50	-	-	

1979

	F	M	A	M	J	J	A	S	O	N	D
E	-	35	45	45	(~ev)	-	45	-	~ev	-	-
N	-	35	50	50	(15)	100	115	-	-	>200	(~ev)

1980

J	F
-	80
-	60

50 km, suggesting the presence of the short wavelength modes: (2,4), (2,5) or (2.6). A summary of the wavelengths deduced

from the observed phase gradients can be found in Table 7.2.

In contrast to the regular behaviour of autumn, the spring equinox profiles show large variations of phase associated with a rather rapid change from winter phase values to summer values. Especially large variations occurred during October 1978.

The seasonal variation of the amplitude and phase can be seen more clearly from Fig. 7.5 where the monthly mean values at 90 km are plotted. The phase is fairly steady throughout winter with only a slight retardation with time. The eastward component achieves maximum values significantly earlier in 1978 than in 1979 - 10.5h compared with 12h - indicating a certain amount of interannual variability. The northward phase typically lags the eastward phase by 2 to 4 hours, consistent with a counter-clockwise rotation of the velocity vector. In spring an abrupt phase change of approximately 5 hours occurs in both tidal components. This occurs between September and October in 1979, but slightly earlier in 1978 for the northward component. During summer the eastward phase at 90 km shows large changes associated with the irregular phase gradient noted earlier. A change in autumn occurs between February and March, but its magnitude of 2.5 - 3h is not as large as in spring. Instead the phase shows a steady retardation during autumn to reach the winter phase values. The timing of the equinox phase changes are not symmetrical with respect to season; the autumn change occurs close to the end of summer while the September/October change is closer to the middle of the season.

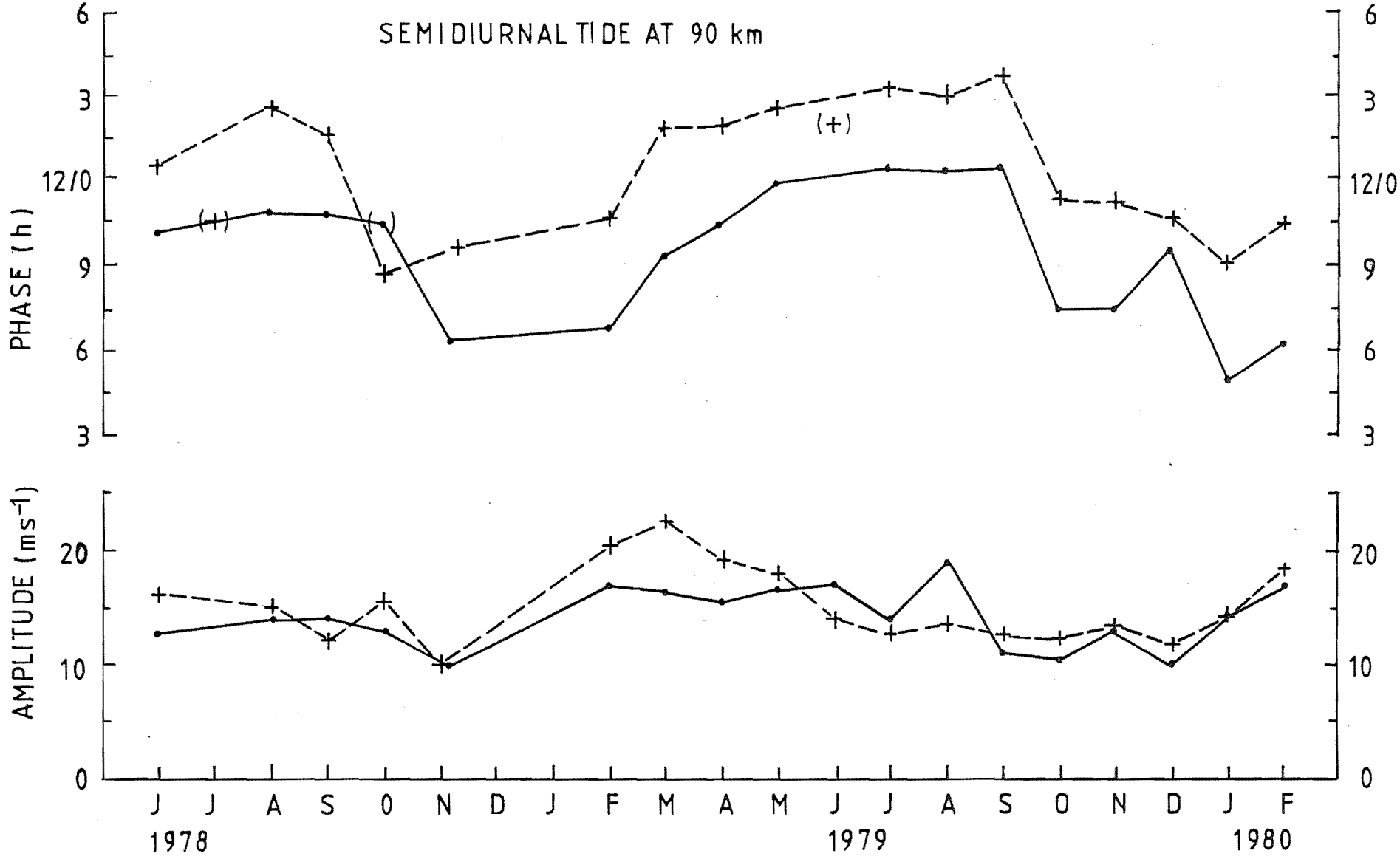

Figure 7.5: Seasonal variation of the semidiurnal tide at 90 km.

The amplitude variation of the semidiurnal tide at 90 km is predominantly annual with largest values occurring in early autumn and smallest values in late spring. There is little difference between summer and winter amplitudes. The eastward and northward amplitudes are similar in value to each other except in late summer/early autumn when the northward component consistently exceeds the eastward component.

7.3.2 Comparison with Other Results

Tidal measurements using the partial reflection drifts experiment have not previously been attempted at Christchurch. However, 35 days of meteor radar observations spread over a year were reported by Wilkinson and Baggaley (1975) for a height interval of 90 - 100 km. The annual variation of amplitude of the semidiurnal tide was quite different to that observed here, but those results were based on samples of only several days per month. The tidal phase did show some similarities at times. In particular, Wilkinson and Baggaley noted a fairly steady eastward phase during autumn and winter with typical values of 10.5h. This value, corresponding to a mean height of 95 km, is in agreement with the present results. The abrupt phase change of nearly 180^{o} in spring was also seen. Meteor radar wind measurements with height determination were made by Poulter (1980) for a 9 day period in July, 1977. The observed phases at 90 km are in good agreement with the present results. However, the phase gradients indicated the dominance of an evanescent semidiurnal mode

while the present data suggests contributions from higher order modes particularly in the eastward component.

A comparison with other mid-latitude results is shown in Table 7.3. For the purposes of comparison, the northern

Table 7.3: Amplitudes (A) and phases (ϕ) of semidiurnal tidal wind components near 90 km.

Lat.	Winter				Summer				Ref.
	U		V		U		V		
	A ms^{-1}	ϕ h	A ms^{-1}	ϕ h	A ms^{-1}	ϕ h	A ms^{-1}	ϕ h	
44S	15	10 -12.5	14	.5-3.5	15	5-9.5	16	9-11	1
43S	25	11 -13	23	1.5-4					2
43S	16	9 -11	16	11-2	13		9	~9	3
35S	13	10.6	11	3.8	12	7.3	16	0.6	4
47N	20	9.5			10	7.0			5
40N			26	4.6			21	2.8	6
53N	18	5.6-7.7	21	9-10.4	9	2.6-4.1	12	7.4-8	7
52N	15		15	3.5	16	12-13	14	11-13	8
45	29	9.8			18	10.7			9

References to data sources:

1: Present results; 2: Poulter (1980); 3: Wilkinson and Baggaley (1975); 4: Elford (1959); 5: Fellous et al. (1974); 6: Hess and Geller (1976); 7: Greenhow and Neufeld (1961); 8: Stening et al. (1978); 9: Walterscheid et al. (1980).

hemisphere meridional phases have been adjusted by 6h to account for their clockwise rotation of the velocity vector. The comparatively small correction of -0.5h to the Christchurch phases due to the difference between L.T. and local mean solar time has not been made. The majority of the data is from meteor radar measurements, but also shown are partial reflection results from Saskatoon (52^{o}N) and theoretical values obtained by Walterscheid et al. (1980). It can be seen that the winter results for phase near Christchurch overlap, but that larger amplitudes were measured by Poulter (1980) in July, 1977. The other southern hemisphere station, at Adelaide (35^{o}S), also shows reasonable agreement, but the higher latitude, northern hemisphere results of Greenhow and Neufeld (1961) show some significant differences in phase values. A comparison between measurements made at different locations and times can only be expected to give a qualitative indication of tidal behaviour since the exact values of amplitude and phase will depend on both the combination of modes present and upon latitude.

The theoretical value of zonal phase at mid-latitudes, as determined by Walterscheid et al. (1980), is in general agreement with the observations in winter. However, the summer value of 10.7h differs significantly from the observed typical value of 7h. It happens that the value of 7h is in agreement with models using the earlier distribution of thermal forcing.

The most well defined short wavelength (higher order) modes were observed during autumn, although such modes also

appeared in September, 1978 (Table 7.2). In winter the contribution from long wavelengths dominated. This is in contrast to the observations of Fellous et al. (1975) who found that short wavelength modes prevailed in winter at 47°N. Their results at the equinoxes were averaged over periods spanning 3 months. There is a danger with such coarse averaging at times of changing and variable tidal phase (particularly in October), that regular features are smeared out; the same problem arises for significant changes within a month in the present results. The presence of short wavelength modes in autumn is also in direct conflict with the model of Lindzen and Hong (1974) who predicted longest wavelengths at this time. The improved model heating rates of Forbes and Garrett (1978b) with their narrower vertical extent may ameliorate this situation.

A prominent feature of the phase at Birdlings Flat is the rapid change during autumn. Greenhow and Neufeld (1961) also found that a rapid change occurred between September and October at 53°N, while a more gradual change was observed during the northern hemisphere spring. Rapid phase changes during October have also been reported by Fellous et al. (1975) at 47°N and Schminder and Kürschner (1978) at 51°N. The fact that the rapid phase transition occurs regularly at approximately the same time of year in both hemispheres suggests that this is a global phenomenon rather than a local effect.

Greenhow and Neufeld also found a largely annual variation in amplitude with minimum values in spring and early summer, as found in the present work. An exception to this trend was

a sharp dip in October. It is not clear whether they used the amplitude of a vectorial average or the average of individual amplitude estimates. If it was the former then this dip would be caused by the rapid phase variations occurring at this time.

7.3.3 Discussion

The phase of the semidiurnal tide in summer is observed to be 4-5h in advance of the winter value. The simplest explanation of this fact is in terms of a large contribution from antisymmetric tidal modes which, under simple thermal forcing, would differ by 180° between summer and winter. Such components must be unexpectedly large in amplitude to explain the observed phase shift; theoretical models (Walterscheid et al., 1980) predict the dominance of the symmetric (2,2) and (2,4) modes at solstices. The likely presence of the antisymmetric modes at the equinoxes poses further problems for the theoretical models. The latitudinal distribution of ozone about the equator is one factor that may engender the generation of antisymmetric modes in these seasons. The ozone content varies markedly with season and latitude, with maxima at the spring pole in the northern hemisphere and at $\sim 60^{\circ}$S in the southern hemisphere spring (e.g. Pyle and Rogers, 1980). Although most of this variation occurs below the height of maximum ozone thermotidal forcing, Teitelbaum and Cot (1979) took the latitudinal distribution of ozone into account by using actual equinoctal ozone measurements to calculate the semidiurnal tidal response.

They found that antisymmetric modes were in fact excited but that the amplitudes in the upper atmosphere were very dependent on the local temperature profile. Amplitudes were small at mid-latitudes.

The importance of background winds in the excitation of antisymmetric modes through mode coupling was shown by Lindzen and Hong (1974). Lindzen (1976) noted that the hemispheric difference in winds at the same seasons could give rise to differences in mode structure between summer and winter, and autumn and spring. In this regard it is noted that the seasonally asymmetric change in the semi-diurnal phase observed here, at the end of February and between September and October, is parallelled by a change in the direction of the prevailing zonal winds in the meso-sphere. Hemispheric differences in circulation at the equinoxes may be able to explain why the abrupt tidal phase change occurs during September/October both in the northern and southern hemispheres.

The latitudinal dependence of the zonal and meridional components of the (2,2),(2,3), (2,4) and (2,6) modes has been illustrated by Lindzen and Hong (1974). At a latitude of 44^{o} the two components achieve similar amplitudes for the first 3 of these modes. However, the (2,6) mode has a meridional velocity component which is smaller in amplitude than the zonal component, being closer to a node. Thus if the (2,6) mode was excited it would be likely to affect the zonal phase profiles most. This is consistent with the observation that average zonal wavelengths tend to be smaller than the meridional wavelengths.

The most common behaviour of the semidiurnal tidal amplitudes is for weak decay with height to a minimum near 90 km, followed by slow growth above. This results in energy densities which decay with height throughout the year except for a few occasions in early summer above 95 km. Destructive modal interference could result in amplitude decay, but would not explain the regularity of the minimum at 87-90 km in view of the variety of the modes excited at different times of the year. Molecular viscosity and thermal conductivity are not thought to be important below 110 km (Walterscheid and Venkateswaran, 1979a), but eddy viscosity may be strong in this region. Of particular significance, is the fact that the strongly forced (2,2) mode becomes evanescent in the thermodecline of the mesosphere, and tidal energy is reflected downwards.

7.4 THE DIURNAL TIDE

7.4.1 Results

It has already been noted that the bahaviour of the diurnal tide is more irregular than the semidiurnal tide, as found by other experimenters. Yet the monthly mean profiles (Fig. 7.6) often exhibit a regular behaviour in the vectical. The phase behaviour indicates both evanescent modes and vertical wavelengths as short as 22-25 km. In addition standing waves - such as would be formed by the combination of an upward wave and a downward reflected wave - appear. The inferred vertical wavelengths are summarized in

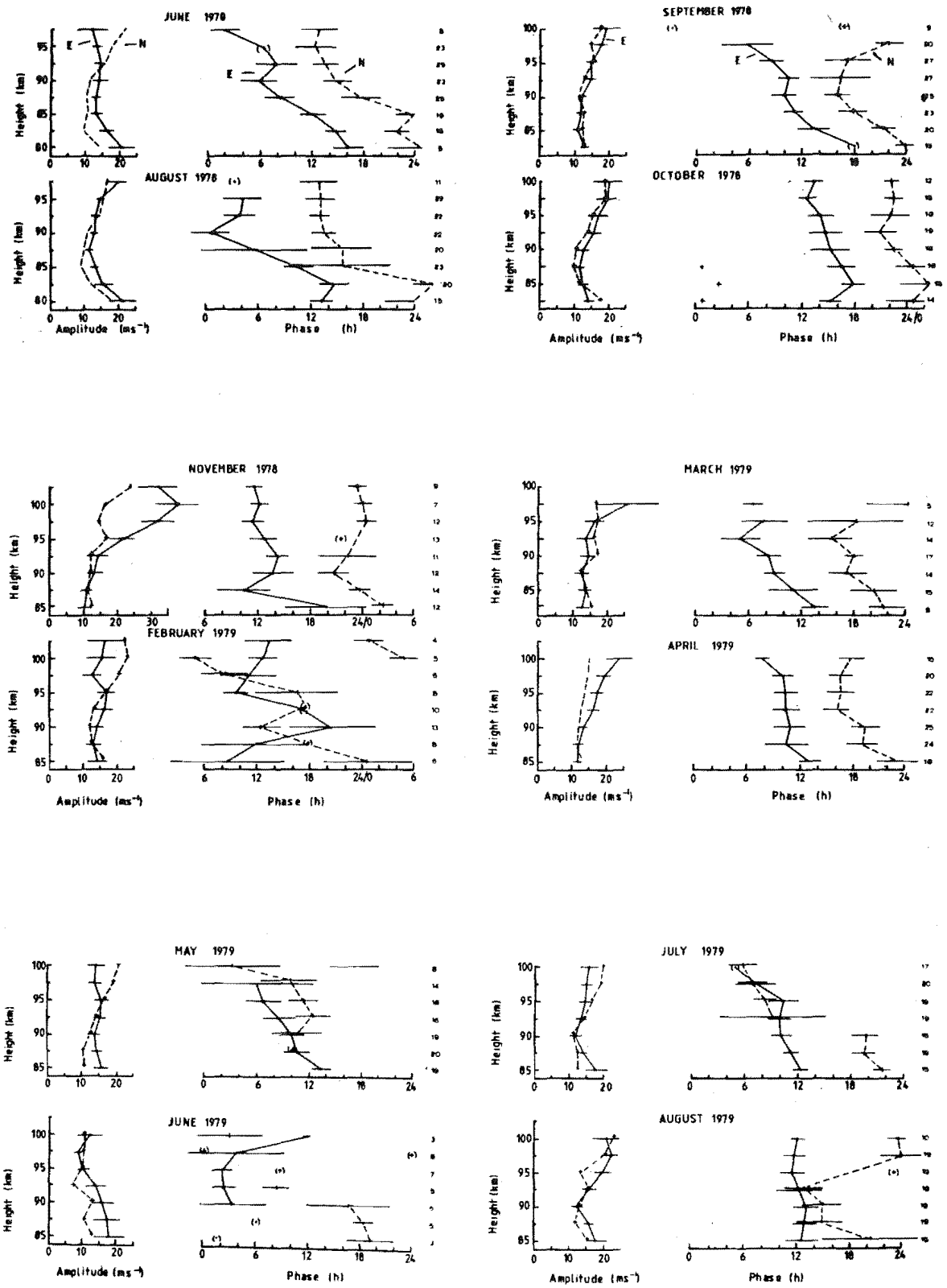

Figure 7.6: Height variation of the diurnal tide, June 1978 to February 1980.

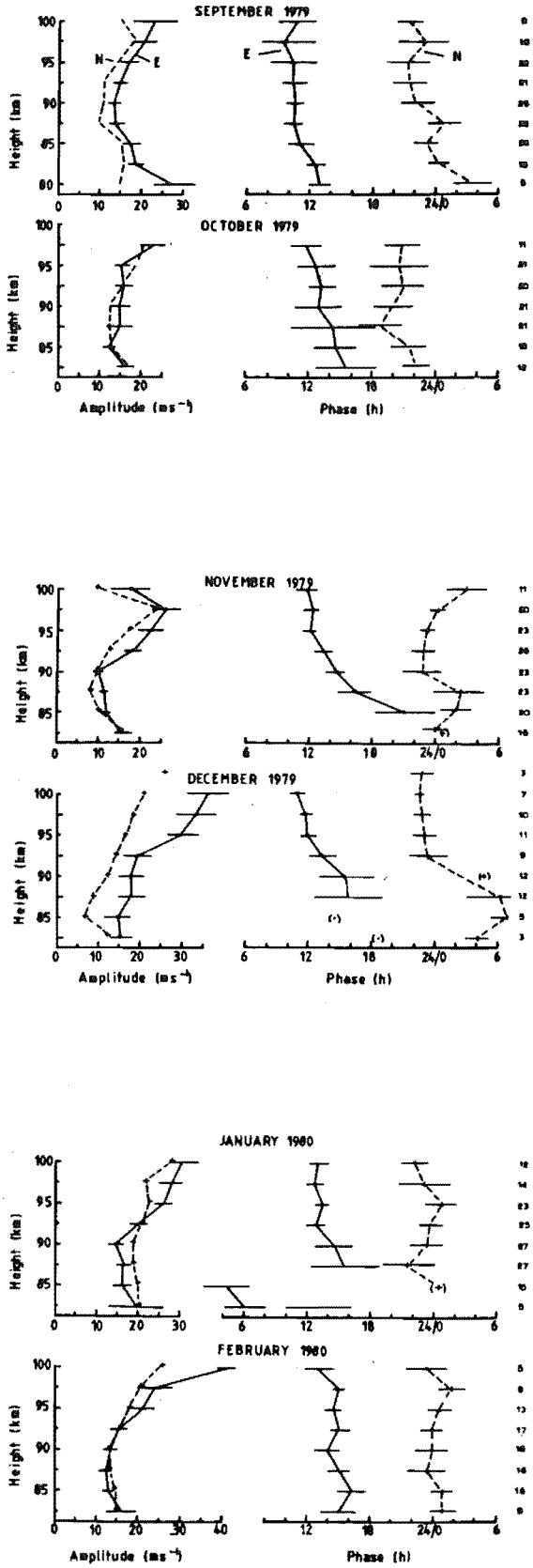

Figure 7.6: Continued.

Table 7.4: Estimated vertical wavelengths (km) of the zonal (E) and meridional (N) components of the diurnal tide. (±5-10 km).

1978

	J	J	A	S	O	N	D
E	22		SW	(40)	60		
N	25		SW	(40)	(120)		

1979

	F	M	A	M	J	J	A	S	O	N	D
E	-	27	ev	39	ev	55	ev	ev	100	(40)	54
N	-	42	26	-	SW	SW	SW	>130	ev	ev	ev

1980

J	F
>150	ev
eV	ev

Table 7.4. In general, the eastward phase leads the northward, but, in contrast to the semidiurnal tide, seldom by 90^{o}.

The smallest vertical wavelengths were observed in June, 1978, with values of 22 km and 25 km for the zonal and meridional components, consistent with the (1,1) mode (cf. Table 7.1). The lack of amplitude growth expected for such a propagating mode at these heights indicates that strong

damping must be occurring. The presence of this single propagating mode is not typical of the winter season however. In particular, standing wave patterns were more common. In August, 1978, for example, the northward component undergoes a phase change of close to 180^{o} over a short height interval near 83 km. This height is also close to an amplitude minimum. The eastward phase showed a 180^{o} phase shift over a broader height range. If this change was to be alternatively interpreted as a downward phase progression, the smallest resolvable vertical wavelength would be about 13 km. This could correspond to the (1,3) mode but Hines (1974, p654) showed that such a short wavelength mode would be severely damped by eddy viscosity. The winter of 1979 showed a contribution to an evanescent mode, in addition to standing wave behaviour.

Short wavelengths were consistently observed in autumn. The shortest wavelengths of 27 km correspond to the (1,1) mode, but the other longer wavelengths observed may represent an unresolved evanescent component.

The phase behaviour in summer is quite regular and indicates the dominance of evanescent modes. Theoretical models indicate that the (1,-2) mode is the most strongly forced evanescent mode, but the strong amplitude growth observed is not anticipated.

The seasonal variation of the amplitude and phase of the diurnal tide at 90 and 100 km is shown in Fig. 7.7. At 90 km the amplitude is remarkably constant throughout the year, except for an increase in the northward component in summer.

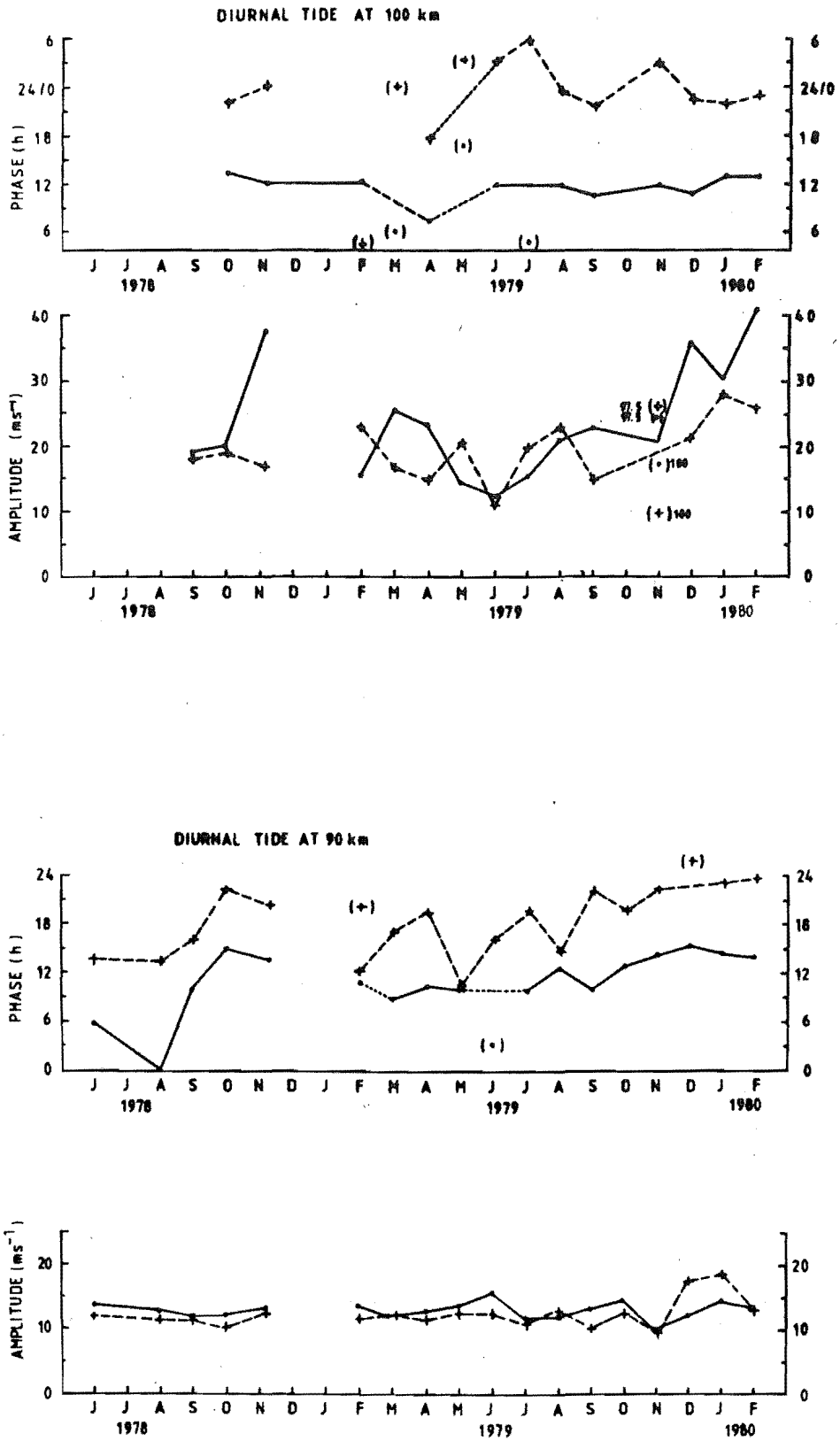

Figure 7.7: Seasonal variation of the diurnal tide at 100km and 90km.

The 1979 zonal phase at 90 km shows a slow increase from winter through to early summer, from 9 to 15h. The diurnal tide maximum winds in the eastward direction therefore occur near noon on average. The zonal phases for June and August 1978 which do not follow this trend are associated with very rapid changes of phase with height. Although the meridional phase is much more variable than the zonal, it also shows a retardation from winter to summer. Only in the spring period do the two components exhibit the phase quadrature expected of a counter-clockwise rotating velocity vector.

The diurnal amplitudes at 100 km (Fig. 7.7) are larger and much more variable than at 90 km. In particular very large values are attained in summer and minimum values in early winter.

The zonal phase at 100 km is very steady throughout the year, maximising very near to 12h (L.T.). The meridional phase shows a weak advance in phase from winter to summer, in contrast to the behaviour at 90 km. The resulting phase difference between components is now closer to 180^{o} than 90^{o}.

7.4.2 Discussion

The phase of the eastward component of the diurnal tide lies within a few hours of local noon. A similar phase was also observed by Stubbs (1976) at 35^{o}S. Most theoretical modelling has concentrated on the semidiurnal tide. At extratropical latitudes, below 110 km, little improvement has

been made upon the study by Lindzen (1967) of the diurnal tide in an isothermal atmosphere at rest. The eastward and northward phases predicted by that model, for a height of 85 km at 45^{o} latitude, are 12h and 19h. The apparent agreement with the present results is fortuitous however, since the short wavelength (1,1) mode was thought to be dominant with a phase shift of ~ 6h between 85 and 90 km.

In contrast to Lindzen's model, short wavelength modes were dominant only in autumn and on occasions in winter, while an evanescent tide was present on other occasions and clearly dominant in summer. The very short wavelengths tend to be confined to below 90-95 km. This may be due to the strong eddy damping such modes encounter above this region. Results at 47^{o}N also show evanescent behaviour dominating in summer, and short wavelengths prevailing, not only in autumn, but also in winter (Fellous et al., 1975).

Since the work of Lindzen (1967), Forbes and Garrett (1978b) have shown that the ozone heating rates for the (1,-2) mode should be larger by a factor of 2. As a consequence, the evanescent tidal response at mesospheric heights should also be larger. Full modelling of the diurnal tide with the inclusion of seasonally varying winds and the improved heating rates is clearly required.

Except for April 1979 below 92 km, the vertical wavelength of the zonal component is smaller than that of the meridional component. This can be accounted for by the relative amplitudes of the zonal and meridional velocity components of the (1,1) and (1,-2) modes. The velocity

expansion functions for these modes, illustrated in Lindzen (1967), show that at 45° latitude the amplitude of the zonal component of the (1,1) mode is twice that of the meridional component, but for the (1,-2) mode this ratio is only one half.

The very small seasonal variation of amplitude at 90 km is in marked contrast to the large amplitudes reached in summer at 100 km. At this time of year the phase profiles indicate that evanescent modes predominate and such a rapid amplitude increase with height is therefore unexpected. The seasonal variation of the northward component of phase at 100 km at this time also differs in sense from that at 90 km. The two-day wave is also strong for a short period in summer, but no relationship between its amplitude variation and that of the diurnal tide was found as might be expected if the large diurnal tide was due to nonlinear interactions of the planetary wave. It is suggested therefore, that the large amplitudes at 100 km are due to a local source of thermal excitation in summer. Such a source could be provided by UV heating which Forbes and Garrett (1976) showed to peak at 100 km with a half-width of about 30 km. Such a heat source may also be expected to affect the prevailing wind. The presence of poleward meridional winds at the time of the suggested maximum summer heating implies a latitudinal distribution biased equatorward of our location.

7.5 MERIDIONAL MOMENTUM FLUX

The presence of significant mean meridional winds in the upper atmosphere presents problems in balancing the angular momentum budget in the mesosphere, as discussed in Chapter 5. The contribution from the divergence of horizontal tidal momentum fluxes is considered here. Vertical velocities are not available so the possible contributions from the divergence of the vertical flux of momentum cannot be determined.

The meridional flux of zonal momentum is represented by $\overline{u'v'} = \frac{1}{2}uv \cos(\phi_u - \phi_v)$ where u and v are the amplitudes and ϕ the phases of the tidal components (Newell and Dickinson, 1967). For a single mode, tidal theory requires that the zonal and meridional wind components be in phase quadrature so that there is no meridional flux of momentum. However, Jones (1963) showed that when several modes of the same wavenumber are present, they may combine in such a way as to produce a net transport of energy and momentum flux. Jones also found significant flux of momentum from the semidiurnal tide at Jodrell Bank. More recently Elford (1979) has examined in detail the tidal momentum transport at Adelaide (35^{o}S).

In the previous section it was seen that the monthly means of the tidal components frequently show significant departures from phase quadrature. The daily values of the meridional flux of eastward momentum have been evaluated and averaged for each month for the diurnal and semidiurnal tides; these are shown at four heights in Fig. 7.8.

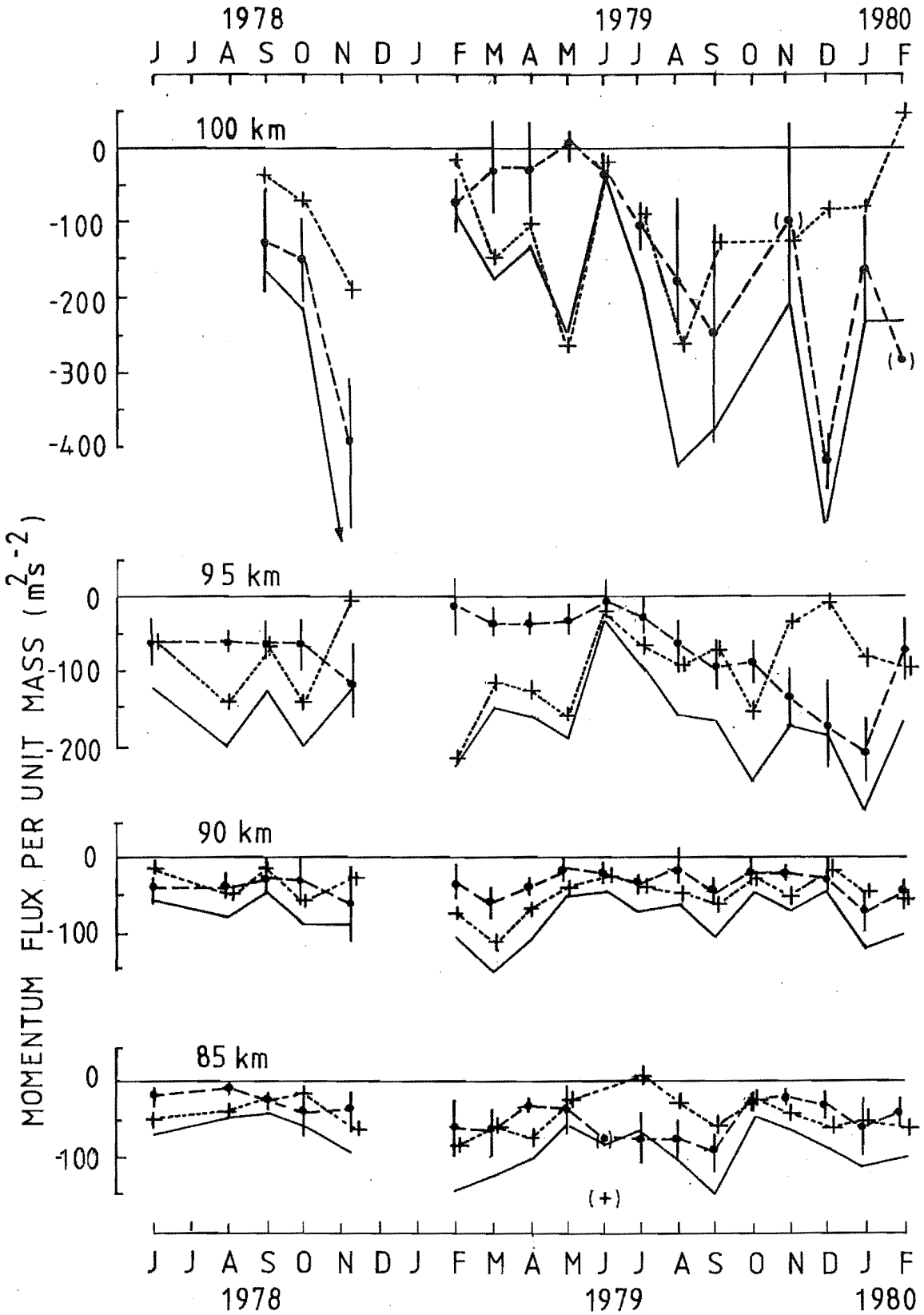

Figure 7.8: Seasonal variation of the northward flux of eastward momentum due to the diurnal (---) and semidiurnal (•••) tides and their sum (——).

The momentum flux of the diurnal tide is poleward at all heights. At the lowest height considered, 85 km, a weak seasonal variation is seen with small values in autumn and spring/early summer in 1979, although the results of 1978 do not follow this trend. BY 90 km there is no significant seasonal variations. However, above this, a distinct pattern emerges, with small poleward magnitudes in autumn and winter increasing to substantial values in excess of $-200\ m^2s^{-2}$ by early summer. This is seen most clearly at 95 km, while the sparser and less reliable data at 100 km is somewhat more erratic. These large summer values are likely to be associated with the increase in amplitude of the evanescent diurnal tide observed at this time. The momentum fluxes are larger than at Adelaide (Elford, 1979) where the (1,-2) mode will be smaller and the (1,1) mode plays a more important role.

The contribution from the semidiurnal tide is also in the poleward direction, tending to have minimum values in winter. At 95 km and above, summer fluxes are also small. The magnitudes overall are larger and more irregular than those of the diurnal tide.

The net tidal momentum transport is also shown in Fig. 7.8. At 85-90 km magnitudes of the southward flux are typically 50 to 100 m^2s^{-2}. The divergence of such a flux is given by

$$-\frac{1}{a\cos^2\theta}\frac{\partial}{\partial\theta}(u'v'\cos^2\theta) = \frac{2\tan\theta}{a}\overline{u'v'} - \frac{1}{a}\frac{\partial}{\partial\theta}(\overline{u'v'})$$

(Elford, 1979), where a and θ are the earth's radius and latitude. If a value of $\overline{u'v'}$ of $-100\ m^2s^{-2}$ is maintained around a latitude circle the first term on the right hand side will increase the zonal wind speed at 44^oS by $+2.6\ ms^{-1}d^{-1}$. The second term will depend upon the latitude range in which the flux divergence occurs. If a flux of $-100\ m^2s^{-2}$ is taken to increase to zero by a latitude of 90^oS (60^oS) then this term is $1.7\ ms^{-1}d^{-1}$ ($5.2\ ms^{-1}d^{-1}$). The horizontal divergence of tidal meridional momentum flux at 85 - 90 km therefore results in an eastward acceleration of the mean flow of typically $4-8\ ms^{-1}d^{-1}$. The flux values increase strongly above this height; for a value of $-200\ m^2s^{-2}$ the contribution to the mean flow acceleration is $9-16\ ms^{-1}d^{-1}$.

These values are certainly not insignificant but must however, be considered in relation to the other terms of the momentum equation. The dominant contribution from mean flow terms is due to the Coriolis torque on the meridional flow: $(2\Omega\sin\theta)\bar{v} = f\bar{v}$, where $\bar{v}$ is the mean meridional flow. This may alternatively be recognized as the flux of angular momentum of the earth's rotation by the mean meridional flow. The observed mean meridional wind has a strong seasonal variation (Chapter 5). In summer, when the tidal momentum flux is large, values of $\bar{v}$ above 85 km are typically $-5\ ms^{-1}$. If this is taken as a typical zonal mean value, it would result in a mean flow eastward acceleration of $44\ ms^{-1}d^{-1}$ but observed zonal flow accelerations are small (less than a few $ms^{-1}d^{-1}$). The tidal momentum flux divergence is not only significantly smaller than this but is in fact of the

opposite sign needed to achieve a balance. During autumn and late winter the meridional wind is typically $+10ms^{-1}$, contributing a mean flow acceleration of $-87ms^{-1}d^{-1}$. Although the tidal fluxes are of the correct sign to effect a balance they are clearly of insufficient magnitude.

A similar conclusion was reached by Elford (1979). He also showed that the convergence of the vertical momentum flux of the theoretical diurnal (1,1) tide was less than $14ms^{-1}d^{-1}$ at meteor heights. The contribution from the (1,-2) mode which dominates the present measurements, must await theoretical modelling or the difficult measurement of vertical velocities. Dissipating internal gravity waves are an alternative likely source of the momentum flux convergence. They achieve large amplitudes at these heights and are also likely to be directly filtered by the intervening wind structure (Hines and Reddy, 1967).

CHAPTER 8

CONCLUSIONS

The development of a real-time drift analysis system has enabled the measuremnt of winds in the mesosphere and lower thermosphere to be made with unprecedented coverage in time.

It was shown in Chapter 2 that full correlation analysis is valid if amplitude correlations, rather than complex correlations, are used, although the deduced spatial scale of the diffraction pattern will be affected. Also, high frequency noise will not seriously affect the calculated velocity. Also in Chapter 2, wind measurements were shown to be in broad agreement with preliminary results from a simultaneous meteor wind experiment.

The real-time wind measurement system at Birdlings Flat, was described in Chapter 3. It meets the requirements of being operator-independent, of having sufficient processing speed and incorporates as much hardware backup as possible.

The optimal data selection criteria were discussed in Chapter 4. One-minute samples were found to produce good quality data at a superior rate to 3-minute samples. The apparent velocity has the advantage that it requires a minimum of calculation. Although the apparent velocity has a greater spread than the 'true' velocity over short time scales, wind averages over 24 hours are in good agreement. Noon winds were shown to be seriously contaminated by the

tides on occasions, but it was found that monthly averages of even 2-hour noon samples, were a good measure of the monthly mean prevailing wind.

The wind measurements spanning 18 months enabled a detailed study of the prevailing wind between 65 and 100km to be made. Such measurements are particularly sparse in the southern hemisphere. A seasonally reversing circulation was observed in the mesosphere with a centre of strong, steady westward winds at 72km in summer and with more variable eastward winds in winter. A rapid changeover from the summer to winter wind regimes occurred in late February. The meridional wind component below 90 km was directed equatorward in summer, and poleward in winter, in accordance with the theoretical, thermally driven mesospheric circulation. The period of poleward winds extends well into the equinoxes, consistent with equinoctal heating at equatorial regions. At the highest levels of measurement, in the lower thermosphere, a different wind regime exists; it is in antiphase with that of the mesosphere. In the intermediate region of 85-100km, the influence of both regimes is evident.

Empirical wind models, based largely upon northern hemisphere measurements, have been used for comparison. The observed zonal wind was in reasonable agreement with the model but the observed summer westward jet formed earlier and at a higher altitude. Above 80 km, autumn and winter winds were more westward than the model. Significant differences were observed in the meridional component. The thermal wind indicated a poleward temperature gradient

up to a height of 100km in winter, while in summer the temperature gradient was reversed above 70km. This is consistent with a warm winter mesosphere.

Long period wind oscillations were observed at all times of the year. The relatively large values of energy density in summer can be explained by the upward penetration of westward travelling planetary waves. A 2-day oscillation dominated the wind spectra in January. There is compelling evidence to suggest that it is in fact the (3,3) atmospheric free, normal mode. A 5-day oscillation, which has been associated with the (1,2) mode, was strong in early and late summer, suggesting that the strong mid-summer winds detune the mesospheric cavity predicted by Geisler and Dickinson (1976). A 10-day oscillation, with a well-defined variation of phase with height, was tentatively associated with the (1,3) mode. In other seasons, both stationary and eastward travelling waves may penetrate the stratospheric winds, making an identification of wind oscillations with atmospheric free modes on the basis of period alone, more dubious.

A further feature in summer was the increase of energy densities with height near 70-75 km. It was shown that the background wind conditions at this time, could support baroclinically unstable waves in this region.

The power spectra of stratospheric winds at 20 km showed the greater relative importance of longer period components. However, common periodicities in the upper and lower regions support the supposition of penetration of planetary waves

into the lower thermosphere from below. A dynamical coupling of the two regions was also implied by concomitant changes in the prevailing wind. The effect was especially pronounced during a stratospheric warming in late August 1978 which was preceded by a major magnetic storm.

The atmospheric tides generally dominated the wind spectra, with the semidiurnal tide more regular than the diurnal tide. The usefulness of complex demodulation in showing the tidal amplitude and phase variations was demonstrated.

The eastward component of the semidiurnal tide usually led the northward component by 90°, indicating a counter-clockwise rotation of the velocity vector. The most notable feature of the seasonal variation of the semi-diurnal tide was the abrupt change in phase of almost 6h in spring and a smaller phase change of the opposite sense in autumn. These changes parallel the timing of the zonal wind changeovers. This behaviour suggests that antisymmetric modes may be important, and are possibly enhanced by mode coupling induced by the background wind. Short wavelength, semidiurnal modes were consistently observed in autumn while long wavelength modes were most common in winter. The amplitude of the tide generally showed a weak decrease with height to a minimum near 90 km, followed by a slow growth above.

The diurnal tide, in contrast, showed little seasonal variation of phase. However, the amplitude grew to very large values at 100km in summer. At this time, the vertical

variation of phase indicated the dominance of evanescent modes. It is therefore suggested that there is a local diurnal heat source near 100km which increases in strength in summer. Short wavelength, diurnal modes predominated in autumn; the shortest wavelength of 27 km corresponds to the (1,1) mode. The wavelengths associated with the zonal component of the diurnal tide were generally shorter than those of the meridional component, in accordance with the relative amplitudes of the velocity expansion functions of the dominant (1,1) and (1,-2) modes at mid-latitudes. The meridional flux of tidal momentum was directed poleward throughout the year. The horizontal convergence of this flux appears unable to balance the angular momentum budget.

For future work, the feasability of shifting to a new frequency is worthy of serious consideration, since interference has severely degraded the quality and quantity of night-time data. The data acquisition rate for D-region partial reflections may also be improved by the use of a smaller antenna spacing which would result in higher levels of cross-correlation. A more detailed study of the winds in conjunction with satellite temperature measurements, when they become available, would be valuable in elucidating the role of planetary waves and stratospheric warmings in the dynamics of the upper mesosphere and lower thermosphere. Co-operative ventures with other stations have already proved their worth in the study of the 2-day wave. Further co-operation is essential for the measurement of the spatial structure of the large-scale planetary and tidal waves. A

study of internal gravity waves and their possible interaction with the background wind is an important field of its own, which may be studied with the present data collection system.

APPENDIX A

LEAST SQUARES MINIMIZATION OF TIME DELAY ERRORS

A least squares method of fitting V_a and ϕ_a as parameters to values of V_i', derived from the observed time delays between antennae, was described by Fooks (1965). However, Fraser (1970) noted that the method gave zero weight to points where $\tau' = 0$, thus introducing an unreasonable bias. Fraser derived an alternative least squares estimate of V_a and ϕ_a which minimized the squared differences between the observed time shifts and those calculated from (V_a, ϕ_a) for 3 antennae. Meek (1978) has expressed the problem more generally for any number of antennae positioned at (d_i, ψ_i). The time delays for an apparent velocity (V_a, ϕ_a) are given by

$$\tau_i' = \frac{d_i}{V_a}\cos(\psi_i - \phi_a)$$

$$= \frac{\cos\phi_a}{V_a}(d_i\cos\psi_i) + \frac{\sin\phi_a}{V_a}(d_i\sin\psi_i)$$

This is a linear regression problem with τ_i' the measured time delays, and $\frac{\cos\phi_a}{V_a}$ and $\frac{\sin\phi_a}{V_a}$ the parameters to be determined.

In the matrix notation of Appendix C the problem can be expressed as

$$\underline{y} = A\underline{x} + \underline{\epsilon}$$

with

$$\underline{x} = \begin{pmatrix} \frac{\cos\phi_a}{V_a} \\ \frac{\sin\phi_a}{V_a} \end{pmatrix} \quad \underline{y} = \begin{pmatrix} \tau_1' \\ \tau_2' \\ \vdots \\ \tau_n' \end{pmatrix} \quad A = \begin{pmatrix} d_1\cos\psi_1 & d_1\sin\psi_1 \\ \vdots & \vdots \\ d_n\cos\psi_n & d_n\sin\psi_n \end{pmatrix}$$

The unweighted least squares solution, as noted by Meek, is

$$\hat{\underline{x}} = (A^T A)^{-1} A^T \underline{y} \tag{A.1}$$

The fixed matrix A for the 3 antennae geometry of Fig. 2.1 at Birdlings Flat, and measuring ψ_i and ϕ_a counter-clockwise from the x-direction, is

$$A = d\begin{pmatrix} 1 & 0 \\ 0 & -1 \\ -1 & 1 \end{pmatrix} .$$

d is the spacing of antenna along the shortest sides of the triangle. The solution (A.1) reduces to

$$\hat{\underline{x}} \equiv \begin{pmatrix} \frac{\cos\phi_a}{V_a} \\ \frac{\sin\phi_a}{V_a} \end{pmatrix} = \frac{1}{d}\begin{pmatrix} \tau_{12}' - \frac{T_e}{3} \\ -\tau_{23}' \quad \frac{T_e}{3} \end{pmatrix} = \frac{1}{d}\begin{pmatrix} \tau_x' \\ \tau_y' \end{pmatrix} \tag{A.2}$$

where the following definitions have been made:

$$T_e \equiv \tau_{12}' + \tau_{23}' + \tau_{31}' \qquad \text{(the 'time delay error')}$$

$$\tau_x' \equiv (\tau_{12}' - T_e/3)$$

$$\tau_y' \equiv -(\tau_{23}' - T_e/3) .$$

Thus the equally weighted least squares requirement gives rise to a very simple correction to the time delays observed between antennae in the x and y directions, satisfying the need for computational speed in the real-time drifts system. For a weighted least squares analysis, the correction $-T_e/3$ must be replaced by a factor of T_e which is dependent upon the weights. V_a and ϕ_a can be obtained from (A.2) as

$$\frac{1}{V_a^2} = \frac{1}{d^2}\,(\tau_x'^2 + \tau_y'^2)$$

$$\phi_a = \tan^{-1}\frac{\tau_y'}{\tau_x'} \quad . \tag{A.3}$$

The covariance matrix for $\underline{\hat{x}}$ is given by $C_{\underline{\hat{x}}} = \sigma^2(A^TA)^{-1}$, where σ^2 is estimated by

$$\sigma^2 = (\underline{y} - A\underline{x})^T\,(\underline{y} - A\underline{x}) \tag{A.4}$$

(Appendix C.3). For a configuration of only 3 antennae, the estimation of the 2 parameters allows only one degree of freedom. This will reduce the reliability of (A.4). σ^2, the sum of the squared resuduals, has the value $T_e^2/3$ here, giving a covariance matrix of

$$C_{\underline{\hat{x}}} = \frac{T_e^2}{9d^2}\begin{pmatrix} 2 & 1 \\ 1 & 2 \end{pmatrix}$$

The variances $\frac{\cos\phi_a}{V_a}$ and $\frac{\sin\phi_a}{V_a}$ are therefore estimated to be

$\frac{2T_e^2}{9d^2}$. The error in V_a and ϕ_a can then be found by the law of propagation of errors outlined in Appendix C.3.

APPENDIX B

PROGRAMMABLE ATTENUATORS

Attenuators capable of being controlled directly by the computer as well as manually were required to optimize the signal level entering the receivers. The attenuators are built in the standard rack-mounted modules which are connected to power supplies and the Station Control Register (SCR) through a McMurdo plug. The SCR selects the attenuator module by setting the clock line low; the data lines (loaded from the accumulator) then contain the octal multiple of 5 dB attenuation steps required. Reed relays introduce the appropriate attentuation network (Fig. B.1). The analogue circuitry is based on a design by Wratt (1974).

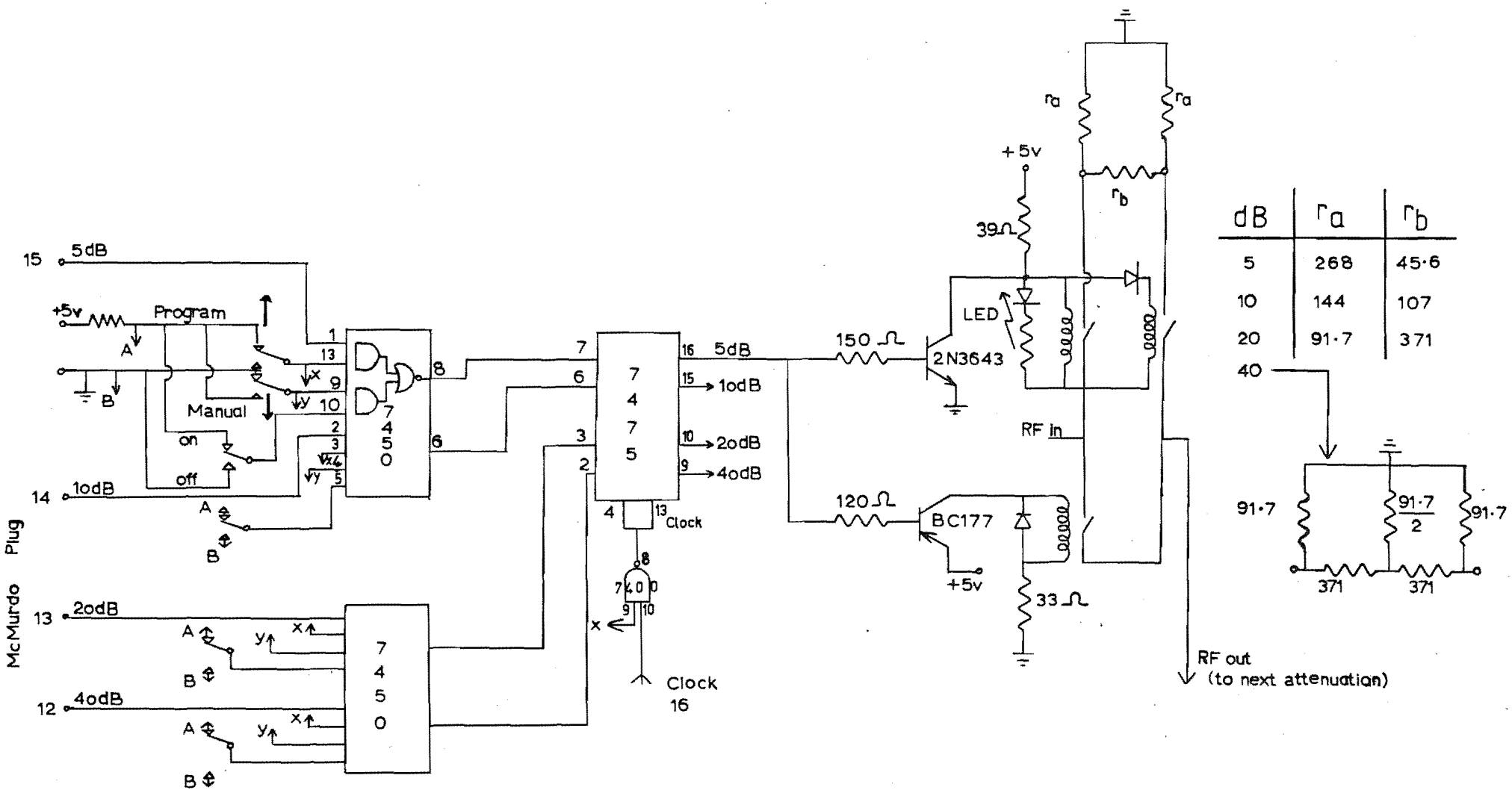

Figure B.1: Programmable attenuator circuit.

APPENDIX C

WEIGHTED LINEAR REGRESSION ANALYSIS

C.1 INTRODUCTION

Linear regression is a method of fitting a set of linear functions to an observed data series. The most important example in the present work is the determination of the amplitude and phase of the diurnal and semi-diurnal tides. Although a sinusoid of the form $A\cos(\omega t + \phi)$ is non-linear in A and ϕ, it can be expanded as

$$A\cos(\omega t + \phi) = (A\cos\phi)\cos\omega t + (A\sin\phi)\sin\omega t \qquad (C.1)$$

$$= a\cos\omega t + b\sin\omega t$$

which is a linear function of the parameters a and b. Tidal analysis requires the determination of the constant term and at least 2 of the tidal harmonics. Then the j'th data point, y_j, of a series with a total of n points can be represented by:

$$y_j = x_1 + x_2\cos\omega_1 t_j + x_3\sin\omega_1 t_j + x_4\cos\omega_2 t_j + x_5\sin\omega_2 t_j$$

$$+ \ldots + x_m\sin\omega_m t_j + \epsilon_j \qquad (C.2)$$

where (m-1)/2 frequencies are to be fitted. ϵ_j represents a residual (error) contribution to the measurements with zero mean and a variance σ_j^2. The object of the analysis

is to determine the coefficients x_i such that the sum of the squares of the residuals is minimized.

C.2 THE LEAST SQUARES SOLUTION

The linear problem of (C.2) can be expressed in the general form of

$$y_j = a_{j_1} x_1 + a_{j_2} x_2 + \ldots a_{jm} x_m + \epsilon_j$$

or in matrix notation:

$$\underline{y} = A\underline{x} + \underline{\epsilon}$$

where $\underline{y}$ is the vector of data values,

$\underline{x}$ is a vector of parameters to be determined,

$\underline{\epsilon}$ is the vector of error terms,

and A is the matrix $\begin{pmatrix} a_{11} & a_{12} & \ldots & a_{1m} \\ \cdot & & & \\ \cdot & & & \\ a_{n_1} & & & a_{nm} \end{pmatrix}$

(e.g. Brandt, 1976).

The variances, σ_j^2, of the measurements are assumed to be independent and can therefore be expressed as a diagonal covariance matrix:

$$C_y = \begin{pmatrix} \sigma_1^2 & & & 0 \\ & \sigma_2^2 & & \\ & & \ddots & \\ 0 & & & \sigma_n^2 \end{pmatrix}$$

In weighted linear regression, emphasis is placed upon measurements with a small variance, by using a matrix of weights, W, which is simply the inverse of C_y:

$$W = \begin{pmatrix} \frac{1}{\sigma_1^2} & & & 0 \\ & \frac{1}{\sigma_2^2} & & \\ & & \ddots & \\ 0 & & & \frac{1}{\sigma_n^2} \end{pmatrix} = C_y^{-1}$$

The least squares criterion requires that the weighted sum of the squared residuals be minimized. Thus,

$$M = \underline{\epsilon}^T W \underline{\epsilon} = (\underline{y} - A\underline{x})^T W (\underline{y} - A\underline{x})$$

must be minimized by setting the partial derivatives with respect to the parameters to zero i.e. $\frac{\partial M}{\partial x_i} = 0$ for $i = 1, \ldots m$. these conditions give

$$2A^T W(\underline{y} - A\underline{x}) = 0 \qquad \text{for } i = 1, \ldots m$$

This can be rearranged to obtain the 'normal equations':

$$A^T WA\underline{x} = A^T W\underline{y}$$

When $m \leqslant n$ these equations can be solved to give

$$\hat{\underline{x}} = (A^T WA)^{-1} A^T W\underline{y} \qquad (C.3)$$

where $\hat{\underline{x}}$ is the vector of least squares best estimates of the parameters.

In the case of equal weights (i.e. $\sigma_j^2 = \sigma^2$),(C.2) gives

$$\hat{\underline{x}} = (\frac{1}{\sigma^2} A^T IA)^{-1} A^T \frac{1}{\sigma^2} I\underline{y}$$

$$= (A^T A)^{-1} A^T \underline{y} \qquad (C.4)$$

which is independent of the variance and is the same result as from an unweighted least squares calculation.

In the case of *harmonic analysis* where the frequencies are harmonically related to the inverse of the data length, and the weights are unity, the off-diagonal terms of the matrix $A^T A$ in (C.4) are orthogonal resulting in $(A^T A)^{-1} A^T$ being diagonal. Then the equations reduce simply to

$$\hat{x}_i = \frac{\sum_{j=1}^{N} y_j \cos\omega_i t_j}{\sum_{j=1}^{N} \cos^2\omega_i t_j} \qquad (C.5)$$

C.3 ERROR ANALYSIS

Two approaches may be taken in order to find the errors in the coefficients. If the variance of each data point is known, then the errors may be *propagated*, otherwise the errors must be obtained from *calculation* from the sum of the squared residuals, M (Clifford, 1973). In the first case use is made of the fact that in (C.3) $\underline{\hat{x}}$ is a linear transformation of $\underline{y}$. i.e. $\underline{x} = T\underline{y}$, where $T = (A^TWA)^{-1}A^TW$. Then the covariance matrix of $\underline{\hat{x}}$ is given by

$$C_{\underline{\hat{x}}} = TC_{\underline{y}}\, T^T \qquad (C.6)$$

(Brandt, 1976). Assuming that the weighting matrix, W, is C_y^{-1}, and using the facts that W, W^{-1} and A^TWA are symmetric, (C.6) reduces to

$$C_{\underline{\hat{x}}} = (A^TWA)^{-1} \qquad (C.7)$$

In the numerical implementation of the analysis, it is convenient that this matrix was previously calculated while solving for $\underline{\hat{x}}$ in (C.3).

The variances of the parameters are consequently given by the diagonal elements of $C_{\underline{\hat{x}}}$.

For equal weights, $W = \sigma^2 I$ and $C_{\underline{\hat{x}}} = \sigma^2(A^TA)^{-1}$ (C.8)

A measure of the accuracy of the fit can be obtained from $M = \underline{\epsilon}^T W \underline{\epsilon}$. If the errors are normally distributed then

M follows a χ^2 distribution with n-m degrees of freedom.

When the variances of the measurements are unknown, a weight which is judged to be inversely proportional to the relative variance ($\sigma_j'^2$) of each measurement can still be applied. Then

$$W = \sigma^2 \begin{pmatrix} \frac{1}{\sigma_1'^2} & & & 0 \\ & \frac{1}{\sigma_2'^2} & & \\ & & \ddots & \\ 0 & & & \frac{1}{\sigma_n'^2} \end{pmatrix}$$

where σ^2 is an unknown factor. An estimate of σ^2 is $\frac{M}{n-m}$, and the covariance matrix of the parameters is then $\sigma^2 (A^T W A)^{-1}$.

The parameters, $\hat{\underline{x}}$, can easily be converted to amplitudes and phases of the appropriate periodic components. For example, for the first frequency, $A = (x_2^2 + x_3^2)^{\frac{1}{2}}$ and $\phi = \tan^{-1} \frac{x_3}{x_2}$. The errors calculated refer to x_j, but the parameters x_2 and x_3 are not simply related to A and ϕ by a linear transformation matrix T to enable a propagation of errors as in (C.6). However, a Taylor expansion of A and ϕ to first order can be used to approximate a linear transformation. Then,

$$T = \begin{pmatrix} \frac{\partial A}{\partial x_2} & \frac{\partial A}{\partial x_3} \\ \frac{\partial \phi}{\partial x_2} & \frac{\partial \phi}{\partial x_3} \end{pmatrix} \qquad (C.9)$$

and the covariance matrix of A and ϕ, $C_{A\phi}$, is related to the covariance matrix of x_2 and x_3, C_x, by $C_{A\phi} = TC_xT^T$ as in (C.6). This is the well-known law of propagation of errors (Brandt, 1976). The off-diagonal terms of C_x in this case cannot be neglected.

C.4 REGRESSION ANALYSIS PROGRAM

The program HARMONIC was written in Burrough's Extended Algol to perform a linear regression analysis with maximum flexibility. As in the program SPECTRAL (Appendix G), a variety of simple commands are used to drive HARMONIC, and use is made of the Burrough's B6700 interrupt system to enable interactive operation.

Among the variables which are accessible are: the number of periods to be fitted (NHARM), the actual periods to be fitted (the frequencies need not be harmonically related), the time step between calculations (STEPX) which can be set to peform 'running periodic regression', the type of errors required (ERRTYPE = 1 for error calculation, or 2 for error propagation), the type of weighting required, with options of:

WTMODE = 0 for equal weights

WTMODE = 1 for weighting by N/variance

WTMODE = 2 for weighting by 1/variance

WTMODE = 3 for weighting by N.

(N is the number of distinct measurements contributing to each data point). The default values are periodic regression

on 24h and 12h periods weighting by the number of points per hourly interval, at 24h intervals.

A program listing is not included here since use is made of many installation dependent facilities, but the following is a typical command sequence.

```
RUN OBJECT/HARMONIC;  DATA CARD
INPUT1 JANDATA.                    % OPEN DATA FILE
NHARM = 4; PERIODS = 48,24,12,8    % FIT HARMONICS TO THESE PERIODS
NPTS = 48; STEPX = 48              % IN 2 DAY SEGMENTS
WTMODE = 2; ERRTYPE = 2            % USE PROPAGATION OF ERRORS
GO
CLOSE1                             % CLOSE THE OUTPUT FILE OF
                                   % ANALYSED PARAMETERS
FINISH
```

APPENDIX D

THE GOVERNING EQUATIONS OF THE ATMOSPHERE

The governing equations of an atmosphere which assumed to be an inviscid, compressible perfect gas are:
the equations of motion,

$$\frac{D\underline{V}}{Dt} + 2\underline{\Omega} \times \underline{V} = -\frac{1}{\rho}\nabla p + \underline{g} \qquad (D.1)$$

the equation of mass continuity,

$$\frac{D\rho}{Dt} + \rho\nabla.\underline{V} = 0 \qquad (D.2)$$

the thermodynamic energy equation,

$$\frac{Dp}{Dt} = \frac{\gamma p}{\rho}\frac{D\rho}{Dt} + (\gamma-1)\rho J \qquad (D.3)$$

where $\underline{V}, \rho, P$ are velocity, density and pressure, Ω and g are the earth's angular velocity and acceleration due to gravity, γ is the ratio of specific heats, J is the external heating rate per unit mass and $\frac{D}{Dt} \equiv \frac{\partial}{\partial t} + \underline{V}.\underline{\nabla}$ is the 'substantial derivative'.

In spherical coordinates of (λ,θ,z), where λ is longitude, θ is latitude and z is the vertical distance above the earth's surface, the three equations of motion become:

$$\frac{Du}{Dt} - 2\Omega v\sin\theta - \frac{uv\tan\theta}{a} + \frac{uw}{a} = -\frac{1}{\rho}\frac{1}{a\cos\theta}\frac{\partial p}{\partial \lambda} \qquad (D.1a)$$

$$\frac{Dv}{Dt} + 2\Omega u\sin\theta + \frac{u^2\tan\theta}{a} + \frac{vw}{a} = -\frac{1}{\rho a}\frac{\partial p}{\partial \theta} \qquad (D.1b)$$

$$\frac{Dw}{Dt} - \frac{u^2+v^2}{a} = -\frac{1}{\rho}\frac{\partial p}{\partial z} - g \qquad (D.1c)$$

(Holton, 1972), where a is the Earth's radius and u,v,w are the eastward, northward and vertical velocity components. Terms involving the component of the earth's rotation vector parallel to the earth's surface have been neglected following the 'traditional approximation' that z is small compared to the distance to the earth's centre. The terms involving $\frac{1}{a}$ in D.1a-c, the curvature terms, are about an order of magnitude smaller than the others for global scale motions and can be neglected to a first approximation.

The linear wave equations are obtained by considering the expansion of the field variables in terms of a small parameter. It is assumed that the zero-order terms (denoted by a subscript zero) are independent of time and horizontal coordinates and that there is no background flow ($\underline{V}_o = 0$). Equation (D.1c) to zeroth order gives the hydrostatic equation $\frac{\partial p_o}{\partial z} = -g\rho_o$. The first order linearized equations are then:

$$\frac{\partial u'}{\partial t} - 2\Omega v'\sin\theta = -\frac{1}{\rho_o a\cos\theta}\frac{\partial p'}{\partial \lambda} \qquad (D.4)$$

$$\frac{\partial v'}{\partial t} + 2\Omega u'\sin\theta = -\frac{1}{\rho_o a}\frac{\partial p'}{\partial \theta} \qquad (D.5)$$

$$\frac{\partial p'}{\partial z} = -\rho' g \qquad (D.6)$$

$$\frac{\partial \rho'}{\partial t} + w' \frac{d\rho_o}{\partial z} + \rho_o \chi' = 0 \qquad (D.7)$$

$$\frac{\partial p'}{\partial t} + w' \frac{dp_o}{dz} = \gamma g H_o \left(\frac{\partial \rho'}{\partial t} + w' \frac{d\rho_o}{dz} \right) + (\gamma - 1) \rho_o J \qquad (D.8)$$

where the velocity divergence is given by

$$\chi' = \frac{1}{a\cos\theta} \frac{\partial u'}{\partial \lambda} + \frac{\partial}{\partial \theta} (v'\cos\theta)] + \frac{\partial w'}{\partial z}$$

and the scale height $H_o = \frac{RT_o}{g}$.

It is assumed that the perturbation variables are periodic in longitude and time i.e. of the form $\exp[i(s\lambda - \omega t)]$, where s is a zonal wavenumber and ω the wave frequency. Letting $f = \frac{\omega}{2\Omega}$, (D.4) and (D.5) may be solved for u' and v':

$$u' = \frac{f}{2a\Omega(f^2 - \sin^2\theta)} \left[\frac{s}{\cos\theta} + \frac{\sin\theta}{f} \frac{\partial}{\partial \theta} \right] \frac{p'}{\rho_o} \qquad (D.9)$$

$$v' = - \frac{i}{2a\Omega} \frac{f}{(f^2 - \sin^2\theta)} \left[\frac{\tan\theta}{f} + \frac{\partial}{\partial \theta} \right] \frac{p'}{\rho_o} \qquad (D.10)$$

With a new variable, G, defined by

$$G \equiv \chi - \frac{\kappa J}{g H_o}$$

the variables u',v',w',p' and ρ' can be eliminated from (D.4) - (D.8) to obtain a single equation for G alone:

$$H_o \frac{\partial^2 G}{\partial z^2} + \left(\frac{dH_o}{dz} - 1 \right) \frac{\partial G}{\partial z} = \frac{g}{4a^2\Omega^2} F \left[\left(\frac{dH_o}{dz} + \kappa \right) G - \frac{\kappa J}{\gamma g H_o} \right] \qquad (D.11)$$

(Kasahara, 1976), where

$$F \equiv \frac{1}{\cos\theta}\frac{\partial}{\partial\theta}\left[\frac{\cos\theta}{(f^2-\sin^2\theta)}\frac{\partial}{\partial\theta}\right] + \frac{1}{(f^2-\sin^2\theta)}\left[\frac{s}{f}\left(\frac{f^2+\sin^2\theta}{f^2-\sin^2\theta}\right) - \frac{s^2}{\cos^2\theta}\right]$$

If it is assumed that both G and J can be expanded in terms of a (complete) set of functions $\Theta_n(\theta)$ (the Hough functions) for a given s and f, then (D.11) can be solved by the method of separation of variables with a separation constant h_n. The two equations obtained are:

Laplace's tidal equation,

$$F(\Theta_n) + \frac{4\Omega^2a^2}{gh_n}\Theta_n = 0 \qquad \text{(D.12)}$$

and the vertical structure equation,

$$H_o\frac{d^2G_n}{dz^2} + \left(\frac{dH_o}{dz} - 1\right)\frac{dG_n}{dz} + \frac{1}{h_n}\left(\frac{dH_o}{dz} + \kappa\right)G_n = \frac{\kappa J_n}{\gamma g H_o h_n} \qquad \text{(D.13)}$$

(e.g. Siebert, 1961). (D.12), the horizontal structure equation, is called Laplace's tidal equation after Laplace (1799) who first derived it. It is independent of the thermal forcing which is contained entirely in the vertical structure equation.

Three types of long period wave solution to these equations are of importance to upper atmospheric studies.

(i) With no thermal forcing (J=0) and with a lower boundary condition of w = 0 at z = 0, the solutions describe atmospheric free oscillations whose frequencies appear as eigenvalues of (D.12) (Section 6.2).

(ii) When J describes the thermotidal forcing and when the lower boundary condition is $w = 0$ at $z = 0$, the equations describe the atmospheric tides with the h_n obtained from (D.12) as eigenvalues (Section 7.1).

(iii) With $J = 0$, stationary planetary wave solutions may be represented by specifying the effect of surface topography as a lower boundary condition on the vertical velocity (e.g. Charney and Drazin, 1961).

APPENDIX E

NUMERICAL FILTERS

It is often desirable to attenuate certain temporal variations from a time series. This can be accomplished by numerical filtering, whereby each point of the time series is replaced by a weighted sum of neighbouring points. If the weights, w_k, are symmetrical about the central weight, w_o, then the filter produces no phase shift in the filtered series. The filtering process is then one of convolution of the filter weights with the time series. A low-pass filter whose weights sum to 1 will not alter the mean data value.

The frequency response, R(f), of the filter is described by the Fourier transform of the weights:

$$R(f) = \int_{-\infty}^{\infty} w(t)\exp(2\pi i f t)\,dt$$

where f is the frequency. For a discrete filter with M weights distributed equally either side of w_o (i.e. $w_{-k} = w_k$),

$$R(f) = \sum_{k=-M}^{M} w_k \cos(2\pi f k) + i \sum_{k=-M}^{M} w_k \sin(2\pi f k)$$

It is convenient to consider the frequency in terms of cycles per data interval; this is done here. The Nyquist frequency is then f = 0.5. Since the set of weights, w_k, is even, the term involving sines is zero and R(f) is therefore real (i.e. there is no phase shift). Thus,

$$R(f) = w_o + 2 \sum_{k=1}^{M} w_k \cos(2\pi fk) \qquad (E.1)$$

E.1 SIMPLE LOW PASS FILTERS

Low-pass filters are used to remove rapid variations in the time series. The Hanning filter is a simple 3-point filter useful both for smoothing data, and also smoothing the raw periodograms to reduce spectral leakage. It has weights: $w_o = 1/2$, $w_1 = w_{-1} = 1/4$. The frequency response is, from (E.1),

$$R(f) = \frac{1}{2}(1 + \cos 2\pi f) \qquad (E.2)$$

As shown in Fig. E.1, the frequency response has a slow roll-off. Repeated applications of the Hanning filter produce a correspondinglingly narrower response.

A 2M+1 point equally weighted moving average is frequently used as a low-pass filter. The weights in this case are $w_k = \frac{1}{2M+1}$. The frequency response of a moving average filter of length T can be shown analytically to be $R(f) = \frac{\sin \pi fT}{\pi fT}$, the sinc function, in the case of continuous data. For discrete data the response must be modified to $R(f) = \frac{\sin(\pi fT)}{T\sin(\pi f)}$, where $T = 2M+1$ (Kennedy, 1980). The frequency response of a 3-point moving average is shown in Fig. E.1 for both the continuous and discrete cases. It can be seen that this filter introduces undesirable sidelobes which are larger for discrete data than for continuous data. With longer filter lengths both the amplitude of the sidelobes and the difference between the continuous and discrete cases

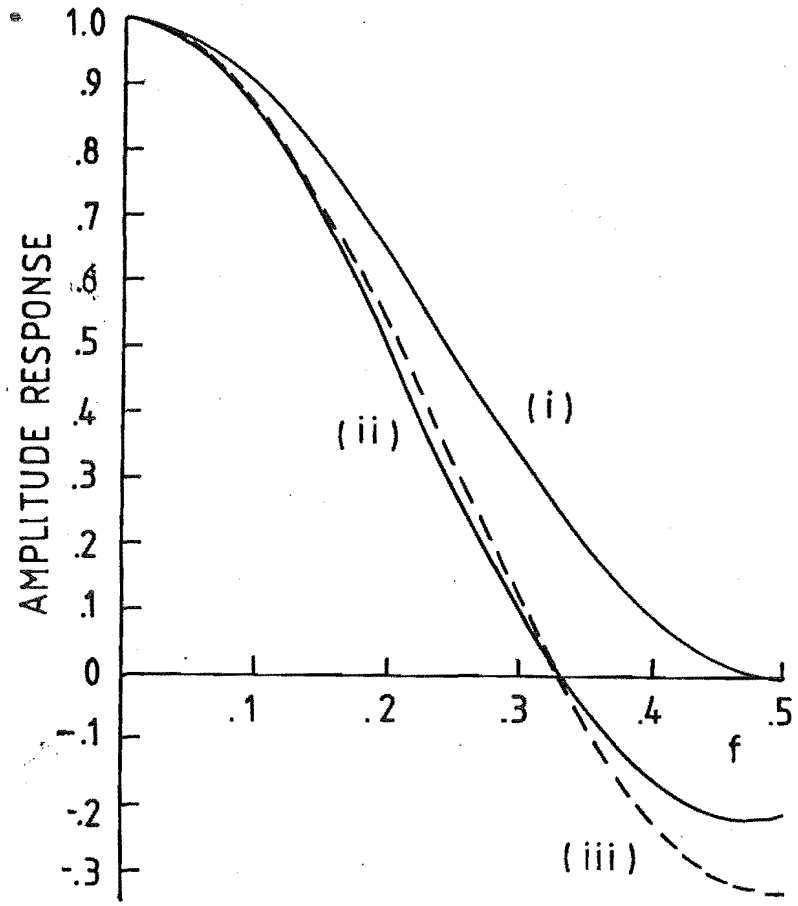

Figure E.1: Filter responses of the Hanning filter (i), and equally weighted moving averages in the continuous case (ii), and for a 3-point discrete filter (iii).

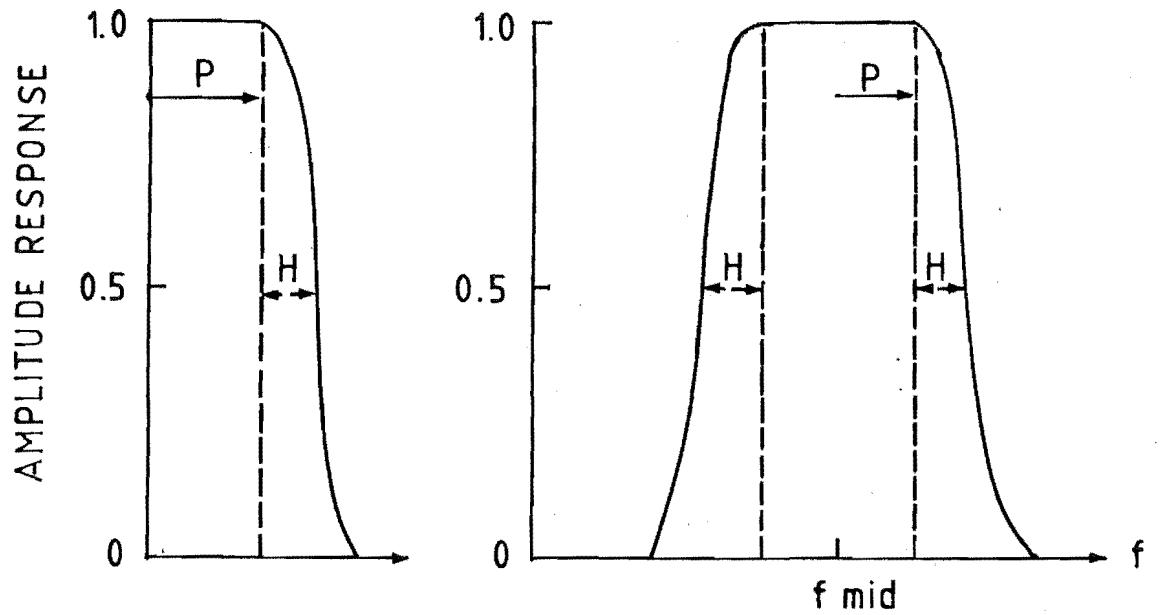

Figure E.2: Parameters used to specify the Behannon and Ness (a) low-pass and (b) band-pass filters.

decreases. In contrast, it can be seen that the Hanning filter, although having a slightly slower roll-off, does not introduce the sidelobe oscillations.

E.2 BEHANNON AND NESS FILTERS

An ideal filter will have a sharp termination at the desired frequency cut-off, P. Behannon and Ness (1966) derive weights which approximate the actual filter response to the ideal filter cut-off in a least squares sense. The filters are linear and have 2M+1 symmetrical weights. However, a sharp cut-off results in large overshoot on either side of this point (Gibbs phenomena). Behannon and Ness overcome this by introducing a quarter cycle of a cosine termination of width H, instead of the sharp cut-off (Fig. E2a). H is required to be as small as possible in order to match the ideal cut-off, but must be large enough to reduce the side-lobe oscillations to an acceptable level. Behannon and Ness recommend that for a filter of length M, H should be approximately $\frac{1}{2}$M. Use of a larger M will permit a sharper cut-off without increasing the oscillations.

The equation for generating the weights, L_k, is

$$L_k = \frac{\cos 2\pi kH^2}{1-16k^2H^2} \frac{\sin 2\pi k\ (P+H)}{\pi k} \qquad \text{(E.3)}$$

(Behannon and Ness, 1966). A further factor can then be added to these weights in order to normalize the gain to 1.0 at f = 0:

$$w_k = L_k + \frac{1 - (L_o + 2 \sum_{i=1}^{M} L_i)}{2M+1} \qquad (E.4)$$

M data points will be lost at the beginning and end of the data series. With P = 0 it can be seen from Fig. E.2a that an ultra-low-pass filter is obtained.

The low-pass filter can be simply shifted to a central frequency of interest, f_{mid}, creating a band-pass filter by utilizing the shift theorem of Fourier transforms. This shift is achieved by multiplying the weights of the low-pass filter in (E.4) by 2 cos $2\pi f_{mid}$ t. Such a band-pass filter is illustrated in Fig. E.2b. Thus a low-pass, band-pass or high-pass filter can be synthesized by the suitable specification of 4 parameters: M, f_{mid}, P and H.

Figures E.3 and E.4 illustrate the frequency response of several filters referred to in this thesis.

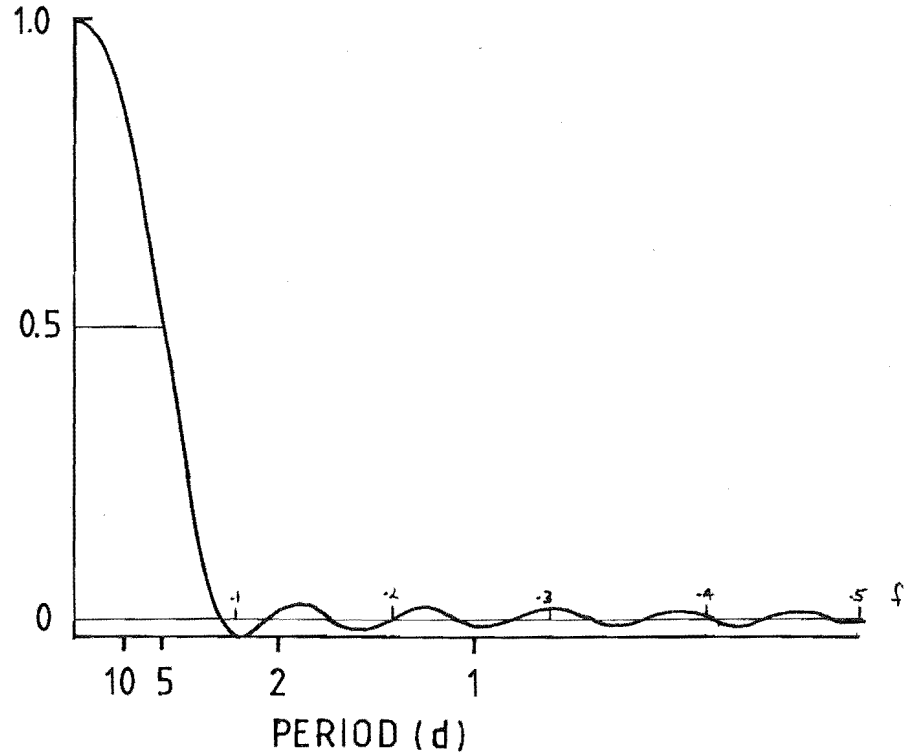

Figure E.3a: Amplitude response of the low-pass filter used in section 6.5.1 with a half-amplitude point at 5d. M = 12, f_{mid} = 0, P = .01, H = .04.

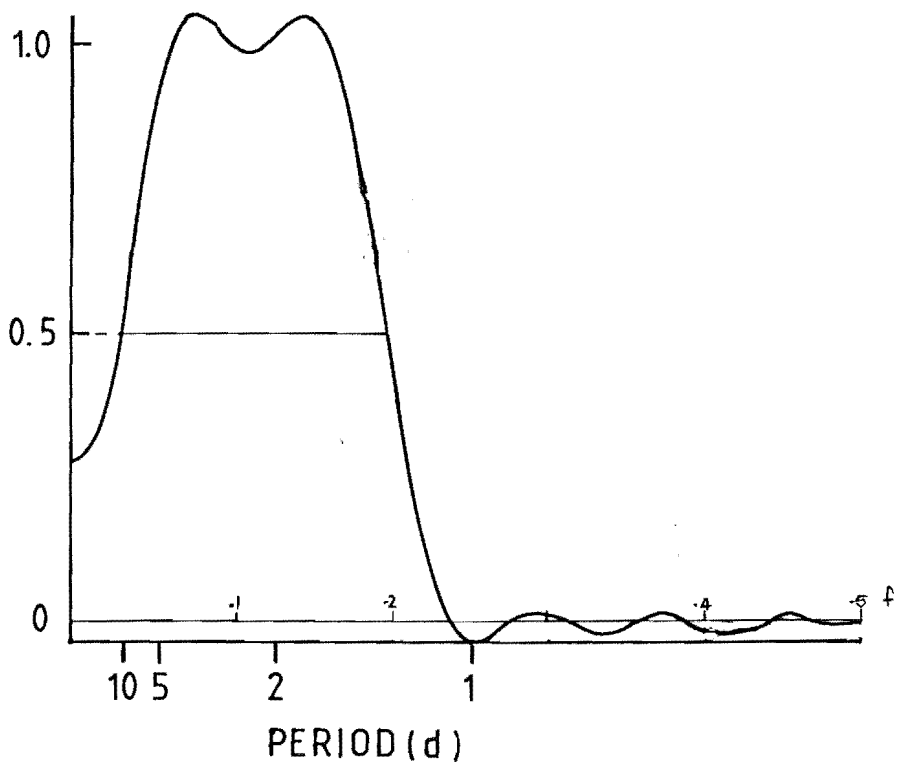

Figure E.3b: Amplitude response of the band-pass filter used in Section 6.5.1 with half-amplitude points at 11.1 and 1.3d. M = 12, f_{mid} = .11, P = .0475, H = .04.

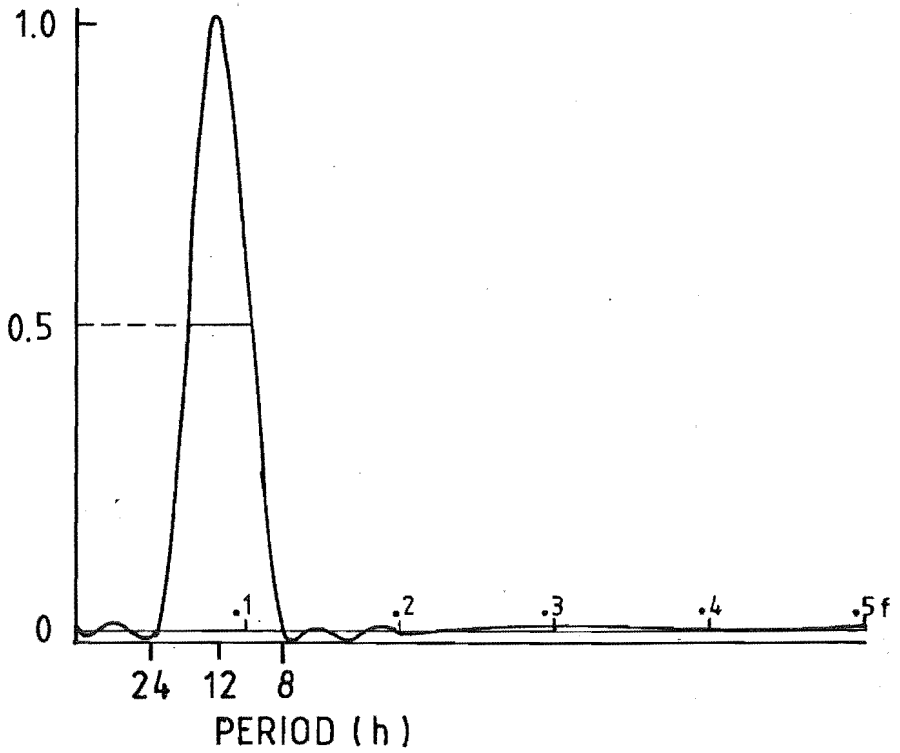

Figure E.4a: Amplitude response of the band-pass filter used in Section 7.2 centred at 12h with half-amplitude points at 16 and 9.7h. M = 25, f_{mid} = .0833, P = 0, H = .02.

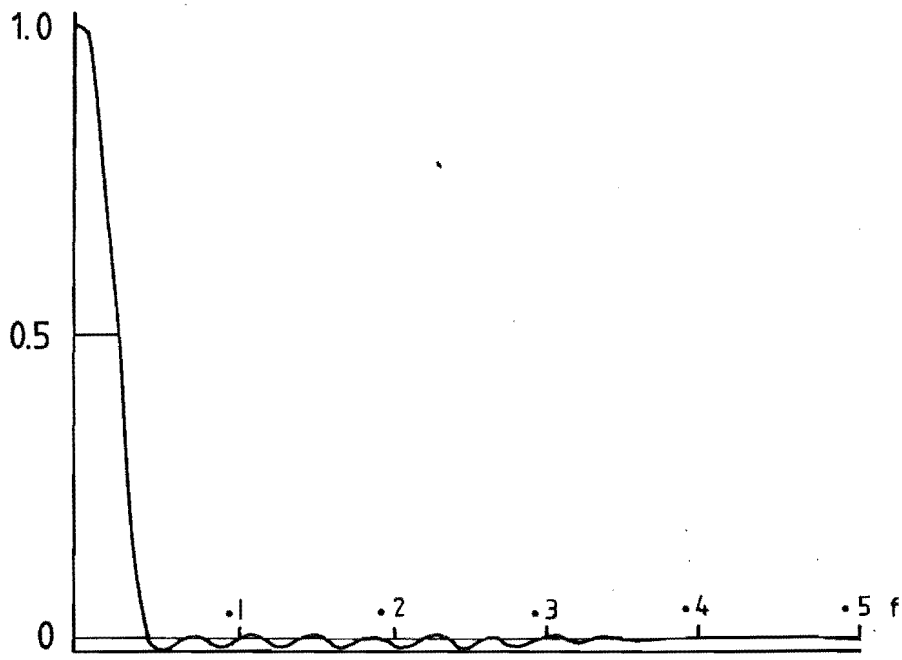

Figure E.4b: Amplitude response of the low-pass filter used in complex demodulation in Section 7.2. M = 25, f_{mid} = 0, P = 0, H = .02.

APPENDIX F

COMPLEX DEMODULATION

The aim of complex demodulation is to isolate the 'time-local' amplitude and phase of a particular spectral band. This is especially useful when the time series is non-stationary. The method has been described in detail by Granger and Hatanaka (1964) and more efficient computational approaches have been introduced by Bingham et al. (1965).

The process is implemented by first shifting the frequency band of interest centred at ω_o down to zero frequency by multiplying each term in the series by $\exp(-i\omega_o t)$. Then a suitable low-pass filter with bandwidth $\Delta\omega$ is applied. The amplitude and phase of spectral components within the frequency band $\omega_o \pm \Delta\omega/2$ can then be directly obtained from this complex, demodulated time series.

As a means of illustrating this, suppose a real time series, $x(t)$, contains a frequency component at ω_o. Then $x(t) = A(t)\cos(\omega_o t + \phi(t))$, where A and ϕ may be slowly varying functions of time. After mixing down to zero frequency, a time series $x_D(t)$ is obtained:

$$x_D(t) = x(t)\ \exp(-i\omega_o t)$$

$$= (A(t)/2)[\exp\{i(\omega_o t + \phi(t))\} + \exp\{-i(\omega_o t + \phi(t))\}]\ x$$

$$\exp(-i\omega_o t)$$

$$= (A(t)/2)\exp i\phi(t) + (A(t)/2)\exp\{-i(2\omega_o t + \phi(t))\}$$

The modulus of the first term is A(t)/2 and its phase is the required phase of the sinusoidal signal. The second term, at a frequency of $-2\omega_o$, muat be removed by the low-pass filter. Filters to do this are described in Appendix E.

More generally, the complex demodulate represents the amplitude and phase variation of oscillations within the filter bandwidth, $\Delta\omega$. If the frequency of demodulation, ω_o, does not coincide exactly with a strong spectral peak within the bandwidth considered, $\phi(t)$ will exhibit a linear phase variation in time which can be used to determine the actual frequency of the peak.

Several further points may be noted. Care should be taken in the choice of filter in order that sidelobes do not introduce spurious variations in the demodulated phase. Since the data is filtered, not every point of the complex demodulate is independent and computational effort can be reduced by making use of this fact. Banks (1975) has utilized the fast Fourier transform to apply the frequency shifting and filtering in the frequency domain. Finally, 'time-local' power and cross-spectra may be formed from the complex demodulates of the respective time series (Granger and Hatanaka, 1964).

APPENXIX G

SOFTWARE FOR WINDS DATA ANALYSIS

The program SPECTRAL serves the dual purposes of data manipulation and analysis. It is written mainly in Burrough's Extended Algol, with some Fortran subroutines 'bound' in, and makes use of the Burrough's interrupt system for interactive, remote-terminal operation. A repertoire of some 70 simple commands is recognized and includes the facility to execute a chain of commands from a separate file. The functions of the program are outlined below under three general categories of commands.

(i) Data Handling and Manipulation.

Data input to the program usually consists of wind velocities within a certain time-averaging interval, together with the corresponding number of velocities and standard deviation. SPECTRAL enables the compression of this data (to a longer time-averaging interval), the combination of adjacent heights, the combination of different data files, the shifting of data in time and the selection of data from particular time intervals. The data so processed, can then be output to a new data file, or passed on for further analysis.

(ii) Raw Data Analysis.

The main purpose here is to display the raw data in various states. Commands may specify that the data is to be:

interpolated, averaged according to any of a variety of weighting functions (depending upon the number of points and standard deviation of the sampling interval), smoothed (with a Hanning filter), filtered (using the Behannon and Ness filters described in Appendix E), smoothed with an m-point moving average, graphed or output to a new data file.

(iii) Spectral Analysis.

Three types of spectral analysis can be used: auto- and cross-periodograms, auto- and cross-power spectra calculated from the Fourier transform of the correlation functions, or MEM power spectra. Complex demodulation can also be performed on the data.

In the first two methods it is necessary to apply a window to either the raw data or the correlations in order to reduce spectral leakage. The two types of window used were the Hanning and Parzen windows. M points at each end of the time series involved, are tapered with weights w_i given by:

(a) $$w_i = \frac{1}{2}(1 + \cos\frac{\pi i}{M}), \qquad i \leqslant M$$

for the Hanning window (i.e. a cosine tapered square window) or

(b) $$w_i = \begin{cases} 1 - 6(\frac{i}{M})^2 + 6(\frac{i}{M})^3, & i \leqslant \frac{M}{2} \\ 2(1 - \frac{i}{m})^3, & \frac{M}{2} < i \leqslant M \end{cases}$$

for the Parzen window.

The spectral estimator obtained using the Parzen window has a smaller variance than that from the Hanning window, but larger bias (Jenkins and Watts, 1968).

Each spectral estimator of the periodogram has only 2 degrees of freedom (γ) resulting in a 'noisy' spectrum. Therefore smoothing is generally required to reduce the variance associated with each value. Confidence intervals for smoothed spectral estimators, $S_{xx}(f)$, each of γ degrees of freedom, can be obtained if we approximate their distribution to a χ^2-distribution. Then there is a $(1-\alpha)100\%$ probability that the population value lies between

$$S_{xx}(f) \frac{\gamma}{\chi^2_{(\gamma,1-\alpha/2)}} \quad \text{and} \quad S_{xx}(f) \frac{\gamma}{\chi^2_{(\gamma,\alpha/2)}}$$

where $\chi^2_{\gamma,\alpha}$ are the α points of the χ^2-distribution with γ degrees of freedom (Jenkins and Watts, 1968). The number of degrees of freedom for the smoothed periodogram is

$$\gamma = 2p\left(\frac{N-N_T}{N_O}\right)$$

where N is the number of data points, N_T is the number of points tapered by the data window, N_O is the total number of points after zeroes have been added (to enable the use of a fast Fourier transform and p is the effective number of points involved in smoothing of the raw periodogram.

When the power spectrum is estimated from the Fourier transform of the correlation,

$$\gamma \simeq 2\left(\frac{N}{M}\right)$$

where M is the maximum number of correlation lags used.

The coherence is also determined from the cross-spectra. The coherence, β, that is exceeded by random data with a probability, α, is given by

$$\beta = \left(1-\alpha^{1/(\gamma/2-1)}\right)^{\frac{1}{2}}$$

(Julian, 1975).

The MEM spectra were calculated according to the algorithm given by Andersen (1979).

Examples of the use of the program are given below.

Example 1.

Create filter weights for a low-pass filter, then interpolate, filter and graph the data while outputting a new file.

```
RUN   OBJECT/SPECTRAL; DATA CARD
INPUT1   JANDATA.
NODEMEAN; INTERPOLATE
FILTER 25  0  0  .02  GRAPH LIN LOG DR=3
% SET UP FILTER WEIGHTS FOR AN ULTRA LOW-PASS FILTER
% GRAPH THE RESPONSE ON BOTH A LINEAR AND LOG SCALE (WITH 30DB DYNAMIC RANGE)
% M=25, FMID=0, P=0, H=.02
GRAPHDATA
OUTPUT1  FIL/D.   % CREATE OUTPUT FILE: "FIL/D"
GO
CLOSE1
```

EXAMPLE 2.

Graph the power spectra obtained from the smoothed periodograms, the Fourier transform of the correlations, and from MEM.

```
RUN OBJECT/SPECTRAL;  DATA CARD
INPUT1  JANDATA.
INTERPOLATE
POWER GRAPH LIN
TAPER PARZEN 0.2  % TAPER 20% OF DATA WITH A PARZEN WINDOW
SMOOTHSP 3        % SMOOTH THE RAW PERIODGRAMS 3 TIMES
%
BAT AUTO GRAPH LIN 1
% REQUEST BLACKMAN AND TUKEY TYPE AUTO-SPECTRA
%
MEM 50   0   0.5   .002 GRAPH LOG
% GRAPH MEM SPECTRA WITH A FILTER LENGTH OF 50,
% FROM A FREQ OF 0 to 0.5 (NYQUIST), IN .002 STEPS
%
GO                % PROCESS ALL HEIGHTS IN THIS FILE
```

Example 3.

Calculate and graph the auto-spectra, and the amplitude, phase and coherence of the cross-spectra between the zonal and meridional wind components.

```
RUN OBJECT/SPECTRAL; DATA CARD
INPUT1  JANDATA.              % POSITION AT E/W WINDS
INPUT2  JANDATA.; SPACE2  84  % POSITION AT N/S WINDS
NDATASETS=1                   % 1 HEIGHT AT A TIME
TAPER PARZEN 0.2              % TAPER 20% OF DATA
```

```
CROSSPECTRUM GRAPH LIN 7

SMOOTHSP 3                          % SMOOTH THE CROSS-SPECTRA

GO                                  % 1ST HEIGHT

THRU 4 DO

BEGIN SPACE1 84; SPACE2 84; GO; END

% WORK THROUGH 4 MORE HEIGHTS WITH INPUT1 SET

% TO E/W WINDS AND INPUT2 TO N/S WINDS
```

REFERENCES

Andersen, N., 1974: On the calculation of filter coefficients for maximum entropy spectral analysis. Geophys., 39, 69-72.

Angell, J.K. and J. Korshover, 1970: Quasi-biennial, annual, and semiannual wind and temperature harmonic amplitudes and phases in the stratosphere and low mesosphere of the northern hemisphere. J. Geophys. Res., 75, 543-550.

Awe, O., 1964a: Errors in correlation between time series. J. Atmos. Terr. Phys., 26, 1239-1255.

Awe, O., 1964b: Effects of errors in correlation on the analysis of the fading of radio waves. J. Atmos. Terr. Phys., 26, 1257-1271.

Babcock, R.R. and J.V. Evans, 1979: Seasonal and solar cycle variations in the thermospheric circulation observed over Millstone Hill. J. Geophys. Res., 84, 7348-7352.

Baggaley, W.J. and E.M. Poulter, 1978: The radio meteor wind facility at Christchurch, New Zealand. J. Atmos. Terr. Phys., 40, 941-943.

Banks, R.J., 1975: Complex demodulation of geomagnetic data and the estimation of transfer functions. Geophys. J. Roy. Astr. Soc., 43, 87-101.

Barber, N.F., 1956: A correlation treatment of fading signals. J. Atmos. Terr. Phys., 8, 318-330.

Barnett, J.J., 1974: The mean meridional temperature behaviour of the stratosphere from November 1971 derived from measurements by the Selective Chopper Radiometer on Nimbus IV. Quart. J. Roy. Meteorol. Soc., 100, 505-530.

Behannon, K.W. and N.F. Ness, 1966: The design of numerical filters for geomagnetic data analysis. NASA Report TN D-3341, 35pp.

Beland, M., 1978: The evolution of a nonlinear Rossby wave critical level: effects of viscosity. J. Atmos. Sci., 35, 1802-1815.

Belmont, A.D., D.G. Dartt and G.D. Nastrom, 1974: Periodic variations in stratospheric zonal wind from 20-65 km at 80°N to 70°S. Quart. J. Roy. Meteorol. Soc., 100, 203-211.

Belmont, A.D. and G.D. Nastrom, 1979: Long-period waves in mesospheric winds at Saskatoon (52°N). J. Geomag. Geoelectr., 31, 165-171.

Beynon, W.J.G. and J.C. Wright, 1969: The analysis of ionospheric drift data in the closely spaced receiver method. J. Atmos. Terr. Phys., 31, 593-596.

Bingham, C., M.D. Godfrey and J.W. Tukey, 1967: Modern techniques of power spectrum estimation. I.E.E.E. Trans. Audio and Electroacoustics, AU-15, 56-66.

Blamont, J.-E. and H. Teitelbaum, 1968: La rotation du vecteur vitesse horizontal dans les marées atmosphériques.

Bloomfield, P., 1976; Fourier Analysis of Time Series: An Introduction. Wiley, 258pp.

Bramley, E., 1951: Diversity effects in Spaced-aerial reception of ionospheric waves. Proc. I.E.E.E., 98, 19-26.

Brandt, S., 1976: Statistical and Computational Methods in Data Analysis. North-Holland Publ. Co., 322pp.

Briggs, B.H., 1968: On the analysis of moving patterns in geophysics - I. Correlation analysis. J. Atmos. Terr. Phys., 30, 1777-1788.

Briggs, B.H. 1972: Recent work on ionospheric irregularities and drifts. Geofys. Publik., 29, 121-134.

Briggs, B.H., 1977: The analysis of moving patterns by correlation methods. Rep.ADP 148, Dept. of Phys., University of Adelaide.

Briggs, B.H., G.J. Phillips and D.H. Shinn, 1950: The analysis of observations on spaced receivers of the fading of radio signals. Proc. Phys. Soc., B63, 106-121.

Briggs, B.H. and M. Spencer, 1955: The variability of time shifts in measurements of ionospheric movements. In: The Physics of the Ionosphere, The Physical Society, London, 123-135.

Briggs, B.H., W.G. Elford, D.G. Felgate, M.G. Golley, D.E. Rossiter and J.W. Smith, 1969: Buckland Park Aerial Array. Nature, 223, 1321-1325.

Briggs, B.H. and A.D. Maude, 1978: Spaced sensor observations of pattern motion. J. Geophys. Res., 83, 5309-5311.

Brown, G.M. and J.W. Chapman, 1972: An investigation of the ground diffraction pattern of radio waves reflected by the ionosphere. J. Atmos. Terr. Phys., 34, 1445-1454.

Brown, G.M. and J.I. John, 1979: Vertical penetration of planetary scale waves into the lower ionosphere. J. Atmos. Terr. Phys., 41, 379-385.

Burns, A.G., 1980: Travelling planetary waves: cross spectral analysis of stratospheric radiances and ionospheric parameters. M.Sc. Thesis, University of Canterbury, 174pp.

Burpee, R.W., 1976: Some features of global-scale 4-5 day waves. J. Atmos. Sci., 33, 2292-2299.

Butler, S.T. and K.A. Small, 1963: The excitation of atmospheric oscillations. Proc. Roy. Soc. A274, 91-121.

Cavalieri, D.J., 1976: Travelling planetary-scale waves in the E-region. J. Atmos. Terr. Phys., 38, 965-977.

Chandra, H., 1978: On the triangle size effect in spaced receiver drifts experiments. Ind. J. Radio Space Phys., 7, 13.

Chapman, S. and R.S. Lindzen, 1970: Atmospheric Tides. D. Reidel. 200pp.

Charney, J.G. and P.G. Drazin, 1961: Propagation of planetary-scale disturbances from the lower into the upper atmosphere. J. Geophys. Res., 66, 83-109.

Chen, W.Y. and G.R. Stegen, 1979: Experiments with maximum entropy power spectra of sinusoids. J. Geophys. Res., 79, 3019-3022.

Ching, B.K. and Y.T. Chiu, 1972: Annual and sub-annual effects of EUV heating - I. Harmonic Analysis. Planet. Space Sci., 20, 1745-1759.

CIRA, Cospar International Reference Atmosphere, 1972. Akademie-Verlag, Berlin, 450 pp.

CIRA, Cospar International Reference Atmosphere, 1965. North-Holland Publ. Co., Amsterdam.

Clark, J.H.E., 1975: The theory of the vertical propagation of quasi-geostrophic disturbances in the presence of distorted background flows.

Clemmow, P.C., M.A. Johnson and K. Weekes, 1955: A note on the motion of a cyclindrical irregularity in an ionized medium. In: The Physics of the Ionosphere, The Physical Society, London, 136-139.

Clifford, A.A., 1973: Multivariate Error Analysis. Wiley, 112pp.

Coy, L., 1974: A possible 2-day oscillation near the tropical stratos-pause. J. Atmos. Sci., 36, 1615-1618.

Craig, R.L., 1979: Quasi two-day wave at 90 km. XVIIth General Assembly I.U.G.G., Canberra.

Craig, R.L., R.A. Vincent, G.J. Fraser and M.J. Smith, 1980: The quasi 2-day wave in the Southern Hemisphere mesosphere. Nature, 287, 319-320.

Crane, A.J., J.D. Haigh, J.A. Pyle and C.F. Rogers, 1980: Mean meridional circulations of the stratosphere and mesosphere. Pure Appl. Geophys., 118, 307-328.

Cunnold, D.M., 1975: Vertical transport coefficients in the mesosphere obtained from radar observerations. J. Atmos. Sci., 32, 2191-2200.

Cunnold, D., F. Alyea, N. Phillips and R. Prinn, 1975: A three-dimensional dynamical-chemical model of atmospheric ozone. J. Atmos. Sci., 32, 170-194.

Deland, R.J. and R.M. Freidman, 1972: Correlation of fluctuations of ionospheric absorption and atmospheric planetary scale waves. J. Atmos. Terr. Phys., 34, 295-304.

Deland, R.J., 1973: Comments on "Further evidence of global-scale, 5-day pressure waves". J. Atmos. Sci., 30, 934-935.

Dickinson, R.W., 1968a: Planetary Rossby propagating vertically through weak westerly wind wave guides. J. Atmos. Sci., 25, 989-1002.

Dickinson, R.W., 1968b: On the exact and approximate linear theory of vertically propagating planetary Rossby waves forced at a spherical lower boundary. Mon. Weather Rev., 96, 405-415.

Dickinson, R.E., 1970: Development of a Rossby wave critical level. J. Atmos. Sci., 27, 627-633.

Dickinson, R.E. 1975: Meteorology of the upper atmosphere. Rev. Geophys. Space Phys., 13, 771-862.

Dickinson, R.E. and P.C. Williamson, 1972: Free oscillations of a discrete stratified fluid with application to numerical weather prediction. J. Atmos. Sci., 29, 623-640.

Dickinson, R.E., E.C. Ridley and R.G. Roble, 1975: Meridional circulation in the thermosphere. I. Equinox conditions. J. Atmos. Sci., 32, 1737-1754.

Dickinson, R.E., E.C. Ridley and R.G. Roble, 1977: Meridional circulation in the thermosphere. II. Solstice conditions. J. Atmos. Sci., 34, 178-192.

Diky, L.A. and G.S. Golitsyn, 1968: Calculation of the Rossby wave velocities in the Earth's atmosphere. Tellus, 20, 314-317.

Dunkerton, T., 1978: On the mean meridional mass motions of the stratosphere and mesosphere. J. Atmos. Sci., 35, 2325-2333.

Dunkerton, T., 1979: On the role of the Kelvin wave in the westerly phase of the semiannual zonal wind oscillation. J. Atmos. Sci., 36, 43-41.

Ebel, A., 1974: Heat and momentum sources of mean circulation at an altitude of 70 to 100 km. Tellus, 26, 325-333.

Elford, W.G., 1959: A study of winds between 80 and 100 km in medium latitudes. Planet. Space Sci., 1, 94-101.

Elford, W.G., 1976: Prevailing winds in the lower thermosphere. Nature, 261, 123-124.

Elford, W.G. 1979: Momentum transport due to atmospheric tides. J. Geophys. Res., 84, 4432-4436.

Eliasen, E. and B. Machenhauer, 1965: A study of the fluctuations of the atmospheric planetary flow patterns represented by spherical harmonics. Tellus, 17, 220-238.

Eliasen, E. and B. Machenhauer, 1969: On the observed large-scale atmospheric wave motion. Tellus, 21, 149-165.

Eliassen, A. and E. Palm, 1960: On the transfer of energy in stationary mountain waves. Geofys. Publ., 22, 1-23.

Emery, B.A., 1978: Neutral thermospheric winds above Millstone Hill:2. Seasonal wind variations, 1970-1971. J. Geophys. Res., 83, 5704-5716.

Essex, E.A. and F.W. Morton, 1974: Stratospheric-ionospheric coupling in the Southern Australia region. J. Atmos. Terr. Phys., 36, 1945-1956.

Fedor, L.S., 1967: A statistical approach to the determination of three-dimensional ionospheric drifts. J. Geophys. Res., 72, 5401-5415.

Fedor, L.S. and W. Plywaski, 1972: The interpretation of ionospheric drift measurements - IV. The effects of signal coupling among spaced sensor channels. J. Atmos. Terr. Phys., 34, 1285-1303.

Felgate, D.G., 1970: On the point source effect in the measurement of ionospheric drifts. J. Atmos. Terr. Phys., 32, 241-245.

Felgate, D.G. and M.G. Golley, 1971: Ionospheric irregularities and movements observed with a large aerial array. J. Atmos. Terr. Phys., 33, 1353-1369.

Felgate, D.G., A.N. Hunter, S.P. Kingsley and H.G. Muller, 1975: Comparative studies of E-region ionospheric drifts and meteor winds. Planet. Space Sci., 23, 389-400.

Fellous, J.L., A. Spizzichino, M. Glass and M. Massebeuf, 1974; Vertical propagation of tides at meteor heights. J. Atmos. Terr. Phys., 36, 385-396.

Fellous, J.L., R. Bernard, M. Glass, M. Massebeuf and A. Spizzichino, 1975: A study of variations of atmospheric tides in the meteor zone. J. Atmos. Terr. Phys., 37, 1511-1524.

Flattery, T.W., 1967: Hough functions. Ph.D. thesis, University of Chicago. 168pp.

Fooks, G.F., 1965: Ionospheric drift measurements using correlation analysis; methods of computation and interpretation of results. J. Atmos. Terr. Phys., 27, 979-989.

Forbes, J.M. and H.B. Garrett, 1976: Solar diurnal tide in the thermosphere. J. Atmos. Sci., 33, 2226-2241.

Forbes, J.M. and H.B. Garrett, 1978a: Seasonal-latitudinal structure of the diurnal thermospheric tide. J. Atmos. Sci. 35, 145-159.

Forbes, J.M. and H.B. Garrett, 1978b: Thermal excitation of atmospheric tides due to insolation absorption by O_3 and H_2O. Geophys. Res. Lett., 5, 1013-1016.

Forbes, J.M. and H.B. Garrett, 1980: Theoretical studies of Atmospheric Tides. Rev. Geophys. Space Phys., 17, 1951-1981.

Fraser, G.J. 1965: The measurement of atmospheric winds at altitudes of 64-120 km using ground-based radio equipment. J. Atmos. Sci., 22, 217-218.

Fraser, G.J. 1968: Seasonal variation of southern hemisphere mid-latitude winds at altitudes of 70-100 km. J. Atmos. Terr. Phys., 30, 707-719.

Fraser, G.J., 1970: Minimising time shift errors in spaced receiver arrays. Unpublished Report. University of Canterbury.

Fraser, G.J. 1977: The 5-day wave and ionospheric absorption. J. Atmos. Terr. Phys., 39, 121-124.

Fraser, G.J. and A. Kochanski, 1970: Ionospheric drifts from 64-108 km altitudes at Birdlings Flat. Ann. Geophys., 26, 675-687.

Fraser, G.J. and R.A. Vincent, 1970: A study of D-region irregularities. J. Atmos. Terr. Phys., 32, 1591-1607.

Fraser, G.J. and M.R. Thorpe, 1976: Experimental investigations of ionospheric/stratospheric coupling in southern mid-latitudes - I. Spectra and cross-spectra of stratospheric temperatures and the ionospheric f-min parameter. J. Atmos. Terr. Phys., 38, 1003-1011.

Fraser, G.J., B.B. Lim, G.K. Prisk and M.J. Smith, 1981: An association between mesospheric winds and electron densities. Submitted to J. Atmos. Terr. Phys.

Geisler, J.E. and R.E. Dickinson, 1968: Vertical motions and nitric oxide in the upper mesosphere. J. Atmos. Terr, Phys., 30, 1505-1521.

Geisler, J.E. and R.E. Dickinson, 1975: External Rossby modes on a β-plane with realistic vertical wind shear. J. Atmos. Sci., 32, 2082-2093.

Geisler, J.E. and R.E. Dickinson, 1976: The five-day wave on a sphere with realistic zonal winds. J. Atmos. Sci., 33, 632-641.

Geller, M.A., H. Tanaka and D.C. Fritts, 1975: Production of turbulence in the vicinity of critical levels for internal gravity waves. J. Atmos. Sci., 32, 2125-2135.

Glass, M., J.L. Fellous, M. Massebeuf, A. Spizzichino, I.A. Lysenko and Yu. I. Portniaghin, 1975: Comparison and interpretation of the results of simultaneous wind measurements in the lower thermosphere at Garchy (France) and Obninsk (U.S.S.R.) by meteor radar technique. J. Atmos. Terr. Phys., 37, 1077-1087.

Glass, M., R. Bernand, J.L. Fellous and M. Massebeuf, 1978: The French meteor radar facility. J. Atmos. Terr. Phys., 40, 923-931.

Golley, M.G. and D.E. Rossiter, 1970: Some tests of methods of analysis of ionospheric drift records using an array of 89 aerials. J. Atmos. Terr. Phys., 32, 1215-1233.

Golley, M.G. and D.E. Rossiter, 1971: Some aspects of ionospheric drifts using partial and total reflections from the lower ionosphere. J. Atmos. Terr. Phys., 33, 701-714.

Granger, C.W.J. and M. Hatanaka, 1964: Spectral Analysis of Economic Time Series. Princeton Univ. Press, 299 pp.

Green, J.S.A., 1972: Large-scale motion in the upper stratosphere and mesosphere: an evaluation of data and theories. Phil. Trans. Roy. Soc. Lond., A271, 577-583.

Greenhow, J.S. and E.L. Neufeld, 1961: Winds in the upper atmosphere. Quart. J. Roy. Meteor. Soc., 87, 472-489.

Gregory, J.B., 1961: Radio wave reflections from the mesosphere. I. Heights of occurrence. J. Geophys. Res., 66, 429-445.

Gregory, J.B., 1965: The influence of atmospheric circulation on mesospheric electron densities in winter. J. Atmos. Sci., 22, 18-23.

Gregory, J.B. and A.H. Manson, 1975a: Winds and wave motions to 110 km at mid-latitudes. II. Mean winds at 52°N,1969-73. J. Atmos. Sci., 32, 1667-1675.

Gregory, J.B. and A.H. Manson, 1975b: Winds and wave motions to 110 km at mid-latitudes. III. Response of mesospheric and thermospheric winds to major stratospheric warmings. J. Atmos. Sci., 32, 1676-1681.

Gregory, J.B., C.E. Meek, A.H. Manson and D.G. Stephenson, 1979: Developments in the radiowave drifts technique for measurements of high-altitude winds. J. Appl. Meteorol, 18, 682-691.

Groves, G.V., 1969: Wind models from 60 to 130 km altitude for different months and latitudes. J. Brit. Interplanet. Soc., 22, 285-307.

Groves, G.V., 1971: Atmospheric structure and its variation in the region from 25 to 120 km. Air Force Cambridge Research Laboratories, Environ. Res. Pap., No. 368.

Groves, G.W., 1972: Annual and semi-annual zonal wind components and corresponding temperature and density variations, 60-130 km. Planet. Space Sci., 20, 2099-2112.

Hagen, J.B. and D.T. Farley, 1973: Digital-correlation techniques in radio science. Radio Sci., 8, 775-784.

Hargreaves, J.K., 1973: Mid-latitude winter anomalies in radio absorption and stratospheric temperature distribution: Observations concerning the influence of auroral and magnetic activity. J. Atmos. Terr. Phys., 35, 291-304.

Hartmann, D.L., 1976: The dynamical climatology of the stratosphere on the southern hemisphere during late winter 1973. J. Atmos. Sci., 33, 1789-1802.

Haug, A. and H. Pettersen, 1970: An interpretation of asymmetric cross-correlation functions in D- and lower E-region drift measurements. J. Atmos. Terr. Phys., 32, 397-403.

Haurwitz, B., 1940a: The motion of atmospheric disturbances. J. Marine Res., 3, 35-50.

Haurwitz, B., 1940b: The motion of atmospheric disturbances on the spherical earth. J. Marine Res., 3, 254-267.

Hess, G.C. and M.A. Geller, 1976: The Urbana meteor-radar system: Design, development and first observations. Aeronomy Rep. No. 74, University of Illinois, 336 pp.

Hines, C.O., 1960: Internal atmospheric gravity waves at ionospheric heights. Canad. J. Phys., 38, 1441-1481.

Hines, C.O., 1968: Some consequences of gravity wave critical layers in the upper atmosphere. J. Atmos. Terr. Phys., 30, 837-843.

Hines, C.O., 1972: Motions in the ionospheric D and E regions. Phil. Trans. Roy. Soc. Lond., A271, 457-471.

Hines, C.O., 1974: The Upper ATmosphere in Motion. Am. Geophys. Union, Wash., 1027pp.

Hines, C.O., 1975: Unpublished paper on Specular Point theory.

Hines, C.O., I. Paghis, T.R. Hartz and J.A. Fejer, 1965: Physics of the Earth's Upper Atmosphere. Prentice-Hall, N.J., 434pp.

Hines, C.O., and C.A. Reddy, 1967: On the propagation of atmospheric gravity waves through regions of wind shear. J. Geophys. Res., 72, 1015-1034.

Hirota, I., 1971: Excitation of planetary Rossby waves in the winter stratosphere by periodic forcing. J. Meteorol. Soc. Japan, 49, 439-448.

Hirota, I., 1976: Seasonal variation of planetary waves in the stratosphere observed by the Nimbus 5 SCR. Quart. J. Roy. Meteorol. Soc., 102, 757-770.

Hirota, I. and J.J. Barnett, 1977: Planetary waves in the winter mesosphere - preliminary analysis of Nimbus 6 PMR results. Quart. J. Roy. Meteorol. Soc., 103, 487-498.

Hocking, W.K., 1979: Angular and temporal characteristics of partial reflection from the D-region of the ionosphere. J. Geophys. Res., 84, 845-851.

Hodges, R.R., 1967: Generation of turbulence in the upper atmosphere by internal gravity waves. J. Geophys. Res., 72, 3455-3458.

Hodges, R.R., 1969: Eddy diffusion coefficients due to instabilities in internal gravity waves. J. Geophys. Res., 74, 4087-4090.

Holloway, J.L., 1958: Smoothing and filtering of time series and space fields. In: Advances in Geophysics, Vol. 4, Academic Press, N.Y., 351-389.

Holton, J.R., 1972: An introduction to dynamic meteorology. Academic, N.Y., 319 pp.

Holton, J.R., 1975: The dynamic meteorology of the stratosphere and mesosphere. Am. Meteorol. Soc., Vol. 15, Boston, 218 pp.

Holton, J.R., 1980: The dynamics of sudden stratospheric warmings. Ann. Rev. Earth Planet. Sci., 8, 169-190.

Holton, J.R. and W.M. Wehrbein, 1980: A numerical model of the zonal mean circulation of the middle atmosphere. Pure Appl. Geophys., 118, 284-306.

Hong, S.-s. and R.S. Lindzen, 1976: Solar semidiurnal tide in the thermosphere. J. Atmos. Sci., 33, 135-153.

Hook, J.L., 1972: Wind patterns at meteor altitudes (75-105 km) above College, Alaska, associated with midwinter stratospheric warmings. J. Geophys. Res., 77, 3856-3868.

Hough, S.S., 1898: On the application of harmonic analysis to the dynamical theory of tides, II, On the general integration of Laplace's dynamical equations. Phil. Trans. Roy. Soc. London, A191, 139-185.

Houghton, J.T., 1978: The stratosphere and mesosphere. Quart. J. Roy. Meteorol. Soc., 104, 1-29.

Jenkins, G.M. and D.G. Watts, 1968: Sepectral Analysis and its Applications. Holden-Day, San Francisco, 525 pp.

Jones, D. and A.D. Maude, 1965: Evidence for wave motions in the E-region in the ionosphere. Nature, 206, 177-179.

Jones, W.L., 1963: Energetics of the solar semidiurnal tide in the atmosphere. Ph.D. Thesis, MIT, 162 pp.

Jones W.L., 1976: Linear internal gravity waves in the atmosphere. Handbuch der Physik, 49, 177-216.

Julian, P.R., 1975: Comments on the determination of significance levels of the coherence statistic. J. Atmos. Sci., 32, 836-837.

Kal'chanko, B.V. and S.V. Bulgakov, 1973: Study of periodic components of wind velocity in the lower thermosphere above the equator. Geomag. Aeron., 13, 955-956.

Kane, R.P., 1979: Maximum entropy spectral analysis of some artificial samples. J. Geophys. Res., 84, 965-966.

Kantor, A.J. and A.E. Cole, 1964: Zonal and meridional winds to 120 km. J. Geophys. Res., 69, 5131-5140.

Kasahara, A., 1976: Normal modes of ultralong waves in the atmosphere. Mon. Weather Rev., 104, 669-690.

Kasahara, A., 1980: Effect of zonal flows on the free oscillations of a barotropic atmosphere. J. Atmos. Sci., 37, 917-928.

Kato, S., 1966: Diurnal atmospheric oscillation, 1, eigenvalues and Hough functions. J. Geophys. Res., 71, 3201-3209.

Kelleher, R.F., 1966: Some statistical properties of the ground diffraction patterns of vertically reflected radio waves. J. Atmos. Terr. Phys., 28, 213-223.

Kellogg, W.W., 1961: Chemical heating above the polar mesopause in winter. J. Meteorol., 18, 373-381.

Keneshea, T.J., M.E. Gardner and W. Pfister, 1965: Analysis of ionospheric winds and turbulence over Puerto Rico with a correlation method.

Kennedy, J.S., 1980: Comments on 'On detrending and smoothing random data' by A.J. Owens. J. Geophys. Res., 85, 219-220.

Kent, G.S. and R.W.H. Wright, 1968: Movements of ionospheric irregularities and atmospheric winds. J. Atmos. Terr. Phys., 30, 657-691.

Kochanski, A., 1972: Semiannual variation at the base of the thermosphere. Mon. Weather Rev., 100, 222-234.

Labitzke, K., 1972: The interaction between stratosphere and mesosphere in winter. J. Atmos. Sci., 29, 1395-1399.

Labitzke, K., 1980: Climatology of the stratosphere and mesosphere. Phil. Trans. Roy. Soc. Lond., A296, 7-18.

Laplace, P.S., 1799: Méchanique Céleste, Paris, 145-167.

Lauter, E.A. and R. Knuth, 1967. Precipitation of high energy particles into the upper atmosphere at medium latitudes after magnetic storms. J. Atmos. Terr. Phys., 29, 411-417.

Leovy, C., 1964: Simple models of thermally driven mesospheric circulation. J. Atmos. Sci., 21, 327-341.

Leovy, C.B. and P.J. Webster, 1976: Stratospheric long waves: Comparison of thermal structure in the northern and southern hemispheres. J. Atmos. Sci., 33, 1624-1638.

Lindzen, R.S., 1966: On the theory of the diurnal tide. Mon. Weather Rev., 94, 295-301.

Lindzen, R.S., 1967: Thermally driven diurnal tide in the atmosphere. Quart. J. Roy. Meteorol. Soc., 93, 18-42.

Lindzen, R.S., 1971: Tides and gravity waves in the upper atmosphere. In: Mesospheric models and related experiments. Ed. G. Fiocco, Reidel, Holland, 122-130.

Lindzen, R.S., 1972: Equatorial planetary waves in shear: Part II. J. Atmos. Sci., 29, 1452-1463.

Lindzen, R.S., 1976: A modal decomposition of the semidurnal tide in the lower thermosphere. J. Geophys. Res., 81, 2923-2926.

Lindzen, R.S., 1978: Effect of daily variations of cumulonimbus activity on the semidiurnal tide. Mon. Weather Rev., 106, 526-533.

Lindzen, R.S., 1979: Atmospheric tides. Ann. Rev. Earth Planet. Sci., 7, 199-225.

Lindzen, R.S. and D. Blake, 1971: Internal gravity waves in atmospheres with realistic dissipation and temperature. Part II. Thermal tides excited below the mesopause. Geophys. Fluid Dyn., 2, 31-61.

Lindzen, R.S. and D. Blake, 1972: Lamb waves in the presence of realistic distributions of temperature and dissipation. J. Geophys. Res., 77, 2166-2176.

Lindzen, R.S. and S.s-. Hong, 1974: Effects of mean winds and horizontal temperature gradients on solar and lunar semidiurnal tides in the atmosphere. J. Atmos. Sci., 31, 1421-1466.

Little, L.T. and R.D. Ekers, 1971: A method for analysing drifting random patterns in astronomy and geophysics. Astron. Astrophys., 10, 306-309.

Longuet-Higgins, M.S., 1968: The eigenfunctions of Laplace's tidal equations over a sphere. Phil. Trans. Roy. Soc. Lond., A269, 511-607.

Lysenko, J.A., Yu. I. Portnyagin, K.M. Greisiger and K. Sprenger, 1975: Some peculiarities of the atmospheric circulation at the altitude of 90-100 km over Europe in winter 1972-73. Zeit. Meteorol., 25, 213-217.

MacDougall, J.W. 1966: The interpretation of ionospheric drift measurements. J. Atmos. Terr. Phys., 28, 1093-1109.

McGee, C.R., 1966: On the nature of movements in the ionosphere. J. Atmos. Terr. Phys., 28, 861-869.

McNulty, R.P. 1976: Vertical energy flux in planetary-scale waves: Observational results. J. Atmos. Sci., 33, 1173-1183.

Madden, R.A., 1975: Oscillations in the winter stratosphere: Part 2. The role of horizontal heat transport and the interaction of transient and stationary planetary-scale waves. Mon. Weather Rev., 103, 717-729.

Madden, R.A., 1978: Further evidence of travelling planetary waves. J. Atmos. Sci., 35, 1605-1618.

Madden, R.A., 1979: Observations of large-scale travelling Rossby waves. Rev. Geophys. Space Phys., 17, 1935-1949.

Madden, R.A. and P. Jullian, 1972: Further evidence of global-scale, 5-day pressure waves. J. Atmos. Sci., 29, 1464-1469.

Madden, R.A. and P. Julian, 1973: Reply. J. Atmos. Sci., 30, 935-940.

Manabe, S. and J.D. Mahlman, 1976: Simulation of seasonal and interhemispheric variations in the stratospheric circulation. J. Atmos. Sci., 33, 2185-2217.

Manson, A.H., 1968: Coupling effects between the ionosphere and stratosphere in Canada (45N, 75W), 1962-1966. J. Atmos. Terr. Phys., 30, 627-632.

Manson, A.H., 1969: The effect of solar corpuscular radiation on the 1963 final spring warming in the Antarctic. J. Atmos. Sci., 26, 587-693.

Manson, A.H., 1971: The concentration and transport of minor constituents in the mesosphere and lower thermosphere (70-110 km) during periods of anomalous absorption. J. Atmos. Phys., 33, 715-721.

Manson, A.H., 1976: Stratospheric-ionospheric-magnetospheric coupling at mid-latitudes in the Southern Hemisphere, 1969-1974. J. Atmos. Terr. Phys., 38, 1617-1020.

Manson, A.H., J.B. Gregory and D.G. Stephenson, 1973: Winds and wave motions (70-100 km) as measured by a partial reflection radiowave system. J. Atmos. Terr. Phys., 35, 2055-2067.

Manson, A.H., J.B. Gregory and D.G. Stephenson, 1974: Winds and wave motions up to 110 km and mid-latitudes I. Partial reflection radiowave soundings, 1972-73. J. Atmos. Sci., 31, 2207-2215.

Manson, A.H., and C.E. Meek, 1976: Internal gravity waves in the mesosphere and lower thermosphere at mid-latitudes. J. Atmos. Sci., 33, 1650-1656.

Manson, A.H. and C.E. Meek, 1977: Gravity waves in the lower thermosphere at 35°S (South Australia). J. Atmos. Terr. Phys., 39, 1411-1416.

Manson, A.H., J.B. Gregory, C.E. Meek and D.G. Stephenson, 1978: Wind and wave motions to 110 km at mid-latitudes. V. An analysis of data from September 1974 - April 1975. J. Atmos. Sci., 35, 592-599.

Manson, A.H., C.E. Meek and R.J. Stening, 1979: The role of atmospheric waves (1.5h - 10 days) in the dynamics of the mesosphere and lower thermosphere at Saskatoon (52°N, 107°W) during four seasons of 1976. J. Atmos. Terr. Phys., 41, 325-335.

Manson, A.H., and C.E. Meek, 1980: Gravity waves of short period (5-90 min), in the lower thermosphere at 52°N (Saskatoon, Canada). J. Atmos. Terr. Phys., 42, 103-113.

Massebeuf, M., R. Bernard, J.L. Fellous and M. Glass, 1979: The mean Zonal circulation in the meteor zone above Garchy (France) and Kirana (Sweden). J. Atmos. Terr. Phys., 41, 647-655.

Matsuno, T., 1971: A dynamical model of the stratospheric sudden warming. J. Atmos. Sci., 28, 1479-1494.

Matsuno, T., 1966: Quasi-geostrophic motions in the equatorial area. J. Meteorol. Soc. Japan, 44, 25-43.

Mechtly, E.A. and L.G. Smith, 1968: Seasonal variation of the lower ionosphere at Wallops Island during IQSY. J. Atmos. Terr. Phys., 30, 155-1561.

Meek, C.E., 1978: The analysis of ionospheric drift measurements. Report, Inst. Space and Atmos. Studies, University of Saskatchewan, 127 pp.

Meek, C.E., A.H. Manson and J.B. Gregory, 1979: Internal consistency analysis for partial and total reflection drifts data. J. Atmos. Terr. Phys., 41, 251-258.

Mitra, S.N., 1949: A radio method of measuring winds in the ionosphere. Proc. I.E.E.E., 96, 441-446.

Muller, H.G., 1972: Long-period meteor wind oscillations. Phil. Trans. Roy. Soc. Lond., A271, 585-598.

Muller, H.G. and Kingsley, 1974: Long period meteor wind oscillations. J. Atmos. Terr. Phys., 36, 1933-1943.

Muller, H.G. and L. Nelson, 1978: A travelling wuasi 2-day wave in the meteor region. J. Atmos. Terr. Phys., 40, 761-766.

Murgatroyd, R.J., 1965: Winds in the mesosphere and lower thermosphere. Proc. Roy. Soc., A288, 575-589.

Murgatroyd, R.J., 1971: Dynamical modelling of the stratosphere and mesosphere. In: Mesospheric Models and Related Experiments, ed. G. Fiocco, Reidel, Holland, 104-121.

Murgatroyd, R.J. and R.M. Goody, 1958: Sources and sinks of radioative energy from 30 to 90 km. Quart. J. Roy. Meteorol. Soc., 84, 225-234.

Murgatroyd, R.J. and F. Singleton, 1961: Possible meridional circulations in the stratosphere and mesosphere. Quart. J. Roy. Meteorol. Soc., 87, 125-135.

Murphy, C.H., 1969: Seasonal variation of ionospheric winds over Barbados, West Indies. J. Geophys. Res., 74, 339-347.

Nastrom, G.D. and A.D. Belmont, 1980: Apparent solar cycle influence on long-period oscillations in stratospheric zonal wind speeds. Geophys. Res. Lett., 7, 457-460.

Newell, R.E., 1966: The energy and momentum budget of the atmosphere above the tropopause. In: Problems of Atmospheric Circulation. Ed. R.V. Garcia and T.F. Malone, MacMillan, London, 106-125.

Newell, R.E. and R.E. Dickinson, 1967: On the application of a proposed global system for measuring meteor winds. Pure Appl. Geophys., 69, 162-172.

Offerman, D., 1979: Recent advances in the study of the D-region winter anomaly. J. Atmos. Terr. Phys., 41, 735-752.

Otnes, R.K. and L. Enochson, 1972: Digital Time Series Analysis. Wiley, 467 pp.

Owens, A.J., 1978: On detrending and smoothing random data. J. Geophys. Res., 83, 221-224.

Pawsey, J.L., 1935: Further investigations of the amplitude variations of downcoming wireless waves. Proc. Camb. Philosoph. Soc., 31, 125-144.

Pfister, W., 1971: The wave-like nature of inhomogeneities in the E-region. J. Atmos. Terr. Phys., 33, 999-1025.

Phillips, G.J. and M. Spencer, 1955: The effects of anisometric amplitude patterns in the measurement of ionospheric drifts.

Poulter, E.M., 1978: Radio-meteor investigations of atmospheric motion. Ph.D. Thesis, University of Canterbury, 367 pp.

Poulter, E.M., 1980: Winter motions in the southern hemisphere meteor region. J. Atmos. Terr. Phys., 42, 661-672.

Pyle, J.A. and C.F. Rogers, 1980: A modified diabatic circulation model for stratospheric tracer transport. Nature, 287, 711-714.

Quiroz, R.S., 1978: The contribution of satellite remote-sounding data in stratospheric research. In: Remote Sounding of the Atmosphere from Space. Ed. H.-J. Bolle, Pergamon Press, 69-82.

Ratcliffe, J.A., 1956: Some aspects of diffraction theory and their application to the ionosphere. Rep. Prog. Phys., 19, 188-226.

Reed, R.J. 1966: Zonal wind behavior in the equatorial stratosphere and lower mesosphere. J. Geophys. Res., 71, 4223-4233.

Rodgers, C.D., 1976: Evidence for the five-day wave in the upper stratosphere. J. Atmos. Sci. 33, 710-711.

Roper, R.G., 1966: Atmospheric turbulence in the meteor region. J. Geophys. Res., 71, 5785-5792:

Roper, R.G. 1975: Meteor winds over Atlanta (34N, 84W). XVIth General Assembly I.U.G.G., Grenoble.

Roper, R.G., 1978: Winds from the Atlanta (34°N, 84°W) radio meteor wind facility. J. Atmos. Terr. Phys., 40, 891-894.

Roper, R.G. and W.G. Elford, 1963: Seasonal variation of turbulence in the upper atmosphere. Nature, 197, 963-964.

Rossby, C.-G., and collaborators, 1939: Relations between variations in the intensity of the zonal circulation of the atmosphere and the displacements of the semipermanent centers of action. J. Marine Res., 2, 38-55.

Rossiter, D.E. 1971: A comparison of ionospheric drifts with radio meteor measurements of the neutral wind. Aust. J. Phys., 24, 103-117.

Salby, M.L., 1979: On the solution of the homogeneous vertical structure problem for long-period oscillations. J. Atmos. Sci., 36, 2350-2359.

Salby, M.L., 1980a: The influence of realistic dissipation on planetary normal structures. J. Atmos. Sci., 37, 2186-2199.

Salby, M.L., 1980b: Rossby normal modes in asymmetric and realistic background configurations. Part I: Simple nonuniformities. Submitted to J. Atmos. Sci.

Salby, M.L., 1980c: Rossby normal modes in asymmetric and realistic background configurations. Part II: Equinox and solstice conditions. Submitted to J. Atmos. Sci.

Salby, M.L. and R.G. Roper, 1980: Long-period oscillations in the meteor region. J. Atmos. Sci., 37, 239-244.

Schminder, R. and D. Kürschner, 1978: On the behaviour of wind systems in the upper mesosphere region during the transition from summer to winter conditions. J. Atmos. Terr. Phys., 40, 165-168.

Schminder, R. and D. Kürschner, 1979: On the behaviour of wind systems in the upper mesopause region in winter and during the transition from winter to summer conditions. J. Atmos. Terr. Phys., 41, 119-122.

Schoeberl, M.R., 1978: Stratospheric warmings: Observations and theory. Rev. Geophys. Space Phys., 16, 521-538.

Schoeberl, M.R. and J.H.E. Clark, 1980: Resonant planetary waves in a spherical atmosphere. J. Atmos. Sci., 37, 20-28.

Shapley, A.H. and W.J.G. Beynon, 1965: 'Winter anomaly' in ionospheric absorption and stratospheric warmings. Nature 206, 1242-1243.

Siebert, M., 1961: Atmospheric tides. In: Advances in Geophysics, Vol. 7, Academic Press, N.Y., 105-182.

Simmons, A.J., 1974a: Planetary-scale disturbances in the polar winter stratosphere. Quart. J. Roy. Meteorol. Soc., 100, 76-108.

Simmons, A.J., 1974b: Baroclinic instability at the winter stratopause. Quart. J. Roy. Meteorol. Soc., 100, 531-540.

Simmons, A.J., 1977: Baroclinic instability in the summer mesosphere. Quart. J. Roy. Meteorol. Soc., 103, 211-215.

Sinno, K. and M. Higashimura, 1969: Development of ionospheric absorption associated with stratospheric warmings in 1958 and 1963. J. Atmos. Terr. Phys., 31, 1353-1357.

Slack, M., 1946: The probability distributions of sinusoidal oscillations combined in random phase. J. Instn. Elect. Engrs., 93, PtIII, 76-86.

Smith, M.J., 1980: Atmospheric tides from 80 to 100 km at 44S. XVIIth General Assembly I.U.G.G., Canberra, 1979.

Spizzichino, A., 1969: Theorie des interactions non linearires entre les ondes atmosphériques. Ann. Geophys., 25, 773-783.

Spjeldvik, W.N. and R.M. Thorne, 1975: The cause of storm after effects in the middle latitude D-region. J. Atmos. Terr. Phys., 37, 777-795.

Sprenger, K. and R. Schminder, 1967: Results of ten years' ionospheric drift measurements in the l.f. range. J. Atmos. Terr. Phys., 29, 183-199.

Sprenger, K. and R. Schminder, 1969: Solar cycle dependence of winds in the lower ionosphere. J. Atmos. Terr. Phys., 31, 217-221.

Stenning, R.J., C.E. Meek, A.H. Manson and D.G. Stephenson, 1978: Winds and wave motions to 110 km at midlatitudes. VI. Tidal gravity and and planetary waves.

Strobel, D.F., D.M. Hunten and M.B. McElroy, 1970: Production and diffusion of nitric oxide. J. Geophys. Res., 75, 4307-4321.

Stubbs, T.J., 1973: The measurement of winds in the D-region of the ionosphere by the use of partially reflected radio waves. J. Atmos. Terr. Phys., 35, 909-919.

Stubbs, T.J., 1976: Mean and periodic components of ionospheric drifts in the D-region at 35°S during 1972. J. Atmos. Terr. Phys., 38, 979-989.

Stubbs, T.J. and R.A. Vincent, 1973: Studies of D-region drifts during the winter of 1970-72. Aust. J. Phys., 26, 645-660.

Stubbs, T.J., 1977: A study of ground diffraction pattern parameters associated with D-region partial reflections. J. Atmos. Terr. Phys., 39, 589-594.

Teitelbaum, H. and C. Cot, 1979: Antisymmetric tidal modes under equinoctal conditions induced by ozone heating. J. Atmos. Terr. Phys., 41, 33-41.

Tsedelina, Ye. Ye., 1965: Movements of inhomogeneities in plasma (ionosphere). Geomag. Aeron., 5, 525-530.

Tung, K.K., 1979: A theory of stationary long waves. Part III: Quasi-normal modes in a singular waveguide.

Tung, K.K. and R.S. Lindzen, 1979: A theory of stationary long waves. Part I: A simple theory of blocking. Mon. Weather Rev. 107, 714-734.

Ulrych, T.J. and T.N. Bishop, 1975: Maximum entropy spectral analysis and auto-regressive decomposition. Rev. Geophys. Space Phys., 13, 183-200.

Villars, F. and H. Feshback, 1963: The effect of the earth's magnetic field on irregularities of ionization in the E layer. J. Geophys. Res., 68, 1303-1320.

Vincent, D.G., 1968: Mean meridional circulation in the Northern Hemisphere lower stratosphere during 1964 and 1965. Quart. J. Roy. Meteorol. Soc., 94, 333-349.

Vincent, R.A. and S. Ball, 1977: Tides and gravity waves in the mesosphere at mid- and low- latitudes. J. Atmos. Terr. Phys., 39, 965-970.

Vincent, R.A., T.J. Stubbs, P.H.O. Pearson, K.H. Lloyd and C.H. Low, 1977: A comparison of partial reflection drifts with winds determined by rocket techniques. J. Atmos. Terr. Phys., 39, 813-821.

Vincent, R.A. and J.S. Belrose, 1978: The angular distribution of radio waves partially reflected from the lower ionosphere. J. Atmos. Terr. Phys. 40, 35-47.

Vincent, R.A. and J. Rottger, 1980: Spaced antenna VHT radar observations of tropospheric velocities and irregularities. Radio Sci., 15, 319-335.

Wallace, J.M. and R.F. Tadd, 1974: Some further results concerning the vertical structure of atmospheric tidal motions within the lowest 30 kilometers. Mon. Weather Rev., 102, 795-803.

Walterscheid, R.L. and S.V. Venkateswaran, 1979a: Influence of mean zonal motion and meridional temperature gradients on the semidiurnal atmospheric tide: A spectral study. Part I: Theory. J. Atmos. Sci., 36, 1623-35.

Walterscheid, R.L. and S.V. Venkateswaran, 1979b: Influence of mean zonal motion and meridional temperature gradients on the semidiurnal atmospheric tide: A spectral study. Part II: Numerical results. J. Atmos. Sci., 36, 1636-1662.

Walterscheid, R.L., J.G. De Vore and S.V. Venkateswaran, 1980: Influence of mean zonal motion and meridional temperature gradients on the solar semidiurnal atmospheric tide: A revised spectral study with improved heating rates. J. Atmos. Sci., 37, 455-470.

Webster, A.R. and G.F. Lyon, 1975: On the use of running means in the power spectrum analysis of ionospheric data. Planet. Space Sci., 21, 153-157.

Weisman, M.L. and J.J. Olivero, 1979: Evidence for vertical motions in the equatorial middle atmosphere. J. Atmos. Sci., 36, 2169-2182.

Wilkinson, P.J. and W.J. Baggaley, 1975: Southern hemisphere atmospheric winds in the meteor region. Planet. Space. Sci., 23, 509-521.

Woodman, R.F. and A. Guillen, 1974: Radar observations of winds and turbulence in the stratosphere and mesosphere. J. Atmos. Sci., 31, 439-505.

Wratt, D.S., 1974: Atmospheric physics: electron density variations in the mesosphere. Ph.D., University of Canterbury, 228 pp.

Wright, J.W., 1968: The interpretation of ionospheric radio drift measurements - I. Some results of experimental comparisons with neutral wind profiles. J. Atmos. Terr. Phys., 30, 919-930.

Wright, J.W., 1972: The interpretation of ionospheric radio drift measurements - V. Demonstration of the point source effect in time-averaged correlations and drift calculations.

Wright, J.W., M. Glass and A. Spizzichino, 1976: The interpretation of ionospheric radio drift measurements - VIII. Direct comparisons of meteor radar winds and kinesonde measurements: mean and random motions.

Zipf, E.C., W.L. Borst and T.M. Donahue, 1970: A mass spectrometer observation of NO in an auroral arc. J. Geophys. Res., 75, 6371-6376.

ACKNOWLEDGEMENTS

I am indebted to Dr Grahame Fraser, my supervisor, for suggesting this project and for his valuable contribution to the software development at Birdlings Flat.

I have enjoyed many stimulating and informative discussions with Professor Walt Jones.

It is also a pleasure to thank the following people:

Justin Cooper and Murray Lynn who initiated me into the esoteric art of dealing with idiosyncratic hardware and software at Birdlings Flat;

Murray Poulter for many lively encounters, and for supplying the meteor wind data;

Kim Prisk for sharing in the data collection during 1978 and for the graphs of f_{min} and ΣK;

Graham Lees who assisted with the data collection and aerial maintenance throughout;

John de Voil for his conscientious maintenance of the transmitter and receivers;

Alec Black, who was responsible for the PDP-8 hardware;

Laurie Hunter for the photographic work and Janet Warburton for the typing.

The geomagnetic and absorption data was supplied by the Geophysical Observatory of the DSIR and the 1978 stratospheric data by the N.Z. Meteorological Service. The software for reading and plotting the stratospheric data, was written by Dr David Wratt.

Finally, I would like to thank Professor A.G. McLellan for providing the opportunity to pursue this research and for financial assistance in the form of a Teaching Fellowship.

ERRATA

page 8, line 8. "with the geometry of Fig. 2.1 (and with $\xi_o = \eta_o$)"

Page 60. The following numbers should appear descending down the right hand side of Fig. 4.2: 5, 3, 8, 10, 9, 17, 6, 4, 3

Page 79, line 7. $(U/2\Omega L)$ not $(U/2L)$

Page 79, line 17. N not N^2

Page 98, line 19. 65 not 85

Page 110. The phase scale of the upper diagram is incorrect. It should have the following symbols just after the large scale marks:
J M M J S N J
Caption should conclude with: "The circled points are values at Adelaide from Elford (1976)"

Page 127, line 7. 6.2b not 6.2a. Line 9. node not mode.

Page 140, line 9. 1977 not 1976

Page 156, lines 26, 27. Zonal and meridional should be interchanged.

Page 210. February 1980 not February 1979.

Page 216. Add to caption: "•——• zonal; +--+ meridional"

Page 228. As for page 216.

Page 220, line 17. Spring not autumn.

Page 53, line 20. "at all heights"

Page 103, line 24. Fig. 52 not Fig. 7.2

CORRECTIONS TO REFERENCES

Blamont, J.-E. and H. Teitelbaum, 1968: La rotation du vecteur vitesse horizontal dans les marées atmosphériques. Ann. Geophys., 24, 387-391.

Bossalasco M. and A. Elena, 1963: Absorption de la couche D et temperature de la mesosphere. Compte. Rend., 256, 4491.

Clark, J.H.E., 1975: The theory of the vertical propagation of quasi-geostrophic disturbances in the presence of distorted background flows. J. Atmos. Sci., 32, 2217-2228.

Clark, R.R., 1975: Meteor wind measurements at Durham, New Hampshire (43N, 71W). J. Atmos. Sci., 32, 1689-1693.

Forbes, J.M. and H.B. Garrett, 1980 - should be 1979

Kelleher R.F., 1965. In Proc. 2nd Intl. Symp. on Equatorial Aeronomy, ed. F. de Mendonca, 272.

Keneshea, T.J., M.E. Gardner and W. Pfister, 1965: Analysis of ionospheric winds and turbulence over Puerto Rico with a correlation method. J. Atmos. Terr. Phys., 27, 7-30.

Phillips, G.J. and M. Spencer, 1955: The effects of anisometric amplitude patterns in the measurement of ionospheric drifts. Proc. Phys. Soc., 68B, 481-492.

Rogers, R.R. and G.B. Walker, 1973: Autocorrelations of detected radar signals. J. Appl. Meteorol., 12, 1078-1080.

Stening, R.J., C.E. Meek, A.H. Manson and D.G. Stephenson, 1978: Winds and wave motions to 110 km at midlatitudes. VI. Tidal, gravity and planetary waves. J. Atmos. Sci., 35, 2194-2204.

Tung, K.K., 1979: A theory of stationary long waves. Part III: Quasi-normal modes in a singular waveguide. Mon. Weather Rev., 107, 751-774.

Vincent, R.A. and T.J. Stubbs, 1977: A study of motions in the winter mesosphere using the partial reflection drift technique. Planet. Space Sci., 25 441-455.

Wright, J.W., 1972: The interpretation of ionospheric radio drift measurements - V. Demonstration of the point source effect in time-averaged correlations and drift calculations. J. Atmos. Terr. Phys. 38, 1365-1378.

Wright, J.W., M. Glass and A. Spizzichino, 1976: The interpretation of ionospheric radio drift measurements - VIII. Direct comparisons of meteor radar winds and kinesonde measurements: mean and random motions. J. Atmos. Terr. Phys., 38, 713-729